UNIVERSITY OF SOUTHAMPTON

FACULTY OF NATURAL & ENVIRONMENTAL SCIENCES

CHEMISTRY

SELECTIVE OXIDATIONS OF ALCOHOLS AND ALDEHYDES IN A MICROFLUIDIC ELECTROLYSIS CELL

by

Robert Aaron Green

Thesis for the degree of Doctor of Philosophy

February 2014

UNIVERSITY OF SOUTHAMPTON

ABSTRACT

FACULTY OF NATURAL & ENVIRONMENTAL SCIENCES

Chemistry

Thesis for the degree of Doctor of Philosophy

SELECTIVE OXIDATIONS OF ALCOHOLS AND ALDEHYDES IN A MICROFLUIDIC ELECTROLYSIS CELL

ROBERT AARON GREEN

Electrosynthesis uses electrical current to drive reactions as an alternative to stoichiometric reagents that may be toxic, expensive or create substantial waste. Despite the attraction, electrosynthesis has, however, never become routine procedure in the laboratory. The reasons for the apparent underuse are the perception that specialist knowledge and equipment is often required. The recent advances in microflow technology over the past decade have generated a number of electrosynthetic devices that address the perceived problems. Our own research into electrochemical microflow devices has led to the development of a now commercially available electrochemical flow cell.

To fully advertise the benefits of electrochemical microflow technology synthetically useful reactions need to be developed. The optimisation of such reactions has been the focus of this Ph.D. research. The first reaction investigated was a selective electrochemical 2,2,6,6-tetramethyl-1-piperidinyloxy (TEMPO) mediated oxidation of alcohols to aldehydes and ketones. Cyclic voltammetry techniques were used to investigate the mechanism, and optimise the procedure, with 15 examples tested with excellent conversions and yields achieved in a single pass.

We then turned our attention to the development of procedures for an electrochemical oxidative esterification and amidation mediated by *N*-heterocyclic carbenes (NHCs). The optimisation process was directed by a Design of Experiment (DoE) approach and supported by cyclic voltammetry (CV) experiments. 20 examples of esterification and 23 examples of amidation were demonstrated respectively in excellent yields in a single pass.

Contents

List of Tables

List of Figures

DECLARATION OF AUTHORSHIP

I, Robert Green

declare that the thesis entitled

SELECTIVE OXIDATIONS OF ALCOHOLS AND ALDEHYDES IN A MICROFLUIDIC ELECTROLYSIS CELL

and the work presented in the thesis are both my own, and have been generated by me as the result of my own original research. I confirm that:

- this work was done wholly or mainly while in candidature for a research degree at this University;
- where any part of this thesis has previously been submitted for a degree or any other qualification at this University or any other institution, this has been clearly stated;
- where I have consulted the published work of others, this is always clearly attributed;
- where I have quoted from the work of others, the source is always given. With the exception of such quotations, this thesis is entirely my own work;
- I have acknowledged all main sources of help;
- where the thesis is based on work done by myself jointly with others, I have made clear exactly what was done by others and what I have contributed myself;
- parts of this work have been published as: *ChemSusChem* **2012**, *5*, 326-331 and *Electrochimica Acta*, **2013**, *113*, 550-556.

Signed: ……..

Date:……

Acknowledgements

First I would like to give a deep thank you to my supervisor Richard Brown for giving me the opportunity to work on a new and exciting project. Richard's guidance and wisdom throughout the project has enabled me to make this research a success, and has sparked my interest to keep working within this exciting area.

A lot of the success of this project was due to the insightful teachings of my second supervisor Derek Pletcher, who I owe a huge thank you. Derek's lessons in electrochemistry and how to perform and interpret cyclic voltammetry (to someone who knew very little), has been immensely valuable to this research, and continues to be so.

I would like to thank my industrial supervisor Stuart Leach for his help and guidance throughout my research. In particular Stuart's suggestion of using Design of Experiment software during the optimisation of the esterification and amidation reactions, which was implemented with great success, saving me lots of time. I would also like to thank him and everybody else at GSK for making my time on placement incredibly enjoyable and useful.

A special thanks needs to be given to my friend and colleague Joe Hill-Cousins, for him teaching me how to use the flow chemistry equipment, and the work we did on the optimisation of the electrochemical TEMPO oxidation. Also I would like to thank Joe for the helpful and often perceptive discussions throughout the project and his helpful feedback on my thesis.

I would also like to thank Lynda, Sam, Valerio, Mohammed, Alex Holt, Alex Pop, Rob, Azzam, Gareth, Marco and Alex Leader for making my time during my Ph.D. enjoyable. The many funny conversations (especially Mohammed's crazy stories) and nights out (mostly in the Stags) helped me through the tough times during my research.

Thank you to John Langley and Julie Herniman for their help with the mass spectroscopy analysis and Neil Wells for help with the NMR experiments.

I would also like to say a huge thank you to my parents for always being supportive during my academic studies and always being there when I needed them. Your love and support have always enabled me to reach my goals.

Finally, I would like to thank Becky for all your help and support. Especially when things were not going so well, thank you for putting up with me, you always made it seem brighter. Your love and support throughout my Ph.D. has helped me to succeed and become the person I am today.

Abbreviations

A	Amp
Ac	Acetate
Aq.	Aqueous
Bn	Benzyl
br	Broad
Bu	Butyl
C	Chemical reaction
CV	Cyclic Voltammetry
d	Doublet
DBU	1,8-Diazabicyclo[5.4.0]undec-7-ene
DCC	Dicyclohexylcarbodiimide
DCM	Dichloromethane
DMF	*N,N*-Dimethylformamide
DMS	Dimethyl sulphide
DMSO	Dimethylsulfoxide
E	Electron transfer
EC	Electron transfer followed by chemical reaction
EI	Electron impact
Equiv.	Equivalents
ESI	Electrospray Ionisation
Et	Ethyl
EWG	Electron Withdrawing Group
FFKM	Perfluoroelastomer
FT	Fourier Transform
GC	Gas Chromatography
h	Hour(s)
HFIP	1,1,1,6,6,6-Hexafluoro-propan-2-ol
HOAt	1-Hydroxy-7-azanenzotriazole
HRMS	High Resolution Mass Spectrometry
i	Current
IBX	2-Idoxybenzoic acid
IR	Infrared
j	Current density
J	Coupling constant
LRMS	Low Resolution Mass Spectrometry

ms	Mass spectrometry
m	Multiplet
Me	Methyl
mmol	Millimole(s)
min	Minutes
MW	Molecular Weight
NHC	*N*-Heterocyclic Carbene
NMR	Nuclear Magnetic Resonance
TEMPO	2,2,6,6-Tetramethyl-1-piperidinyloxy
p	Para
PCC	Pyridinium Chlorochromate
PDC	Pyridinium Dichromate
Ph	Phenyl
ppm	Parts Per Million
PVDF	Polyvinylidene fluoride
q	Quartet
rt	Room temperature
RTIL	Room Temperature Ionic Liquid
ð	Chemical shift
sat.	Saturated
SCE	Saturated Calomel Electrode
spt	Septet
sxt	Sextet
sol.	Solution
t	Triplet
^{t}Bu	*Tert*-butyl
Tf	Trifluoromethane sulfonyl
THF	Tetrahydrofuran
TLC	Thin Layered Chromatography

1 Organic Electrochemistry

1.1 Organic Electrosynthesis

1.1.1 Introduction

Chemical transformations involve the transfer of electrons. Whether electrons are lost (oxidations) or gained (reductions) determines the products. Typically, in organic synthesis the addition or removal of electrons is facilitated by oxidants or reductants. Electrodes can be thought of as macromolecules that can accept or provide electrons. In addition the potential can be finely tuned to oxidise or reduce specific functionality within a molecule, therefore increasing selectivity.[1,2] Selectivity is often a problem with harsh chemical oxidants or reductants.

The concept of using electrochemistry to drive chemical transformations has been investigated for a long time, with the foundations laid down by Faraday and Kolbe in the 1800's.[1] Nowadays many procedures are known, of which some examples will be discussed later.

The research discussed within this thesis utilises electrochemistry to drive chemical transformations and investigate the mechanisms by which they occur. Therefore it is important to discuss the underlying concepts of organic electrosynthesis along with examples, to understand the presented research.

1.1.2 Electrosynthesis Concepts

Oxidations and reductions induced by chemical oxidants and reductants differ from electrochemical oxidations and reductions. Typically chemical oxidations and reductions are considered to undergo a series of two-electron reactions with the concomitant transfer of atoms or groups to form a covalent bond.[1,2] For example in the reduction of a ketone with sodium borohydride, two-electrons are transferred to the carbonyl centre by the attack of the hydride, forming a new C–H bond and breaking the π C–O bond. The resultant alkoxide picks up a proton during work-up generating an alcohol (**Scheme 1.1.2.1**).

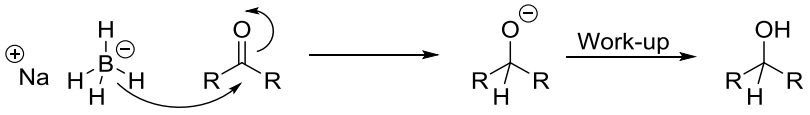

Scheme 1.1.2.1 - Mechanism of ketone reduction by sodium borohydride.

Electrochemical oxidations and reductions are driven by the transfer of single electrons to or from the substrate leading to reactive radical cation or anion intermediates. These species generally undergo chemical reactions followed by a further electron transfer. For example the reduction of aromatic ketones involves an initial single electron transfer, followed by reaction with a proton to give a radical. This then undergoes another electron transfer followed by reaction with a proton to give the alcohol (**Scheme 1.1.2.2**).[1,2]

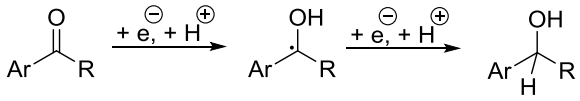

Scheme 1.1.2.2 - Mechanism of electrochemical reduction of aromatic ketones.

To perform electrosynthetic reactions typically two electrodes are placed in a solution, a working electrode and a counter electrode (**Figure 1.1.2.1**). The electrodes are connected to a power supply and charge is passed between the two electrodes, which requires the addition of inert electrolyte to ensure that the charge can pass through the solution.[1,2]

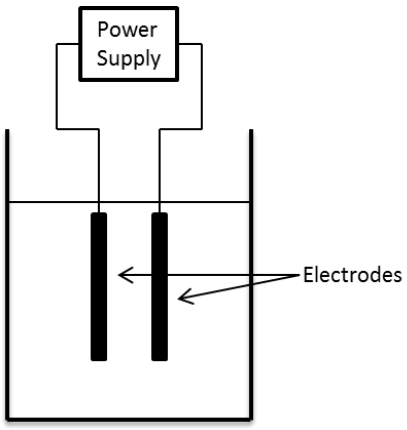

Figure 1.1.2.1 - Electrochemical beaker cell.

At the anode an electron passes from a species in the bulk solution to the electrode, which is an oxidation. At the cathode an electron is passed from the

electrode to a species in the bulk solution, which is a reduction. The transfer of the electron only occurs close to the electrode; therefore the process can be thought to involve three steps:[2]

- Mass transport of material to the electrode
- The electron transfer
- Mass transport of material away from the electrode

The rate of the reaction is determined by the slowest step. The modes of mass transport are diffusion, convection or migration. Diffusion is the physical process of balancing concentration throughout the mixture. As a reaction proceeds, the starting material is consumed, so the concentration at the electrode is reduced. Therefore the starting materials diffuse to the electrode to balance the concentration. The concentration of products increases at the electrode; as a consequence it diffuses out into the bulk solution (**Figure 1.1.2.2**).[2]

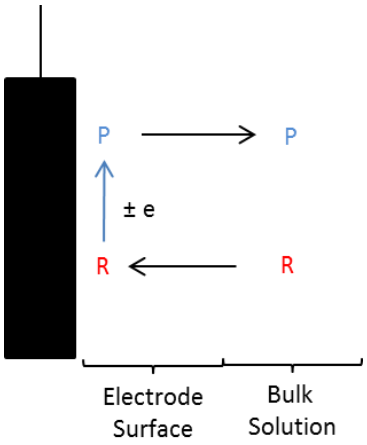

Figure 1.1.2.2 - Diffusion of reactants to electrode surface and products away. Key: Black arrow - direction of diffusion. Blue arrow - electron transfer. R - Reactant. P - Product.

Convection is the movement of species by external mechanical forces, such as stirring the solution with a stirrer bar. Controlling the rate of convection allows for mechanistic and kinetic studies to be conducted. Migration is the movement of charged species in a potential field. Often this mode of transport does not need to be considered for reactant or product, as the excess of electrolyte that is present carries the charge through the solution.[2]

At the working electrode the desired electron transfer occurs. For charge to pass between the electrodes, the counter electrode needs to balance the reaction by providing the opposite electron transfer. Therefore it is important to consider the balanced overall reaction during electrosynthesis. If the reaction is reversible, the reverse of the reaction at the working electrode can balance the reaction. This unproductive process reduces the efficiency of the reaction and can be avoided by performing the electrolysis in a divided or two-compartment cell (**Figure 1.1.2.3**). The two compartments are usually separated by an ion-permeable membrane, so that charge can still be passed across the reaction mixture.[2]

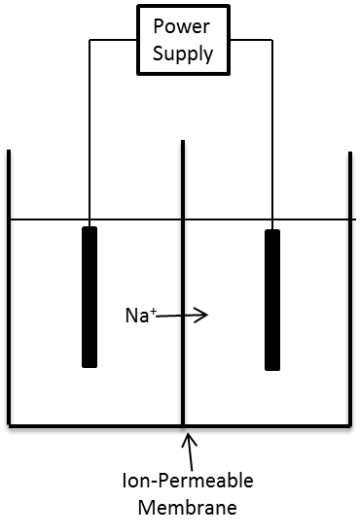

Figure 1.1.2.3 - Electrochemical cell divided with an ion-permeable membrane.

Electrosynthesis allows for greater control of oxidations and reductions, by being able to finely control the applied potential. To drive electrosynthesis an overpotential (η) needs to be applied. If a positive potential is applied to the reaction an anodic current will generally be observed, leading to an oxidation. If the negative potential is applied a cathodic current is normally observed, leading to a reduction.[2]

Electron transfer to the reactive substrate leads to reactive intermediates. These intermediates can be radical ions, anions, cations or radicals, depending on potential applied during the reaction. Higher concentrations of reactive intermediates are formed at the electrode surface and then diffuse into the bulk solution. Due to their reactive nature subsequent reactions occur quickly, usually in a thin layer at the electrode surface, often leading to different

selectivity to that observed in traditional synthesis. When describing these reaction mechanisms E is used to denote the electron transfer and C is used to portray further chemical reaction. Therefore a mechanism that starts with an electron transfer followed by subsequent chemical reaction is known as an EC mechanism.[2]

1.1.3 Examples of Organic Electrosynthesis

There is extensive literature describing the use of electrochemistry in organic synthesis. In this section a few examples are presented to illustrate the power of electrosynthesis in organic chemistry.

One of the oldest and well-known reactions is the Kolbe electrolysis, which was first reported in 1849. The reaction converts carboxylic acids under partially neutralised conditions, usually with a platinum electrode, *via* a one-electron oxidation, to give a radical and CO_2. Therefore it can be considered an electrochemical decarboxylation. The formed radical can then go on to self-condense, cross-couple, abstract a hydrogen atom or add to an olefin, which can lead to a mixture of products (**Scheme 1.1.3.1**).[1] This is an example of an ECC mechanism.

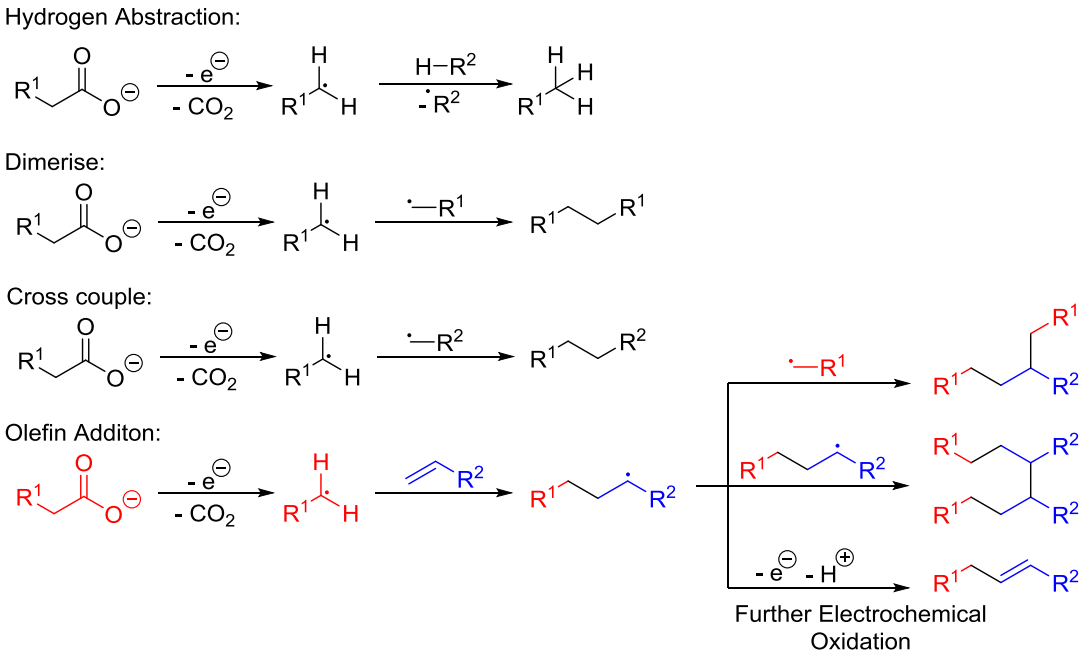

Scheme 1.1.3.1 - Examples of Kolbe electrolysis reactions.

Careful selection of the conditions dictates the outcome of the Kolbe reaction, although mixtures are observed in cross coupling examples. Typically partially neutralised conditions are employed in an undivided cell. Control of the conditions is important as under acidic environments a two-electron oxidation to the carbenium ion dominates, albeit this reaction has been used to synthesise other useful products such as ethers (**Scheme 1.1.3.2**).[1]

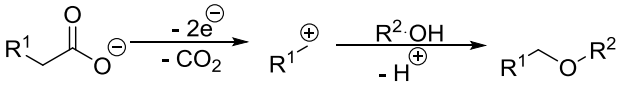

Scheme 1.1.3.2 - Carbenium ion formation and ether formation.

The importance of the reaction is demonstrated by its use on an industrial scale, in the synthesis of sebacic acid (**1.01**) (**Scheme 1.1.3.3**). The acid **1.02** is dimerised to ester **1.03**, which is then hydrolysed to sebacic acid (**1.01**). Sebacic acid is applied as an additive in plasticizers and cosmetics, as well as other industries and is synthesised on a multi-tonne scale.[1]

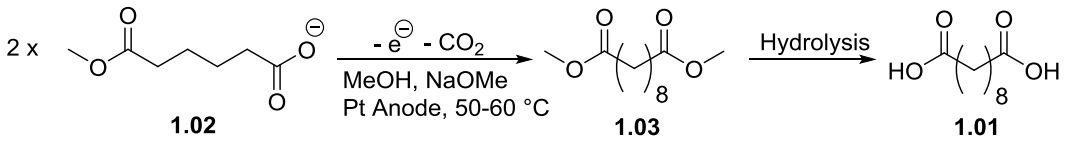

Scheme 1.1.3.3 - Synthesis of Sebacic acid (**1.01**) by Kolbe electrolysis.

Another interesting example of Kolbe electrolysis, involves the formation of a trifluoromethyl radical ($CF_3^{\cdot}$, **1.04**) from trifluoroacetic acid (**1.05**). The radical can then add to olefins and arenes, which is a mild and economical way of adding a CF_3 functional group (**Scheme 1.1.3.4**).[1] This is important particularly to the pharmaceutical industry, where the CF_3 group is found in many drugs and pre-clinical drug candidates.[3,4]

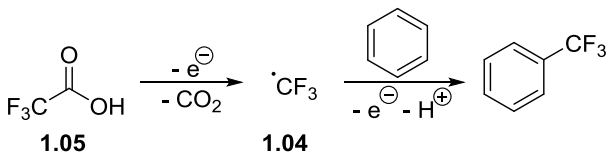

Scheme 1.1.3.4 - Trifluoromethyl addition via Kolbe electrolysis.

Selective fluorination is also another important reaction for the pharmaceutical and fine chemicals industries. This is because the C–F bond is often inert to

bio-degradation pathways, meaning the selective insertion can prolong the half-life of drug candidates.[4-6] Fluorination can also confer specific properties in materials and polymers, must notably the polymers used within fuel cells, such as Nafion.[7] Typically chemoselective fluorination methods require toxic or expensive reagents such as F_2, $FClO_3$, CF_3OF, XeF_2, Et_2NSF_3 (DAST), *N*-fluoropyridinium salts and *N*-fluorotriethylenediamine derivatives (selectfluor).[1] Whereas electrochemical fluorination has been shown to provide a relatively mild alternative approach.[1,8]

Salts such as $Et_3N \cdot HF$ and $Et_3NF \cdot 3HF$ are employed, to act as electrolytes and fluoride source.[1,8] The mechanism is expected to be an ECEC process, where an initial radical cation is formed, followed by loss of a proton and a second electron transfer, and finally attack by a fluoride ion (**Scheme 1.1.3.5**). A dry aprotic solvent is usually employed, and undivided cells can be used.[1]

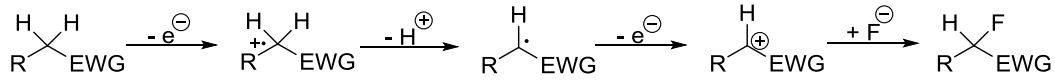

Scheme 1.1.3.5 - Mechanism of electrochemical fluorination.

There is now a vast array of examples of selective fluorination on a range of molecules. This includes substrates containing aromatic, carbonyl and sulfide moieties (**Scheme 1.1.3.6**).[1,8]

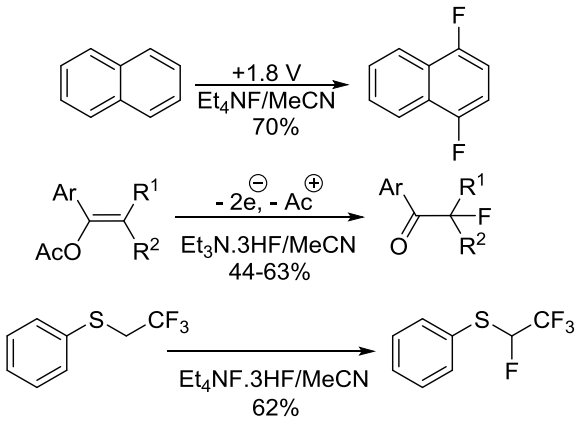

Scheme 1.1.3.6 - Examples of selective electrochemical fluorinations.

Electrosynthesis provides an alternative tool for synthetic chemists, as shown in the examples discussed. The major advantage of using electrochemistry to drive chemical transformations is the removal of the need to use toxic and

often expensive oxidants or reductants. Therefore electrosynthesis can be classified as a sustainable technology. Often electrosynthesis allows for alternative reactive species to be generated, such as radical cations and anions which are not readily accessible with traditional reagents. Therefore novel products can frequently be achieved. Despite these benefits, electrosynthesis is not widely used by organic chemists, due to the perception that specialist knowledge and equipment is required. To combat the underuse, new technologies such as flow chemistry are being combined with electrochemistry, to allow electrosynthesis to be accessible to more synthetic chemists.

1.2 Microfluidic Organic Electrosynthesis

1.2.1 Introduction

In recent years there has been a lot of interest in using flow chemistry as a tool in organic synthesis. Flow chemistry differs from traditional synthetic methods by flowing reagents in solution through devices that facilitate rapid mixing and heating (**Figure 1.2.1.1**). At any one point only a small amount of reactive materials mix, reducing risks of runaway reactions. The improved safety along with the easy scalability, by running the reaction for longer, makes flow chemistry an attractive option for organic chemists.[9-15]

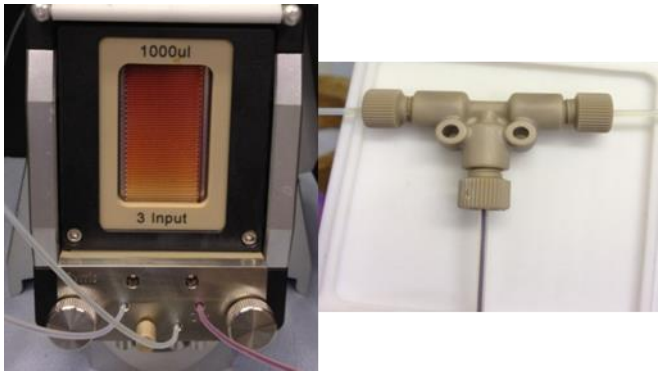

Figure 1.2.1.1 - Examples of microflow reactors.

As previously discussed electrosynthesis is a powerful tool for organic chemists, but has largely been underused. The reason for this is often long reaction times are needed for high conversions, difficulty in scaling-up the reaction and the excess of electrolyte often required. Combining electrosynthesis and microflow technology provides an opportunity to develop electrochemistry into a more user convenient format. The small inter-electrode gaps that can be generated in electrochemical microflow devices can reduce reaction times by lowering the distance of mass transfer to the electrode surface. This small gap, can also lead to lower amounts of electrolyte being required, or in some devices completely removing the need for added electrolyte altogether. Furthermore, the reactions can achieve high conversions in a single pass and be scaled-up by simply increasing the length of time the reaction is run for. A useful addition is the ability for in-line analysis and purification which can be incorporated, leading to automated systems.

In this section examples of reactions performed in electrochemical microflow cells will be presented. Also the different types of devices will be discussed, along with their advantages and disadvantages. Finally the development of novel microfluidic electrolysis devices used within this research will be discussed.

1.2.2 Electrochemical Microflow Reactors

There are now many examples in the literature of electrochemical flow cells for organic synthesis applications. Parallel plate reactors are the most common cell designs in electrochemical technology. However, high conversion is only achieved by recycling the reactant solution many times through the cell and a reservoir. In microflow systems the target is a high conversion in a single pass. In all microflow designs the size of the inter-electrode gap has been minimalized, generally achieved by using a spacer or gasket. In some cases the inter-electrode gap has been reduced so that no electrolyte is required.[16-21] This is accomplished by reducing the inter-electrode gap to an extent where the diffusion layers at the two electrodes overlap.[22,23] Therefore the cations and anions produced from the working and counter electrodes are enough to act as electrolyte in the reaction.

One of the simplest designs is to have a single rectangular channel passing between two electrodes clamped together (**Figure 1.2.2.1**). To create the channel a rectangle is cut into adhesive tape which is used as a spacer between the two electrodes. Inter-electrode gaps have been reported between 80-320 μm thick and a variety of materials have been used as the electrodes.[24] Path-lengths for these devices are usually in the order of 30 mm.[16-21,24-27] A similar cell with a longer path-length of 100 mm, comprised of ten 10 mm working electrodes, has also been reported.[28,29]

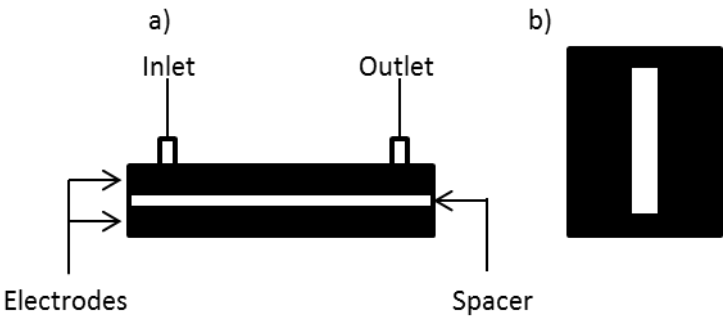

Figure 1.2.2.1 - Diagram of a parallel plate reactor. a) Electrode arrangement separated by a spacer. b) Channel created by spacer.

A variation on parallel plate reactor design is to machine multiple microchannels into the electrodes, providing a path for the reaction mixtures to flow through (**Figure 1.2.2.2**). The electrodes were again separated by a spacer or a gasket, with the inter-electrode gap around 100 μm.[30-33] To ensure good distribution between the channels an angled path entering and exiting the cell was shown to be beneficial.[30]

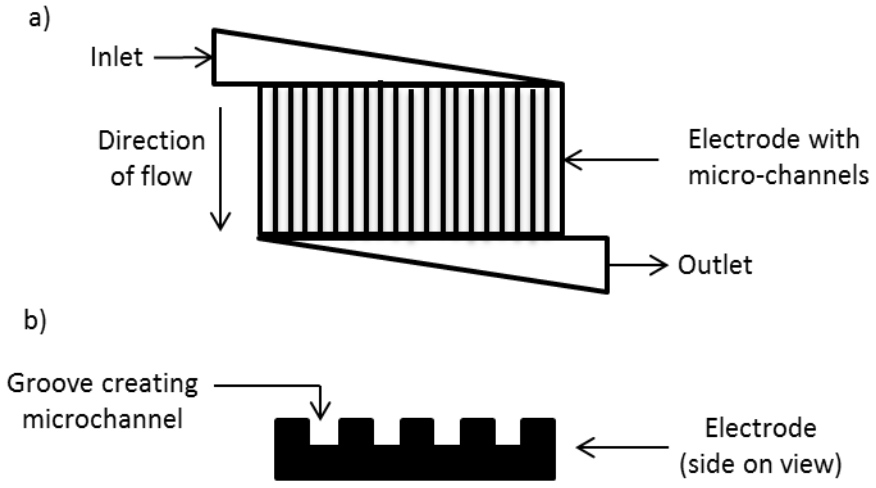

Figure 1.2.2.2 - a) Electrochemical microflow cell with machined channels. b) Side view of electrode with microchannels

Often the counter electrode reactions produce gas which causes bubbles, which can reduce the residence time in the cell lowering the conversion.[27,28,31,32] Therefore it is often beneficial to perform reactions under back-pressure, to supress bubble formation. A micro-channel cell capable of withstanding 20 bar has been fabricated. The design used a floating electrode arrangement, to double the path-length (**Figure 1.2.2.3**).[31] This was created by sandwiching a

glassy carbon electrode between two micro-channelled counter electrodes, separated by two gaskets. The floating electrode allows charge to pass through it; therefore it can act as both an anode and cathode on the two surfaces.

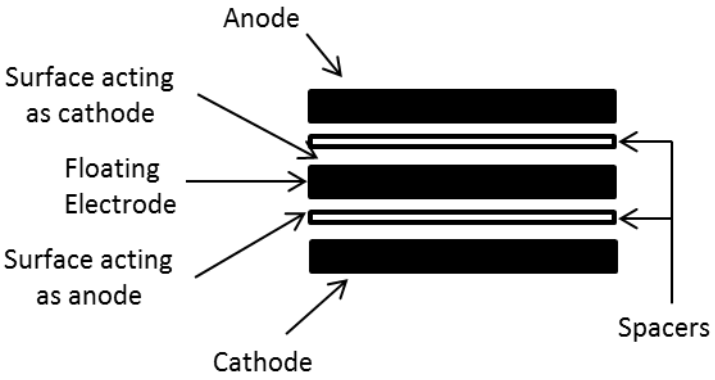

Figure 1.2.2.3 - Floating electrode arrangement.

An alternative approach using carbon felt electrodes and a porous spacer has also been reported (**Figure 1.2.2.4**).[34] Carbon felt electrodes allow for a very high surface area between the reaction mixture and electrodes to be achieved. The porous spacer (pore size 3 μm) permits the reaction mixture to pass between the anodic and cathodic chambers, whilst keeping the inter-electrode gap around 75 μm.

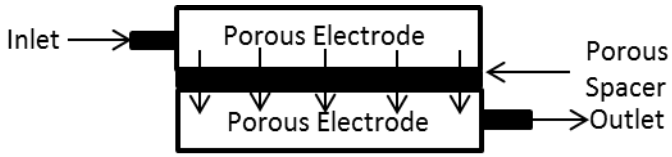

Figure 1.2.2.4 -Electrochemical microflow cell with porous spacer.

The final type of reactor utilises multiple floating electrodes, which create channels for the reaction mixture to flow between (**Figure 1.2.2.5**).[35-37] The frame of the reactor kept the inter-electrode gap constant at 100 μm.[35,37] The distribution between channels was irregular in this cell design, leading to a poorer performance than the single channel examples. Although it was anticipated that when scaling up this reactor, the multiple electrode channels would be advantageous.[35,37]

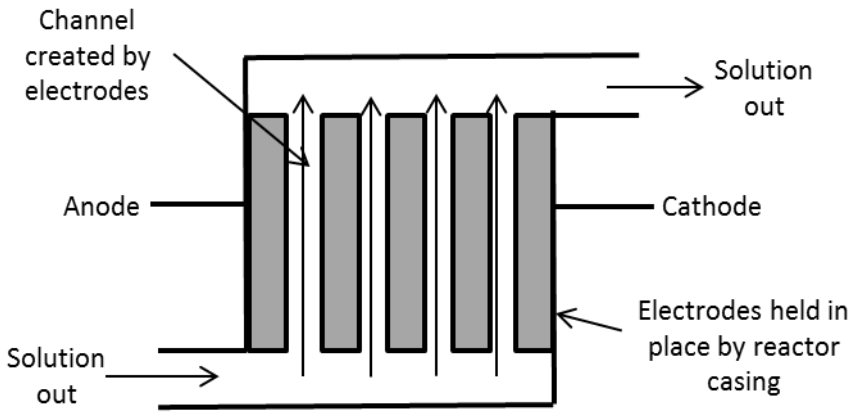

Figure 1.2.2.5 - Electrochemical microflow cell with channel created by multiple electrodes.

Flow rates for these electrochemical microflow cells vary from < 0.1 mL min^{-1} to 10 mL min^{-1}. The amount of products produced in these short path length cell is usually in the region of 10 mg h^{-1}, although placing multiple devices in parallel can improve this.[17] A high conversion in a single pass necessitates a much longer channel. Most of the cells suffer from reduced performance when bubbles are generated; therefore pressurised systems are usually required.[31,33]

1.2.3 Organic Electrochemical Microflow Synthesis

As electrochemical microfluidic cells become more readily available, the number of reported synthetic procedures increases. Over the past decade many reactions have been reported. Some of these are discussed in this section.

The most reported reaction is the methoxylation of 4-methoxytoluene (**1.06**), because this is often the reaction used to characterise the performance of different electrochemical microflow cells (**Scheme 1.2.3.1**).[28,29,31,33-35]

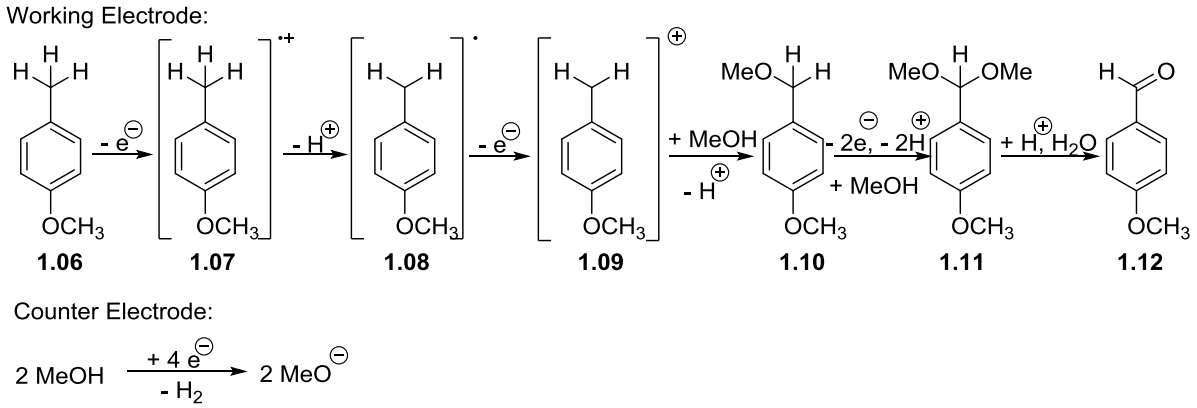

Scheme 1.2.3.1 - Electrochemical methoxylation of **1.06** to synthesise acetal **1.11** or aldehyde **1.12**.

The reaction has been conducted in a variety of cells, at different flow rates and inter-electrolyte gaps and without the addition of electrolyte.[34] Furthermore the methoxylation reaction has been carried out on an industrial scale using a cell with a series of narrowly spaced carbon discs 1 m in diameter. The reaction begins with the anodic electron transfer from **1.06** to give the radical cation **1.07**, which loses a proton to give the more stable benzyl radical **1.08**. A second electron transfer occurs giving the cation **1.09**, which then reacts with methanol to give mono-methoxylated product **1.10** after the loss of a proton. This process of electron transfer, proton loss and reaction with methanol is then repeated to generate the dimethylacetal **1.11**. The mechanism can be described as two ECEC steps. Some groups have reported the selective formation of 4-methoxybenzaldehyde (**1.12**) in the presence of aqueous acid, through hydrolysis of the acetal group.[28] The counter electrode reaction is the reduction of methanol to form H_2 and methoxide, which then reacts with the proton formed at the anode to balance the cell pH. To counter the formation of H_2 bubbles in the cell, and consequent increase of the resistance between the electrodes, back pressure is often required for good yields.

An alternative reaction that has been used to characterise single channelled electrochemical microflow cells, is the methoxylation of furan (**1.13**) to give the 2,5-dimethoxylated 2,5-dihydrofuran **1.14** (**Scheme 1.2.3.2**). The cells used to perform this reaction had inter-electrode spaces <100 μm allowing the removal of electrolyte from the reaction mixture. Good yields were achieved in a single pass.[20,27]

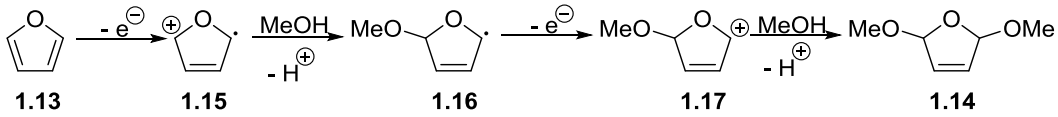

Scheme 1.2.3.2 - Electrochemical methoxylation of furan (**1.13**).

The reaction follows an ECEC mechanism, with the first electron transfer giving the radical cation **1.15**. The radical cation then reacts with methanol, to give the radical **1.16**, after the loss of a proton. Another electron transfer follows to give the cation **1.17**, which reacts with another equivalent of methanol to give the dimethoxylated product **1.14**. Methoxide is formed by the reduction of the methanol solvent at the counter electrode, balancing the overall pH of the reaction.

Yoshida showed that at low temperatures iminium ions could be generated from pyrrolidine **1.18**, in an electrochemical microflow cell, using a carbon felt electrode in the presence of electrolyte (tetrabutylammonium tetrafluoroborate).[38] The anodic and cathodic compartments were separated by a PTFE membrane. The reaction mixture was flowed through the anode chamber in DCM at -78 °C, where a two-electron transfer followed by loss of a proton occurs to generate the iminium ions. The reaction mixture was then treated with an excess of nucleophile to form a range of C-C bonded products, with conversions between 49-69% (**Scheme 1.2.3.3**.). To balance the electrochemistry a solution of trifluoromethanesulfonic acid (TfOH) was reduced generating H_2 in the cathode compartment, using a platinum wire electrode with added electrolyte. The reaction was monitored online using FTIR. A significant shift in the carbonyl stretch was observed when pyrrolidine **1.18** was oxidised to the iminium ion. The size of the observed transmittance was related to the amount of imminium present, which was controlled by the current used during the reaction, allowing the reaction to be monitored.

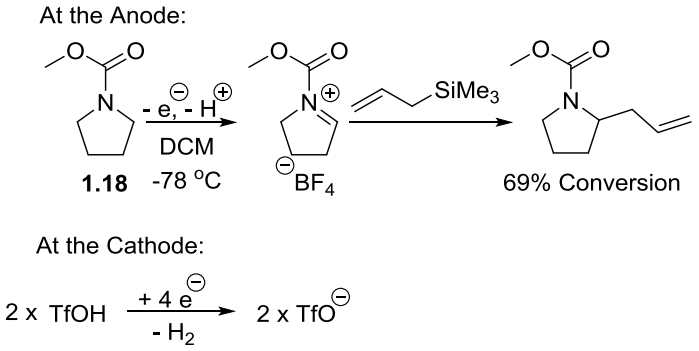

Scheme 1.2.3.3 - Electrochemical generation of iminium ions.

Further examples of carbon-carbon bond forming reactions have been demonstrated utilising the reductive couplings of benzylbromides (**1.19**). Initially dimerization products **1.20** were reported, but this was soon extended to include coupling with excess acetic anhydride and olefins to give **1.21** and **1.22** respectively (**Scheme 1.2.3.4**).[17,19,21]

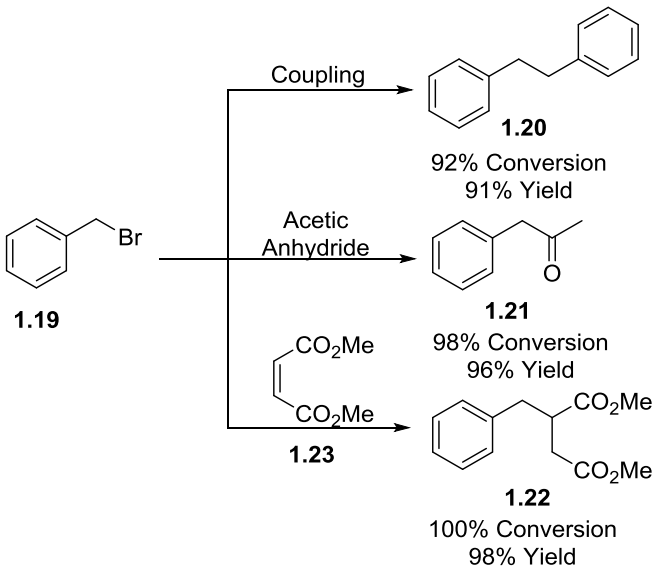

Scheme 1.2.3.4 - Electrochemical reductive C-C bond forming reactions.

Reactions were performed in a single channelled electrochemical microflow cell, without the addition of electrolyte. Excellent conversions and yields were achieved (> 95%), with flow rates at ~10 μL min^{-1} and 5 mM solutions of benzyl bromide.[17,19,21] Scaled-up versions of the reaction were achieved by using four cells in parallel, which gave a four-fold increase in the production of products.[17] An ECE mechanism is followed starting with cathodic reduction of the electron-poor olefin **1.23** to give a radical anion **1.24**. The radical anion reacts with the

benzylbromide (**1.19**), which loses a bromide ion, to give the radical **1.25**. Further cathodic electron transfer followed by protonation generates the product **1.22** (**Scheme 1.2.3.5**).[19]

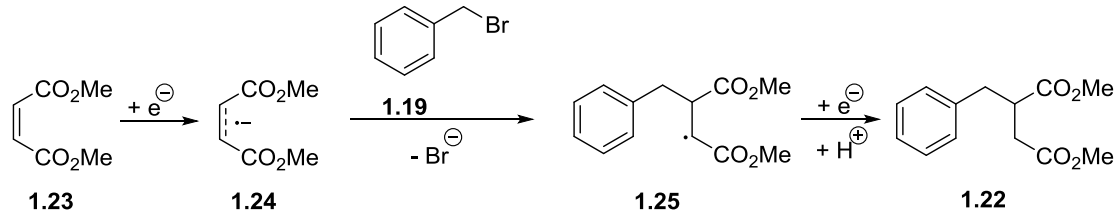

Scheme 1.2.3.5 - Mechanism of formation of **1.22** by electrochemical reductive coupling.

The formation of carbon-sulfur bonds has also been demonstrated. The process involves the electrochemical oxidation of catechols (**1.26**) under basic conditions to give the quinone **1.27**, which is followed by reaction with a benzenethiol to generate the product **1.28** (**Scheme 1.2.3.6**).[25,26]

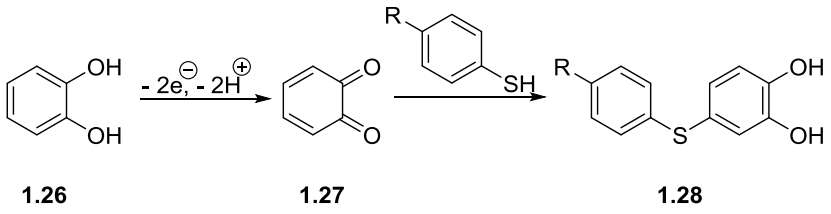

Scheme 1.2.3.6 - Electrochemical oxidations of catechols.

The procedure utilises a single channel electrochemical microflow cell, with an inter-electrode gap of 80 μm. Additional electrolyte is added, with flow rate of 0.1 mL min^{-1}, giving approximately 14 mg h^{-1} of product. The reaction was compared in batch and flow, showing an increase from 13% to 88% yield when the reaction was perform under flow conditions. The counter electrode reaction is the formation of H_2 from the electrochemical reduction of the protons generated from the oxidation of the catechol **1.26**.[25,26]

Furthermore diaryliodinium salts **1.29** have also been synthesised in an electrochemical microflow cell. This is achieved by electrochemically oxidising iodoarenes **1.30** and coupling with another arene to give **1.29** (**Scheme 1.2.3.7**).[27]

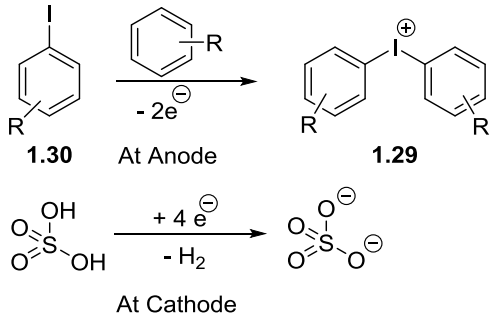

Scheme 1.2.3.7 - Electrochemical formation of the idonium salt **1.29**.

The reaction is performed in a single channelled cell, at a flow rate of 80 μL min^{-1}, which provides a residence time of 17 seconds. Yields up to 72% were achieved in a single pass. An ECE mechanism is followed, where an electron transfer from **1.30** to give a radical cation is followed by the coupling to another arene. The radical cation then undergoes another anodic electron transfer, with loss of a proton to give the product **1.29** (**Scheme 1.2.3.8**). The reaction is conducted in an acetonitrile, acetic anhydride and sulfuric acid mixture, which improved the selectivity of the reaction. The sulfuric acid is reduced at the cathode, generating H_2 and producing a counter-ion for the product.[27]

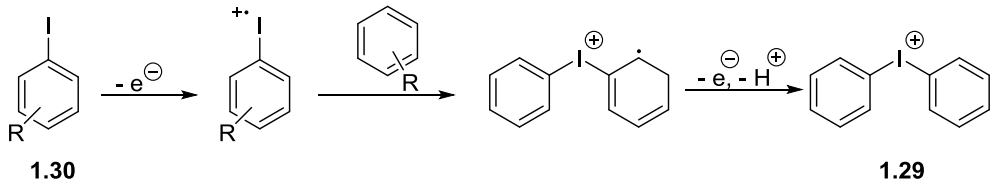

Scheme 1.2.3.8 - Mechanism of the electrochemical formation of idonium salt **1.29**.

In this section a selection of example reactions performed in electrochemical microflow cells have been presented. Examples of both oxidations and reductions have been reported leading to an array of interesting compounds. However, most of the procedures shown are only capable of producing milligrams of material per hour, although in principal this can be improved by running cells in parallel.[17] Some of the early electrochemical reactor designs attempted to minimise the inter-electrode gap, in order to remove or greatly reduce the electrolyte. Although, this was achieved at the expense of flow rate, impacting the practicality of these devices to synthetic chemists. Therefore

many of the reported procedures still use additional electrolyte, though at lower loadings than that required for batch electrosynthesis. As demonstrated in this section microfluidic electrosynthesis has the potential to be a helpful tool to synthetic chemists. As the interest grows more interesting methodologies will continue to be developed, leading to a wider up-take of this technology.

1.2.4 Development of an Electrochemical Microflow Reactor

The majority of the electrochemical microflow devices described to date consist of a straight channel flowing through two parallel electrodes. The rather short channel length limited high conversions to very slow flow rates, which reduces the rate of product formation. Many conventional microflow reactors used in organic synthesis comprise of a convoluted channel design to extend the path-length, and enhance mixing. It was thought that combining a convoluted channel design between two parallel electrodes would be advantageous. Therefore a research project was initiated in our laboratory to construct such a cell.

In 2011 Kuleshova *et al.*[39] reported the first microfluidic electrochemical cell with a convoluted parallel plate design (**Figure 1.2.4.1**). An inert spacer/gasket is used to create a path, between the two parallel electrodes.[39] In this case a star-shaped channel design path was created in Viton, which gave a path-length of 600 mm and inter-electrode gap of 500 μm. To ensure that a constant pressure was applied across the cell to prevent leakage, eleven evenly spaced sealing bolts, tightened to a constant torque, were used to clamp the cell together. The electrode materials were a carbon PVDF composite (anode) and stainless steel (cathode).[39] These materials were selected for their applicability in a wide range of electrochemical transformations, ease of machining and cost.

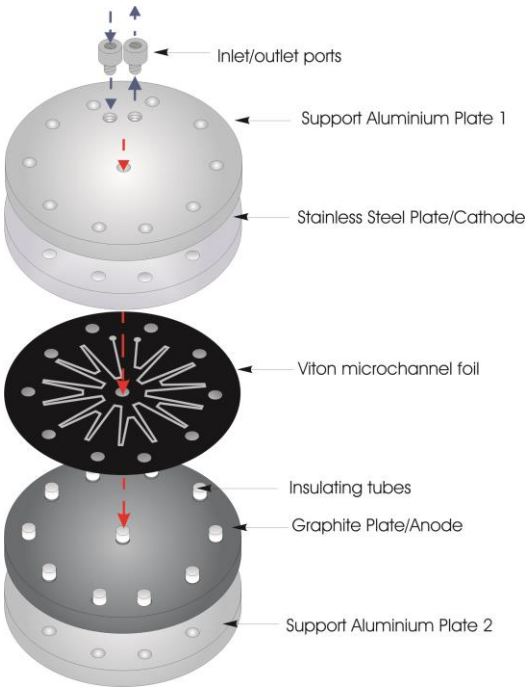

Figure 1.2.4.1 - Diagram of the Southampton prototype electrochemical microflow cell.[39]

The home-made prototype cell was then characterised using the methoxylation of *N*-formylpyrrolidine (**1.31**) to give **1.32** (**Scheme 1.2.4.1**). This is an excellent example of electrosynthesis, following an ECEC mechanism. At the anode pyrrolidine **1.31** undergoes a two-electron oxidation with concomitant proton loss to yield the iminium ion intermediate **1.33**. The iminium ion reacts with the solvent methanol, followed by the loss of a proton to give the methoxylated product **1.32**. On the counter electrode methanol is reduced to give methoxide and H_2, to balance the pH of the reaction. Excellent conversions (>95%) were achieved, in a single pass at 0.1 mL min^{-1} at 70 mA, which equated to a production of 78 mg h^{-1} of **1.32**. Remarkably, when the reaction was conducted at increased flow rate (3.5 mL min^{-1}) and current (400 mA) the methoxylated product **1.32** was produced selectively at a rate of 945 mg h^{-1}, although the conversion dropped to 33%.[39]

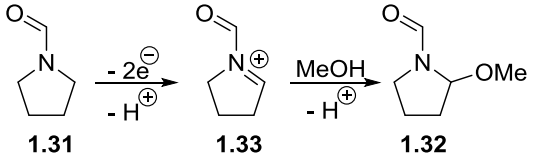

Scheme 1.2.4.1 - Electrochemical methoxylation of pyrrolidine **1.31**.

To promote the uptake of flow electrosynthesis by organic chemists, it was considered that further miniaturisation and compatibility with other microflow equipment was required. Therefore a collaboration with Syrris Ltd. was initiated and a new cell was developed as a 'plug and play' addition to their existing flow chemistry systems. The key requirements for this commercialised cell were that high conversions in a single pass should be achieved with a good rate of product formation. It was also considered that the addition of temperature monitoring would be a feature that users of the cell would find desirable. This led to the development of the electrochemical microflow cell shown in **Figure 1.2.4.2**.[40]

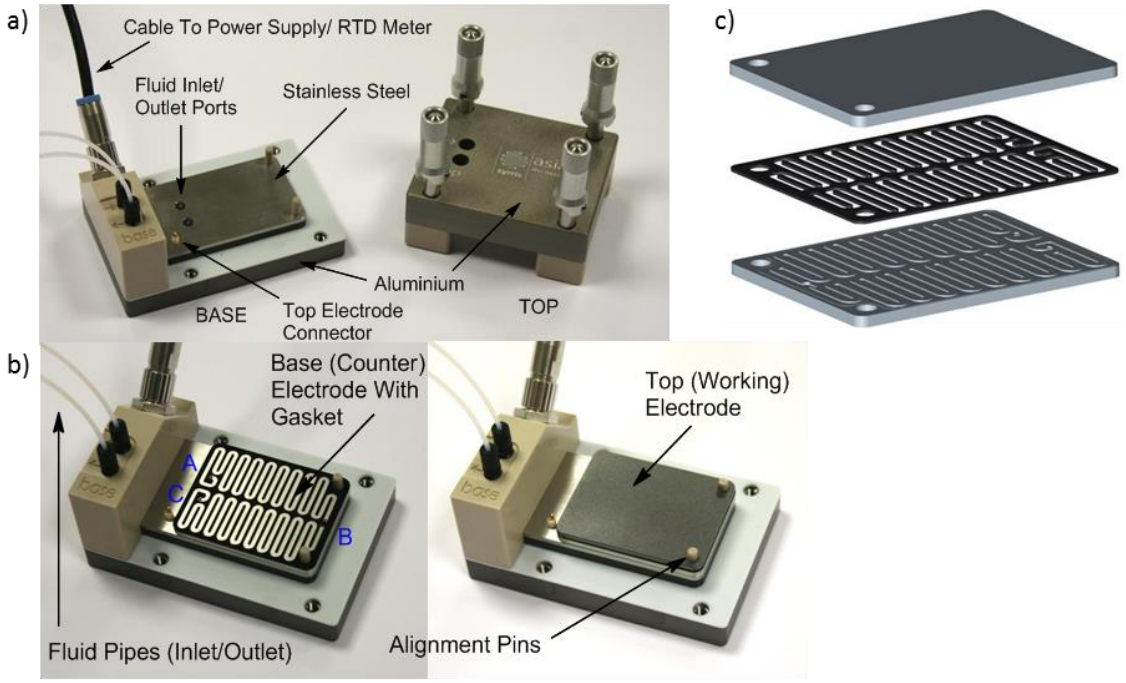

Figure 1.2.4.2 - The electrochemical microflow cell developed in collaboration with Syrris Ltd. a) Cell holder. b) Cell holder fitted with recessed electrode and gasket, then carbon electrode. c) Arrangement of electrodes and gasket/spacer.

The cell was constructed from two rectangular electrode plates (53 mm x 40 mm x 2 mm). The working electrode is a carbon PVDF blend, and the counter electrode is stainless steel. The counter electrode has a 250 μm recessed channel cut into it. Into the channel fits an FFKM gasket (500 μm thick), which creates the snaking channel of 700 mm long. The path length can be extended by employing a double stacked 'floating electrode' arrangement. When the two

electrodes are compressed with the cell holder, the inter-electrode gap is ~200 μm giving a total volume of ~0.21 cm^3, and a working electrode surface area of 1050 mm^2. The cell holder is designed to allow rapid heating or cooling of the cell.[40]

The electrochemical properties of the cell were then characterised using the methoxylation of *N*-formylpyrrolidine (**1.31**) as the test reaction. Again excellent conversions (>95%) were achieved in a single pass and the double stacked arrangements (with a floating electrode), generating 1.8 and 2.3 g h^{-1} of product respectively at 3.0 mL min^{-1} and 800 mA. When this cell was compared to the Southampton prototype and other cells within the literature, a vast improvement in the rate of product formation has been achieved, although electrolyte has been added, which needs to be removed on work-up. Furthermore these reactions are not conducted with back pressure regulation so there is significant bubble production. The formation of bubbles does not reduce cell performance, and may actually aid the mass transport in the cell as well as mixing.[40] The cell developed in conjunction with Syrris Ltd. was used to develop the reactions discussed within this thesis and a modified version is now commercially available.

1.3 Cyclic Voltammetry

Cyclic voltammetry is an experimental technique that allows electrochemical reactions to be quickly investigated. Throughout this research cyclic voltammetry has been used to assist reaction development, through increased understanding of the electrochemistry. Qualitative and quantitative information can be obtained within a few seconds, and that information directly applied to instruct the next experiments. The speed and ease of experimentation makes cyclic voltammetry the method of choice to investigate electrochemical reactions.[1,2]

1.3.1 Experimental Set-up

In the cyclic voltammetry experiment, the potential is swept through a potential range of interest, and then swept back to the starting potential. At the potential where an electrochemical reaction occurs, a response is observed which is an increase in the current (*i*) or current density (*j*). Current density is the current divided by the electrode surface area.

Differences in the peak shape are related to whether the electron transfer is reversible or irreversible and if any chemical steps are involved.[2] This subject will be discussed in more detail later. Further mechanistic and kinetic information can be obtained, by changing the scan rate, the number of scans, and the potential ranges used. Also changing the concentration, temperature and pH of the solution of interest can bring useful insights into the reaction under study.[2]

The dominant mode of mass transfer during a cyclic voltammetry experiment is diffusion. Whether the diffusion is the rate limiting step during the reaction under investigation can be determined from the shape of the observed voltammograms. **Figure 1.3.1.1** shows how a typical cyclic voltammetry experiment is set-up. A three electrode system is most often employed, which is controlled by a potentiostat. The observed current response is measured at the working electrode, which acts as anode or cathode, depending on the potential being applied. A counter-electrode is present to balance the overall electrochemistry, and allow current to flow. Finally a reference electrode is

used to measure the potential against, and it is important to define the type of reference electrode used.[2]

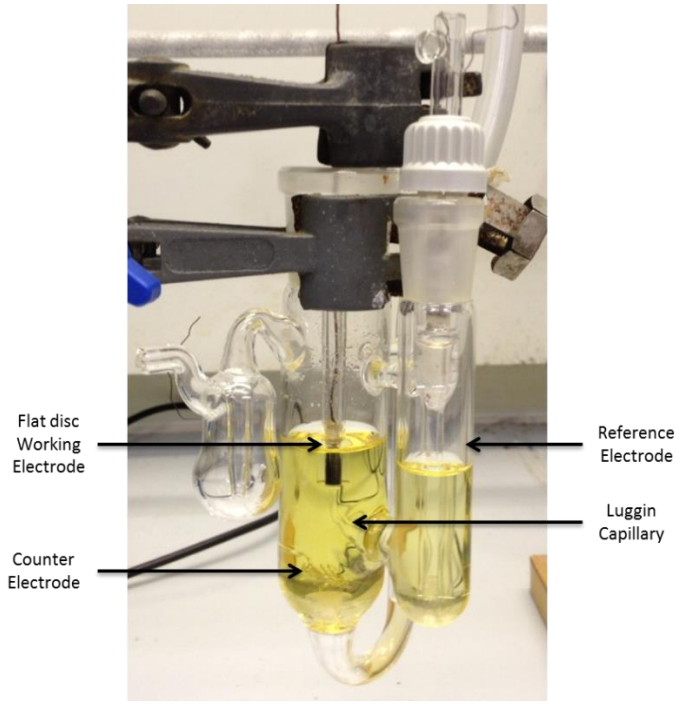

Figure 1.3.1.1 - Experimental set-up to perform CV experiments.

In the experimental cell shown in **Figure 1.3.1.1**, the working and counter electrode are in close proximity to each other to make sure good consistent data is achieved. The reference electrode is also held in close proximity due to the luggin capillary. The working electrode needs to be held close to the luggin capillary to achieve good data by reducing the experimental IR drop. IR drop is the resistance in the cell, affecting the observed current, which is minimalized in the set-up shown. Often an excess of electrolyte is added to allow current to pass across the cell, so a response can be observed.[2]

The working electrode is often a flat disc electrode, made of platinum, gold or glassy carbon. The surface should be regularly polished between experiments, to reduce the build-up of impurities on the electrode surface that can affect the results. The counter-electrode is usually a platinum wire, with a high surface area. High purity solvents should be used to achieve the best results. They should also be degassed, as dissolved oxygen within the solvent can affect the results.[1,2] This is because O_2 is electroactive, meaning that at the correct potential a response can be observed, obscuring other important information.

1.3.2 Interpreting Results from Cyclic Voltammograms

The simplest scenario to interpret is a reversible one-electron transfer reaction. A typical response for this is shown in **Figure 1.3.2.1**. As the potential is swept forward (towards a more positive potential) eventually a point is reached that drives the transfer of an electron which causes a response that is observed through an increase in current density (*j*). At all potentials above this point the electron transfer is occurring. The highest point (E^{a}_{p}) is observed when all the electroactive material at the surface is consumed, and therefore mass transport is at the highest rate. This is the oxidation potential for that species. At higher potentials the current begins to decrease, giving the characteristic peak shape. The observed decrease in current is due to an increase in the thickness of the diffusion layer at the electrode surface. The increase in the thickness reduces the current as it lowers the concentration gradient of the electroactive species between the bulk solution and the electrode surface, which drives the mass transport of the material to the electrode. When the upper limit of the potential scan is reached, the scanning direction is reversed (to a more negative potential). When the potential sweep reaches the point where the reverse electron transfer occurs, a cathodic current response is recorded giving the observed reverse peak. The same principals discussed in the forward scan also apply to the reverse scan, where E^{c}_{p} is the reduction potential. $E^{a}_{p/2}$ is the potential at half the oxidation peak, and is the value for the redox potential of the species.[1,2]

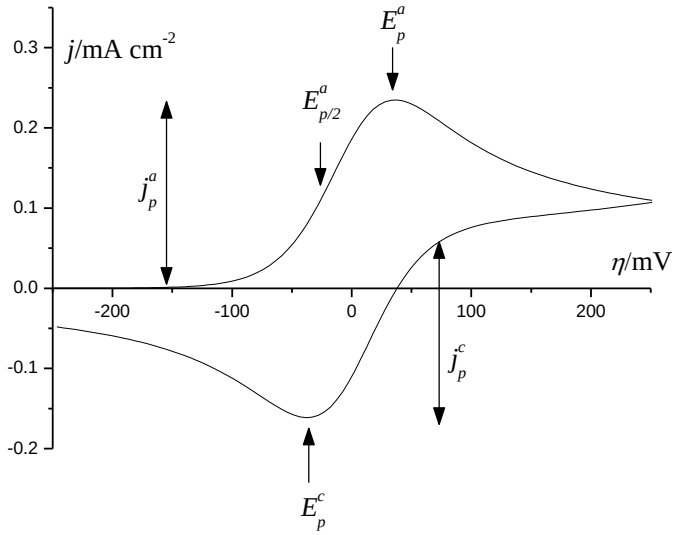

Figure 1.3.2.1 - Typical CV for a reversible one-electron transfer.

The response shown in **Figure 1.3.2.2** compares an electrochemically reversible electron transfer CV (curve a) with an irreversible CV (curve b). In a reversible scenario the separation between the two peaks is <59 mV. Whereas in the irreversible case the separation of the peaks has become more drawn out and is now greater than 59 mV in a one-electron process.[1,2]

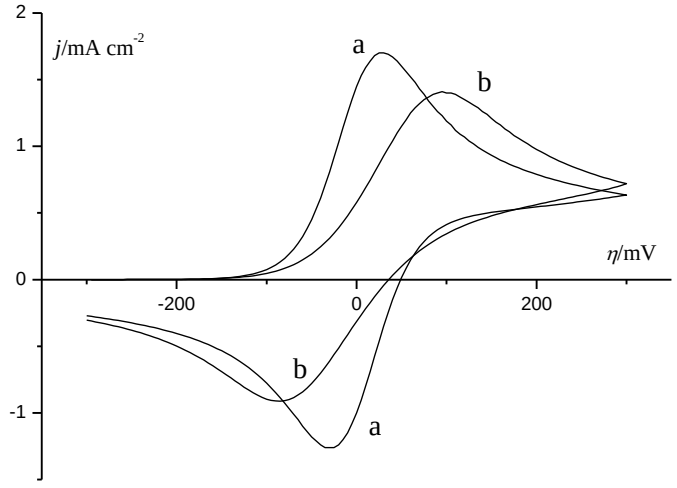

Figure 1.3.2.2 – Comparison between an electrochemically reversible electron transfer (a) and irreversible electron transfer (b) cyclic voltammogram.

Further differences between electrochemical reversible and irreversible electron transfers can be observed when the scan rate is varied (**Figure 1.3.2.3**). In the electrochemically reversible example the peaks become larger and are proportional to the square root of the scan rate. The increase is due to rapid changes in the reactant concentration at the surface of the electrode. Therefore less diffusion can occur on the timescale of the potential sweep as the sweep rate is increased, causing a larger flux of material. The amount of flux to the electrode surface is related to the size of the observed response. When increasing the scan rate for an irreversible electron transfer, the peaks become more drawn out. This provides another opportunity to differentiate between reversible and irreversible electron transfer processes.[1,2]

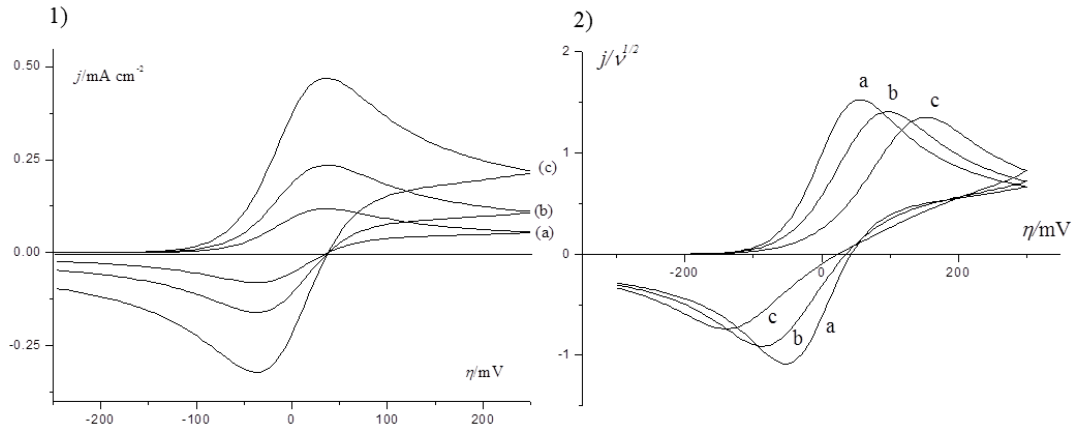

Figure 1.3.2.3 - Comparison of the effect of increasing scan rate on electrochemically reversible (1) and irreversible (2) electron transfers. a-c: increasing scan rate.

Cyclic voltammetry can also be used to investigate more complex reactions that involve electron transfers and chemical steps. When considering an EC reaction, where the chemical step has a short half-life compared to the scan rate, a voltammogram such as the one shown in **Figure 1.3.2.4** will be observed.[1,2]

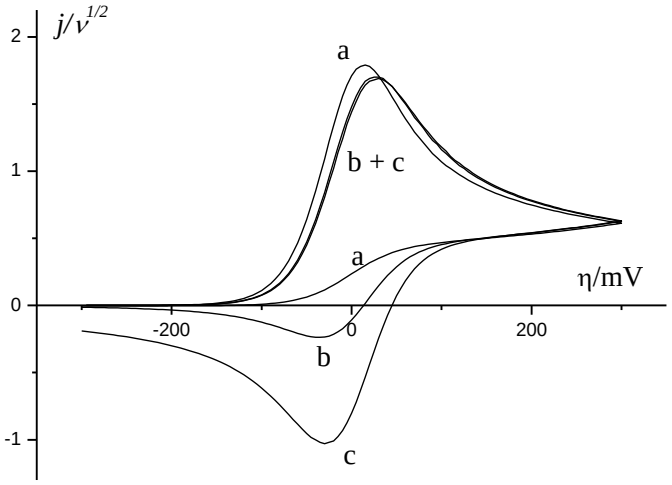

Figure 1.3.2.4 - Cyclic voltammogram showing the effect of scan rate on an EC system. a-c increasing scan rate.

The voltammogram shows a peak corresponding with the initial forward sweep, which is consistent with the electron transfer occurring, to form an intermediate. When the sweep is reversed, the reverse peak is no longer observed (a). This is because the intermediate formed during the forward scan has undergone a chemical reaction (curve a in **Figure 1.3.2.4**), which occurs at a faster rate than the scan. Therefore it is possible to investigate the rate of chemical reaction of an electrochemically generated species by adjusting the CV scan rate (curve b + c). As the scan rate is increased, the reverse peak is observed, partially initially (curve b), but eventually the full reduction peak is detected (curve c). The reduction peak is now observed because the half-life is now longer than the scan rate, meaning the reverse electron-transfer can occur.[1,2]

The ability to generate important data rapidly explains why cyclic voltammetry is one of the most used tools to investigate electroactive species. The discussion in this section has focused more on demonstrating a qualitative approach to reaction investigation. Throughout this research a qualitative interpretation of cyclic voltammograms was used to optimise reactions and investigate mechanisms. A quantitative interpretation can be performed,[1,2] but this has not been discussed as it was not used during this research.

2 Electrochemical TEMPO Mediated Alcohol Oxidations

2.1 Introduction

2.1.1 Alcohol Oxidations

The oxidation of alcohols to aldehydes and ketones is an important transformation in organic synthesis. As a consequence there is now a large array of procedures reported.[41,42] Some of the most popular original methods use reagents derived from chromium trioxide (CrO_3, **2.1**), as an oxidant, although there are many less toxic procedures now widely used. CrO_3 (**2.1**) is itself explosive,[41,43] so is often used as a complex with aqueous sulfuric acid (Jones reagent **2.2**),[44] pyridine (Sarett or Collins reagent **2.3** and pyridinium dichromate, PDC, **2.4**),[43,45] or HCl and pyridine (pyridinium chlorochromate, PCC **2.5**) (**Figure 2.1.1.1**).[41,46]

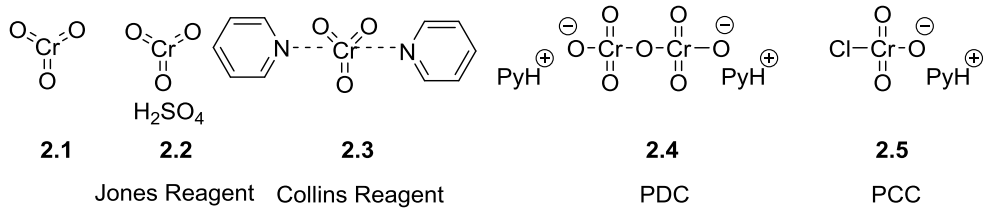

Figure 2.1.1.1 - Chromium based oxidants.

These oxidations are often high yielding for a range of substrates, with short reaction times. Typically these oxidants are used in stoichiometric amounts, generating a lot of highly toxic chromium waste (**Scheme 2.1.1.1**). Over-oxidation of primary alcohols to acids can occur, especially in the presence of water.[41]

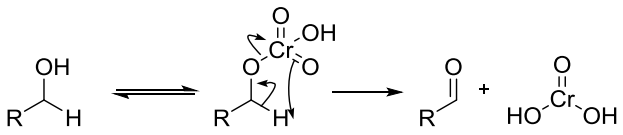

Scheme 2.1.1.1 - Mechanism of alcohol oxidation by chromium salts.

A popular alternative utilises activated DMSO species to drive alcohol oxidations.[41] Perhaps the best known of these is the Swern oxidation, which uses oxalyl chloride **2.6** to form the activated chlorosulfonium species **2.7**.[47] Under cryogenic conditions, DMSO (**2.8**) is treated with oxalyl chloride (**2.6**), to give intermediate **2.9**. This collapses releasing carbon monoxide and carbon dioxide, to give the activated chlorosulfonium species **2.7**. The alcohol is then added to give **2.10**, which after deprotonation by triethylamine forms the ylide **2.11**. The ylide can then rearrange to give a carbonyl and dimethyl sulfide **2.12** (**Scheme 2.1.1.2**).[41] Although this is often a highly efficient process, the Swern oxidation is associated with pungent odours originating from various organosulfur species produced, including the co-product Me_2S (DMS).

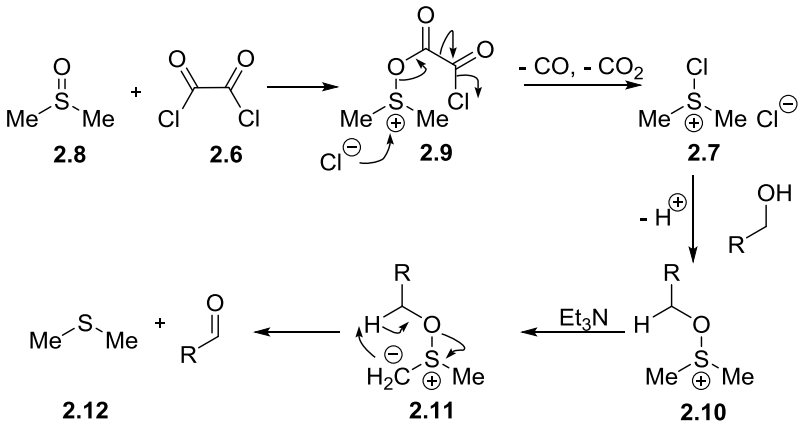

Scheme 2.1.1.2 - Swern oxidation mechanism.

A range of alternative activating agents have been used to generate activated DMSO species (**Figure 2.1.1.2**). Reagents such as dicyclohexylcarbodiimide (**2.13**) (DCC, Pfitzner-Moffatt oxidation),[48] acetic anhydride (**2.14**) (Albright-Goldman oxidation),[49] phosphorous pentoxide (**2.15**) (Albright-Onodera oxidation),[50] sulfur trioxide (**2.16**) (Parikh-Doering oxidation) and trifluoroacetic anhydride (**2.17**) (Omura-Sharma-Swern oxidation) have all been used.[51,52]

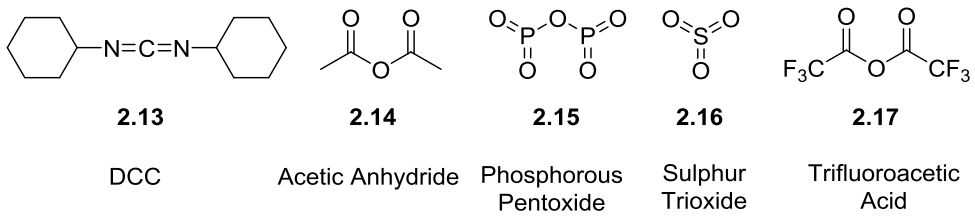

Figure 2.1.1.2 - Examples of reagents used to activate DMSO.

These oxidation procedures have been applied to a vast range of alcohol substrates on a laboratory scale to generate aldehydes and ketones in excellent yields. Often strict control of temperature is needed in order to avoid side reactions. The formation of stoichiometric amounts of CO, CO_2 and DMS as waste, along with the pungent smell produced, often make these procedures unattractive, especially on an industrial scale.[41]

Hypervalent iodine complexes have also been shown to be effective in alcohol oxidations when used in stoichiometric amounts (**Scheme 2.1.1.3**).[41] The most common complexes are the Dess-Martin periodinane (**2.18**) and iodoxybenzoic acid (**2.19**, IBX).[53,54]

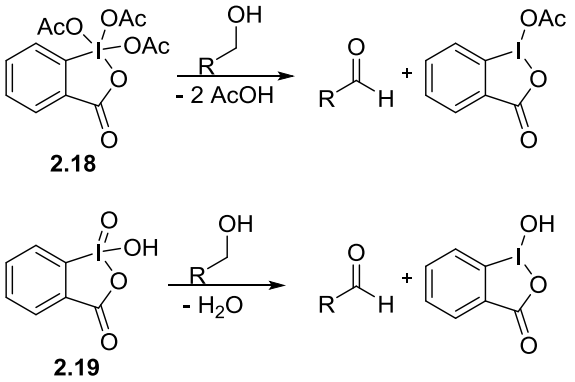

Scheme 2.1.1.3 - Dess-Martin periodinane and IBX oxidation of alcohols.

Dess-Martin periodinane (**2.18**) is more stable than IBX, which has been known to be explosive.[41] Also IBX is only soluble in DMSO, whereas **2.18** is soluble in most organic solvents. Both have been shown to oxidise a range of alcohols efficiently, with a good tolerance of other functional groups.[41]

Catalytic oxidation procedures have been demonstrated, making use of the different oxidation states of ruthenium complexes, and utilising *N*-methyl morpholine *N*-oxide (**2.20**) as a secondary oxidant (**Scheme 2.1.1.4**).[41,42] Tetra-*n*-propylammonium perruthenate (**2.21**, TPAP) is the most commonly used ruthenium complex due to its stability in organic solvents.[55]

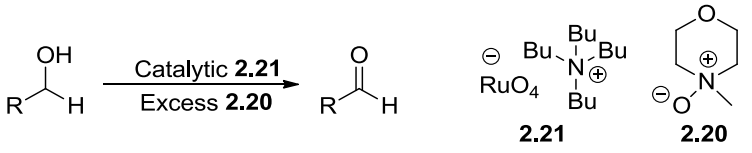

Scheme 2.1.1.4 - Catalytic TPAP alcohol oxidation

A range of alcohols have also been oxidised using these procedures, with a good functional group tolerance. Although substoichiometric loadings of the expensive ruthenium complexes can be used, an excess of a secondary oxidant is required to complete the oxidation, creating excess waste.[41]

With the exception of the TEMPO oxidation, the most common alcohol oxidation procedures used in organic synthesis have been discussed above. It is important to note that there are many more methods for alcohol oxidation reported in the literature, highlighting the fundamental importance of this functional group interconversion in organic synthesis.[41,42] Although there are numerous alcohol oxidation procedures, many of these are often avoided for industrial applications.[56] The reasons for this are the need for stoichiometric amounts of expensive reagents, leading to substantial waste. Many of these reagents are also highly toxic, such as the chromium salts.

The problems highlighted above have led to research into environmentally benign alcohol oxidations or at least procedures with reduced environmental impact. Use of catalytic species, coupled with oxygen or hydrogen peroxide as a terminal oxidant has led to some improvements.[42] Organic oxidants such as TEMPO have also been a fruitful area of research, which is discussed in the next section.

2.1.2 TEMPO Mediated Alcohol Oxidations

2,2,6,6-Tetramethyl-1-piperidinyloxy (TEMPO, **2.22**) is the most common member of the nitroxy radical family, also known as nitroxides (**Figure 2.1.2.1**). They are classified by containing an *N*-disubstituted N–O group with a single unpaired electron.[57-59] The unpaired electron is delocalised over the N–O bond, making nitroxyl radical stable when there are no α-hydrogens present.[58,59] Nitroxides have been identified as environmentally benign oxidants for an array of functional groups, leading to a vast number of publications and reviews.[57-64]

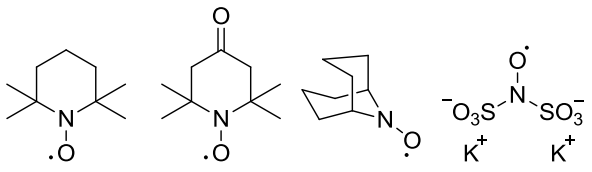

Figure 2.1.2.1 - Examples of nitroxides.

Nitroxides are weak oxidants,[64] but they themselves can undergo a one-electron oxidation to the corresponding oxoammonium cation, which is a relatively strong oxidant.[57] Early work by Golubev *et al*. in 1965 showed that the oxoammonium chloride salt (**2.26**) could be used as a stoichiometric oxidant to convert simple alcohols (present in a large excess) to aldehydes and ketones, leaving the hydroxylamine (**2.27**), and HCl (**Scheme 2.1.2.1**).[65]

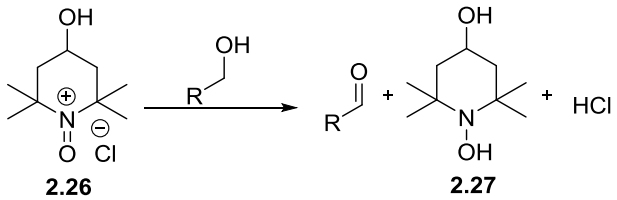

Scheme 2.1.2.1 - Golubev oxidation of alcohols with stoichiometric **2.26**.

Anelli *et al.* first showed that the oxoammonium can be generated *in situ*, leading to catalytic TEMPO oxidations. They showed that 4-methoxy-TEMPO (**2.28**, 1 mol %), with KBr (10 mol %), in an aqueous DCM/NaOCl solution (0.35 M) buffered at pH 8.6 with $NaHCO_3$, at 0 ˚C, gave fast and selective oxidations.[66] The generally accepted mechanism is shown in **Scheme 2.1.2.2**. The catalytic cycle involves the oxidation of the alcohol by the active oxoammonium species **2.29** to give the carbonyl and the hydroxylamine **2.30**. **2.30** is then reoxidised by the hypobromide, generating the bromide. The bromide is then recycled by the hypochlorite terminal oxidant.[57]

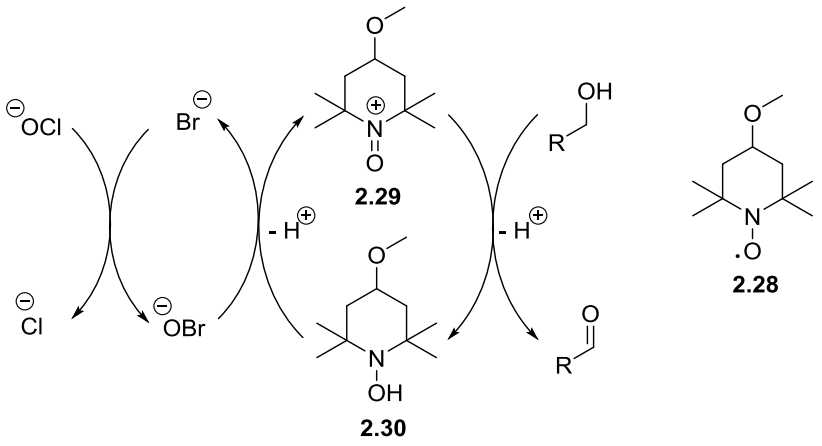

Scheme 2.1.2.2 - Alcohol oxidation mechanism with **2.28** and NaOCl

Excellent yields and turnovers have been achieved with aliphatic, aromatic and heterocyclic alcohols, leading to the wide use of this procedure. Problems include the cost of TEMPO (80-100 $/Kg), making its recovery from homogeneous reaction mixtures very important, especially during procedures that require higher loadings (typical loading 0.1-10 mol %).[63] The high cost has led to procedures using TEMPO analogues functionalised in the 4-position or TEMPO immobilised on solid supports.[57,58,63] Alternative co-oxidants to form the active oxoammonium species have also been reported. Stoichiometric oxidants such as *m*-CPBA, *N*-chlorosuccimide, I_2, Cl_2, Br_2, pyridine/HBr, oxone, periodic acid and H_2O_2 have been employed, although these methods still generate substantial waste.[57,58]

A popular alternative to using stoichiometric oxidants is to use air as an environmentally benign terminal oxidant, coupled with a co-catalyst. The co-catalyst oxidises TEMPO to the active oxidant and recycles the hydroxylamine co-product. The co-catalyst itself is then recycled by air. Many transition metal co-catalysts have been studied, with copper based systems being the most investigated.[58] Different mechanisms for this process have been proposed.[57,58] The first follows a typical mechanism, where an oxoammonium species **2.31** oxidises the alcohol, to give the carbonyl and the reduced hydroxylamine co-product **2.32**. The copper(II) salt then regenerates the oxoammonium species **2.31**, leaving a copper(I) salt, which is recycled by air oxidation (**Scheme 2.1.2.3**).[58] This is thought to be the mechanism occurring when the reported copper based laccase enzyme-TEMPO systems are used to oxidise alcohols.[57,67]

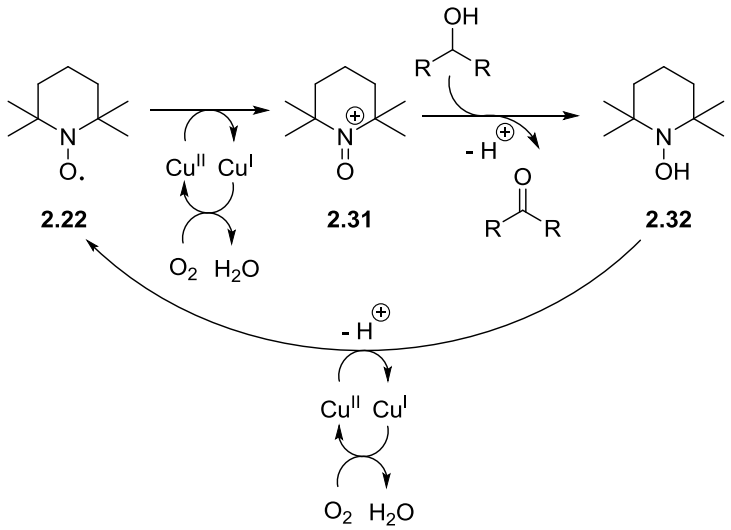

Scheme 2.1.2.3 - Copper co-catalysed TEMPO alcohol oxidation mechanism.

Sheldon has suggested a mechanism involving a copper-TEMPO complex **2.33**, instead of an active oxoammonium species.[57,58] TEMPO (**2.22**) oxidises the copper(I) salt to form a copper(II)-TEMPO complex **2.33**. Ligand exchange with an alcohol forms the adduct **2.34** and a hydroxylamine species **2.32**. The hydroxylamine **2.32** is oxidised to TEMPO by air. Adduct **2.34** undergoes an intermolecular hydrogen transfer with TEMPO, to give the carbonyl, copper(I) salt and a hydroxylamine species **2.32**. Hydroxylamine **2.32** is oxidised to TEMPO by air, restarting the cycle (**Scheme 2.1.2.4**).[57,58]

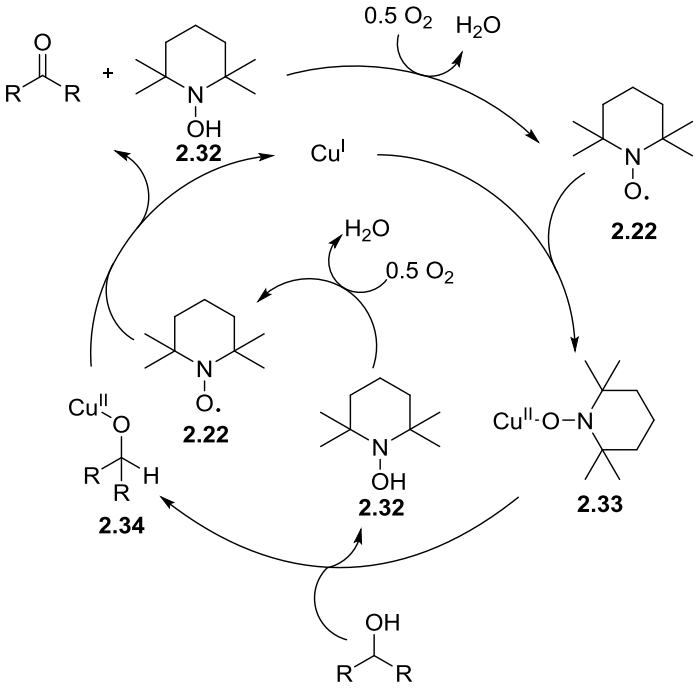

Scheme 2.1.2.4 - Alternative proposed mechanism for oxidative copper co-catalysed TEMPO alcohol oxidations.

Other aerobic transition metal co-catalysed systems have been reported. This includes metals such as vanadium, cerium, iron, ruthenium and manganese.[58] Non-transition metal co-catalytic TEMPO oxidations of alcohols using air as a terminal oxidant are also known. The first was reported by Liang and Hu in 2004.[68] In their system they utilised TEMPO (10 mol %), in conjunction with Br_2 (0.4 equiv.) and $NaNO_2$ (0.4 equiv.) in DCM to oxidise aromatic, allylic and aliphatic alcohols in excellent yield. The proposed mechanism involves recycling of the hydroxylamine **2.32** to the active oxoammonium **2.31**, by Br_2, giving HBr. HBr, is then reoxidised to Br_2 by NO_2, giving water as the by-product. The NO_2 is formed by oxidation of NO using air (**Scheme 2.1.2.5**).

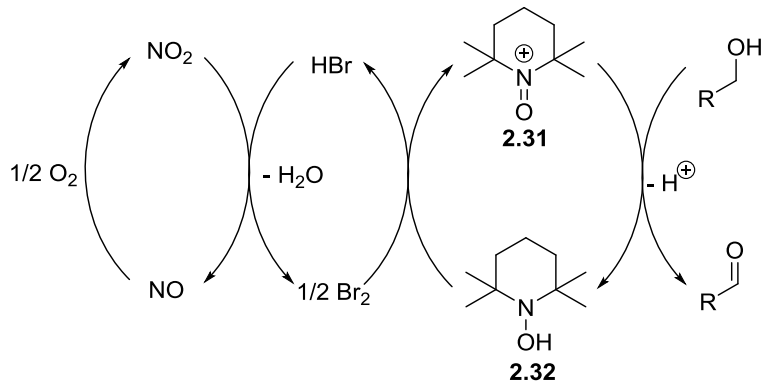

Scheme 2.1.2.5 - Mechanism of TEMPO mediated alcohol oxidation with air as a terminal oxidant.

There are now many examples of TEMPO oxidations used in industrial processes.[63] This demonstrates the importance and robust nature of the reaction. The first to be introduced by Pharmacia and Upjohn was the conversion of bisnoralcohol (**2.35)** to bisnoraldehyde (**2.36**), an important intermediate in the synthesis of many steroids (**Scheme 2.1.2.6**).[63] They utilised 4-hydroxy-TEMPO (**2.37**), as it is more cost effective than TEMPO, with NaOCl and KBr. Since then many other processes have been introduced, often replacing the use of more toxic oxidants. Problems with the cost and recovery of TEMPO have been addressed by developing methodologies based upon solid-supports.[63]

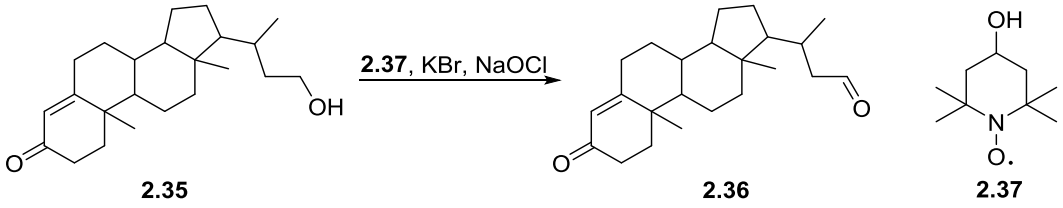

Scheme 2.1.2.6 - TEMPO mediated synthesis of bisnoraldehyde **2.36**.

2.1.3 Electrochemical TEMPO Mediated Alcohol Oxidations

As an alternative to using chemical co-oxidants, Semmelheck in 1983 showed that TEMPO is electrochemically active.[69,70] TEMPO (**2.22**) can undergo a one-electron oxidation at an anode to give an oxoammonium species **2.31**. Conversely, a one-electron reduction occurs at a cathode, which upon protonation gives the hydroxylamine species **2.32** (**Scheme 2.1.3.1**).

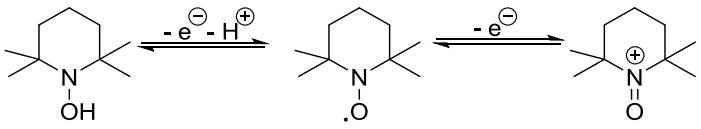

Scheme 2.1.3.1 - Electrochemical oxidation and reduction of TEMPO.

Semmelheck used the electrochemical activity of TEMPO to develop a preparative alcohol oxidation in a divided batch cell (**Scheme 2.1.3.2**).[70] Electrochemical oxidation of TEMPO to the oxoammonium species **2.31** was followed by the addition of the alcohol in sequential steps. A range of alcohols were oxidised to aldehydes or ketones in good yields, with varying reaction times. Improved yields were achieved with the addition of the base 2,6-lutidine (**2.38**).

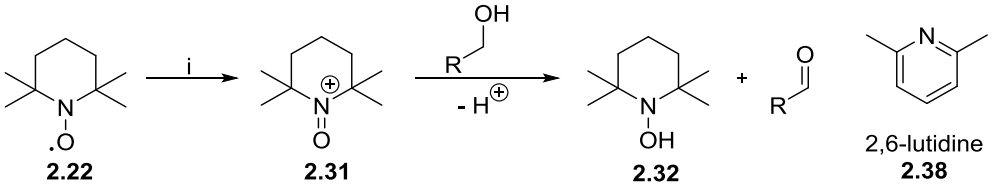

Scheme 2.1.3.2 - Semmelheck's electrochemical alcohol oxidation. *Reagents and conditions* - i) **2.22** (1.6 mmol), **2.38** (1.5 mL) and lithium perchlorate (0.2 M) in MeCN (25 mL), Pt electrode, +0.35 V vs. $AgNO_3$, 23 °C, divided cell, then alcohol addition.

Since Semmelheck's reports, only a handful of preparative procedures utilising the electroactive properties of TEMPO, or its analogues, to oxidise alcohols have been described. Initial attempts to develop a catalytic system required the addition of a bromide source to act as a co-catalyst in a biphasic medium (**Scheme 2.1.3.3**).[71] At the anode the bromide ion is electrochemically oxidised to hypobromite in water, which can oxidise the TEMPO to oxoammonium **2.31** in the organic phase. Alcohol oxidation by oxoammonium **2.31** leads to the aldehyde product and hydroxylamine co-product **2.32**, which is recycled to the oxoammonium species **2.31** by oxidation from the hypobromite.

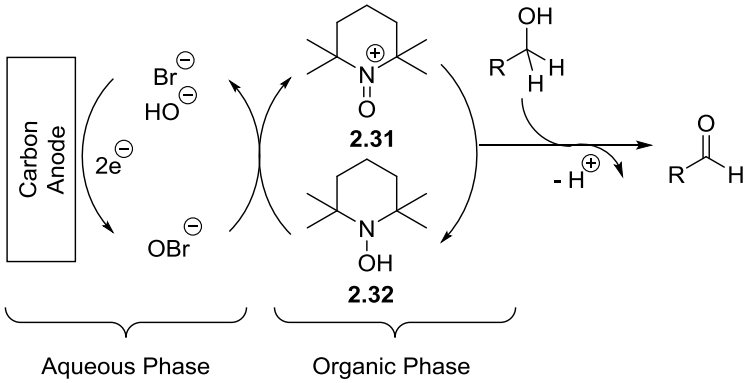

Scheme 2.1.3.3 - Electrochemical co-catalysed biphasic alcohol oxidation.

Subsequent reports have involved direct electrochemical oxidation of TEMPO at the anode in aqueous media. To achieve this, TEMPO has been modified to include water soluble groups,[72,73] water soluble polymers have been synthesised,[74] or nano-emulsions have been used.[75] Furthermore chiral analogues of TEMPO, such as **2.39** have been synthesised, to perform resolutions of racemic secondary alcohols, in an electrochemical system.[76,77] Good yields and enantioselectivities are reported with these procedures (**Scheme 2.1.3.4**).

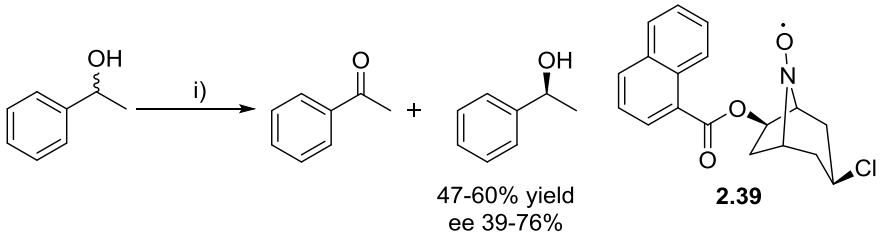

Scheme 2.1.3.4 - Electrochemical enantioselective oxidation of alcohols with TEMPO analogue **2.39**. *Reagents & conditions* - i) **2.39** (0.1 equiv.), NaBr (4.0 equiv.), sat. aq. $NaHCO_3$/DCM, 0 ˚C, Pt electrode, 20 mA.

The redox couple of TEMPO and oxoammonium has been shown to be reversible in various different media, including aprotic solvents, aqueous solutions, ionic liquids, biphasic mixtures and for TEMPO modified electrodes.[62,78-85] Most of these studies have concerned the com-/-disproportionation reaction between TEMPO, oxoammonium species **2.31** and hydroxylamine species **2.32** (**Scheme 2.1.3.5**). Comproportionation of hydroxylamine and oxoammonium has been proposed as an important step in the regeneration of TEMPO during catalytic alcohol oxidation.[86]

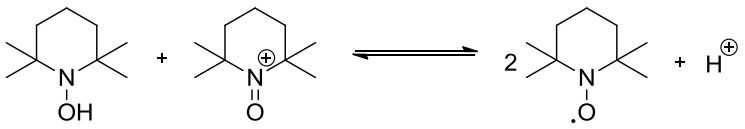

2.32 **2.31** **2.22**

Scheme 2.1.3.5 - Com-/-disproportionation of TEMPO.

The com-/-disproportionation of TEMPO has been shown to be highly pH dependent.[87,88] Most studies have investigated the com-/-disproportionation under acidic conditions, where the equilibrium is to the left (favouring disproportionation). Treating TEMPO with strong acids is often utilised to synthesise oxoammonium salts.[89] Whereas under basic conditions the equilibrium lies to the right (favouring comproportionation) and is reported to be fast.[87] TEMPO mediated alcohol oxidations are usually performed under basic conditions, to shift the com-/-disproptionation equilibrium to favour TEMPO regeneration, leading to improved yields and turnover. Furthermore basic conditions increase the rate of deprotonation of the intermediate adducts **2.40** and **2.41**, again leading to a faster turnover of TEMPO (**Scheme 2.1.3.6**).

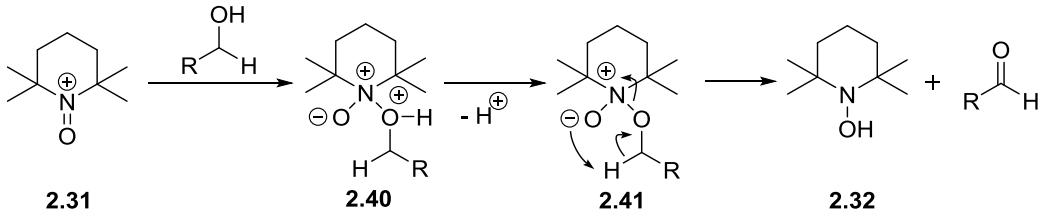

2.31 **2.40** **2.41** **2.32**

Scheme 2.1.3.6 - Mechanism depicting the effect of basic conditions on the rate of deprotonation of adducts **2.40** and **2.41**.

The TEMPO/oxoammonium redox couple and the com-/-disproportionation reaction have been well studied in the literature. On the other hand the TEMPO/hydroxylamine redox couple has not, with only a few reports in the literature.[87,90,91] The TEMPO/hydroxylamine redox couple has been shown to be electrochemically irreversible, and strongly dependent on pH. In acidic solutions (pH 2.5) the oxidation potential of the hydroxylamine species **2.32** is approximately +1.1 V vs. Ag/AgCl. This shifts to around +0.1 V vs. Ag/AgCl under basic conditions (pH 10.2),[87] which is unsurprising for a mechanism involving a proton transfer step.

2.1.4 Research Aims

Alcohol oxidations are fundamental processes and one of the most widely utilised transformations in organic synthesis. TEMPO mediated oxidations are considered to be environmentally benign in relation to other methods, with the ability to be driven electrochemically. As discussed, we have been involved in the development of flow electrosynthesis devices, to improve the accessibility of electrochemical transformations to synthetic chemists. One strand of the research was to develop a TEMPO mediated alcohol oxidation in the electrochemical microflow cell. This was conducted in collaboration with Dr. Hill-Cousins and led to publication in ChemSusChem, which is discussed in **section 2.2**.[92]

Furthermore as an extension of the TEMPO-mediated flow alcohol oxidation, cyclic voltammetry led to an investigation into the effects of the basic conditions on the mechanism. This work has led to another publication in Electrochimica Acta, which is discussed in **section 2.3**.[93]

2.2 TEMPO-Mediated Electrooxidation of Alcohols in an Electrochemical Microflow Cell

Cyclic voltammetry experiments were used to guide the optimisation of an electrochemical TEMPO-mediated alcohol oxidation reaction in the electrochemical microflow cell. A typical three-electrode system (as described in chapter 1) was used to obtain voltammograms, which is described in the experimental section. Before any cyclic voltammetry experiments could be performed, a suitable reaction medium needed to be found. Basic solutions have been shown to increase the rate and yield of TEMPO mediated alcohol oxidations.[70,86,87] Also water has been used as a solvent, which could be considered advantageous in the development of an environmentally benign process. A basic aqueous system would ensure an overall balanced electrochemical process, leading to only hydrogen gas as a waste product, from the reduction of water at the counter electrode. The production of hydroxide also helps to maintain a basic pH during the electrolysis (**Scheme 2.2.1.1**).[92]

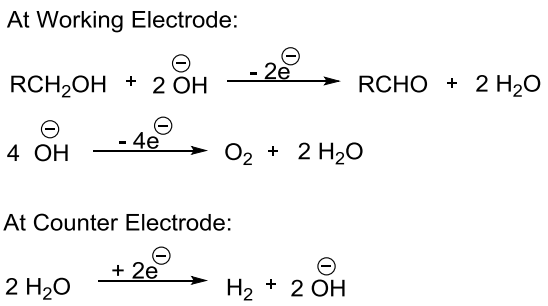

Scheme 2.2.1.1 - Working and counter electrode reactions.

To ensure the solubility of a range of alcohols, *tert*-butanol (^{t}BuOH) was added as a co-solvent. ^{t}BuOH is a preferred solvent in the pharmaceutical industry, due to its favourable safety and handling properties, as determined by the Pfizer Environment, Health and Safety group.[61] To ensure a constant basic pH was maintained throughout the reaction, a sodium carbonate/sodium bicarbonate buffer system was employed.

Cyclic voltammetry experiments were conducted to confirm that the buffered ^{t}BuOH/water reaction medium was suitable. **Figure 2.2.1.1** shows voltammograms of a 10 mM solution of TEMPO (**2.22**) buffered at pH 9.3, at a

vitreous carbon electrode (area 0.07 cm^2), with a potential scan rate of 50 mV s^{-1}. The positive scan is characteristic of a reversible one-electron oxidation of TEMPO (**2.22**) to the oxoammonium species **2.31**, at +0.56 V vs. a saturated calomel electrode (SCE) (**Scheme 2.2.1.2**). This redox couple is similar to that reported in the literature.[62,70,71,78,79,81-85,87,91] Furthermore, when a negative potential scan is performed a drawn out one-electron reduction peak is observed at –0.65 vs. SCE. This is related to the reduction of TEMPO (**2.22**) to the hydroxylamine species **2.32** (**Scheme 2.2.1.2**). The corresponding re-oxidation peak is not observed until +0.20 V vs. SCE. This large peak separation is informative, indicating electrochemical irreversibility (i.e. slower electron transfer), but is still chemically reversible. A redox couple is defined as electrochemically irreversible if the peak separation is greater than 59 mV per electron involved.[2] The slower electrode kinetics is due to the proton transfer step that is involved in the inter-conversion between TEMPO and the hydroxylamine species **2.32**. The potential for the TEMPO/hydroxylamine couple is between –0.1 to –0.3 V vs. SCE, in this solvent mixture.

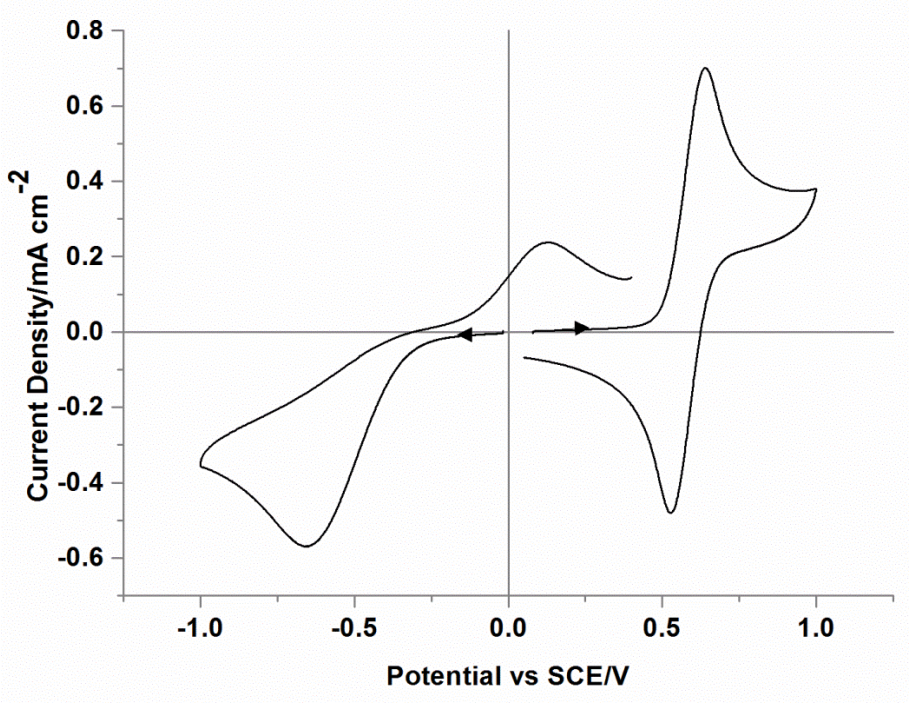

Figure 2.2.1.1 - Cyclic voltammograms at a carbon disc electrode for 10 mM TEMPO in 1:1 ^{t}BuOH/water containing sodium carbonate/bicarbonate at pH 9.3. Scan rate 50 mV s^{-1}. Temperature 20 ˚C.

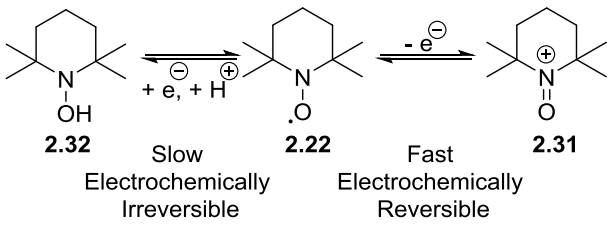

Scheme 2.2.1.2 - Electrochemical oxidation and reduction of TEMPO

The cyclic voltammetry shows that TEMPO (**2.22**) has favourable electrochemistry in the buffered aqueous ^{t}BuOH system, which could be applied to the microflow cell. The cyclic voltammetry suggests that the overpotential to drive the two-electron oxidation of hydroxylamine **2.32** to oxoammonium **2.31**, *via* TEMPO (**2.22**) will be large, and mass transport controlled (**Scheme 2.2.1.3**). The basic conditions have shifted the TEMPO/hydroxylamine redox couple to a lower oxidation potential (+0.20 V). To facilitate the oxidation in the microflow cell the potential will need to be held at a higher potential than the TEMPO/oxoammonium redox couple (> +0.56 V). This is to ensure that TEMPO is rapidly oxidised to the oxoammonium species, therefore facilitating the alcohol oxidation. Holding the potential at > +0.56 V will also rapidly oxidise any hydroxylamine species formed, due to the large difference in potentials (overpotential). In acidic media the potential required for oxidation of hydroxylamine **2.32** has been shown to increase to > 1.0 V (greater than the value for the TEMPO/oxoammonium couple). Therefore the overpotential to drive the oxidation of hydroxylamine **2.32** would be lower, and the oxidation of the hydroxylamine will not occur in the potential range investigated.[87] The shape of the voltammogram indicates whether the electrochemistry is mass transport controlled. A peak like that for the TEMPO/oxoammonium couple suggests the electrochemistry is mass transport controlled. Whereas voltammograms shaped like a wave indicate the reaction is not mass transport controlled.

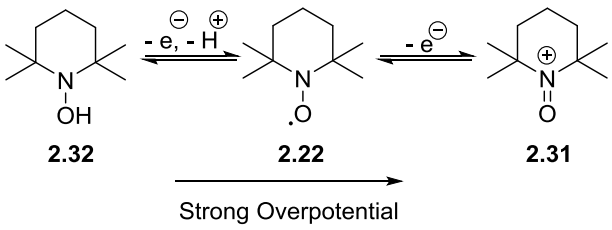

Scheme 2.2.1.3 - Overpotential driving the electrochemical recycling of **2.32**.

In addition, the cyclic voltammetry shows a large separation between the TEMPO/oxoammonium (**2.31**) and TEMPO/hydroxylamine (**2.32**) redox couples. The large separation suggests that the comproportionation reaction will be thermodynamically favourable, to generate two equivalents of TEMPO, under these conditions. This, followed by oxidation of TEMPO (**2.22**) to oxoammonium **2.31**, provides an alternative pathway for the catalytic cycle (**Scheme 2.2.1.4**). A rate constant of ~50 M^{-1} s^{-1} for the comproportionation at pH 10 has been measured, which compares to a rate constant of 0.23 M^{-1} s^{-1} at pH 4.5.[87] Therefore the cyclic voltammetry of TEMPO in the basic buffered aqueous ^{t}BuOH medium suggests that comproportionation to regenerate TEMPO is fast and thermodynamically favourable.

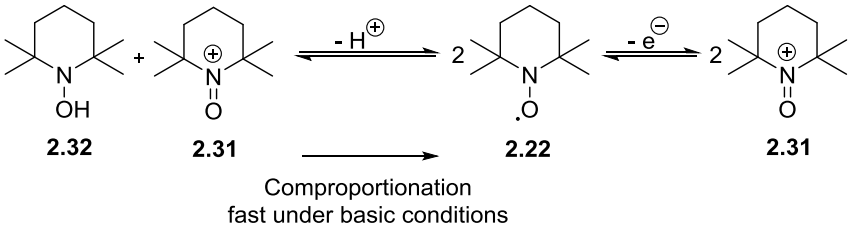

Scheme 2.2.1.4 - Comproportionation as an alternative route to recycle TEMPO.

To continue the development of an electrochemical TEMPO-mediated alcohol oxidation the effect of added alcohol on the cyclic voltammetry of TEMPO was investigated next. This was to confirm that the TEMPO-mediated alcohol oxidation will proceed in the ^{t}BuOH/water medium, and that there are no other electroactive side reactions. Therefore a cyclic voltammogram of 2 mM TEMPO in aqueous ^{t}BuOH buffered at pH 9.3, containing benzyl alcohol (BnOH, **2.42**) (16 mM) was collected (**Figure 2.2.1.2**). With the addition of BnOH to the solution, the positive potential scan changes drastically. The oxidation of TEMPO has become irreversible in the presence of alcohol, as shown by the disappearance of the reduction peak on the reverse scan. Additionally, the limiting current for the oxidation peak has increased. The voltammogram is consistent with an EC' mechanism occurring. An EC' mechanism is where the chemical step leads to an increase in the observed current density, which suggests a catalytic turnover.

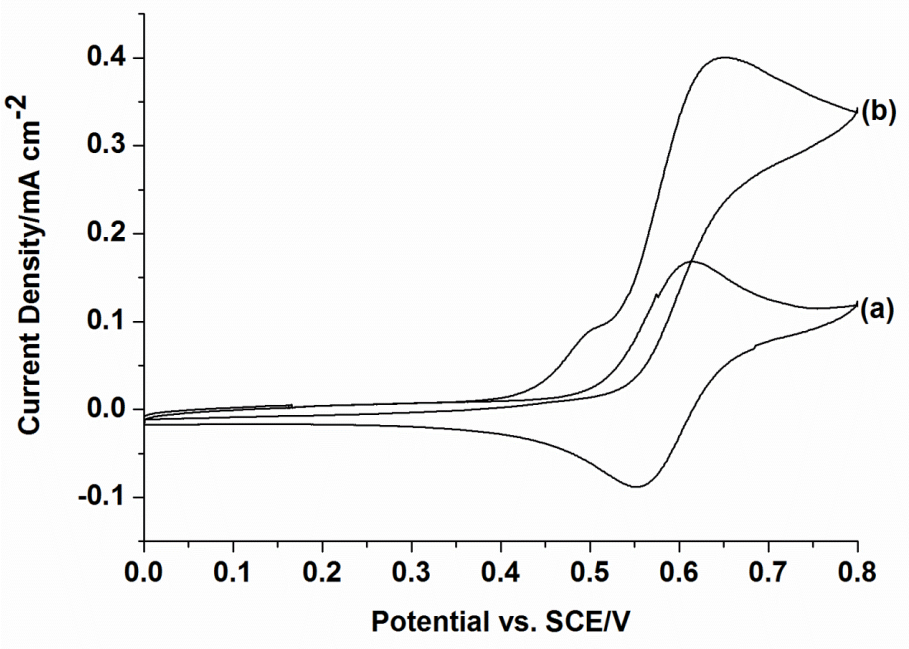

Figure 2.2.1.2 - Cyclic voltammograms at a vitreous carbon disc electrode for 1:1 ^{t}BuOH/water containing sodium carbonate/bicarbonate to show the influence of added benzyl alcohol. a) 2 mM TEMPO, pH 9.3. b) 2 mM TEMPO + 16 mM Benzyl alcohol, pH 9.3. Scan rate 50 mV s $^{-1}$. Temperature 20 °C.

The results from the cyclic voltammograms demonstrate that TEMPO is mediating the oxidation of benzyl alcohol (**2.42**) to benzaldehyde (**2.43**). The disappearance of the cathodic reduction peak, suggests that the oxoammonium species **2.31** is reacting rapidly with BnOH, reducing the concentration of oxoammonium species **2.31** at the electrode surface (**Scheme 2.2.1.5**). The increase in the limiting current in the CV indicates that TEMPO is being recycled by an EC' mechanism, which suggests a catalytic procedure could be developed in the electrochemical microflow cell.

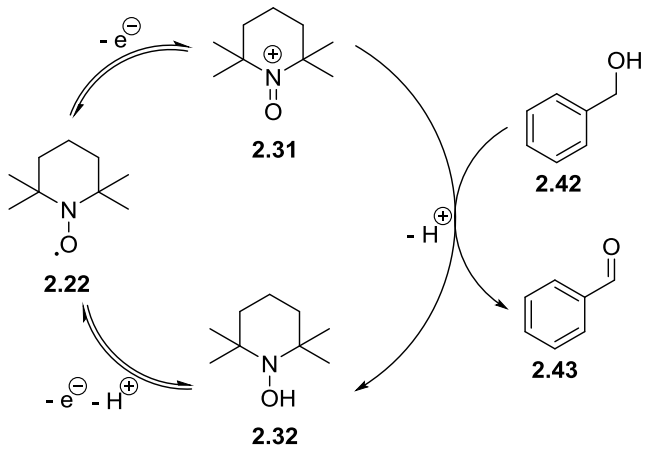

Scheme 2.2.1.5 - Electrochemical TEMPO mediated alcohol oxidation of BnOH.

After demonstrating that the TEMPO mediated alcohol oxidation in the selected reaction medium had favourable electrochemistry, the optimisation of the reaction began. This started with an investigation into the effect of pH on the oxidation of benzyl alcohol (**2.42**). The pH of the buffer solution was adjusted by changing the ratio of carbonate to bicarbonate (see experimental section). TEMPO solutions of pH 9.3 to 11.7, with BnOH were made to investigate the effect of pH on the oxidation of benzyl alcohol. The results are shown in **Figure 2.2.1.3**.

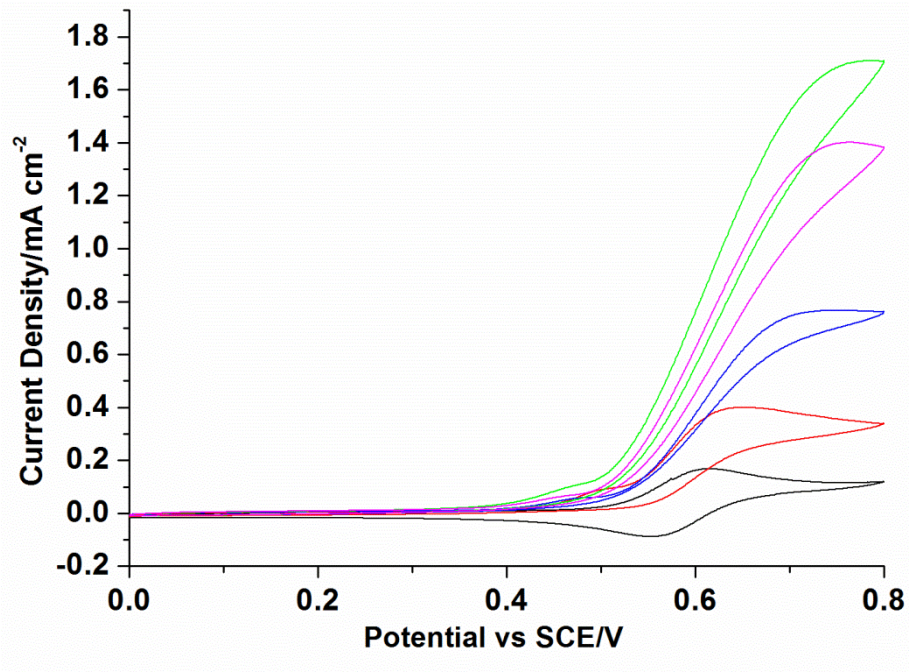

Figure 2.2.1.3 - Cyclic voltammograms at a vitreous carbon disc electrode in 1:1 ^{t}BuOH/water containing sodium carbonate/bicarbonate to show the influence of pH on the rate of the mediated oxidation of benzyl alcohol. Black curve - 2 mM TEMPO, pH 9.3. Red curve - 2 mM TEMPO + 16 mM benzyl alcohol, pH 9.3. Blue curve - 2 mM TEMPO + 16 mM benzyl alcohol, pH 10.6. Green Curve - 2 mM TEMPO + 16 mM benzyl alcohol, pH 11.5. Pink curve - 2 mM TEMPO + 16 mM benzyl alcohol, pH 11.7.

The cyclic voltammograms demonstrate that with increasing pH, larger limiting currents can be achieved. The higher pH allows for faster regeneration of the oxoammonium (**2.31**) oxidant, leading to an increase in the limiting current by a factor of five. **Figure 2.2.1.4** shows the optimum pH to be 11.5 for the TEMPO mediated alcohol oxidation. Increasing the pH further leads to a decrease in limiting current. The reasons for this decrease at higher pH are discussed in the following sections. When the optimal pH of 11.5 was applied in the electrochemical microflow cell improved conversions of BnOH (**2.42**) to benzaldehyde (**2.43**) of up to 98% were observed (**Scheme 2.2.1.6**).[92]

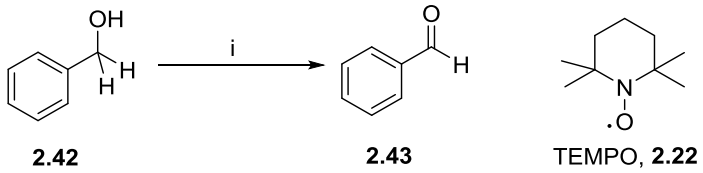

Scheme 2.2.1.6 - Electrochemical TEMPO mediated conversion of BnOH in the electrochemical flow cell. *Reagents & Conditions* - BnOH (0.1 M), TEMPO (30 mol %), 1:1 ^{t}BuOH/H_2O with Na_2CO_3/$NaHCO_3$ buffer, pH 11.5, 20 mA, 0.1 mL min^{-1}. 25 °C

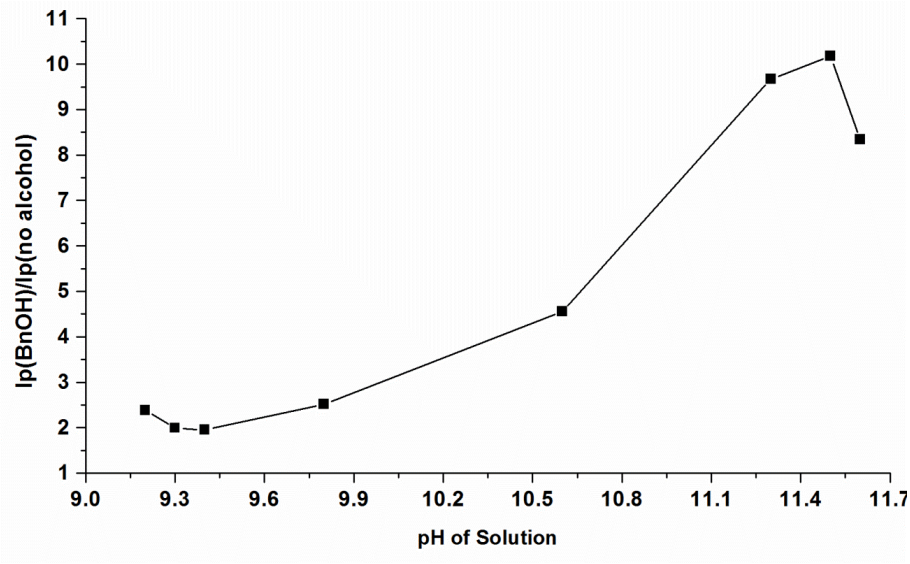

Figure 2.2.1.4 - Graph showing the effect of the pH on the peak current for the electrochemical TEMPO-mediated oxidation of the BnOH in ^{t}BuOH/water.

Finally the effect of temperature on the oxidation was investigated. The cyclic voltammetry cell was placed in a water bath and a solution of TEMPO (2 mM) with benzyl alcohol (**2.42**, 16 mM) in the aqueous ^{t}BuOH buffered to pH 11.5, was added to the cell. Once the solution reached the desired temperature a cyclic voltammogram was collected (**Figure 2.2.1.5**). The cyclic voltammograms show an increase in limiting current at 45 °C, by a factor of 6, which is due to improved rate of mass transfer and kinetics of the chemical reactions in the catalytic cycle. The increased limiting current suggests that a greater conversion rate should be achieved at higher temperature, although in practice, decreased selectivity of the reaction may limit the useful temperature range.

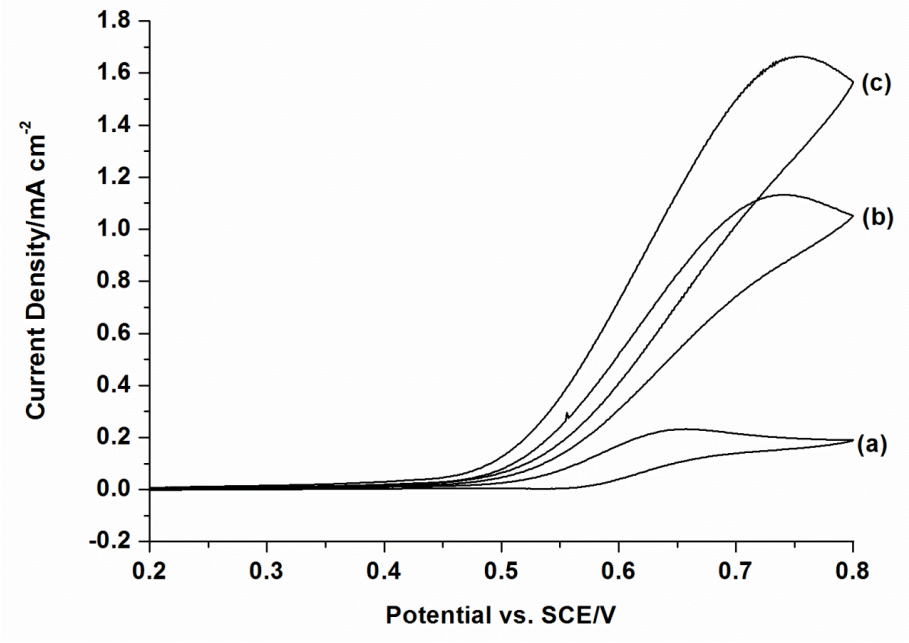

Figure 2.2.1.5 - Cyclic voltammograms showing the effect of temperature on the TEMPO mediated oxidation of benzyl alcohol. 2 mM TEMPO with 16 mM Benzyl alcohol in 1:1 ^{t}BuOH/water with sodium carbonate/bicarbonate at pH 11.5. a) 24 ˚C. b) 35 ˚C. c) 45 ˚C.

Indeed, when higher temperatures were applied to the electrochemical microflow cell, the selectivity decreased and over-oxidation to benzoic acid was observed.[92] The difference in results is due to the change in residence time in the different cells. During the cyclic voltammetry the solution is only being oxidised for approximately 10 seconds, whereas the electrochemical microflow cell has a residence time of 120 seconds at 0.1 mL min^{-1}, increasing the chance of over-oxidation towards the end of the channel at higher temperatures.

To investigate what current to apply during the preparative reactions, a cell current vs. cell voltage plot was obtained using the electrochemical microflow cell (**Figure 2.2.1.6**). The electrochemical microflow cell has a two electrode arrangement so the cyclic voltammogram was obtained by using the stainless steel counter electrode as a reference electrode as well. It is important to note that the current will decrease along the flow path, as the concentration of alcohol drops, if full conversion is achieved. Therefore the current is an integral from along the channel. The solutions were allowed to flow through the cell at 0.1 mL min^{-1}, to fill the cell, which ensured a steady state distribution of solution along the flow path when the potential was applied.

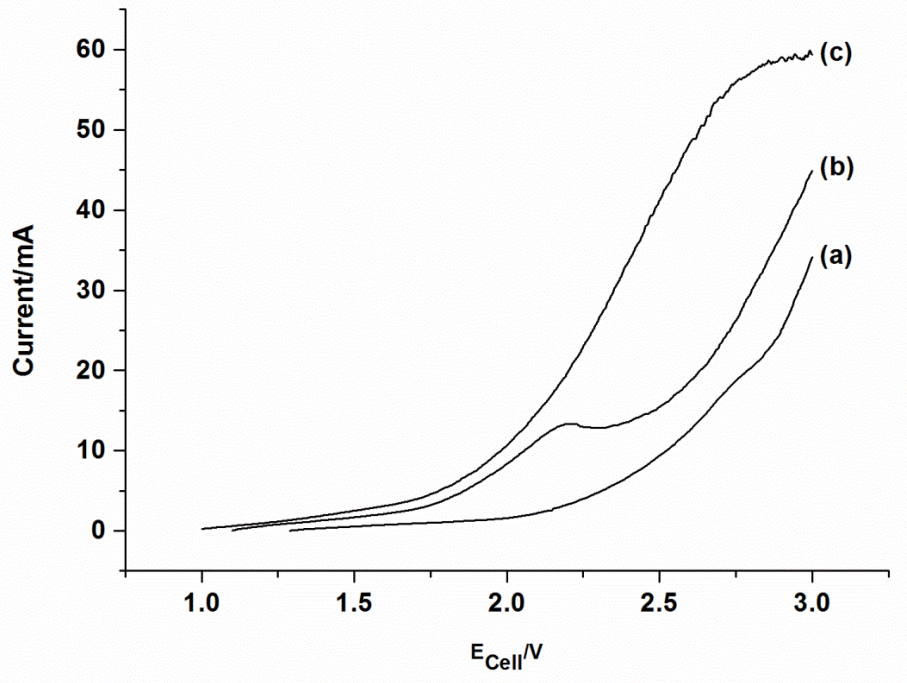

Figure 2.2.1.6 - Cell current vs. cell voltage curves in the electrochemical microflow cell for a) ^{t}BuOH/water containing sodium carbonate/bicarbonate, pH 11.5. b) TEMPO (30 mM). c) TEMPO (30 mM) and 100 mM benzyl alcohol (100 mM). Temperature 25 °C. Flow rate 0.1 mL min^{-1}.

In the absence of TEMPO (line a), no current is observed until 2.5 V, which corresponds to the evolution of oxygen due to electrolysis of the solvent. In the presence of TEMPO (30 mM) (line b) a one-electron oxidation wave is observed, relating to oxoammonium **2.31** formation at ~2.0 V. In the presence of TEMPO (30 mM) and benzyl alcohol (100 mM) (line c), the oxidation wave at ~2.0 V increases from 14 to 58 mA, due to the regeneration of TEMPO. These experiments suggest that successful preparative electrolysis can be achieved in the electrochemical flow cell, at a constant current of 20 mA. At higher currents over oxidation of BnOH occurs leading to reduced selectivity, which was confirmed by preparative experiments. Therefore it is unnecessary to run the electrolysis at higher currents.

On completion of the cyclic voltammetry led optimisation process Dr. Hill-Cousins applied the conditions to 15 alcohol substrates to investigate the scope of the oxidation procedure (**Scheme 2.2.1.7**). The examples along with the isolated yields are shown in **Table 2.2.1.1**.[92]

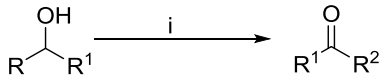

Scheme 2.2.1.7 - TEMPO mediated alcohol oxidation in an electrochemical microflow cell. *Reagents & Conditions* - i) 0.1 M alcohol, 30 mM TEMPO in 1:1 ^{t}BuOH/water buffered with sodium carbonate/bicarbonate at pH 11.5. Temperature 25 °C. Flow Rate 0.1 mL min^{-1}.

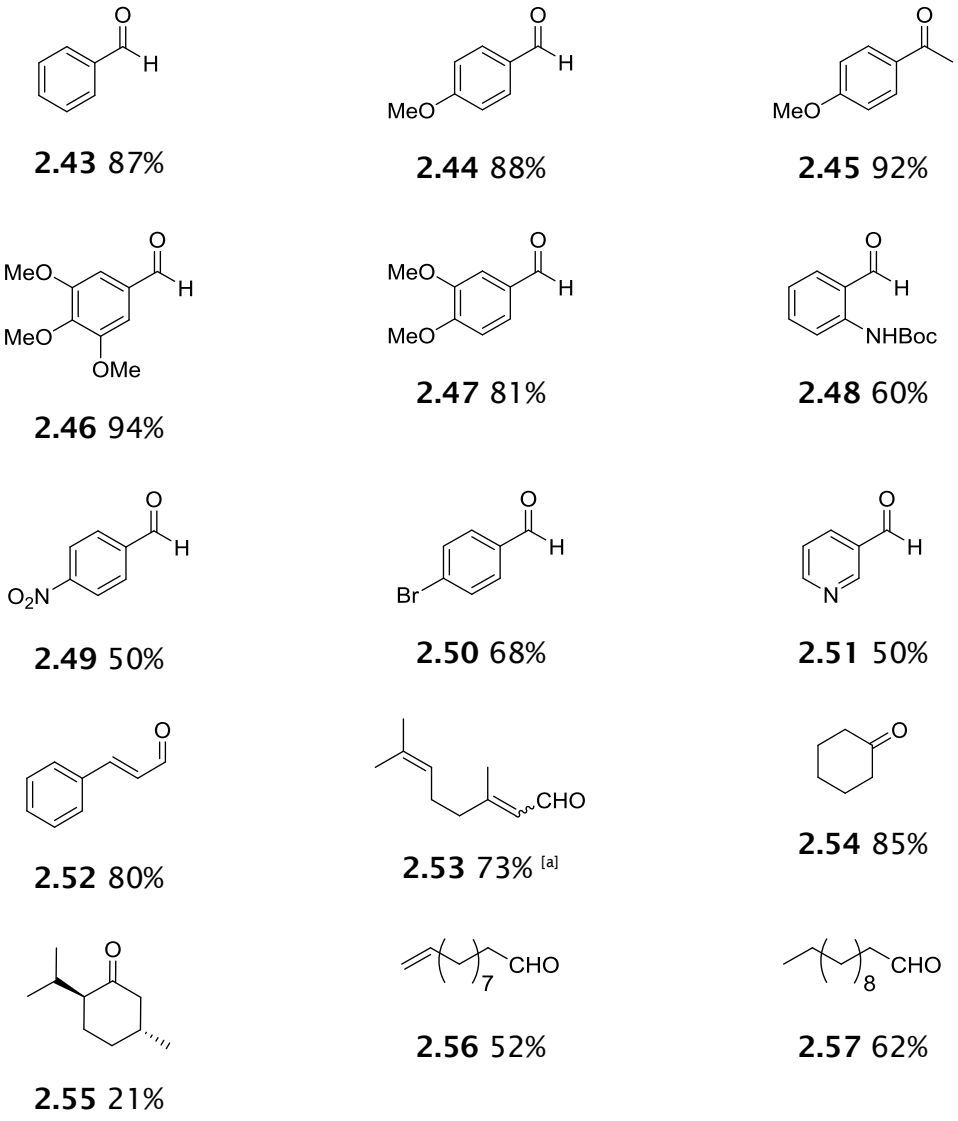

Table 2.2.1.1 - Substrate scope of the TEMPO mediated alcohol oxidation in the electrochemical microflow cell. a E:Z ratio = 1.8:1.

Generally excellent yields were achieved with the benzylic and allylic alcohols as they are easier to oxidise, especially the electron-rich examples (**2.45**, **2.46** and **2.47**). Secondary alcohols were also oxidised to ketones with excellent

yields, despite the slower reactivity. More sterically encumbered and electron-poor benzylic examples (**2.48** and **2.49**) showed reduced yields, due to the slower rate of oxidation. Examples containing electrochemical activity such as nitro and halogen groups were demonstrated (**2.49** and **2.50**), although they gave a lower yield. The reduced yield is presumably due to reaction of the substrate at the cathode, even though no other products were observed. Aliphatic examples, with the exception of cyclohexanone (**2.54**) were slower to oxidise under the optimised conditions. The slower to oxidise examples showed no improvement by lowering the flow rate, but led to over-oxidation products to be observed instead. Over-oxidation products were obtained due to the increased residence time in the electrochemical cell. The optimised conditions normally led to ~30-100 mg of product per hour, depending on the example. The reactions were very clean, with only starting material, catalyst and product recovered, in most cases.[92]

Where high conversions and yields were achieved, high current efficiencies were observed.[92] The current efficiencies are calculated using Faradays law (Q = m x n x f, where Q is charge, m is moles of consumed reactant, n is the number of electrons passed and f is faradays constant) to find the amount of charge passed during the conversion of alcohol to aldehyde. This can then be divided by the actual charge passed (calculated from Q = i x t) to give the current efficiency.

Guided by cyclic voltammetry experiments, a TEMPO-mediated procedure for electrochemical oxidation of alcohols was developed and optimised. Cyclic voltammetry allowed the optimum pH to be found quickly. Not all the improvements suggested by the cyclic voltammetry results translated into improved yields in the preparative synthesis. Therefore it is important to note that this technique can be used to support and guide the development, but additional experimentation is required. Moderate to excellent yields were obtained on a range of alcohols in a single pass through the electrolysis cell, although only 60% of the TEMPO could be recovered. The reasons for this loss of TEMPO led us to conduct further cyclic voltammetry experiments to investigate the fate of the mediator, which is discussed in the next section.

2.3 A Voltammetric Study of the TEMPO Mediated Oxidation of Benzyl Alcohol in ^{t}BuOH/Water

During the optimisation of the TEMPO mediated alcohol oxidation in the electrochemical microflow cell, two significant observations were made. The observation that increasing the pH above 11.5 began to lower the limiting current, and that only 60% of TEMPO was recovered, suggests that side reactions are occurring. To investigate, a cyclic voltammetry study was initiated.

First cyclic voltammograms were collected of TEMPO (2 mM and 10 mM) in the buffered aqueous ^{t}BuOH solution at, both pH 9.3 and pH 11.7 (**Figure 2.3.1.1**). The cyclic voltammograms collected at pH 9.3, are consistent with the reversible one-electron redox couple between TEMPO (**2.22**) and oxoammonium (**2.31**), as discussed earlier. The ratio of the oxidation/reduction (anodic/cathodic) peaks is approximately one and the peak currents are proportional to the concentration of TEMPO.

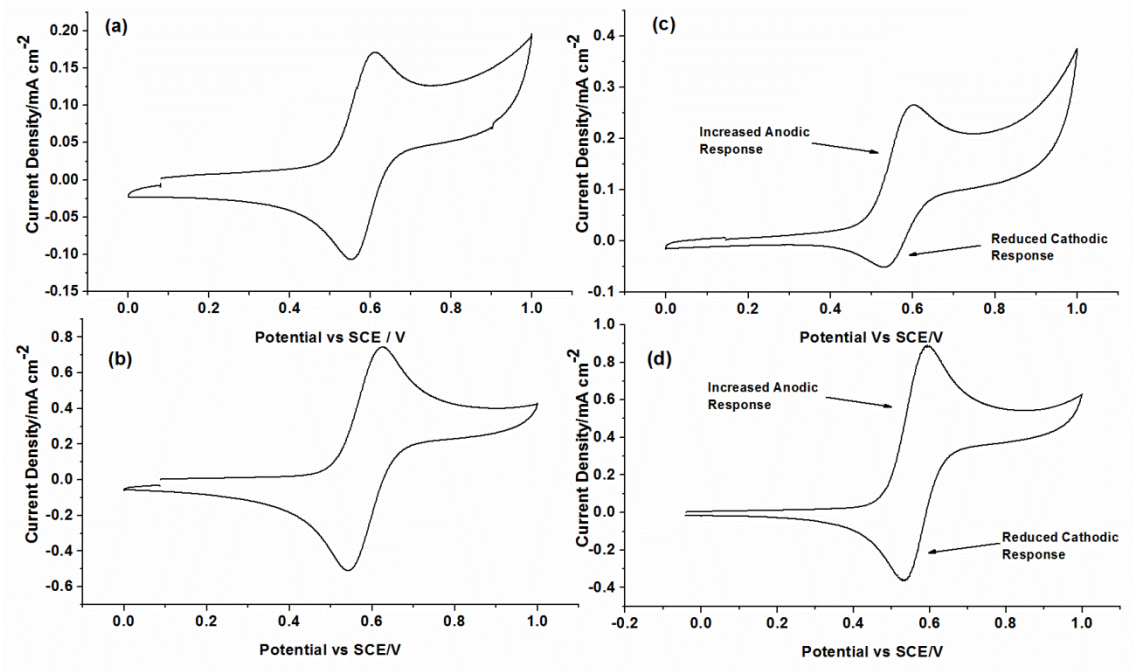

Figure 2.3.1.1 - Cyclic voltammetry at a vitreous carbon disc electrode for the TEMPO in 1:1 ^{t}BuOH/water containing sodium carbonate/bicarbonate. a) 2 mM TEMPO, pH 9.3. b) 10 mM TEMPO, pH 9.3. c) 2 mM TEMPO, pH 11.7. d) 10 mM TEMPO, at pH 11.7. Scan rate 50 mV s^{-1}. Temperature 20 °C.

At the more basic pH (11.7), the voltammograms of TEMPO become more complex. There is an increase in the anodic peak and reduction of the cathodic peak, which is more prominent in the 2 mM TEMPO solutions. The anodic peak is increased by 60%, and the ratio of anodic/cathodic peaks is 0.58. This is consistent with a reaction of the oxoammonium species **2.31** occurring, similar to the observation with added alcohol. The reaction is most likely occurring with hydroxide to give the intermediate **2.58**, as ^{t}BuOH is much bulkier and less nucleophilic (**Scheme 2.3.1.1**). The increase in the anodic current is not related to a TEMPO catalytic cycle, as there is no pathway to reform TEMPO. Therefore the increase in current must be due to further electrochemical oxidation of the intermediate **2.58**, at a similar potential to the oxidation of TEMPO. This also explains why only 60% of TEMPO is recovered in the preparative electrolysis in the microflow cell. The effects are much more reduced in the 10 mM TEMPO solutions, with only a 20% increase in the anodic peak. The reason for this is the reduced effect that the hydroxide is having, because the hydroxide concentration is constant at about 5 mM at pH 11.7, and limits the rate of the side reaction.

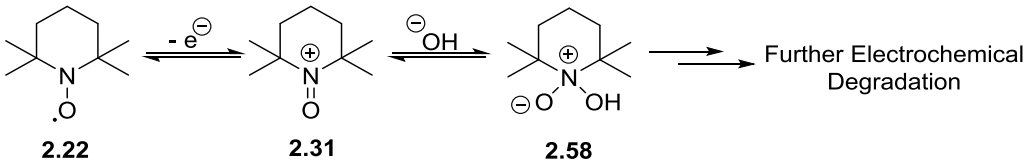

Scheme 2.3.1.1 - Reaction of oxoammonium **2.31** with hydroxide.

To further investigate the effect of high pH on the electrochemistry of TEMPO, a voltammogram in an aqueous NaOH solution at pH 13.2 was collected (**Figure 2.3.1.2**). The redox couple has become completely irreversible and the anodic peak is now consistent with a two-electron oxidation of TEMPO. The voltammogram indicates that at higher pH the reaction of oxoammonium with hydroxide is very fast, and outpaces the electrochemical reduction to TEMPO. At the higher pH a larger concentration of hydroxide is present, leading to a greater proportion of the intermediate **2.58** being present. Under these conditions a second electron transfer occurs and the electrochemical degradation of the intermediate **2.58** is rapid, leading to the observed increase in anodic current.

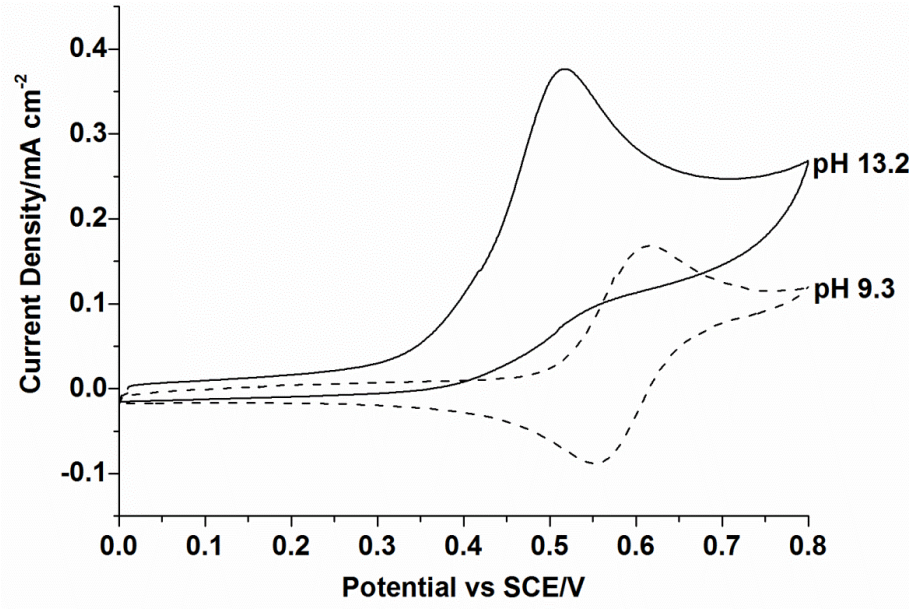

Figure 2.3.1.2 - Cyclic voltammograms at a vitreous carbon disc electrode for 2 mM TEMPO (**2.22**) in 1:1 ^{t}BuOH/water. pH 9.3 contained sodium carbonate/bicarbonate buffer. pH 13.2 contained NaOH. Scan rate 50 mV s^{-1}. Temperature 20 °C.

The effect of pH on the TEMPO/hydroxylamine (**2.22**/**2.32**) redox couple was also investigated (**Figure 2.3.1.3**). Voltammograms were obtained for 10 mM TEMPO (**2.22**) solutions in aqueous ^{t}BuOH buffered solutions at pH 9.3, 10.7 and 11.7. As the basicity of the solution is increased the reduction peak and oxidation peak shift to a more negative potential, at approximately ~70 mV per pH unit. This is consistent with an EC mechanism occurring, where an electron transfer is followed by proton transfer (**Scheme 2.3.1.2**). The change in potential is due to a shift in the equilibrium potential, where under basic conditions the removal of the proton is easier, reducing the potential required to oxidise the hydroxylamine **2.32**.

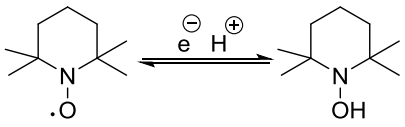

2.22 **2.32**

Scheme 2.3.1.2 - Redox couple of TEMPO and hydroxylamine **2.32**.

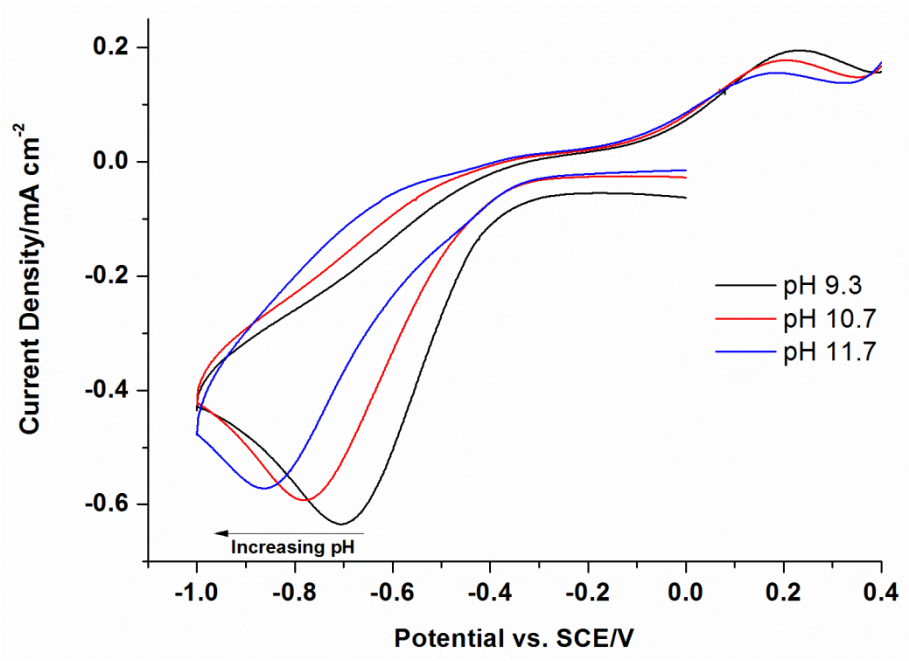

Figure 2.3.1.3 - Cyclic voltammograms at a vitreous carbon electrode for the reduction of TEMPO (10 mM) in 1:1 ^{t}BuOH/water containing sodium carbonate/bicarbonate at pH 9.3, 10.7 and 11.7. Scan rate 50 mV s^{-1}. Temperature 20 °C.

The more basic conditions have a positive effect on the electrochemical regeneration of TEMPO from hydroxylamine **2.32**, by facilitating the removal of a proton. Moreover the comproportionation equilibrium, discussed earlier, favours the regeneration of TEMPO under basic conditions. On the other hand, in an aqueous system increasing the basicity leads to a more rapid reaction between the oxoammonium **2.31** and hydroxide. For successful preparative electrolysis a balance between improved TEMPO turnover and TEMPO degradation needed to be found. The balance was achieved at pH 11.5, as demonstrated by the early cyclic voltammetry and the conditions applied to the electrochemical microflow cell, although only 60% of the TEMPO could be recovered.

The effect of alcohol concentration was also investigated, to help understand the rate of benzyl alcohol oxidation and the mechanism. Cyclic voltammograms were collected in the aqueous ^{t}BuOH solution buffered at pH 11.5, with varying concentrations of benzyl alcohol (**Figure 2.3.1.4**).

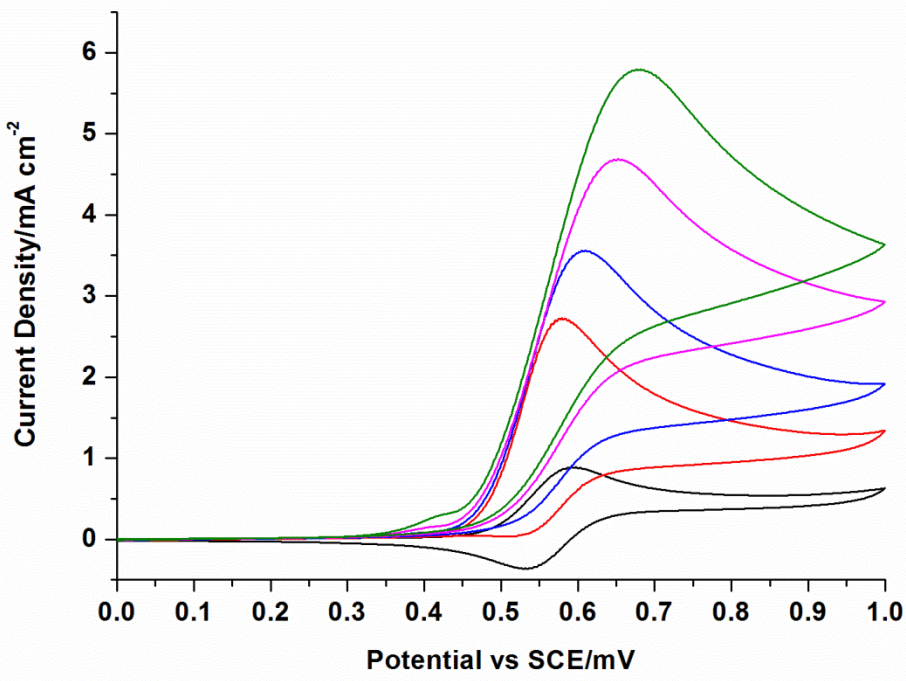

Figure 2.3.1.4 - Cyclic voltammograms at a vitreous carbon electrode for 10 mM TEMPO in 1:1 ^{t}BuOH/water containing sodium carbonate/bicarbonate at pH 11.5. Scan rate 50 mV s^{-1}. Temperature 20 ˚C. Added benzyl alcohol: black curve - 0 mM. Red curve - 10 mM. Blue Curve - 20 mM. Pink curve - 40 mM. Green curve - 80 mM.

Even in a 1:1 mixture of TEMPO and BnOH, the cathodic peak is absent (red curve), suggesting that the initial reaction between the oxoammonium ion **2.31** and BnOH (**2.42**) is fast. Higher loadings of BnOH lead to increases in the anodic peak, but not at a rate expected, if the regeneration of TEMPO is fast. This is further exemplified by **Figure 2.3.1.5**. The data are presented as a plot in dimensionless parameters; the current ratio vs. the excess factor. The current ratio is the ratio of the catalytic current to the peak current for the oxidation of TEMPO at pH 9.3 in the absence of alcohol. The excess factor is the ratio of benzyl alcohol concentration to TEMPO concentration.

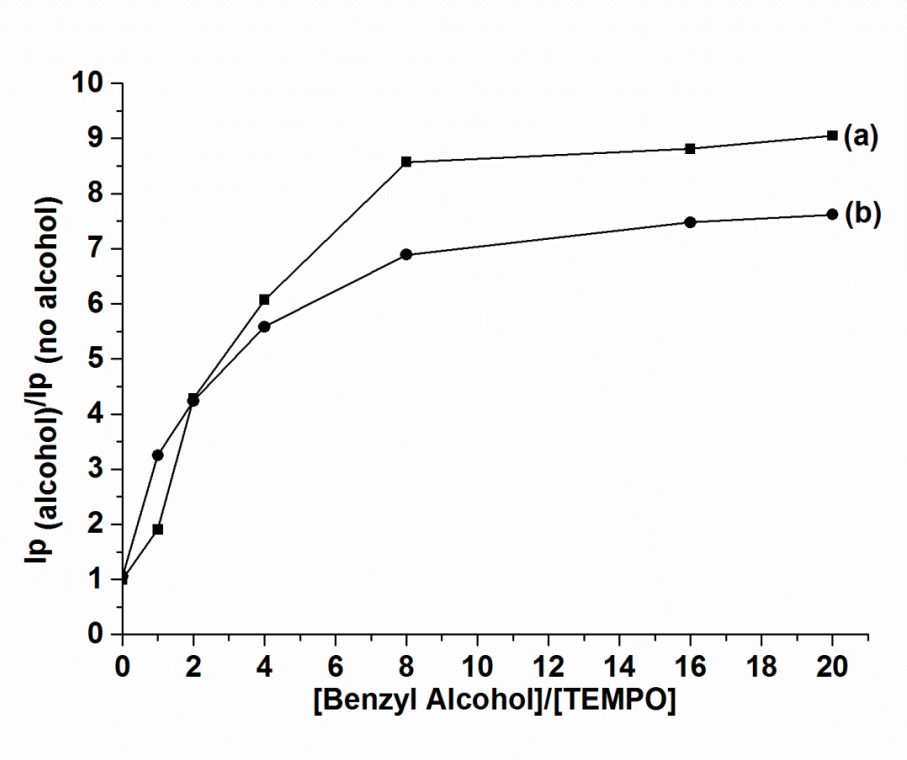

Figure 2.3.1.5 - The influence of TEMPO and benzyl alcohol concentrations on the rate of conversion of benzyl alcohol to benzaldehyde. The data is presented as a plot in dimensionless parameters. a) 2 mM TEMPO. b) 10 mM TEMPO. 1:1 ^{t}BuOH/water with sodium carbonate/bicarbonate at pH 11.5. Temperature 20 °C

Plotting **Figure 2.3.1.5** as dimensionless parameters summarises how the catalytic rate for the benzyl alcohol oxidation varies with alcohol concentration. Although the rate of the regeneration of TEMPO is significant at pH 11.5, and good enough to achieve high conversion in the electrochemical microflow cell, it is not at a mass transport controlled rate. If it was, a current ratio of ~17 would be observed if an 8 mM solution of benzyl alcohol underwent a two-electron oxidation (2 electrons x 8 mM + 1 electron for TEMPO oxidation). The initial reaction between oxoammonium and benzyl alcohol (**2.42**) to give intermediate **2.59** has been shown to be fast by cyclic voltammetry, by the disappearance of the reduction peak of the TEMPO/oxoammonium redox couple. As the cyclic voltammetry is no longer mass transport controlled, a step in the rearrangement of intermediate **2.59** to give benzaldehyde (**2.43**) must be rate determining (**Scheme 2.3.1.3**). The effect of pH on the reaction suggests that the step involves a deprotonation.

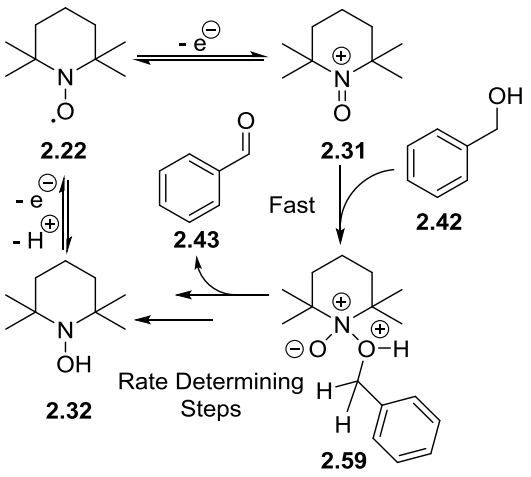

Scheme 2.3.1.3 - Rate determining steps of the TEMPO mediated alcohol oxidation.

These investigations were further supplemented with chemical investigations. The oxidation of benzyl alcohol with an equivalent of oxoammonium salt was monitored by gas chromatography, at pH 11.5 and pH 13.4. The initial oxoammonium salt selected was oxoammonium bromide (**2.60**), which was synthesised by the method of Sheldon *et al.*[67] (**Scheme 2.3.1.4**). Upon more careful analysis of the product, it was shown to be actually oxoammonium tribromide (**2.61**) by elemental analysis. The formation of the tribromide counter-ion could have occurred due to the possible excess addition of bromine to the reaction mixture. Tribromide ion can act as an oxidant, potentially recycling the TEMPO, which would affect the results.

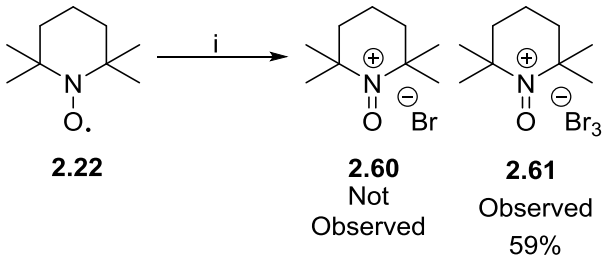

Scheme 2.3.1.4 - Synthesis of oxoammonium salt **2.61**. *Reagents & conditions* - i) TEMPO (**2.22**), Br_2 (1.01 equiv.) in Hexane. 30 min, rt.

Therefore the oxoammonium tetrafluoroborate **2.62** was synthesised instead. This was achieved by disproportionation of TEMPO with aqueous tetrafluoroboric acid (**Scheme 2.3.1.5**).[89]

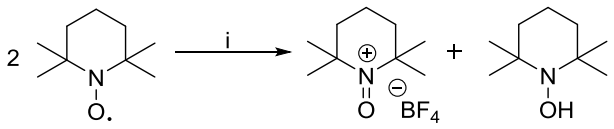

Scheme 2.3.1.5 - Synthesis of oxoammonium salt **2.62**. *Reagents & Conditions* - i) **2.22**, tetrafluoroboric acid (48 % aq. sol.) in water, 30 min, rt.

Benzyl alcohol (**2.42**) was oxidised to benzaldehyde (**2.43**) by adding one equivalent of the oxoammonium salt **2.62**, at pH 11.5 and 13.4, to the reaction mixture (**Scheme 2.3.1.6**). Sufficient buffer was added to maintain the pH during the reaction, as one equivalent of HBF_4 is released during the stoichiometric oxidation.

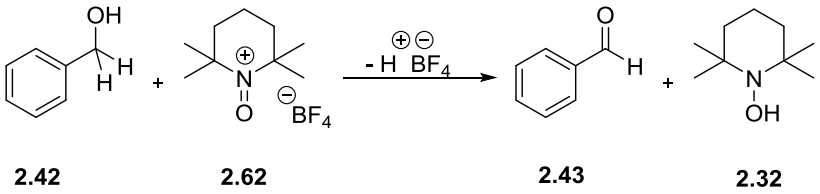

Scheme 2.3.1.6 - Stoichiometric oxidation of BnOH (**2.42**) with oxoammonium salt **2.62** in 1:1 ^{t}BuOH/water at pH 11.5 or 13.4.

The GC yields from the oxidation of BnOH with the oxoammonium salt **2.62** can be observed in **Table 2.3.1.1** (the calibration can be found in the experimental section). Good yields were achieved at pH 11.5, even when 0.5 equivalents of the oxoammonium salt **2.62** was added. Yields were greatly reduced when the reaction was performed at pH 13.4. When the oxoammonium salt **2.62** was pre-mixed in the reaction mixture prior to the addition of BnOH, no alcohol oxidation product was observed.

pH	Reactants		GC Yield of Benzaldehyde
	Benzyl alcohol/ mmol	Oxoammonium 2.62/ mmol	
11.5	0.19	0.19[a]	70%
11.5	0.19	0.10[a]	37%
11.5	0.19	0.19[b]	0%
13.4	0.19	0.19[a]	8%
13.4	0.19	0.19[b]	0%

Table 2.3.1.1 - Reaction of oxoammonium tetrafluoroborate with benzyl alcohol in 1:1 ^{t}BuOH/water at pH 11.5 or 13.4. Yield was determined using a calibrated GC. a) Oxoammonium salt **2.62** added to solution of benzyl alcohol. b) BnOH added to pre-mixed solution of oxoammonium salt **2.62**.

These results are consistent with observations made during the cyclic voltammetry, where under more strongly basic conditions the yield of the alcohol oxidation was reduced. This is believed to be due to the side reaction of the oxoammonium with hydroxide, out-pacing the oxidation of benzyl alcohol. At pH 11.5, the oxoammonium reaction with hydroxide is still occurring, as confirmed with the cyclic voltammetry, but at a reduced rate, allowing the oxidation pathway to dominate.

Attempts were made to isolate the intermediates and products from the destructive reaction between the oxoammonium salt **2.62** and hydroxide. Unfortunately the results were inconclusive. Some studies on oxoammonium analogues have been reported in the literature. Golubev investigated the degradation of the oxoammonium perchlorate salt **2.63**, in a basic NaOH solution.[94] The degradation of the oxoammonium salt **2.63** followed two main pathways leading to the observation of the 4-oxo-TEMPO **2.23** (41%), nitroxide **2.64** (15%), acetone (15%) and dimer **2.65** (25%) as products by HPLC (**Scheme 2.3.1.7**).

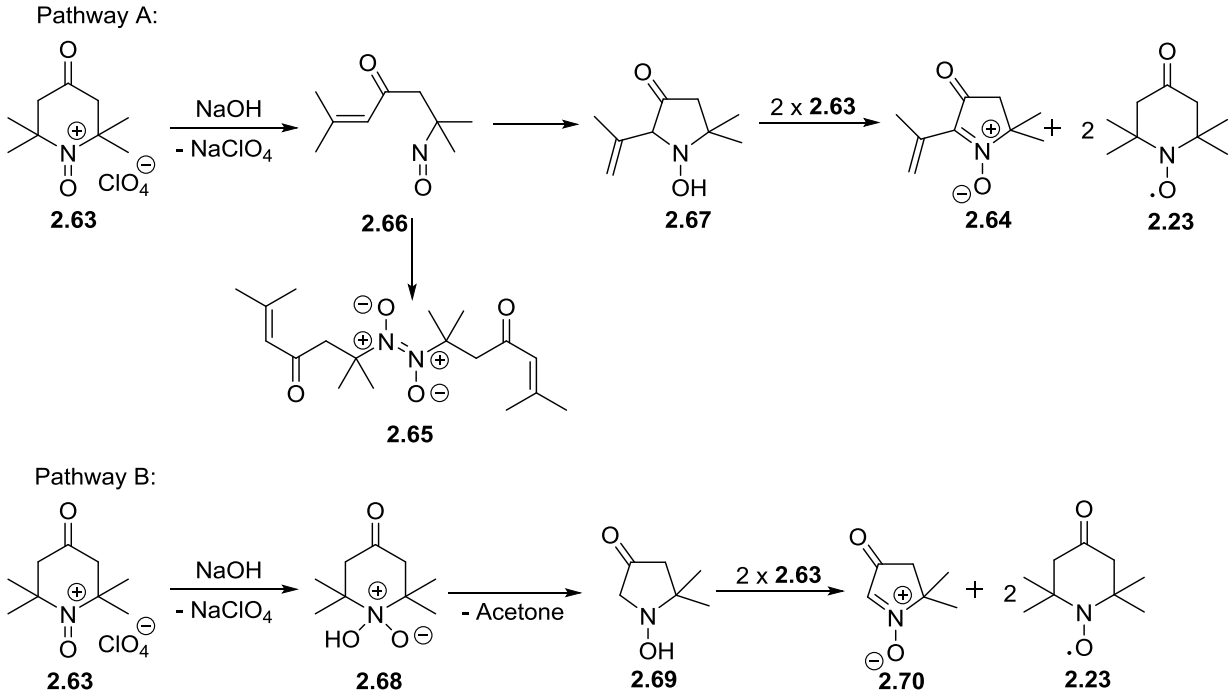

Scheme 2.3.1.7 - Degradation pathways of oxoammonium salt **2.63**.

Degradation pathway A is initiated by the deprotonation of the α-proton to the carbonyl, leading to the ring-opened intermediate **2.66**. Dimerisation of the ring opened intermediate **2.66** leads to dimer **2.65**, which was observed by HPLC. Alternatively **2.66** can cyclise to give the intermediate **2.67**, which can be oxidised using two equivalents of oxoammonium salt **2.63** to the nitrone **2.64**.[94] The oxidation of **2.67** leads to further loss of the oxoammonium salt **2.63**, regenerating the TEMPO analogue **2.23**. The presence of the oxo-group in **2.63**, in the 4-position, increases the acidity of the alpha-protons, facilitating the reported degradation pathways. As an oxo-group is not present in our system, the rate of deprotonation following pathway A would be reduced, as the protons are not as acidic. The alternative degradation route, following pathway B would be more likely in our system. Pathway B begins with an initial attack by the hydroxide at the nitrogen centre to give intermediate **2.68**, which is unstable and eliminates acetone *via* a retro-aldol pathway to give **2.69**.[94] Further oxidation of **2.69** gives the nitrone **2.70** and the TEMPO analogue **2.23**. The oxidation of intermediate species such as **2.69** provides an alternative pathway for further loss of oxoammonium oxidants, reducing the efficiency of alcohol oxidation.[94]

Moad observed the nitrone **2.71** and TEMPO (**2.22**) as products when oxoammonium **2.31** was treated with sodium or silver benzoate (**Scheme 2.3.1.8**), following a similar degradation mechanism as pathway A.[95] The oxoammonium salt **2.31** is present in our system; therefore the reported degradation pathways leading to the nitrone could be possible. In all the discussed possible degradation pathways a significant quantity of nitrone is formed after oxidation.[94,95] Discussed earlier during our cyclic voltammetry experiments was the observation of increased anodic current densities at higher pH. The degradation pathway towards the nitrone could explain the higher current densities observed, either through a direct two-electron oxidation of **2.73** to give the nitrone **2.71**, or through the regeneration of TEMPO as a result of the degradation pathway. Therefore our cyclic voltammetry experiments suggest the presence of nitrone analogues, although through our preparative experiments we were unable to confirm the presence of these species.

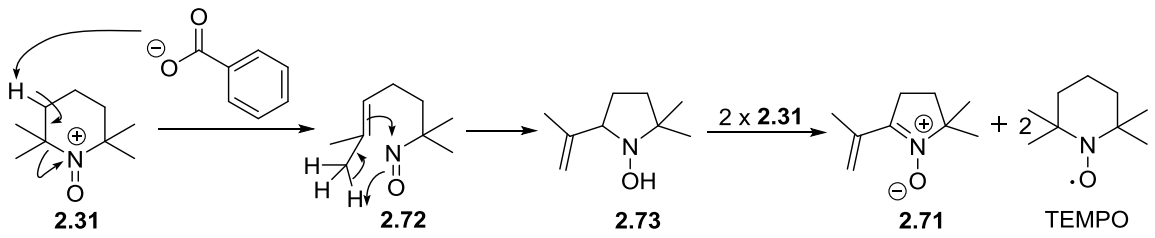

Scheme 2.3.1.8 - Degradation of **2.31** to give nitrone **2.71**.

Combining the information generated from the cyclic voltammetry and chemical reactions provides insights into the overall mechanism of the electrochemical TEMPO mediated alcohol oxidation (**Scheme 2.3.1.9**). Initial rapid nucleophilic attack of the active oxoammonium, generates the intermediate **2.41**, after loss of a proton. This is consistent with the literature and the cyclic voltammetry and is fast at all pH in the range investigated (pH 9.3-11.7). The increased rate of reaction observed with increased pH, suggests that the rate determining step involves a deprotonation. The likely source is the deprotonation to give the intermediate **2.41**, which is followed by a *syn* elimination-type process to give the hydroxylamine **2.32** and the oxidised alcohol product. As a competing process, hydroxide can attack **2.31** to give **2.58**, which then undergoes further degradation, most likely to a

hydroxylamine intermediate, which is electrochemically active giving a nitrone after oxidation, following one of the degradation pathways discussed earlier.

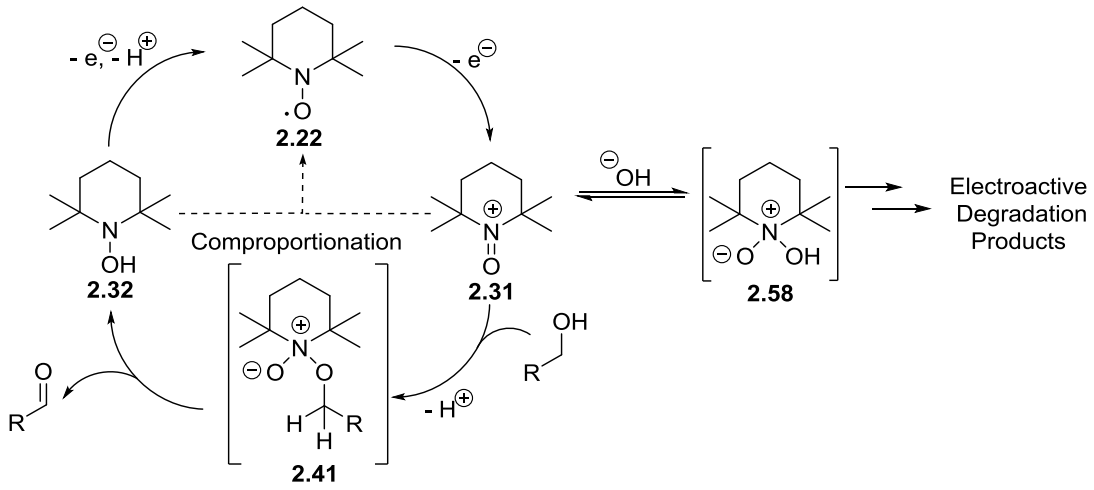

Scheme 2.3.1.9 - Electrochemical TEMPO mediated alcohol oxidation in basic aqueous ^{t}BuOH.

At pH 11.5, the conditions used in the electrochemical microflow cell, good conversions are achieved, although only 60% of TEMPO is recovered. The source of the loss of recovered TEMPO has been shown to be due to a competing reaction with hydroxide to give the intermediate **2.58**. The intermediate **2.58** can then undergo further electrochemical and chemical reaction, leading to the degradation of TEMPO. At pH 11.5 the alcohol oxidation outpaces the reaction with hydroxide, due to the relative concentrations of alcohol and hydroxide. During the reaction in the microflow cell, the alcohol is consumed, leading to the concentration balance being shifted towards a larger ratio of hydroxide to alcohol being present at the end of the flow cell. Therefore as the electrolysis continues the reaction with hydroxide will begin to dominate, leading to the observed 60% recovery of TEMPO. At pH 13.4 the concentration of hydroxide is higher, compared to the alcohol, therefore reaction with the hydroxide becomes the dominant pathway. The cyclic voltammetry shows that the reaction of oxoammonium **2.31** with hydroxide to give the intermediate **2.58** and subsequent electrochemical degradation can outpace the electrochemical reduction of TEMPO, by the disappearance of the cathodic peak. Furthermore the degradation is either electrochemical or regenerates TEMPO shown by the observed increase in current density in the cyclic voltammograms

2.4 Conclusions & Future Work

The research discussed in this chapter has led to the optimisation of a new procedure for the oxidation of alcohols in an electrochemical microflow cell.[92] Cyclic voltammetry was used to guide the optimisation process, by investigating the effect of pH on the electrochemical oxidation of TEMPO. On discovering the optimal conditions of pH 11.5 in an aqueous ^{t}BuOH buffered media, the procedure was successfully applied to the oxidation of a range of alcohols, achieving good to excellent conversions and yields.

The observation that only 60% of TEMPO was recovered in the preparative reaction, led to further investigations, combining synthetic and cyclic voltammetry techniques. The results led to insights on the rate determining step of the oxidation reaction, and the possible electrochemical degradation of TEMPO caused by hydroxide.

Future work could include applying the optimised procedure to more complex substrates, during a total synthesis of a natural product or pharmaceutically relevant target. This would further identify the scope and limitations of the flow electrolysis procedure. Further investigations into the degradation pathways of TEMPO/oxoammonium could also be explored. Isolating the degradation products would lead to a better understanding of the process, so that conditions could be identified to suppress undesired pathways. Reducing the undesired pathways could lead to an improved recovery of TEMPO, improving the environmental impact of the reaction. Moving away from an aqueous system may be required if the dominant degradation is occurring from the reactions with hydroxide ions.

3 Electrochemical Oxidative Esterifications and Amidations in Microflow

3.1 Introduction

3.1.1 *N*-Heterocyclic Carbenes (NHCs)

N-Heterocyclic carbenes (NHCs) are a large class of stable carbenes that have, in recent years, been extensively used as ligands in organometallic complexes and organocatalysts.[96-111] The isolation of **3.01**, the first stable NHC, by Arduengo *et al.* led to an explosion of different NHCs available, typically based upon imidazole, triazole and thiazole rings (**Figure 3.1.1.1**).[96]

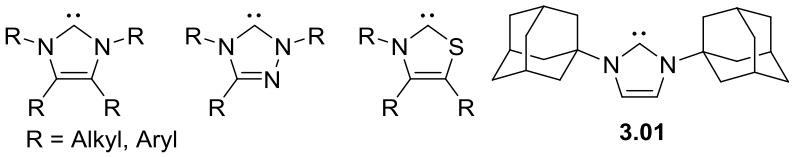

Figure 3.1.1.1 - Types of NHCs.

Like other carbenes, NHCs contain a divalent carbon with a valence electron shell sextet. Unlike other carbenes, they are not just reactive intermediates and can be stable at room temperatures. Some of this stability is due to the presence of bulky substituents surrounding the carbene centre. There is also a strong electronic stabilisation effect from the lone pair of electrons on the nitrogen interacting with the p orbital of the sp^2 hybridised carbene (**Scheme 3.1.1.1**). These electronic effects also explain why NHCs behave as electron-rich nucleophiles, in contrast to other carbenes which are generally electrophilic in character.[99,100,102,105]

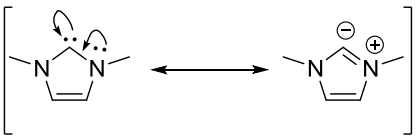

Scheme 3.1.1.1 - Resonance structures of NHCs.

NHCs have been utilised extensively as σ-donor, π-acceptor ligands in organometallic complexes, perhaps most famously in the Grubb's II metathesis

pre-catalyst **3.02** (**Figure 3.1.1.2**). The ability to fine tune the electronic and steric properties of the organometallic complex by changing the substituents surrounding the carbene centre has led to their application in a range of catalysts. This has been well documented in the literature.[105] Our interests here concern the use of NHCs as organocatalysts which will be discussed in the next section.

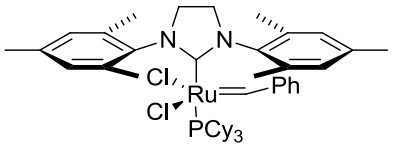

Grubb's II Catalyst

3.02

Figure 3.1.1.2 - Examples of NHCs as ligands.

3.1.2 NHCs as Organocatalysts

The requirement for novel, efficient and environmentally friendly chemical transformations, has led to a huge amount of interest into the area of organocatalysis. One of the most powerful classes of organocatalysts to be identified are NHCs. Over the past 20-30 years there have been numerous publications and reviews on this topic, and some examples will be discussed in the following section.[98,101,102,104,106,108-111]

The development of NHC organocatalysts has led to a huge variety of catalysts available. As discussed earlier, some of these NHCs are 'stable', when stored under an inert atmosphere.[107] The majority of NHCs cannot be isolated under these conditions, so are usually synthesised and stored in the form of precursor salts. The NHCs are then formed by deprotonation, using a suitable base such as DBU (**Scheme 3.1.2.1**). The highly reactive nature of the NHCs means that reactions are typically performed in dry solvents, under an inert atmosphere.[101,108]

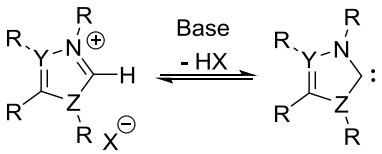

Scheme 3.1.2.1 - Formation of NHC by deprotonation.

The main reaction modes of NHC catalysts can be understood by their σ-donor and π-acceptor properties, which are summarised in **Table 3.1.2.1**.[98,102]

Property	**Reaction Mode**	**Example**
σ-donor	Nucleophilic Attack of Carbonyls	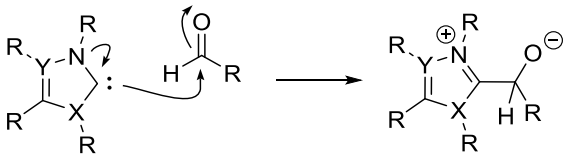
σ-donor	Deprotonation	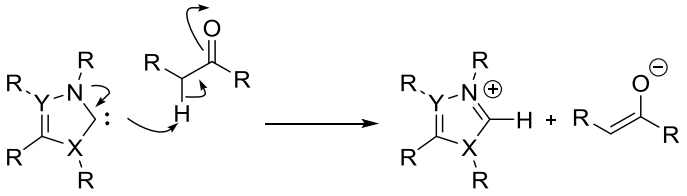
σ-donor	Enamine Reactivity with Electrophiles (Can be Conjugated)	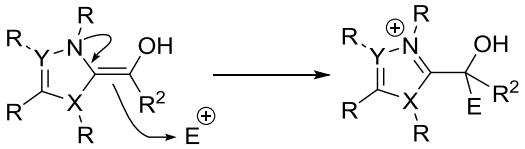
σ-donor	Enamine Reactivity Leaving Group Elimination	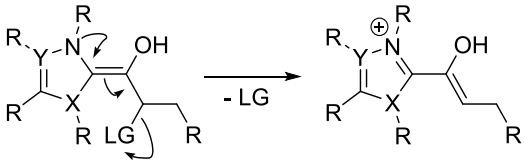
π-acceptor	Leaving group	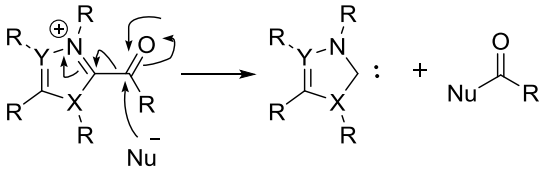 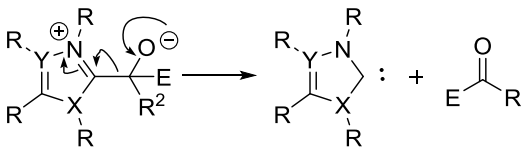
π-acceptor	α-Acidity	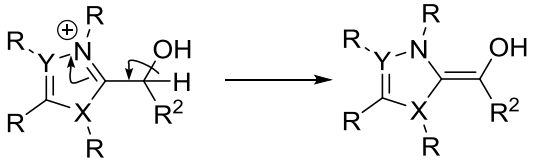

Table 3.1.2.1 - Properties and reaction modes of NHCs.

Additionally other reaction modes have been identified that do not directly involve the NHC moiety, but its presence allows the reaction to occur (**Table 3.1.2.2**). Different combinations of these reaction modes have allowed a wide variety of synthetic transformations to be achieved using NHCs.[98,102]

Reaction Mode
Hydride Transfer 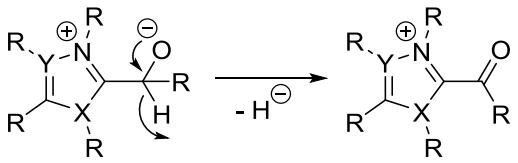
Enolate Reactivity 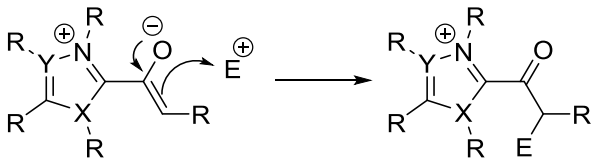
Dual Activation 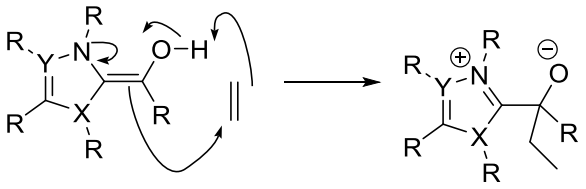

Table 3.1.2.2 - Reaction modes facilitated by NHCs.

A key feature of NHC catalysed reactions is the ability to invert the reactivity of a carbonyl (Umpolung). The umpolung reactivity is exemplified with one of the most studied NHC catalysed reactions; the Benzoin condensation.

The Benzoin condensation is the coupling of two benzaldehydes (**2.43**) to give benzoin (**3.03**) (**Scheme 3.1.2.2**). Cyanide was first noted to catalyse this transformation by Wöhler and Liebig in 1832.[112] The mechanism was postulated by Lapworth in 1903, in which a cyanohydrin intermediate is formed by addition of HCN to the carbonyl of an aldehyde, inverting the reactivity (Umpolung).[113] The inverted reactivity allows the attack of another equivalent of

benzaldehyde, which is followed by elimination of cyanide to give the benzoin product **3.03**.

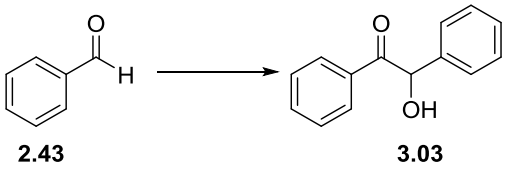

Scheme 3.1.2.2 - Benzoin condensation.

The first example of an NHC used to catalyse the benzoin condensation was demonstrated by Ugai in 1943.[114] Ugai noted that vitamin B_1 (**3.04**), a thiazolium derivative, could catalyse the reaction. An important breakthrough was the discovery of the accepted mechanism by Breslow in 1958 (**Scheme 3.1.2.3**).[115] He postulated that the NHC acted in a similar way to the cyanide in the cyanide-catalysed benzoin condensation, in that the carbonyl's reactivity could be inverted by the NHC.

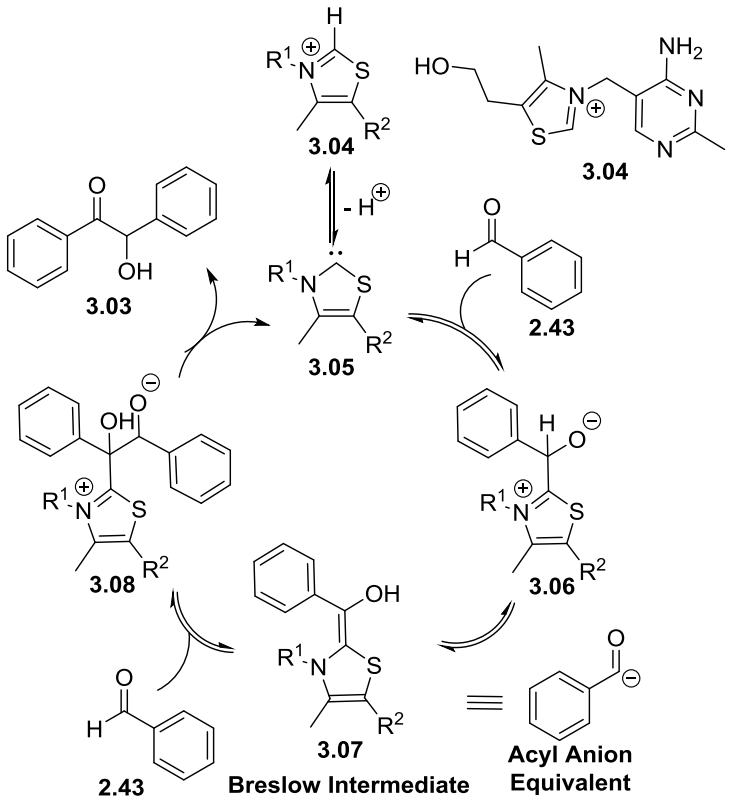

Scheme 3.1.2.3 - NHC catalysed benzoin condensation mechanism.

Breslow realised that vitamin B_1 (**3.04**) can be deprotonated under mildly basic conditions to give the NHC **3.05** *in situ*, which would react with benzaldehyde

(**2.43**) to give the intermediate **3.06**. This then undergoes tautomerisation to give **3.07**, known as the Breslow intermediate. The Breslow intermediate can be considered as an acyl anion equivalent; the reactivity of aldehyde has been inverted. The Breslow intermediate **3.07** can now act as a nucleophile attacking the electrophilic aldehyde to give **3.08**, which eliminates benzoin (**3.03**), regenerating the NHC **3.05**, allowing the catalytic cycle to continue. All the steps shown in this mechanism are covered by the NHC reaction modes discussed earlier.

A key intermediate present in the vast majority of NHC catalysed reactions is the Breslow Intermediate. Its presence is key in another two of the most studied NHC reactions, the Stetter reaction and NHC catalysed homoenolate chemistry.[98,101,102,106,108-110]

In 1976 Stetter extended the NHC's ability to convert the reactivity of aldehydes by coupling them with Michael acceptors.[116] This allows quick and easy access into a variety of 1,4-difunctional molecules (**Scheme 3.1.2.4**).[101] The mechanism is similar to that of the benzoin condensation, forming the Breslow intermediate. The Breslow intermediate can then attack a Michael acceptor, giving the otherwise difficult to achieve substituted 1,4-difunctionalised products, after elimination of the NHC.[101]

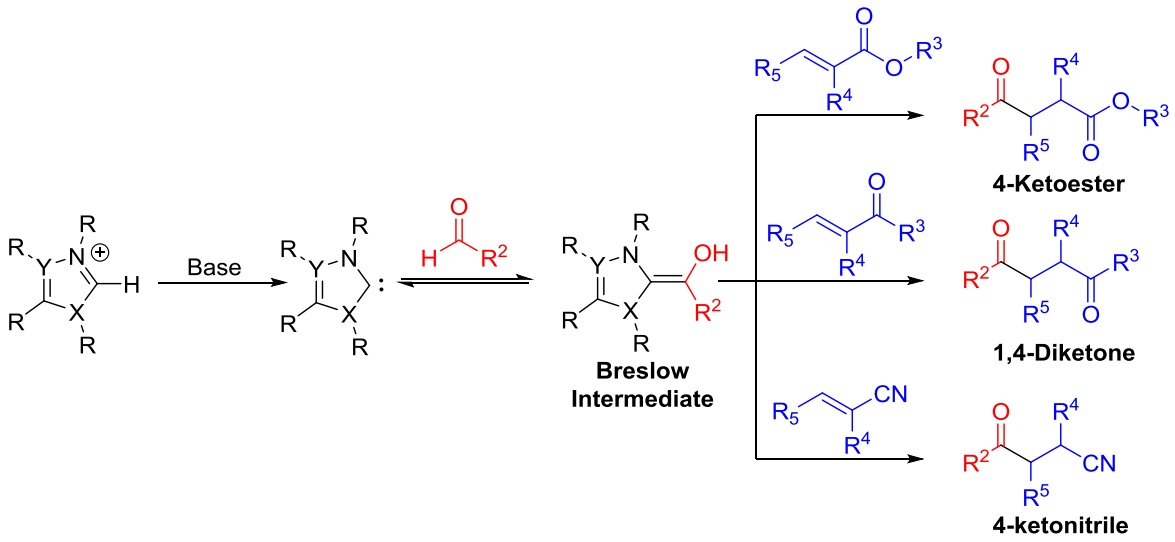

Scheme 3.1.2.4 - Stetter reaction with different Michael acceptors generating diverse 1,4-dicarbonyl products.

Homoenolate chemistry with NHCs was first introduced by Bode and Glorius when they independently presented the formation of γ-butyrolactones (**3.09**), from α,β-unsaturated aldehydes and benzaldehydes in 2004.[117,118] The common Breslow intermediate **3.10** is present, and the method has been extended to produce a variety of highly functionalised products. For example reaction with an imine gives a γ-lactam (**3.11**), or a 1,2-dione gives a spiro-γ-butyrolactones (**3.12**), or finally an aryl-ketone gives a cyclopentene (**3.13**), all with good diastereoselectivity (**Scheme 3.1.2.5**).[98,101,102,106,109]

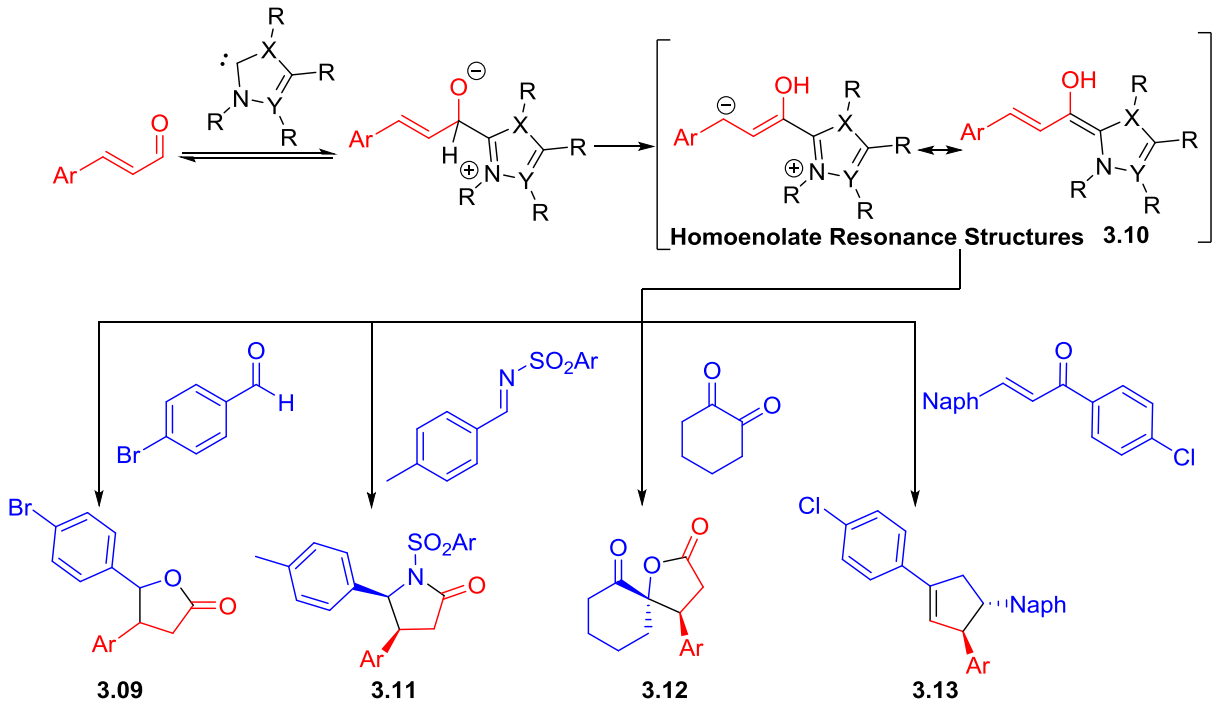

Scheme 3.1.2.5 - Homoenolate formation and examples of further reactions.

The success of these reactions is often dependent on the NHC chosen. Differing electronic and steric effects of the thiazoles, imidazoles and triazoles, can have a large effect on the reaction. As a consequence there are now a variety of NHC catalysts commercially available, including a large selection of chiral NHCs such as triazole salts **3.14** and **3.15**. This has enabled many variations of the discussed reactions to be developed, including asymmetric, inter and intra-molecular versions (**Scheme 3.1.2.6**).[98,101,102,106,109]

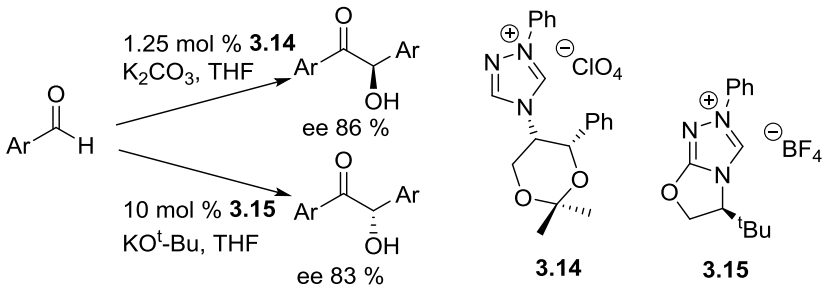

Scheme 3.1.2.6 - Examples of asymmetric benzoin condensation.

The three classes of NHC catalysed reactions briefly discussed, were chosen as they are the most heavily explored and there is now a vast amount of literature dedicated to them. It is important to note other reactions have been reported in this rapidly expanding field, but they still follow the reaction modes discussed earlier.[100,102-104,106,110,111] It is clear though from the examples discussed the power of NHC catalysis to generate challenging products simply, with multiple stereo-centre control.

3.1.3 NHC mediated Oxidative Esterifications

A rapidly expanding area of particular interest to the research described in this thesis is the area of oxidative NHC catalysis. This has been achieved utilising internal redox and external oxidants, and has recently been reviewed.[104,110,111] Oxidative NHC catalysis research has been successfully applied to the conversion of aldehydes to esters, and therefore will be the focus of the discussion in this section.

The field of NHC mediated internal redox catalysis utilises the reduction of α-functionality, to oxidise up to the aldehyde, to give saturated products. The concept was first introduced by Rovis and Bode, when they independently reported the esterification of α-halo aldehydes, and epoxy aldehydes catalysed by the NHCs pre-catalysts **3.16** and **3.17** respectively (**Scheme 3.1.3.1**).[119,120]

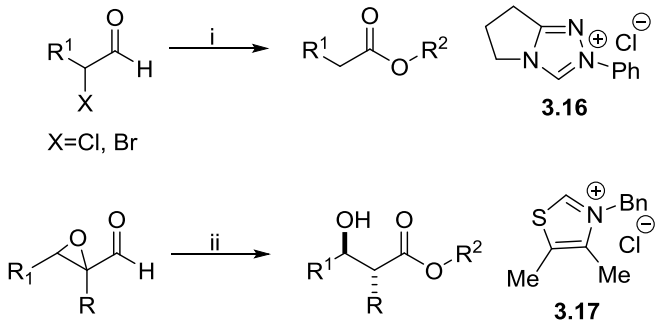

Scheme 3.1.3.1- Redox esterification introduced by Rovis and Bode. *Reagents & conditions* - i) NHC salt **3.16** (20 mol %), alcohol (excess) and Et_3N (1.0 equiv.). ii) NHC salt **3.17** (10 mol %), alcohol (excess) and $^{i}Pr_2NEt$ (8 mol %).

Since the first examples, a variety of α-reducible aldehydes have been demonstrated to undergo NHC redox catalysis to yield a range of products. Aldehydes such as α,β-unsaturated aldehydes (**3.18**), formyl cyclopropane aldehydes (**3.19**), oxacycloalkyl carboxyaldehydes (**3.20**) (intramolecular to give lactones), propargylic aldehydes (**3.21**) and dichloroaldehydes (**3.22**), have been shown to be effective using different NHC catalysts (**Figure 3.1.3.1**).[110]

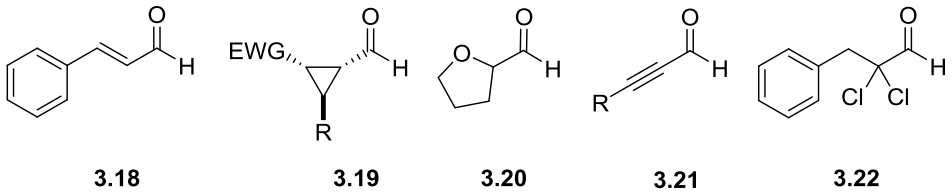

Figure 3.1.3.1 - Examples of α-reducible aldehydes.

The proposed mechanism based on the work of Rovis and Bode follows the reaction modes of NHC catalysts discussed earlier. Initial nucleophilic attack of the NHC to generate intermediate **3.23**, which then rearranges to give the Breslow intermediate **3.24**. Loss of the leaving group follows to give **3.25**, which tautomerises to give **3.26**. The acylated intermediate **3.26** is then intercepted by an alcohol to give an ester and regenerate the NHC (**Scheme 3.1.3.2**).[119,120]

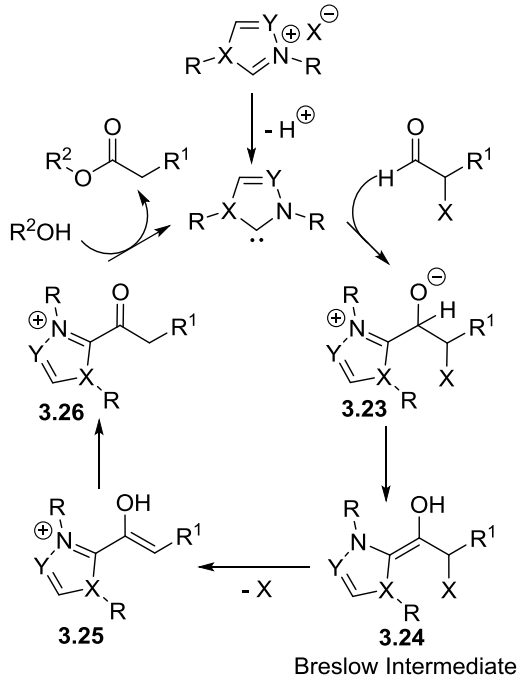

Scheme 3.1.3.2 - Internal redox esterification mechanism.

Bode reported that the strength of the base used to generate the NHC *in situ* can have an important effect on the outcome of the reaction, when using α,β-unsaturated esters.[121] When using KO^{t}Bu a lactone dimer is formed as the major product, whereas use of a tertiary amine base (e.g. DIPEA) leads to the saturated ester. The lactone dimerization occurs by nucleophilic addition of the homoenolate **3.27**, to another equivalent of aldehyde to give **3.28**. Tautomerisation follows to give **3.29**, which can be trapped by the intra-molecular alkoxide to give the lactone **3.30** (**Scheme 3.1.3.3**). The lactone pathway is thought to occur due to the lack of a suitable proton source, caused by the pKa difference between the conjugate acids of the two bases (^{t}BuOH compared to ^{i}Pr$_2$EtNH$^+$).[110,121]

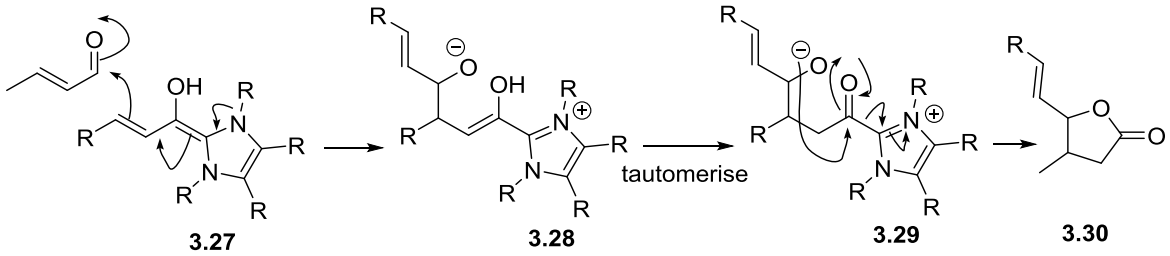

Scheme 3.1.3.3 - NHC catalysed lactone formation when using KO^{t}Bu.

The internal redox method has been successfully applied to yield a range of products, from many substrates, including aromatic alcohols, aliphatic alcohols and phenols. Chiral examples have also been demonstrated, when an appropriate NHC is utilised.[110] The drawback of this approach is the requirement for functionalised aldehydes, which need to be synthesised. Also the leaving group required to drive the internal redox reduces the atom efficiency of the method. These problems led to the development of procedures utilising external oxidants.[104,111]

The origin of external oxidative esterifications can also be traced back to the used of cyanide as a catalyst, when Corey reported its ability to catalyse the conversion of aldehydes to esters, using MnO_2 as an oxidant.[122] Scheidt in 2008 adapted this using NHCs.[123] The mechanism follows a similar path to those already discussed, in that the NHC attacks the aldehyde, leading to the Breslow Intermediate **3.31**. This can then be oxidised by an external oxidant leading to **3.32**. The acylated intermediate then reacts with an alcohol to yield an ester and regenerate the NHC (**Scheme 3.1.3.4**).

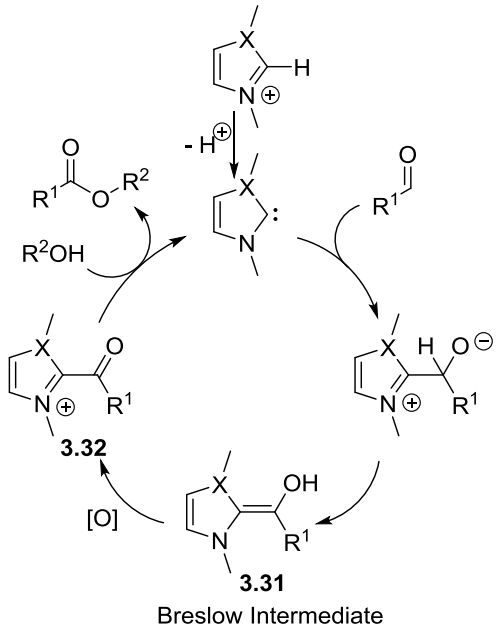

Scheme 3.1.3.4 - NHC mediated esterification with external oxidants.

Since the introduction of MnO_2, many other oxidants have been shown to be effective in this transformation.[104,111] Oxidants such as $K_3[Fe(CN)_6]$, phenazine (**3.33**), acridine (**3.34**), the quinone **3.35**, the riboflavin derivative **3.36**, azobenzene (**3.37**) and nitrobenzene (**3.38**), have been reported

(**Figure 3.1.3.2**). Although it is important to note that the nitrobenzene examples may follow a different mechanism dependent on the substrates involved.[111]

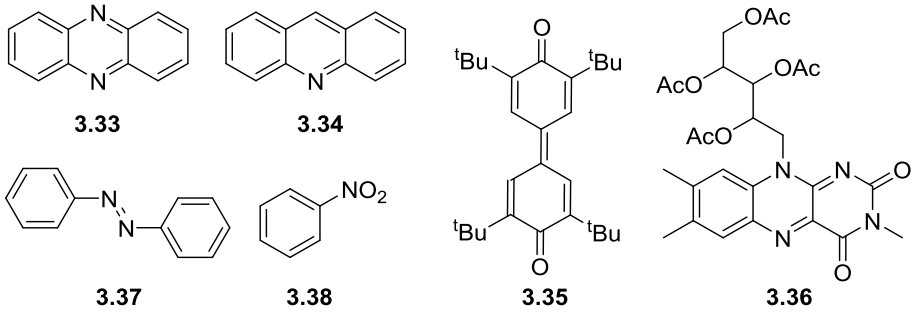

Figure 3.1.3.2 - Reported examples of external oxidants.

The procedures reported work best with aromatic aldehydes, but have demonstrated a good substrate scope with respect to alcohol nucleophiles, although the alcohol is usually present in an excess. Stoichiometric levels of oxidants are required, with some being able to be recovered and reused, after re-oxidation.[104,111] Aldehydes with α-reducible functionality can also be utilised, leading to unsaturated products instead of the saturated products generated through the internal redox mechanism. This was demonstrated by Zeitler in their synthesis of 3,4-dihydrocoumarins **3.39**.[124] They showed that NHCs can convert α,β-unsaturated aldehydes, such as **3.40** to 3,4-dihydrocoumarin (**3.41**), *via* an internal redox of **3.42** and intra-molecular attack by the alcohol. When the reaction was performed in the presence of excess MnO_2, the reaction gave the coumarin **3.39** (**Scheme 3.1.3.5**), suggesting that the external oxidation mechanism can out-pace the internal redox mechanism, allowing unsaturated products to be accessed.

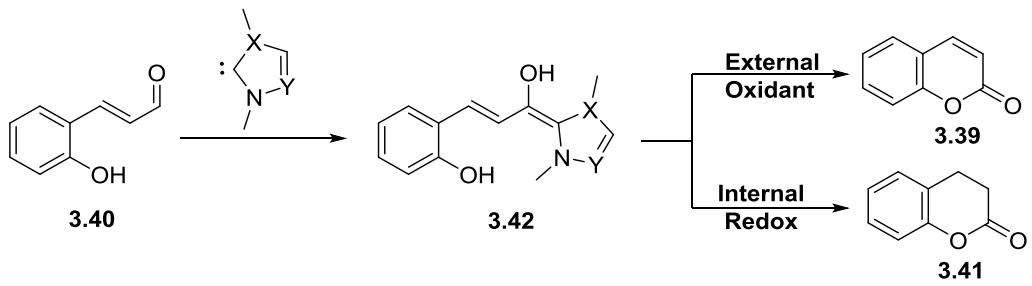

Scheme 3.1.3.5 - Coumarin and 3,4-dihydrocoumarin synthesis

The final oxidative approach utilises O_2 as an oxidant. Liu reported in 2011 the esterification of aldehydes with cinnamyl and allyl bromides, in the presence of oxygen.[125] The mechanism starts with the generation of the Breslow intermediate **3.43**, which after addition of O_2 gives the peroxy intermediate **3.44**. Elimination of the NHC follows, leaving the peracid **3.45**, which can then undergo a Baeyer-Villiger type rearrangement with the starting aldehyde to give two equivalents of acid **3.46**. Finally **3.46** reacts with the bromide to generate the ester under basic conditions (**Scheme 3.1.3.6**). The mechanism has been confirmed with $^{18}O_2$ labelled experiments.[125]

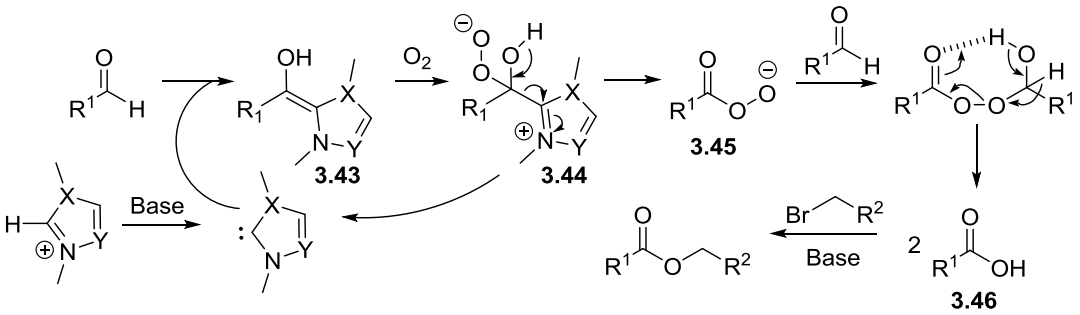

Scheme 3.1.3.6 - Esterification mechanism with O_2 as an oxidant

The discussion in this section has highlighted the key developments of the rapidly growing area of oxidative NHC catalysis. It has been shown to be a particularly powerful procedure for the synthesis of esters, with many examples now reported.[104,110,111]

3.1.4 NHC Mediated Oxidative Amidations

Examples of NHC mediated oxidative amidations have been demonstrated using both internal redox and external oxidant procedures.[104,110,111] Although, there is a lower number of publications in the area compared to oxidative esterifications. One of the reasons for this is the tendency of amines to react rapidly with aldehydes to form imines.[126] The propensity to from imines prevents the NHC from reacting with the aldehydes hindering the amidation pathway. Despite this problem, procedures have been reported, which will be discussed in this section.

The first examples were reported by Rovis and Bode independently in 2007, and are the general approaches taken by others since.[127,128] They combined the internal redox approach with acyl transfer reagents. Rovis employed

4-hydroxy-7-azabenzotriazole (HOAt) in catalytic quantities, whereas Bode used imidazole in stoichiometric amounts (**Scheme 3.1.4.1**). The acyl transfer reagent forms an active intermediate that can be displaced by the amine to give an amide. The amine is typically added after the formation of the reactive intermediate is complete, avoiding the imine formation side reaction.

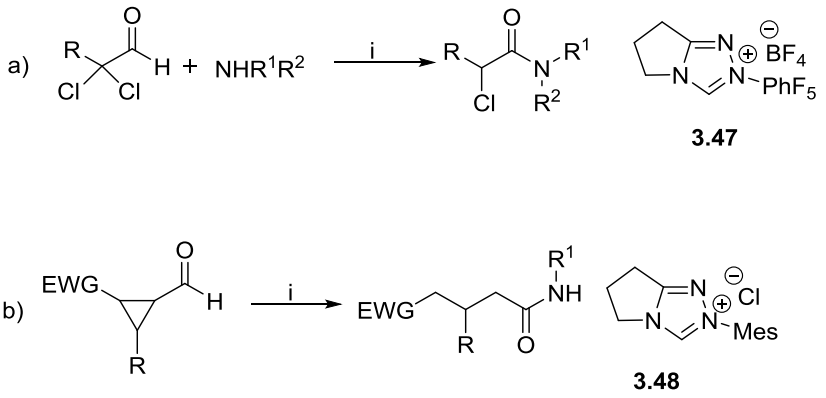

Scheme 3.1.4.1 - Internal redox amidation examples. a) Rovis. b) Bode. *Reagents & conditions* - i) NHC salt **3.47** (20 mol %), HOAt (20 mol %), Et_3N (1.3 equiv.), ^tBuOH (1.0 equiv.) ii) NHC salt **3.48** (5 mol %), DBU (20 mol %), imidazole (1.1 equiv.), then amine.

A similar approach was taken by Struder when using an external oxidant approach.[126] They utilised triazolium salt **3.49** with 1,1,1,3,3,3-hexafluoroisopropanol (HFIP, **3.50**) and the quinone oxidant **3.35** to form an activated ester. HFIP can then be displaced by an amine to yield an amide in a separate reaction (**Scheme 3.1.4.2**).

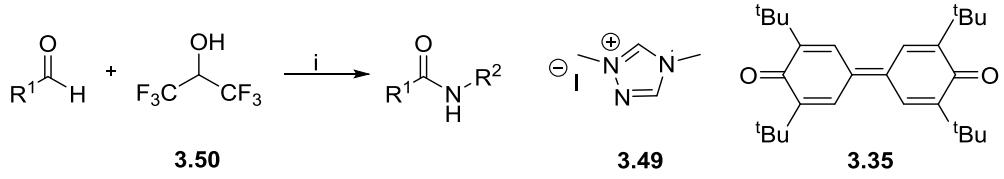

Scheme 3.1.4.2 - Example of an Amidation using an External Oxidant. *Reagents and conditions* - i) NHC salt **3.47** (2 mol %) DBU (20 mol %), quinone **3.35** (1.0 equiv.), HFIP **3.50** (1.0 equiv.), then amine (1.5–2.5 equiv.).

Interestingly, Struder reported on the difference in chemoselectivity of alcohols and amines under external oxidation conditions, without acyl transfer reagents

present.[129] They found that the less nucleophilic alcohols reacted faster than amines, to give esters (**Scheme 3.1.4.3**).

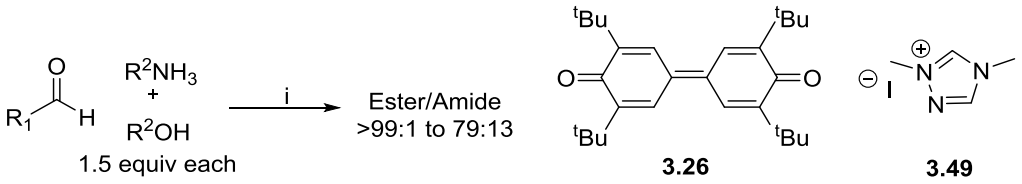

Scheme 3.1.4.3 - Chemoselectivity between Esters and Amides. *Reagents & conditions* - NHC salt **3.49** (2 mol %), DBU (1.1 equiv.), quinone **3.26** (1.0 equiv.), alcohol and amine (1.5 equiv.).

They presented kinetic and DFT studies, that suggested the NHC activates the alcohol, increasing its nucleophilicity through hydrogen bonding. They suggest the NHC plays a dual role catalysing the oxidation and activating the alcohol. There was no mention of whether the side reaction of imine formation was considered during these calculations. The side reaction would severely reduce the rate of amide formation, giving an alternative explanation for the observed selectivity of ester formation.

An alternative approach was taken by Forsyth in the synthesis of the natural product largazole (**Scheme 3.1.4.4**).[130,131] Although they initially attempted the reaction catalytically using an internal redox approach, they found that epoxide **3.51** decomposed. They therefore used a stoichiometric loading of NHC salt **3.17** to give the product **3.52**, avoiding the use of added acyl transfer reagents, and they did not need to protect the acid.

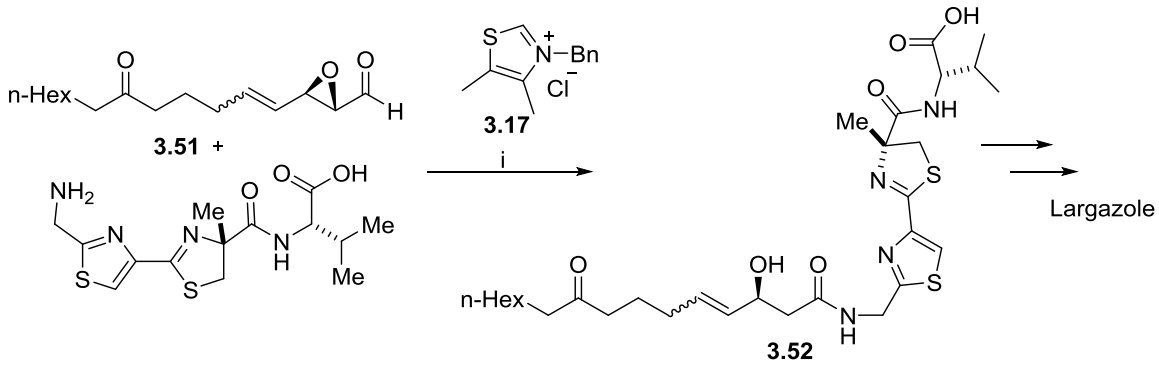

Scheme 3.1.4.4 - Example of amidation in the synthesis of largazole. *Reagents & conditions* - i) NHC salt **3.17** (1.0 equiv.), $^{i}Pr_2EtN$ (1,0 equiv.).

Great progress has been made in the development of NHC mediated oxidative amidations. Due to problems of imine formation indirect routes to amides have been adopted. As interest in the area continues to grow, advances to more efficient procedures will surely follow.

3.1.5 NHC Electrochemistry

In recent years Inesi *et al.* have published many papers on the electrochemistry of NHCs.[132-141] Their focus has been on the generation of NHCs from their pre-salts *via* electrochemical reduction (**Scheme 3.1.5.1**), removing the need for added base.

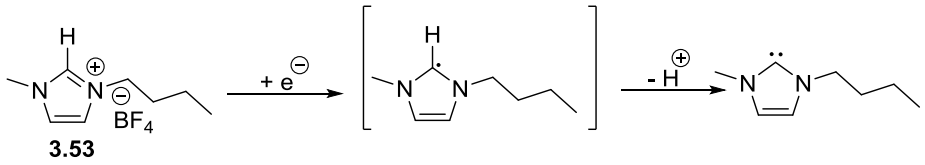

3.53

Scheme 3.1.5.1 - Electrochemical NHC formation.

The electrochemical generation of the NHC is performed in a divided cell, which would be unsuitable for our undivided flow device. The amount of NHC formed can be controlled by the amount of current passed. On formation of the required amount of NHC, the current is switched off and the other reagents are added. The ionic liquid 1-methyl-3-butyl-imidazolium tetrafluoroborate ($[BMIM]^+[BF_4]^-$, **3.53**) also acts as solvent allowing simple extraction of products, and recycling of the ionic liquid.

The electrochemical generation of the NHC procedure has been applied to a range of reactions. For example the approach was shown to be effective in the synthesis of β-lactams, the Staudinger reaction, the formation of chiral oxazolidin-2-ones, the Henry reaction, the benzoin condensation, the Stetter reaction, and the formation of *N*-functionalised benzoxazoles.[132-136,138-141] Inesi *et al*. have also shown that α,β-unsaturated aldehydes can be converted to esters and amides, *via* the internal redox mechanism, using electrochemically generated NHCs in excellent yields (**Scheme 3.1.5.2**).[137,142]

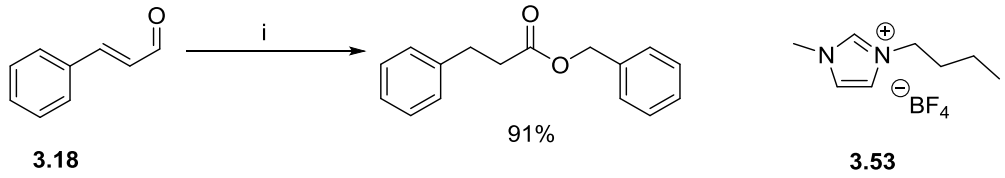

3.18 **3.53**

Scheme 3.1.5.2 - Esterification of α,β-unsaturated aldehydes with electrochemically generated NHC. *Reagents & conditions* - i) $[BMIM]^+[BF_4]^-$ (**3.53**, 2.0 mL), divided cell, Pt electrode, 20 mA, aldehyde **3.18** (1.0 mmol), BnOH (3.0 mmol), 60 ˚C.

A different electrochemical approach for the oxidative synthesis of esters has been reported by Diederich.[143] The thiazole NHC was generated by normal deprotonation procedures, but they electrochemically recycled the electrochemically active riboflavin oxidant **3.36**. This allowed a dual catalytic cycle to be achieved, reducing the environmental impact of the reaction (**Scheme 3.1.5.3**). The method was limited to methyl esters, but good current efficiencies and turnover number were achieved.

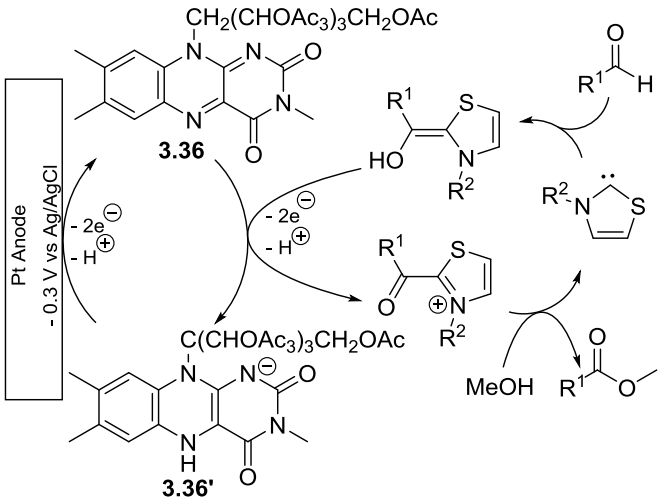

Scheme 3.1.5.3 - Electrochemical dual catalytic esterification.

3.2 Results and Discussion

3.2.1 Research Aims

The aim of this research was to develop an electrochemical conversion of aldehydes to esters and amides in a flow cell. NHC chemistry looked to be a promising strategy to enable this goal. Encouraged by the dual catalytic cycle reported by Diederich,[143] we aimed to achieve a similar dual catalytic cycle in the electrochemical flow cell. From our experience in using TEMPO as an electrochemically active oxidant, we thought this would be an ideal place to start (**Scheme 3.2.1.1**).

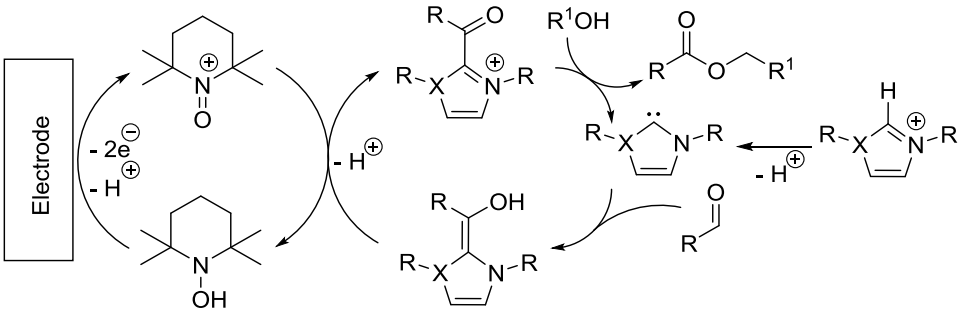

Scheme 3.2.1.1 - Proposed electrochemical dual catalytic oxidative esterification.

3.2.2 TEMPO (2.22) as Oxidant

The NHC 1,4-dimethyl-4*H*-1,2,4-triazol-1-ium iodide (**3.49**) has been demonstrated to be an effective catalyst for oxidative esterifications, so was selected as a starting point. It was synthesised by two sequential methylations with methyl iodide from triazole **3.54**, *via* the mono-methyl-triazole **3.55**, using the method of Belletire *et al*. (**Scheme 3.2.2.1**).[144]

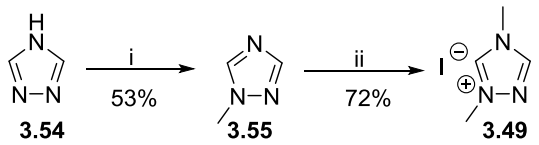

Scheme 3.2.2.1 - Synthesis of NHC salt **3.42**. *Reagents & conditions* - i) Triazole **3.54** (72 mmol), (NaOMe (1.0 equiv.), MeI (1.1 equiv.), methanol (40 mL), reflux 12 h. ii) **3.55** (24 mmol), MeI (2.2 equiv.), methanol (5.0 mL), 4 days, rt.

Attempts to use TEMPO as an oxidant were unsuccessful. The reason for this is due to the formation of TEMPO-esters as reported by Studer.[145] They demonstrated that two equivalents of TEMPO can oxidise the Breslow intermediate, *via* two single electron transfers. The proposed mechanism starts with the formation of the Breslow Intermediate (**3.56**), which undergoes a one electron oxidation, with the first equivalent of TEMPO, to give the radical cation intermediate **3.57**. The reduced TEMPO anion then deprotonates **3.57**, to give **3.58** and the hydroxylamine species **2.32**. The radical **3.58** then undergoes another one-electron oxidation, to give **3.59**, which then rapidly reacts with the resulting reduced TEMPO anion to form a TEMPO-ester (**3.60**). Upon an acidic work-up the TEMPO is eliminated to give an acid (**Scheme 3.2.2.2**). The formation of the TEMPO-ester **3.60** outpaces other nucleophiles, such as alcohols.[145] With this knowledge in hand, an alternative electrochemically active oxidant was investigated.

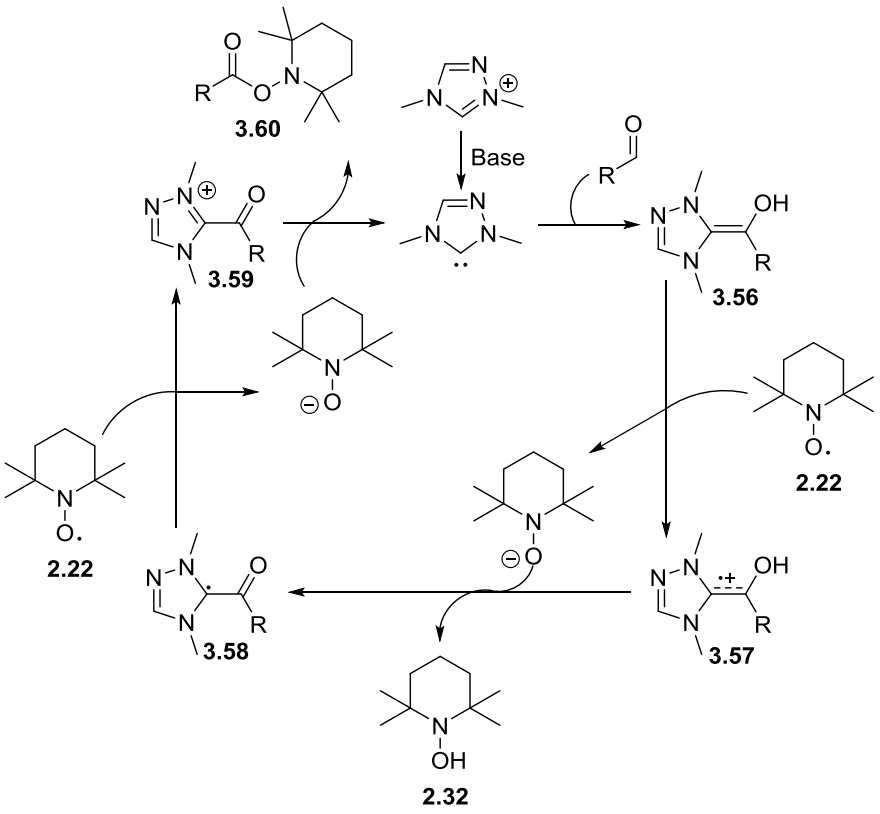

Scheme 3.2.2.2 - Proposed mechanism for TEMPO-ester formation.

3.2.3 3,3',5,5'-Tetra-*tert*-butyl-diphenoquinone (3.35) as Oxidant

3,3',5,5'-Tetra-*tert*-butyl-diphenylquinone (**3.35**) has been shown to be an effective oxidant, in both esterifications and amidations, when used with the NHC salt **3.49.**[126,129] Quinone **3.35** has also been shown to be electrochemically active. Cyclic voltammetry studies conducted in aprotic solvents, such as DMF and pyridine have been reported in the literature, which are consistent with our results (**Figure 3.2.3.1**).[146,147] The cyclic voltammetry suggests that the quinone **3.35** can undergo two successive reversible one-electron reductions, to a di-anion species **3.61** indicative of a reversible EE mechanism (**Scheme 3.2.3.1**). The presence of a radical anion as an intermediate **3.62** after the first reduction was confirmed by Rieker using EPR spectroscopy.[146]

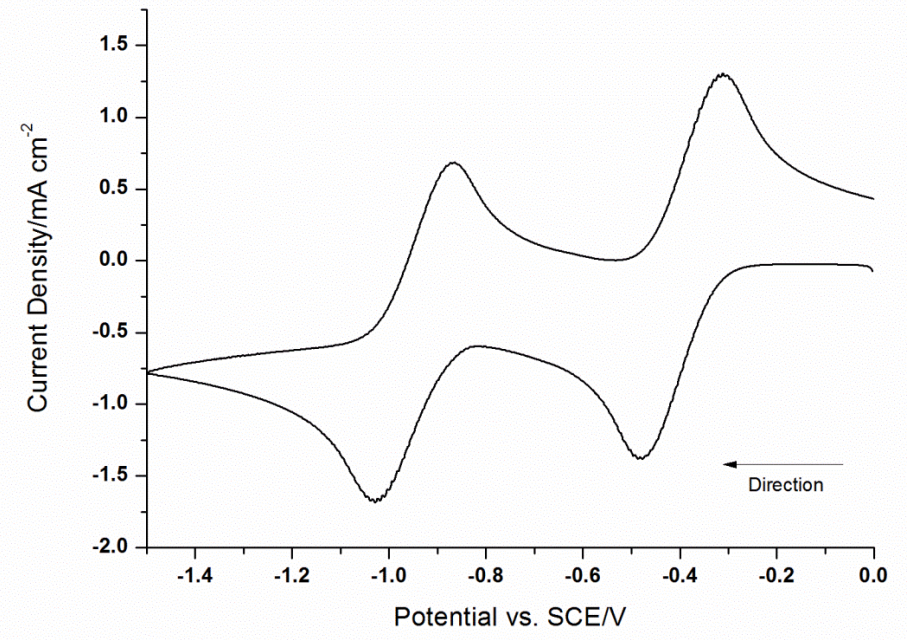

Figure 3.2.3.1 - Cyclic voltammetry of quinone **3.35**. Quinone **3.35** (10 mM), tetrabutylammonium tetrafluoroborate (20 mM) in DMF. 100 mV s^{-1}, rt.

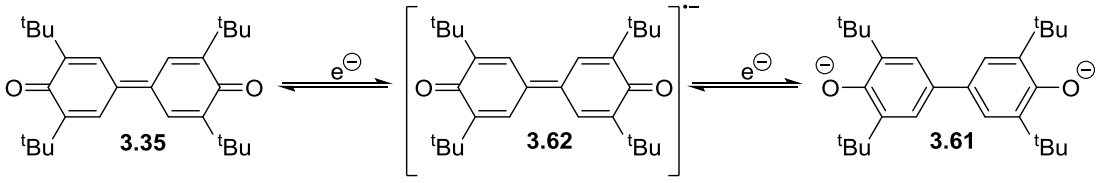

Scheme 3.2.3.1- Electrochemical reduction of quinone **3.35** to di-anion **3.61**.

Encouraged by the literature reports, quinone **3.35** was selected as the oxidant to electrochemically recycle in the flow cell. Quinone **3.35** was synthesised *via* an oxidative phenolic coupling of **3.63**, using I_2 (flakes, not beads) and NaOH (**Scheme 3.2.3.2**).

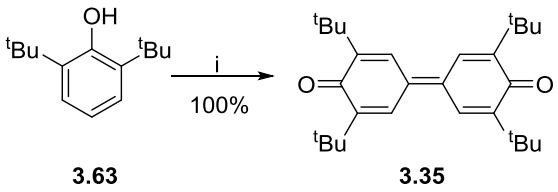

Scheme 3.2.3.2 - Synthesis of quinone **3.35**. *Reagents and conditions* - i) Phenol **3.26** (48 mmol), I_2 (1.01 equiv.), KOH (7.75 equiv.), methanol (150 mL), rt, 30 min.

Initial experiments investigated the conversion of cinnamaldehyde (**3.18**) to the methyl ester **3.54**, to probe whether a catalytic loading of oxidant can outpace the internal redox, which would produce ester **3.65** (**Scheme 3.2.3.3**). A constant current of 10 mA was used with a flow rate of 0.1 mL min^{-1}, with an excess of methanol in THF.

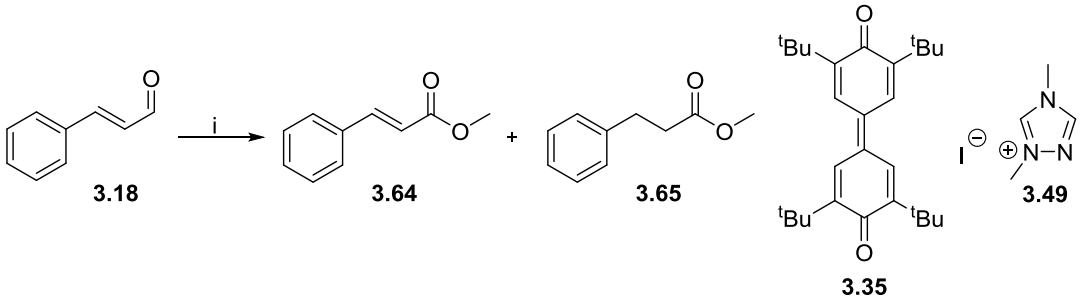

Scheme 3.2.3.3 - Oxidative Esterification with aldehyde **3.18**. *Reagents & conditions* - i) NHC salt **3.49** (2 mol %), quinone **3.35** (20 mol %), DBU (5 mol %), tetrabutylammonium tetrafluoroborate, methanol, THF, rt, 0.1 mL min^{-1}, 10 mA.

Mixtures of the unsaturated and saturated methyl esters **3.64** and **3.65** were collected as an inseparable mixture, with the saturated ester **3.65** as the major product. Yields were modest at between 30-50%. The literature had shown that the external oxidant pathway can outpace the internal redox, when a stoichiometric amount is used.[124] The observation of mixed products suggests that under these conditions the rates are similar, possibly due to the reoxidation of quinone **3.35** being slow. Therefore an aldehyde that doesn't contain an α-reducible moiety was selected for further study.

The conversion of aldehyde **3.66** to the methyl ester **3.67** was selected as the model reaction (**Scheme 3.2.3.4**). Gas Chromatography (GC) was utilised as a rapid way to monitor the reaction, to facilitate optimisation. The GC was calibrated for both the aldehyde **3.66** and the ester **3.67**, so yields could be calculated. Details of the calibration can be found in the experimental section. First the loading of the NHC salt **3.49** was investigated (**Table 3.2.3.1**). DBU loadings were also adjusted accordingly to allow complete formation of the NHC.

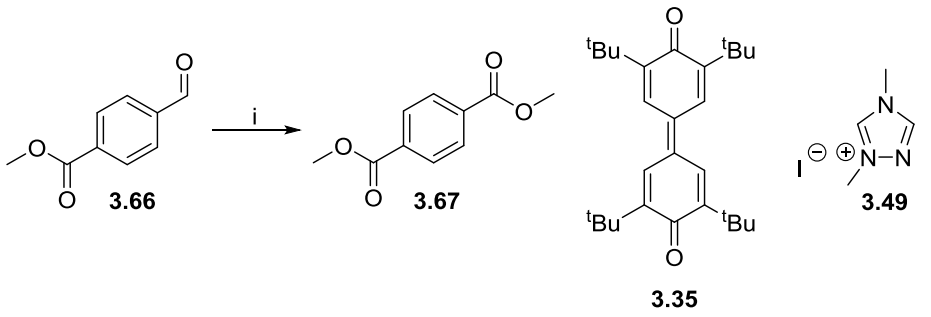

Scheme 3.2.3.4 - Model oxidative esterification reaction of aldehyde **3.66**. *Reagents & conditions* - i) Aldehyde **3.66** (0.1 M), quinone **3.35** (20 mol %), NHC salt **3.49** (see table), DBU (see table), NBu_4BF_4 (0.05 M), MeOH (5.0 equiv.), THF (5.0 mL), 10 mA, 0.1 mL min^{-1}.

NHC Salt 3.49 Loading (mol %)	Loading of DBU (mol %)	GC Yield of Ester 3.67
2	3	17%
5	6	64%
10	11	84%
15	16	61%

Table 3.2.3.1 - Effect of NHC salt **3.49** and DBU loading on yield of esterification.

In some early experiments, excellent yields were achieved with 10 mol % of NHC salt **3.49**. Unfortunately, the early success was marred by our inability to reproduce the high yields, which were typically between 50-70% (isolated). The results show that a loading of 10 mol % of NHC salt **3.49** gives the best results. However, when this method was applied to synthesise ester **3.68**, using HFIP (**3.50**) as the alcohol, the yield reduced to 18% (**Scheme 3.2.3.5**).

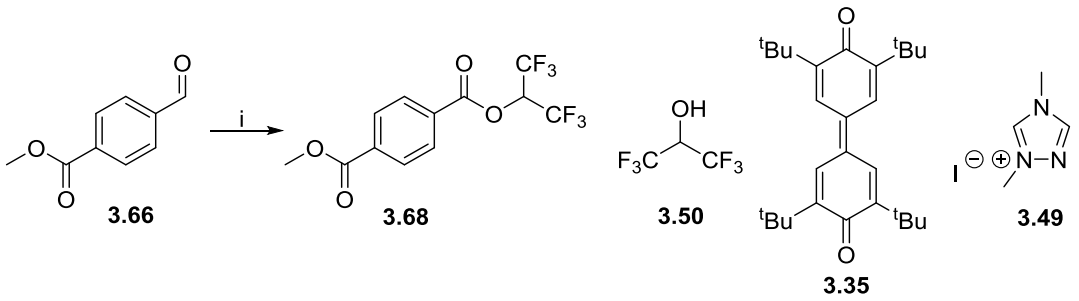

Scheme 3.2.3.5 - Oxidative esterification with hexafluoroisopropanol. *Reagents & conditions* - i) Aldehyde **3.66** (0.1 M), NHC salt **3.49** (10 mol %), quinone **3.35** (20 mol %), HFIP (1.5 equiv.), DBU (12 mol %), NBu_4BF_4 (0.05 M), THF (5.0 mL), 10 mA, 0.1 mL min^{-1}, rt.

The poor alcohol substrate scope, led us to reinvestigate the electrochemistry of the oxidant quinone **3.35**. The cyclic voltammetry discussed earlier showed that the reduction of quinone **3.35** is electrochemically reversible in an aprotic solvent. Cyclic voltammetry of quinone **3.35** has not been performed in the presence of hydrogen bond donors, but studies have been performed on other quinones.[148-151] As a drop in yield was observed when the more acidic alcohol HFIP (pKa 9.3 in water) was used, it was important to consider the effects of HFIP on the electrochemistry of quinone **3.35**.[151]

Cyclic voltammograms of quinone **3.35** with an excess of methanol or HFIP were collected (**Figure 3.2.3.2**). When excess of methanol was added there was a large shift of the second redox couple to a more positive potential, whereas the first redox couple only experiences a small shift. Both redox couples are fully reversible, suggesting that methanol is only weakly interacting with the reduced quinone. When an excess of HFIP is added, there is a clear change in the voltammetry. The reoxidation peak of the second redox couple is lost, suggesting that HFIP is interacting to protonate the dianion to give hydroquinone **3.69** *via* an EEC mechanism (**Scheme 3.2.3.6**). The cyclic voltammetry suggests that the electrochemistry of quinone **3.35** in the presence of HFIP is no longer reversible. This would explain the reduction in yield when using HFIP, as the oxidant is not being electrochemically regenerated.

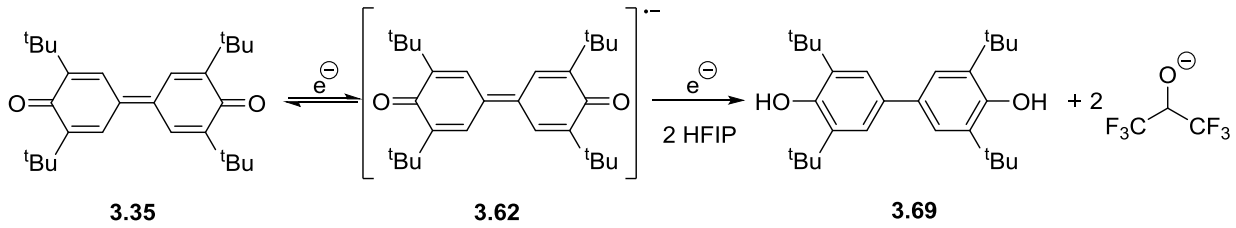

3.35 3.62 3.69

Scheme 3.2.3.6 - Mechanism of formation of hydroquinone **3.69** in the presence of HFIP.

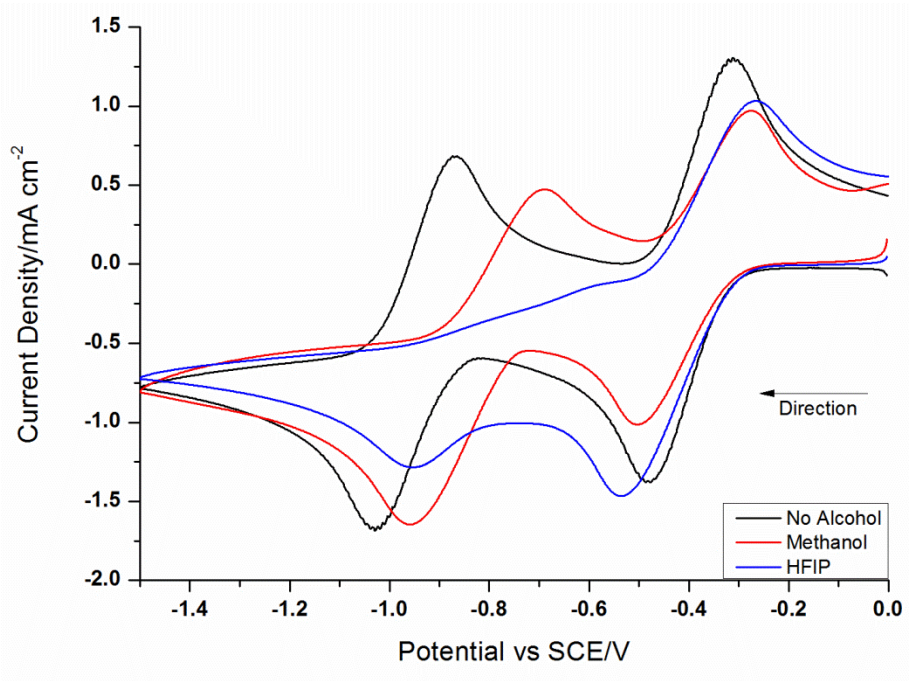

Figure 3.2.3.2 - Cyclic voltammetry of **3.35** with added alcohols. Solid line – quinone **3.35** (10 mM) with tetrabutylammonium tetrafluoroborate (20 mM) in DMF. Dashed line – with methanol (200 mM). Dotted line – with HFIP (200 mM). 100 mV s^{-1}, rt.

Similar cyclic voltammetry studies on the effects of hydrogen bond donors on other quinones have been published in the literature.[148-151] They showed that weak hydrogen bonding species such as ethanol, and stronger hydrogen bonding reagents such HFIP give similar results to the cyclic voltammetry shown in **Figure 3.2.3.2**.[151] They showed that ethanol stabilises the reduction products by hydrogen bonding. Whereas HFIP protonates the reduction products, leading to hydroquinones (**Scheme 3.2.3.7**).[151] Oxidation of hydroquinones requires higher redox potentials, and the loss of a proton,

explaining the observed reduction in yield when HFIP is used instead of methanol.

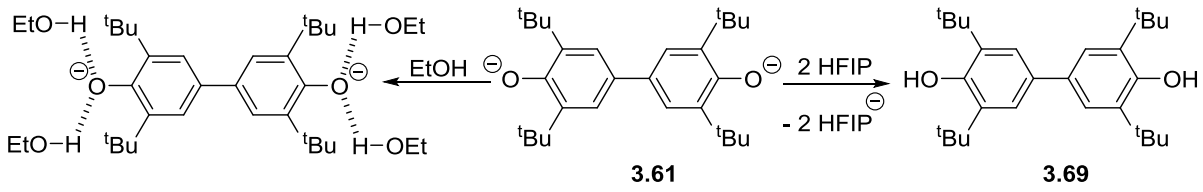

Scheme 3.2.3.7 - Depiction of stabilisation of the dianion **3.61** by hydrogen bonding with ethanol, or formation of hydroquinone **3.69** with HFIP.

Due to the strong effects that different alcohols have on the reoxidation of quinone **3.35**, different electrochemically active oxidants were investigated, along with alternative NHC salts.

3.2.4 Ionic Liquids as source of NHC

Ionic liquids are defined as a compound consisting of anions and cations that melt at or below 100 ˚C. Many are molten at room temperatures leading them to be commonly known as room temperature ionic liquids (RTILs). Ionic liquids have generated a lot of interest over the past decade, because of their potential to be used as environmentally benign solvents. Ionic liquids have very low vapour pressures, therefore they can be considered to be non-volatile. They are typically based upon the structures shown in **Figure 3.2.4.1**.[152-155]

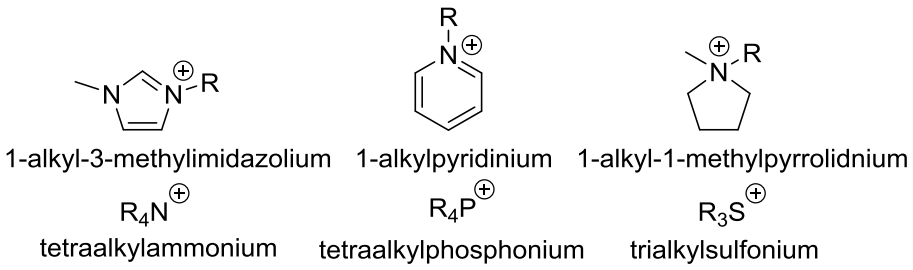

Figure 3.2.4.1 - Types of ionic liquids.

The imidazolium based ionic liquids are of particular interest to this research, due to the ability to form NHCs under basic conditions. This coupled with their conductivity properties, could lead to a system where the ionic liquid acts as solvent, electrolyte and NHC precursor, which can easily be recycled.[137] This

approach was recently demonstrated by Inesi to synthesise esters in good yields, and recover the ionic liquid, with MnO_2 as the oxidant. (**Scheme 3.2.4.1**).[156]

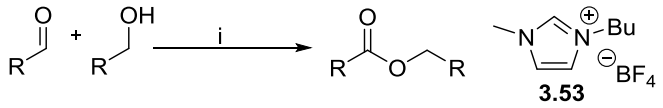

Scheme 3.2.4.1 - Inesi synthesis of esters. *Reagents & conditions* - i) $[BMIM]^+[BF_4]^-$ (**3.53**, 0.5 mL), aldehyde (0.5 mmol), DBU (0.5 mmol), Cs_2CO_3 (1.5 mmol), MnO_2 (1.5 mmol), alcohol (1.5 mmol). 24 h, rt.

A similar approach was investigated using the electrochemically active organic oxidants phenazine (**3.33**) and methyl-riboflavin (**3.36**).[157,158] The cyclic voltammetry of **3.33** shows a reversible two-electron redox couple. Whereas the methyl-riboflavin **3.36** has a more complex cyclic voltammogram, with an initial reversible one-electron redox couple, followed by an electrochemically irreversible one-electron redox couple. (**Figure 3.2.4.2**, **Scheme 3.2.4.2**). The reduction potentials suggest both phenazine **3.33** and methyl-riboflavin **3.36** are both relatively weak oxidants. Despite being weak oxidants both **3.33** and methyl-riboflavin **3.36** have been shown to be effective oxidants in NHC catalysed esterifications, therefore they were selected for further investigation in the electrochemical flow cell.[143,159,160]

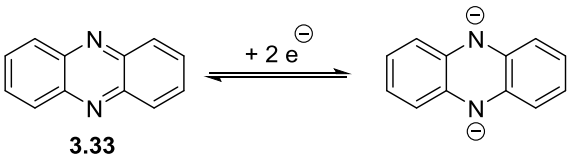

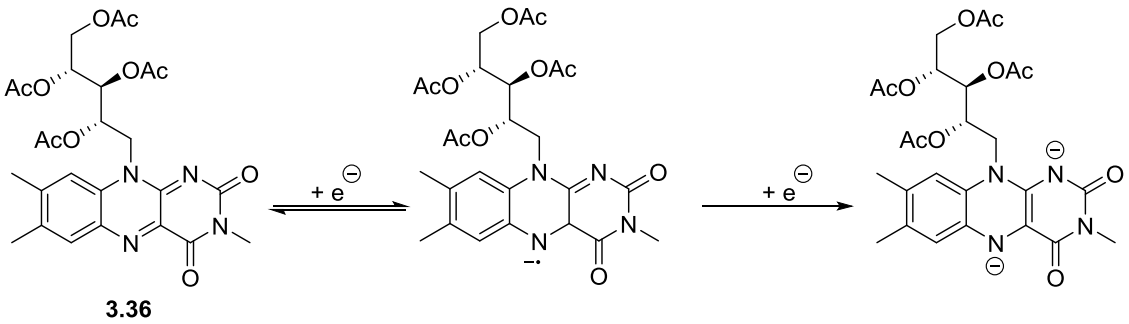

Scheme 3.2.4.2 - Mechanism of electrochemical reduction of oxidants phenazine (**3.33**), and methyl-riboflavin **3.36**.

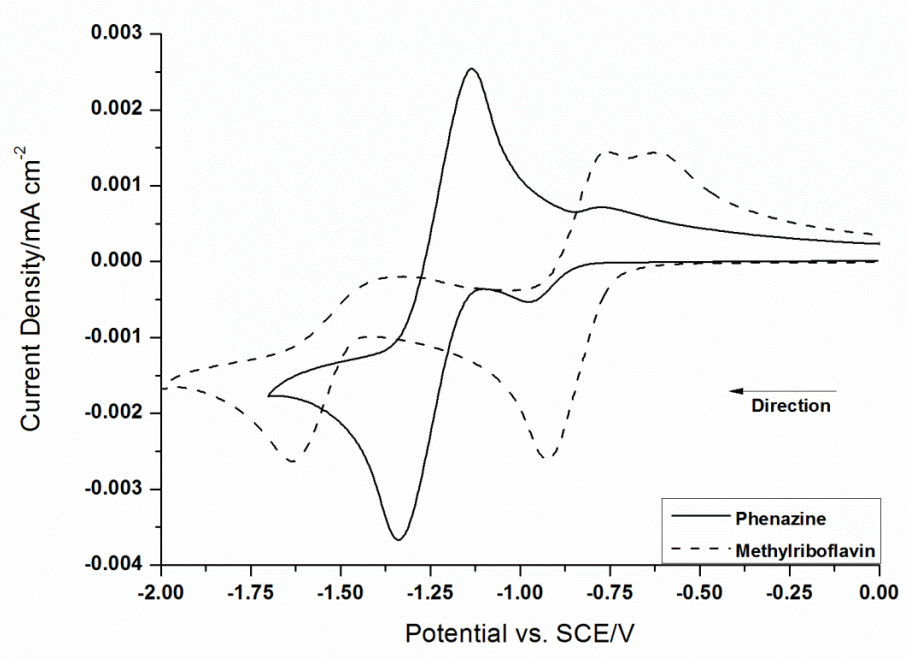

Figure 3.2.4.2 - Cyclic voltammetry of phenazine (**3.33**) and methyl-riboflavin **3.36**. Solid line: Phenazine (**3.33**, 10 mM), NBu_4BF_4 (20 mM) in MeCN. Dashed Line: Methyl-riboflavin **3.36** (10 mM). NBu_4BF_4 (20 mM) in MeCN. 100 mV s^{-1}, rt.

Methyl-riboflavin **3.36** was synthesised in two steps from riboflavin (**3.70**) (**Scheme 3.2.4.3**). The first step involved acetylating the free hydroxyl groups to give **3.71**, which was followed by methylation of the free nitrogen to give **3.36**.

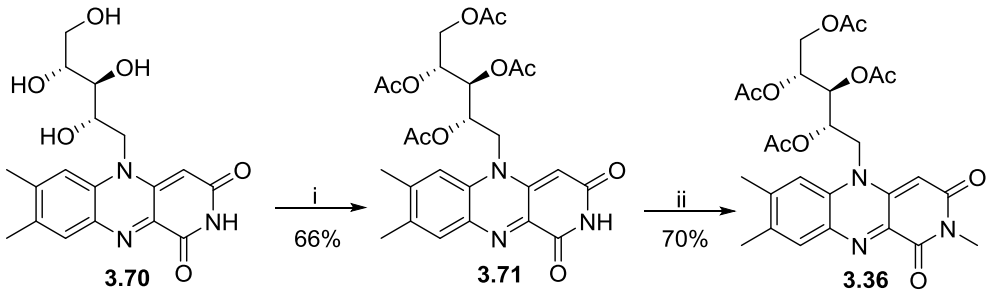

Scheme 3.2.4.3 - Synthesis of methylriboflavin **3.36**. *Reagents and conditions* - i) Riboflavin **3.70** (13 mmol), Ac_2O (60 mL), pyridine (60 mL), reflux, 15 min. ii) **3.71** (7.0 mmol), $CsCO_3$ (1.5 equiv.), MeI (10 equiv.), DMF (50 mL), 16 h, dark.

The ionic liquid 1-butyl-3-methylimidazolium tetrafluoroborate $[BMIM]^+[BF_4]^-$ (**3.53**) was selected as the NHC salt to be investigated. The same esterification

of aldehyde **3.66** to give **3.67** was used as the model reaction, which was monitored by GC. Due to the reactive nature of the Breslow intermediate and the possibility of side reactions occurring in a pre-made solution, the NHC was generated *in situ* by the mixing of two flow streams. This was achieved by adding $[BMIM]^+[BF_4]^-$ to one reservoir, with the other containing a solution of aldehyde, DBU, methanol and oxidant in THF. The two separate solutions were then flowed into a T-piece or glass-plate reactor, where they were mixed. The reaction mixture was then passed through the electrochemical cell (**Figure 3.2.4.3**, **Scheme 3.2.4.4**). Each solution was flowed at 0.05 mL min^{-1}, giving a total flow rate 0.10 mL min^{-1} once mixed. Solutions were based upon 0.2 M of aldehyde **3.66**.

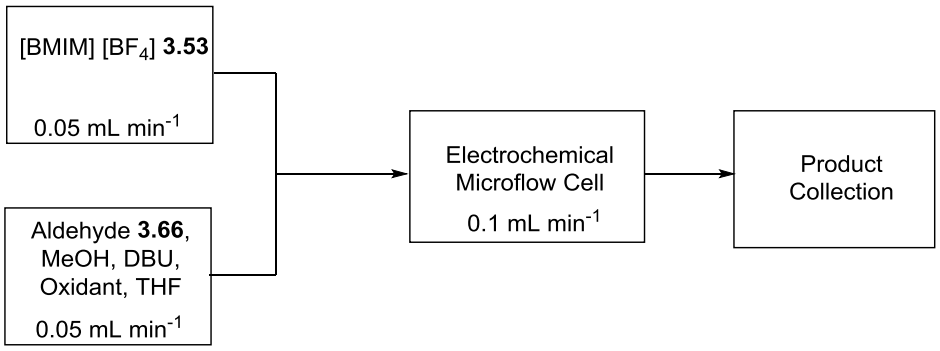

Figure 3.2.4.3 - Schematic of flow set-up using two pumps.

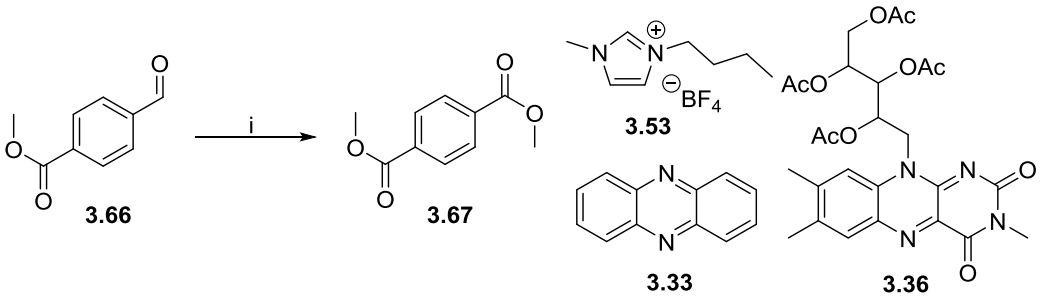

Scheme 3.2.4.4 - Electrochemical oxidative esterification with $[BMIM]^+[BF_4]^-$. *Reagents & conditions* - i) $[BMIM]^+[BF_4]^-$ (**3.53**, 5.0 mL), aldehyde **3.66** (0.1 M), DBU (1.0 equiv.), oxidant (see table), MeOH (5 equiv.), 0.1 mL min^{-1}, current (see table).

Different loadings of the oxidants **3.33** and **3.36** were investigated, as well as different currents, to identify the best conditions (**Table 3.2.4.1**).

Oxidant	Loading/mol %	Current/mA	Yield [a]
Riboflavin **3.36**	20	5	38%
Riboflavin **3.36**	30	5	44%
Riboflavin **3.26**	20	10	53%
Phenazine **3.33**	20	5	48%
Phenazine **3.33**	20	10	55%
Phenazine **3.33**	20	15	94%
Phenazine **3.33**	20	20	89%

Table 3.2.4.1 - The effect of different oxidants and currents of yield. [a] - Yield obtained from a calibrated GC.

The best yields were achieved with 20 mol % phenazine (**3.33**) at a constant current of 15 mA. The methyl-riboflavin oxidant **3.36** possibly decomposed under the reaction conditions, leading to the observed lower yields. To try and reduce the amount of ionic liquid being used an alternative flow arrangement was tested. $[BMIM]^+[BF_4]^-$ was flowed at 0.01 mL min^{-1} and the solution containing the other reagents was flowed at 0.10 mL min^{-1}, giving a total flow rate of 0.11 mL min^{-1} through the electrochemical microflow cell. When tested with the oxidant phenazine (**3.33**) at 15 mA aldehyde **3.66** was converted to ester **3.67** in 84% yield.

After initial promising results using this flow set-up, unfortunately there were reliability problems originating from the viscosity of $[BMIM]^+[BF_4]^-$ leading to inconsistent flow rates, increased pressure within the pumps and leakages. Due to these problems alternative set-ups were investigated.

3.2.5 Design of Experiment Optimisation of Dual Catalytic Esterification

To assist in the optimisation, the Design of Experiment (DoE) software package JMP 9 was used. JMP is a DoE statistical software package that allows reactions to be modelled to find optimal conditions in fewer experiments. For example, a reaction that has three continuous factors (the variables under investigation), the minimum and maximum values of these factors can be represented by the points of a cube (**Figure 3.2.5.1**). The optimum conditions are somewhere within the volume of the cube. To find this systematically many reactions

would be required. DoE software requires only a selection of the minimum and maximum values to be tested along with a centre point. From this the software can predict where the best conditions are mostly likely to lie, which can then be tested by experiment. This drastically reduces the number of experiments required to find the best conditions.

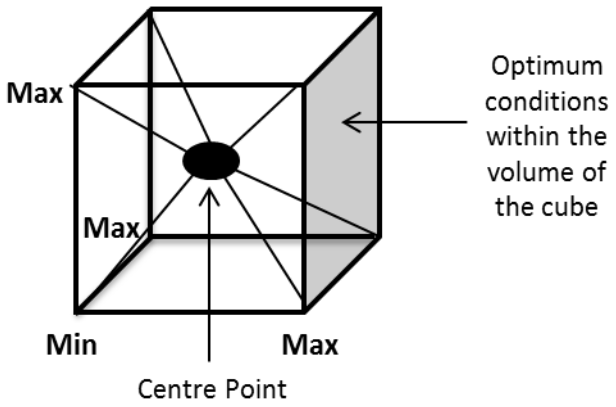

Figure 3.2.5.1 - Representation of Design of Experiment

To produce accurate models of the reaction, accurate data must be collected. Due to the unreliable nature of the flow characteristics $[BMIM]^+[BF_4]^-$ through the cell, a different system was required. Due to the good results achieved using $[BMIM]^+[BF_4]^-$ and the oxidant phenazine (**3.33**), these reagents were investigated in the model esterification reaction to give ester **3.67** (**Scheme 3.2.5.1**).

Before the DoE experiment could be initiated a suitable solvent needed to be found, to solve the reliability problems caused by flowing $[BMIM]^+[BF_4]^-$ through the pumps. Therefore a screen of different aprotic solvents was commenced in batch using the model reaction and a stoichiometric amount of phenazine (**3.33**) (**Scheme 3.2.5.1**). The progress of this was monitored by using a calibrated GC. The results are shown in **Table 3.2.5.1**.

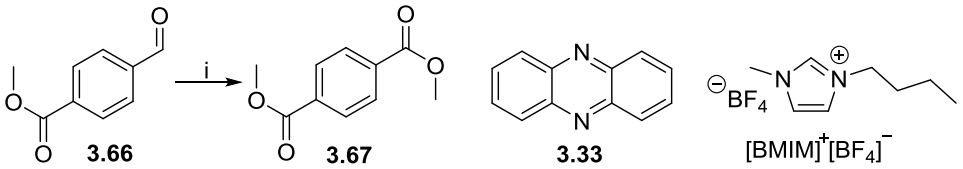

Scheme 3.2.5.1 - Oxidative esterification of aldehyde **3.66**: solvent screen. *Reagents & conditions* - i) $[BMIM]^+[BF_4]^-$ (2.0 equiv.), DBU (0.3 equiv.), methanol (1.1 equiv.), phenazine **3.33** (1.0 equiv.), 4.5 h, rt, various solvents.

Solvent	Yield of 3.67 [a]	Notes
Acetone	70%	Reaction mixture not fully soluble.
DCM	83%	Reaction mixture not fully soluble
DMF	78%	Reaction mixture fully soluble
Acetonitrile	50%	Reaction mixture not fully soluble. Incompatible with flow cell gasket material
DMSO	78%	Reaction mixture not fully soluble
THF	89%	$[BMIM]^+[BF_4]^-$ partially soluble

Table 3.2.5.1 - Results of the effect of solvent on the esterification reaction. [a] - Yield determined by a calibrated GC.

The reaction mixture was not fully soluble in most solvents tested. Acetonitrile causes swelling of the gasket in the electrochemical flow cell, leading to leaks and also gave the worst yield of ester **3.67** in the batch experiments. THF gave the best yield, even though the $[BMIM]^+[BF_4]^-$ is only partially soluble. Therefore 1:1 mixed THF based solvents systems were then tested (**Table 3.2.5.2**).

Solvent Mixture	Yield of 3.67 [a]	Notes
THF/Acetone	51%	Reaction mixture fully soluble
THF/DCM	62%	Reaction mixture fully soluble
THF/DMF	59%	Reaction mixture fully soluble
THF/DMSO	82%	Reaction mixture fully soluble
THF	90%	$[BMIM]^+[BF_4]^-$ not fully soluble

Table 3.2.5.2 - Results of the effect of mixed solvent systems on the esterification reaction. [a] - Yield determined by a calibrated GC.

THF consistently gave the best results despite the partial solubility of $[BMIM]^+[BF_4]^-$. THF is a poor electrochemical solvent, whereas DMSO is often used as an electrochemical solvent due to its high dielectric constant (47, compared to 7 for THF) leading to a wide solubility of electrolytes.[2] Higher dielectric constants allow for the electrolyte salts to dissociate better, leading to lower resistance across the cell.[1] Therefore during the DoE optimisation a THF based solvent system was used, with the addition of 5.0 equivalents of DMSO to help solubilise $[BMIM]^+[BF_4]^-$ and reduce the resistance across the electrochemical microflow cell.

The NHC was generated *in situ* to reduce the possibility of the NHC degrading as the reaction progressed. To achieve the NHC formation and subsequent oxidative esterification a two-pump system was employed again (**Figure 3.2.5.2**). One solution contained the base (DBU) in THF, and the other contained the aldehyde **3.66**, $[BMIM]^+[BF_4]^-$, phenazine oxidant **3.33** and MeOH in the THF/DMSO solvent system (**Figure 3.2.5.2**). The loadings of these reagents as well as the flow rate and current were investigated during the DoE approach.

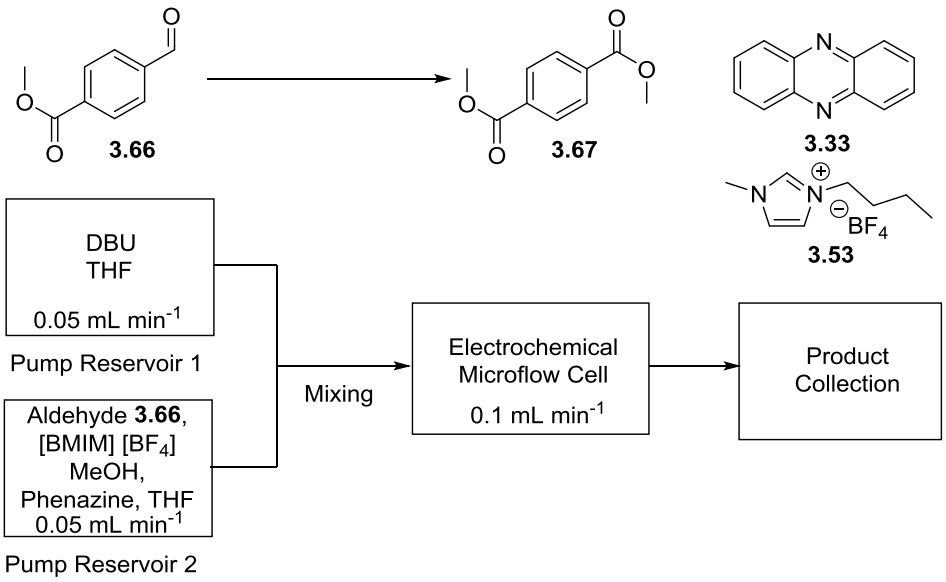

Figure 3.2.5.2 - Schematic of flow set-up during esterification optimisation.

A custom fractional factorial design using JMP 9.0 was used to optimise the model reaction. A full factorial design would investigate all the possible combinations of factors or controlled variables, leading to a large number of experiments. Seven factors were investigated (**Table 3.2.5.3**), therefore a

fractional factorial design allowed a reduced number of experiments to be performed to explore the interactions factors and their effect on the yield of the reaction. The minimum and maximum parameters were determined from previous experiments as a starting point. The ranges between the minimum and maximum values are quite broad, so that the limits of the reaction can be found, with an aim of maximising the amount of product synthesised per hour.

Factor	Minimum	Maximum
Flow Rate	0.1 mL min^{-1}	0.3 mL min^{-1}
Current	5 mA	30 mA
Concentration	0.1 M	0.3 M
Phenazine Loading	10 mol %	30 mol %
$[BMIM]^+[BF_4]^-$ loading	1.0 equiv.	3.0 equiv.
Methanol Loading	1.0 equiv.	5.0 equiv.
DBU Loading	0.2 equiv.	1.0 equiv.

Table 3.2.5.3 - Minimum and maximum values for the seven factors investigated in the DoE.

The fractional factorial model was created to investigate the interaction between each of the factors. The response to be optimised was the yield of ester **3.67** which was set to maximum (i.e. 100%). As a fractional factorial model was employed, it was important to ensure a good general coverage of the investigated interactions between the factors was achieved, to enable an accurate model to be developed. This was assessed by the plot shown in **Figure 3.2.5.3**. The darker blue the square adjacent to the interaction (listed on the side of **Figure 3.2.5.3**), the better that interaction is covered by the experiments performed during the DoE process. In **Figure 3.2.5.3** there is good general coverage of the interactions indicated by the spread of blue across the plot, therefore this model was implemented during the DoE.

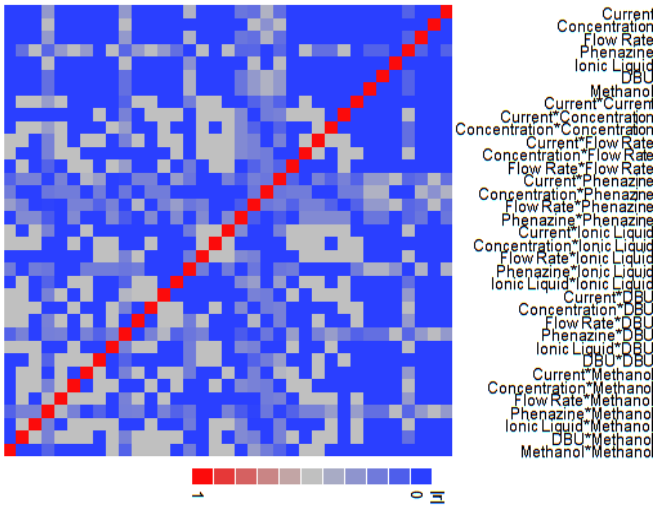

Figure 3.2.5.3 - Evaluation of how well the DoE model covers the interactions of interest. Blue means interaction covered by model. Red means not covered.

The fractional factorial model suggested 18 sets of reaction conditions to be evaluated, which included 2 centre-point reactions. The yields were monitored by a calibrated GC and are shown in **Table 3.2.5.4**

Current mA	Concentration M	Flow Rate mL min^{-1}	Phenazine mol %	$[BMIM]^+[BF_4]^-$ equiv.	DBU equiv.	MeOH equiv.	Yield of **3.67**
20	0.3	0.2	30	1.0	0.2	1.0	43%
20	0.2	0.1	20	1.0	1.0	3.0	49%
10	0.2	0.3	30	2.0	1.0	1.0	38%
20	0.1	0.2	30	3.0	1.0	5.0	57%
20	0.2	0.2	20	2.0	0.6	3.0	46%
20	0.3	0.3	20	2.0	0.6	5.0	34%
20	0.2	0.2	20	2.0	0.6	3.0	44%
20	0.2	0.2	30	2.0	0.6	3.0	49%
20	0.2	0.2	20	2.0	0.6	3.0	49%
30	0.2	0.2	20	3.0	0.6	1.0	59%
30	0.1	0.3	30	1.0	0.6	3.0	52%
20	0.2	0.3	10	3.0	0.2	3.0	39%
30	0.2	0.1	20	2.0	0.2	5.0	62%
10	0.3	0.1	30	3.0	0.6	3.0	62%
10	0.1	0.2	20	2.0	0.2	3.0	36%
20	0.1	0.1	10	2.0	0.6	1.0	26%
30	0.3	0.2	10	2.0	1.0	3.0	52%
10	0.2	0.2	10	1.0	0.6	5.0	26%

Table 3.2.5.4 - Experiments and results using DoE.

After performing the experiments the model was created and assessed for its accuracy. A high RSquare value of 0.99 (close to 1.0) was achieved, which suggested that the model has a high degree of accuracy. Next the plot showing predicted yield verses actual yield was checked (**Figure 3.2.5.4**). A tight straight line, with no out-laying data points is shown, which also suggests a high level of accuracy within the model.

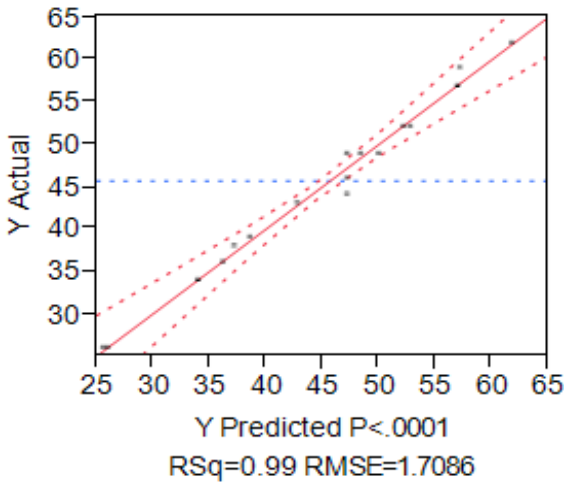

Figure 3.2.5.4 - Plot showing predicted yield vs. actual yield from DoE model.

After assessing the accuracy of the data, the results of the model could be probed. The first point to notice of significance is that the yields for the esterification are only modest to good (up to 62%), suggesting that the optimum conditions may not be in between the ranges tested. Despite this, important information about the reaction can still be obtained. Interestingly the loadings of $[BMIM]^+[BF_4]^-$, methanol and DBU were shown not to influence the yield of the reaction. This means that the minimum loadings of these can be used. The optimum conditions are shown in **Scheme 3.2.5.2** and were shown to be most influenced by:

- Flow Rate - 0.1 mL min^{-1}
- Current - 30 mA
- Concentration of aldehyde **3.66** - 0.3 M
- Phenazine Loading - 30 mol %

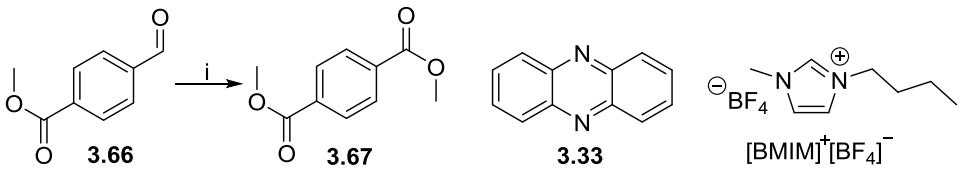

Scheme 3.2.5.2 - Optimum conditions for electrochemical esterification predicted by DoE experimentation. *Reagents & conditions* - i) Aldehyde **3.66** (0.3 M), $[BMIM]^+[BF_4]^-$ (1.0 equiv.), phenazine (**3.33**, 30 mol %), DBU (0.2 equiv.), MeOH (1.0 equiv.), 0.1 mL min^{-1}, 30 mA.

Two experiments were performed to confirm whether the loadings of $[BMIM]^+[BF_4]^-$, methanol and DBU had no overall impact on the yield of the reaction, as predicted by the model. In both experiments the optimum flow rate, current, concentration and phenazine loading conditions were used as shown in **Scheme 3.2.5.2**. The first experiment used the minimal loadings of $[BMIM]^+[BF_4]^-$, methanol and DBU and the second used the highest loadings, as specified in the limits of the DoE model. In both experiments a yield of 67% was obtained, which is within error of the 70% predicted by the DoE model. These results also confirmed that the yields predicted by the DoE model can be matched experimentally.

Figure 3.2.5.5 shows how each of the important factors affects the yield interact. A large effect of flow rate on the yield of the reaction is indicated by the steep gradient of the line. Faster flow rates lead to decreased yields, which are readily understood by the shorter residence time in the cell. If the flow rates were reduced, the yield of the reaction may increase. Importantly, a balance between the amounts of material produced per hour and yield needed to be found for the reaction to be useful. Lower loadings of phenazine **3.33** also have a large effect on yield, suggesting the electrochemical re-oxidation of phenazine may be slow. Alternatively, the oxidation of the Breslow intermediate may be slow. Lower currents and concentration of aldehyde **3.66** do not affect the yield as much. Higher concentrations mean that more product per hour can be synthesised. Another significant result from the DOE is that the yield is apparently independent of the concentration of the organic base DBU, or indeed reduced at higher DBU concentrations.

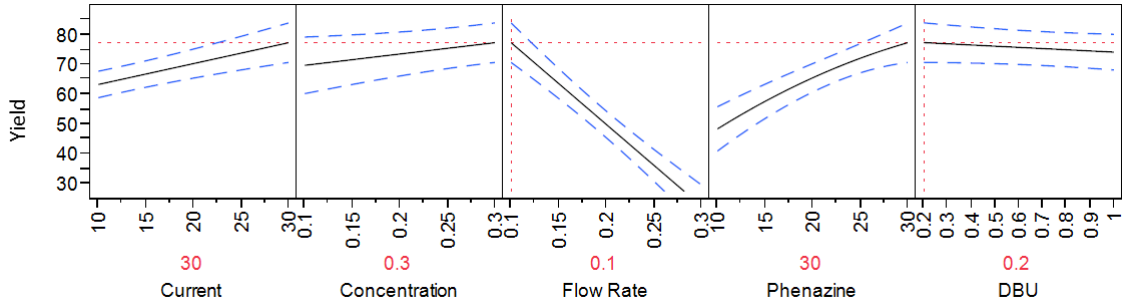

Figure 3.2.5.5 - Graphs showing the effect of the important interactions on yield of ester **3.67** from the DoE.

Efforts to further optimise the yields were attempted. This included investigating the complete removal of DBU. As discussed earlier the electrochemical generation of NHCs directly from their NHC salts has been demonstrated in divided batch cells. Therefore it was envisaged that because DBU was shown not to affect the yield of the reaction, that electrochemical regeneration of the NHC might be occurring. This was tested by flowing the $[BMIM]^+[BF_4]^-$ through the electrochemical flow cell with aldehyde **3.66** phenazine (**3.33**) and methanol. Disappointingly, no product was observed, suggesting that the DBU is required to form the NHC in the current undivided flow cell set-up. The free base, which is sub-stoichiometric, may well be regenerated either directly at the cathode or *via* reaction with methoxide generated at the cathode (**Scheme 3.2.5.3**).

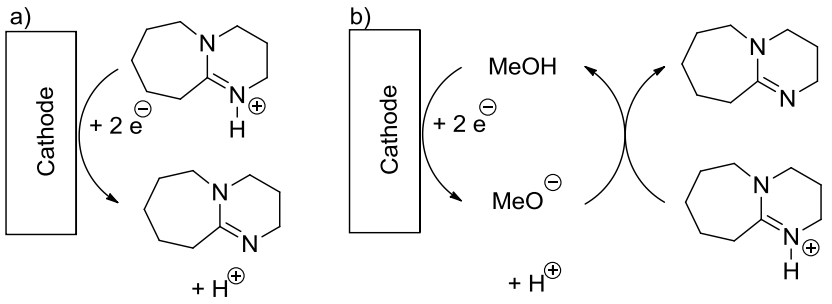

Scheme 3.2.5.3 - Possible routes for electrochemical regeneration of DBU. a) Direct reduction at cathode. b) Methanol reduction at cathode, with subsequent regeneration of DBU.

Further attempts to increase the yield were also unsuccessful, and more worryingly, the reproducibility of the reaction diminished. Yields became inconsistent ranging from 20-50%. All reagents were replaced or purified, yet no improvement could be found. An acid by-product was observed in the NMR suggesting water was present in the reaction, affecting the yield. Water was shown to be present in the $[BMIM]^+[BF_4]^-$ by Karl Fisher titrations and NMR. The $[BMIM]^+[BF_4]^-$ was dried under high vacuum with heating, yet the reaction was still unreliable. The tetrafluoroborate counter-ion has been shown to be unstable in the presence of water from the atmosphere, gradually forming HF and hydroxyl borates (**Scheme 3.2.5.4**).[161,162] It was thought that these products were responsible for the reduction in yield.

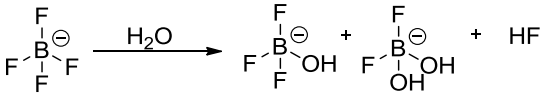

Scheme 3.2.5.4 - Degradation of tetrafluoroborate salts by water.

To investigate this hypothesis, the counter-ion was replaced with the more stable and hydrophobic bis((trifluoromethyl)sulfonyl)amide $(NTf_2)^-$ anion.[163,164] $[BMIM]^+[NTf_2]^-$ (**3.72**) was synthesised in two steps by first alkylating methyl imidazole (**3.73**) with bromobutane (**3.74**) to give $[BMIM^+[Br]^-$ (**3.75**). Counter-ion exchange using $LiNTf_2$ gave $[BMIM]^+[NTf_2]^-$ (**3.62**) in excellent yield (**Scheme 3.2.5.5**).

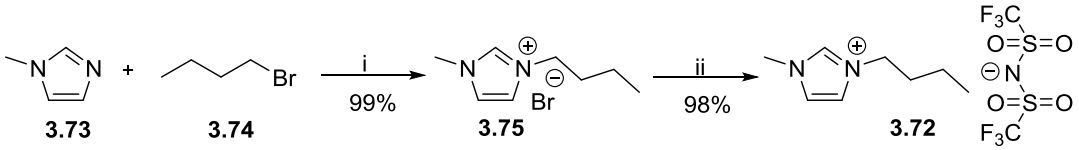

Scheme 3.2.5.5 - Synthesis of $[BMIM]^+[NTf_2]^-$ **3.72**. *Reagents and conditions* - i) **3.73** (125 mmol), **3.74** (1.1 equiv.), 70 ˚C, 12 h. ii) **3.75** (55 mmol) $LiNTf_2$ (1.0 equiv.), water, 12 h.

On replacing $[BMIM]^+[BF_4]^-$ with $[BMIM]^+[NTf_2]^-$, yields were restored to levels close to those obtained in the earlier experiments (~70%). This inferred the degradation of the $^-BF_4$ anion had been the origin of the reduction in yield.

3.2.6 *N*-Heterocyclic Carbene Electrochemistry

Whilst investigating the reliability problems, Boydston published a direct electrochemical oxidative esterification catalysed by NHCs (**Scheme 3.2.6.1**).[165] The thiazolium salt **3.76** was used as the NHC precursor, and the reaction was performed in an undivided batch cell. Good to excellent yields were achieved for a variety of aldehydes and alcohols, although yields dropped by approximately 20% when the reaction was not performed under an inert atmosphere in a dry box.

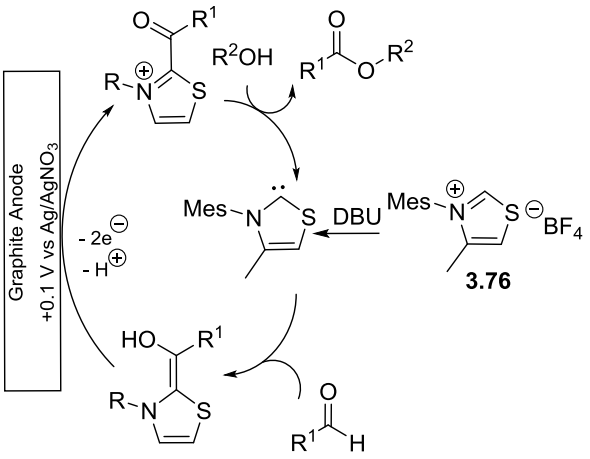

Scheme 3.2.6.1 - Direct electrochemical oxidative esterification reported by Boydston and co-workers.

To investigate the possibility of directly electrochemically oxidising the Breslow intermediate the thiazolium salt **3.77** was synthesised in two steps in order to compare it with imidazolium salts. Thiazolium salt **3.77** was synthesised from simple starting materials in good yield (**Scheme 3.2.6.2**). The NTf_2^- anion was selected as the counter-ion, due to its greater stability and hydrophobicity properties.[163,164]

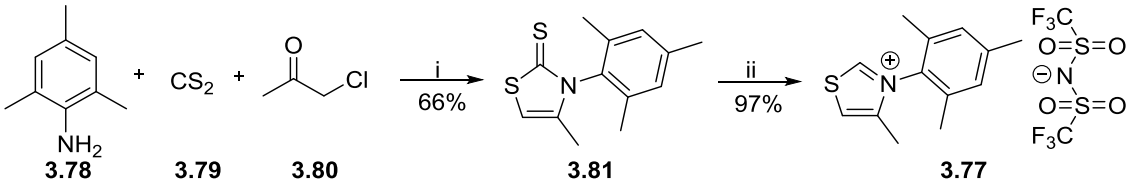

Scheme 3.2.6.2 - Synthesis of thiazolium salt **3.77**. *Reagents & conditions* - i) **3.78** (50 mmol), **3.79** (1.0 equiv.), **3.80** (1.0 equiv.), NaOH (1.0 equiv.), DMSO, 0 °C–rt. ii) **3.81** (24 mmol), H_2O_2 (30% in water, 3.3 equiv.), AcOH (100 mL) then $LiNTf_2$ (1.0 equiv.) in water (50 mL), 24 h.

Cyclic voltammetry studies of the Breslow intermediate have been reported, showing two reversible one-electron redox couples. These results were also confirmed by our own cyclic voltammetry studies (**Figure 3.2.6.1**).[166,167]

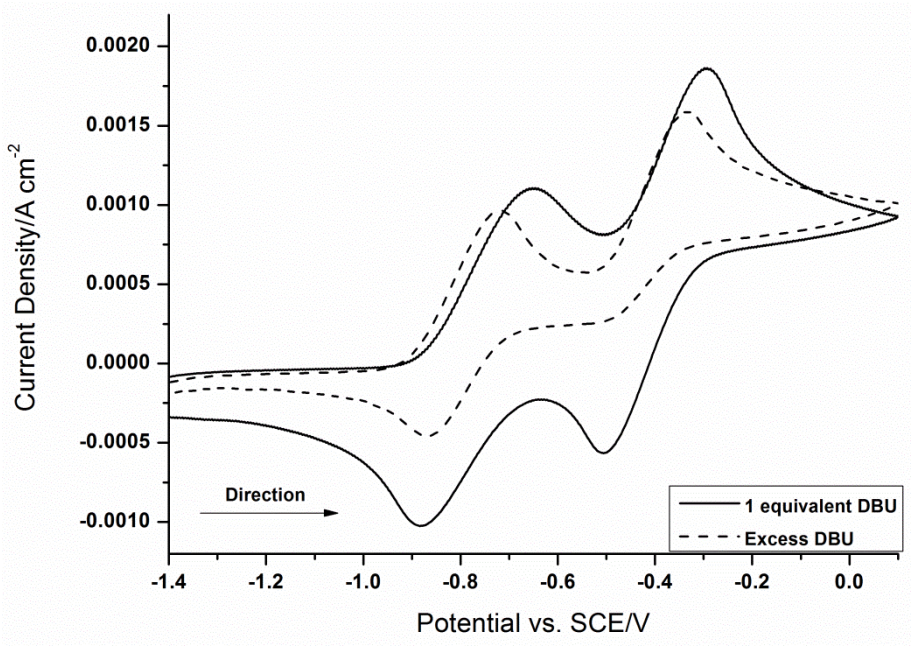

Figure 3.2.6.1 - Cyclic voltammetry of Breslow Intermediate. Thiazolium salt **3.77** (1.0 M), *p*-fluorobenzaldhyde (0.2 M), tetrabutylammonium tetrafluoroborate (0.2 M). Solid line – DBU (0.1 M). Dashed line - DBU (0.2 M). 100 mV s^{-1}, rt.

The Breslow intermediate **3.82** was synthesised *in situ* using the NHC salt **3.77** (0.10 M), and *p*-fluorobenzaldehyde (0.20 M), DBU (0.10 M) and electrolyte tetrabutylammonium tetrafluoroborate (0.20 M) in DMF. From scanning between potentials –1.40 V to 0.10 V at 100 mV s^{-1} two reversible single electrons transfers are observed. This corresponds to the single electron oxidation of **3.82** to the radical species **3.83**, followed by another single electron oxidation to **3.84** (**Scheme 3.2.6.3**). The low oxidation potentials suggest the Breslow intermediate **3.82** is readily oxidised. The presence of the radical species has been reported using EPR spectroscopy.[167] On the addition of excess base the second peak is no longer reversible, suggesting the oxidised species is being intercepted, possibly by DBU or water, meaning the electron transfer is no longer reversible. Attempts to obtain similar cyclic voltammograms with imidazolium salts were unsuccessful, with no peaks observed. This was thought to be due to the Breslow intermediate degrading before the cyclic voltammetry could be performed.

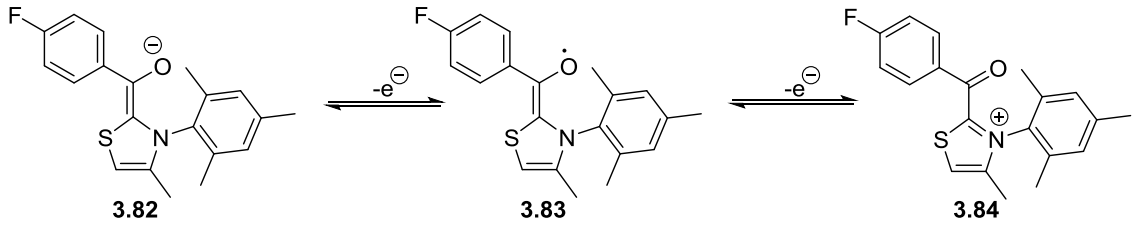

Scheme 3.2.6.3 - Electrochemical oxidation of the Breslow Intermediate **3.72**.

The oxidation potential of the Breslow intermediate (–0.8 V and –0.5 V) suggests it is easier to oxidise than electrochemically active oxidants phenazine **3.33** (–1.25 V) and quinone **3.35** (–1.0 V and –0.5 V), which have previously been investigated as mediators in the reaction. The relative ease of the electrochemical oxidation of the Breslow intermediate is due to the conjugated nature, providing stabilisation to the intermediates formed. Control experiments previously performed without added oxidant gave 20-40% ester products. This suggested that direct electrochemical oxidation of the Breslow intermediate was taking place, instead of electrochemically recycling the oxidant. The added 30 mol % of oxidant increased the yields to those discussed already (~70%). These observations, the favourable cyclic voltammetry and the reports from Boydston, prompted us to investigate the possibility of adapting this for use in the electrochemical flow cell.

3.2.7 Development of Direct Oxidative Esterification

First to test the possibility of a direct electrochemical oxidation of the Breslow intermediate, the NHC salts **3.72** and **3.77** were evaluated in the model reaction (**Scheme 3.2.7.1**). The Breslow intermediate was formed *in situ* using a two pump system. The thiazolium NHC salt **3.77** gave a promising yield of 59%, compared to the imidazolium NHC salt **3.72** giving the ester in 33% yield. The difference in yield is possibly due to the improved resonance stabilisation present in the Breslow intermediate formed from thiazolium salt **3.77**. The increased stability extends the lifetime of the Breslow intermediate leading to more of it being able to be oxidised. Therefore the NHC salt **3.77** was selected for optimisation based on these results and that of the cyclic voltammetry.

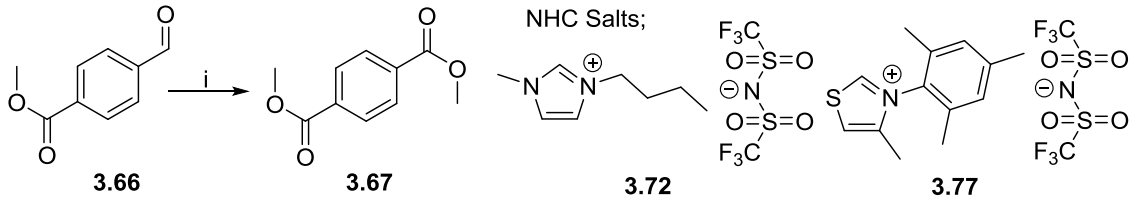

Scheme 3.2.7.1 - Preliminary direct esterification studies using NHCs **3.72** and **3.77**. *Reagents & conditions* - i) Aldehyde **3.66** (0.1 M or 0.3 M), NHC salt **3.72** or **3.77** (1.0 equiv.), DBU (1.0 equiv.), MeOH (1.0 equiv.), DMSO (5.0 equiv.), THF, 0.1 mL min^{-1}, 2.0 V, rt.

A design of experiment approach was taken to optimise the model reaction, which was monitored by GC. A fractional factorial design was created to investigate the interactions between the six factors (**Table 3.2.7.1**). The response was set to maximum, which was related to yield of ester **3.67** (i.e. 100%). The ranges of the factors are quite broad, in order to probe the limits of the reaction and to establish the optimal conditions.

Factor	Minimum	Maximum
Concentration	0.1 M	0.3 M
Voltage	1.0 V	3.0 V
Flow Rate	0.1 mL min^{-1}	0.3 mL min^{-1}
DBU	0.2 equiv.	1.0 equiv.
Methanol	1.0 equiv.	3.0 equiv.
DMSO	2.0 equiv.	5.0 equiv.

Table 3.2.7.1 - Minimum and maximum values used in DoE.

The DoE model was evaluated for how well the desired interactions were covered. The model showed good coverage (**Figure 3.2.7.1**) and therefore the DoE experimental study was initiated.

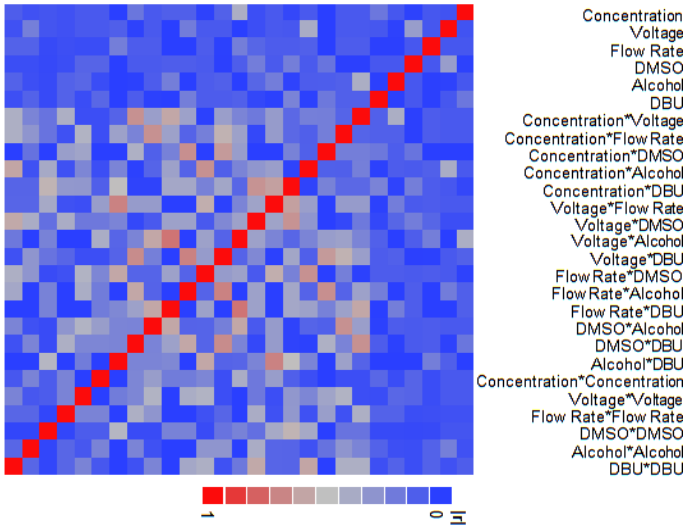

Figure 3.2.7.1 - Design evaluation of DoE model.

The model suggested 20 experiments to run, which included 3 centre-points. The experiments and results are shown **Table 3.2.7.2**.

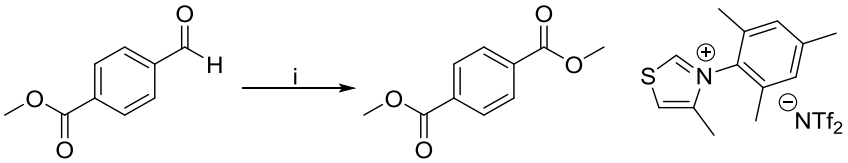

3.66 **3.67** **3.77**

Scheme 3.2.7.2 - Electrochemical oxidative esterification. *Reagents & conditions* - NHC salt **3.77** (1.0 equiv.), rt. Other conditions see table.

	Concentration M	Voltage V	Flow Rate mL min^{-1}	DMSO equiv.	Methanol equiv.	DBU Equiv.	Yield of 3.67
1	0.30	2.00	0.20	2.00	1.00	1.00	37%
2	0.30	3.00	0.30	3.50	3.00	1.00	44%
3	0.30	1.00	0.30	5.00	1.00	0.20	6%
4	0.20	2.00	0.30	3.50	2.00	0.20	15%
5	0.10	1.00	0.20	3.50	2.00	0.60	29%
6	0.30	3.00	0.30	2.00	2.00	0.20	12%
7	0.20	2.00	0.20	3.50	2.00	0.60	29%
8	0.10	2.00	0.10	5.00	3.00	0.60	50%
9	0.30	1.00	0.10	3.50	3.00	0.20	9%
10	0.10	3.00	0.10	2.00	3.00	1.00	44%
11	0.10	1.00	0.10	2.00	1.00	0.20	14%
12	0.20	1.00	0.30	2.00	3.00	0.60	13%
13	0.20	2.00	0.20	3.50	2.00	0.60	25%
14	0.20	3.00	0.20	5.00	3.00	0.20	16%
15	0.30	3.00	0.10	5.00	2.00	0.60	33%
16	0.20	1.00	0.10	5.00	2.00	1.00	30%
17	0.20	3.00	0.10	3.50	1.00	0.60	40%
18	0.20	2.00	0.20	3.50	2.00	0.60	25%
19	0.10	3.00	0.30	5.00	1.00	1.00	35%
20	0.10	2.00	0.10	5.00	1.00	1.00	59%

Table 3.2.7.2 - Experiments and results from the DoE.

On completion of the experiments the yields were placed into the model and the model was assessed for accuracy. The plot in **Figure 3.2.7.2** depicts the predicted yields against the actual yields. It is clear that two data points do not fit the straight line, which corresponds to experiments 2 and 17 in **Table 3.2.7.2**. These data points were removed as they were caused by experimental error and the RSquare increased to 0.996, indicting a high level of accuracy.

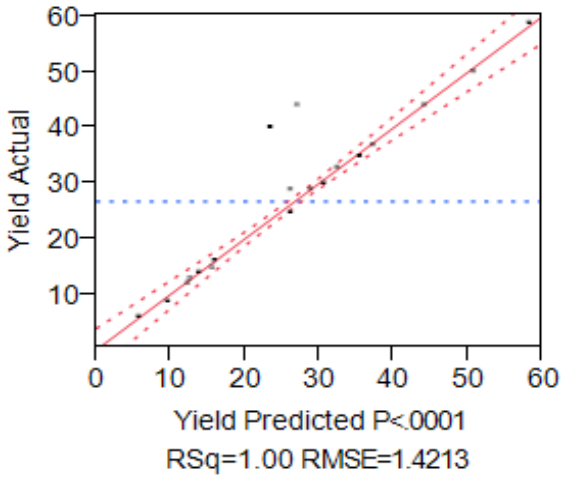

Figure 3.2.7.2 - Plot of predicted yield vs. actual yield from DoE model.

When the results from the model were assessed, the first point of note was that the yields were modest to good. The methanol loading was again shown not to affect the overall yield of the reaction, meaning the loadings can be kept minimal (1.0 equiv. is required for the reaction to proceed to completion). Interestingly, the base DBU was shown to have an effect on the outcome of the reaction this time, with higher loadings leading to improved yields (**Figure 3.2.7.3**). Lower flow rates and concentration were also favourable. The voltage showed a curved relationship with the maximum shown to be at approximately 2.25 V. Due to the broad ranges of the factors investigated the precise profile, and maximum, of this curve was not established. Therefore a second design of experiment with narrower ranges was set-up.

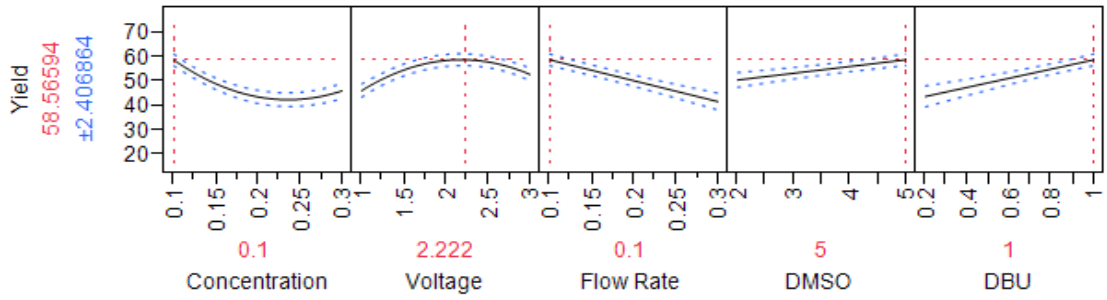

Figure 3.2.7.3 - Graphical depiction of the effects on yield due to the important factors from the DoE.

As the methanol loading was shown not to affect the overall yield of the reaction, it was reduced to the stoichiometric minimum value 1.0 equiv. The optimal DMSO loading was shown to be dependent on flow rate. The flow rate

affects the efficiency of mixing during the reaction. DMSO is present to aid the solubility of the NHC salt, which leads to increased dissociation of the ions, reducing the resistance in the flow cell, allowing the current to pass more efficiently, aiding the oxidation. At higher flow rates the mixing in the flow cell is greater leading to a better distribution of ions, meaning a lower loading of DMSO can be used. At lower flow rates, the mixing is reduced therefore requiring a higher loading of DMSO. Lower flow rates were of interest in the second DoE model, therefore the DMSO loading was kept at 5.0 equivalents. The minimum and maximum for the remaining factors of voltage, concentration and flow rate were focused around the optimum values determined in the previous DoE (**Table 3.2.7.3**).

Factor	Minimum	Maximum
Voltage	2.25 V	2.75 V
Concentration	0.08 M	0.12 M
Flow Rate	0.08 mL min^{-1}	0.12 mL min^{-1}
DBU	1.00 equiv.	2.00 equiv.

Table 3.2.7.3 - Minimum and maximum values for factors from the DoE.

A fractional factorial design was created and was shown to have good coverage of the factors investigated (**Figure 3.2.7.4**).

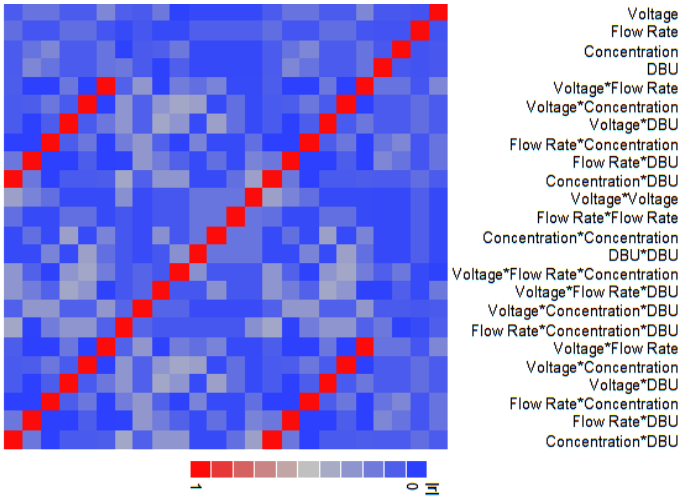

Figure 3.2.7.4 - Evaluation of model from DoE.

The design suggested 19 experiments which included 3 centre-points. The experiments and yields are shown in **Table 3.2.7.4**.

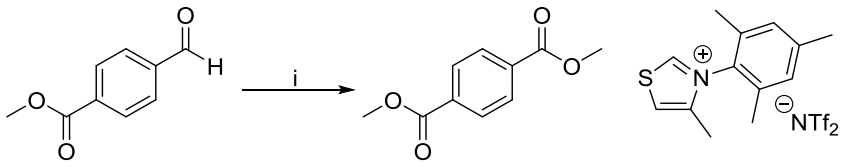

3.66 **3.67** **3.77**

Scheme 3.2.7.3 - Electrochemical oxidative esterification. *Reagents & conditions* - NHC salt **3.77** (1.0 equiv.), MeOH (1.0 equiv.), DMSO (5.0 equiv.), rt. Other conditions see table.

Experiment	Voltage V	Flow Rate mL min^{-1}	Concentration M	DBU equiv.	Yield of 3.67
1	2.75	0.12	0.08	2.00	70%
2	2.50	0.10	0.10	1.50	75%
3	2.50	0.10	0.10	1.50	71%
4	2.50	0.10	0.10	1.50	74%
5	2.75	0.08	0.08	2.00	75%
6	2.75	0.08	0.10	1.00	53%
7	2.25	0.12	0.08	2.00	57%
8	2.25	0.08	0.12	1.00	51%
9	2.50	0.08	0.12	2.00	71%
10	2.25	0.08	0.08	1.50	70%
11	2.75	0.12	0.08	1.00	59%
12	2.50	0.12	0.10	1.50	64%
13	2.25	0.10	0.10	2.00	64%
14	2.75	0.12	0.12	1.00	52%
15	2.25	0.12	0.12	2.00	56%
16	2.50	0.10	0.08	1.00	61%
17	2.75	0.12	0.12	2.00	56%
18	2.75	0.10	0.12	1.50	60%
19	2.25	0.12	0.08	1.00	45%

Table 3.2.7.4 - Experiments and results from DoE.

The model was evaluated to assess the accuracy. The RSquare value of 0.97 was obtained with no out laying data points (**Figure 3.2.7.5**). Therefore the model was considered accurate, and the information was analysed.

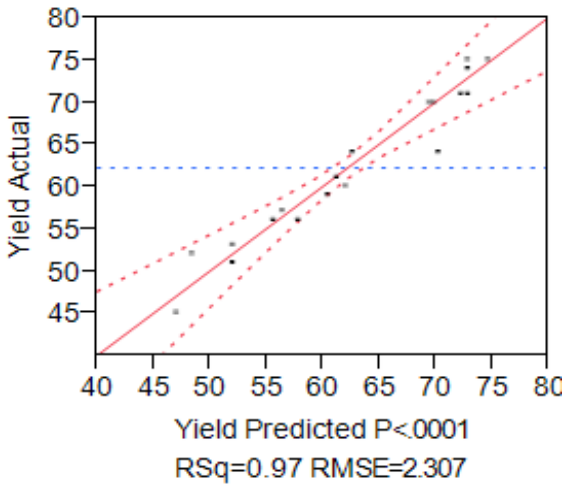

Figure 3.2.7.5 - Plot of predicted yield vs. actual yield from DoE.

The first point of note is the increase in yield to very good levels (75%) (**Figure 3.2.7.6**). Focusing the minimum and maximum values for the factors has allowed the precise profile of the curves to be identified. The actual optimum voltage was predicted to be at around 2.50 V, instead of 2.25 V which was predicted by the previous DoE. Slower flow rates were favourable, possibly due to the increased residence times in the cell, allowing more time for the oxidation to occur. Lower concentrations also had a predicted positive affect on yields, although the improvement was small.

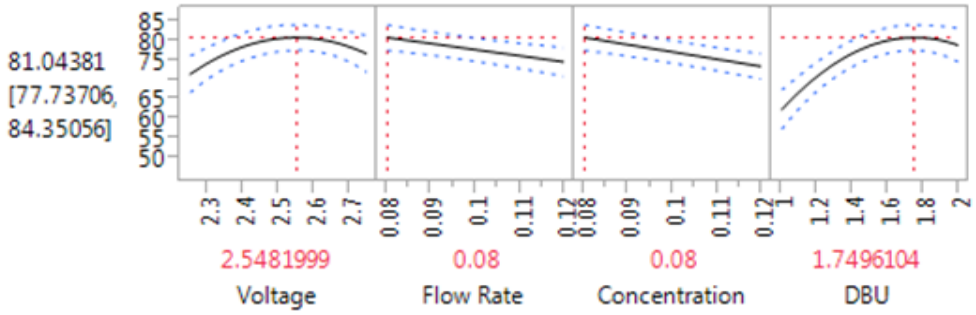

Figure 3.2.7.6 - Results generated from DoE model.

The loading of DBU has a steep curved relationship with the predicted optimum conditions between 1.5-1.8 equivalents. To further investigate the effect of DBU cyclic voltammetry experiments varying the loading of DBU were performed (**Figure 3.2.7.7**). Cyclic voltammograms were obtained for a solution containing the thiazolium NHC salt **3.77** (10 mM), *p*-fluorobenzaldehyde (20 mM) with the electrolyte tetrabutylammonium tetrafluoroborate (20 mM) in DMF. DMF was selected as the solvents as it was used previously in the earlier

cyclic voltammograms. To the solution increased loadings of DBU were sequentially added and cyclic voltammograms generated.

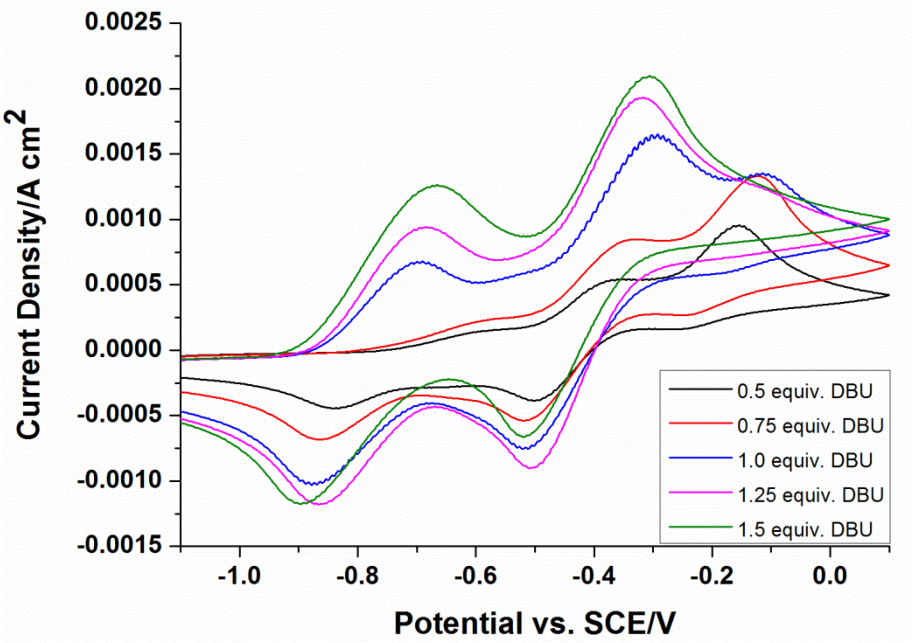

Figure 3.2.7.7 - Cyclic voltammograms showing the effect of DBU on the oxidation of the Breslow intermediate. NHC salt **3.67** (0.1 M), *p*-fluorobenzaldehyde (20 mM), NBu_4BF_4 (0.2 M) in DMF, rt. Scan rate 100 mV s^{-1}.

When no DBU is present in the solution, no peaks are observed in the cyclic voltammogram as the NHC has not formed *in situ* and reacted with the aldehyde to form the Breslow intermediate. When sub-stoichiometric loadings of DBU are present (black line and red line in CV) the two oxidation peaks are not well-formed and they are shifted to less negative potential. As the DBU loading is increased two reversible one-electron oxidation peaks are observed, which have shifted to a lower oxidation potential (blue, pink and green line in CV). The CV results suggest that the oxidation of the Breslow intermediate is more favourable when a higher loading of DBU is present (1.25-2.00 equiv.), which supports the results from the DoE. The first equivalent of DBU is required to form the NHC and subsequent Breslow intermediate. The excess DBU is thought to aid the deprotonation of the Breslow intermediate giving the alkoxide **3.85**. The deprotonated Breslow intermediate can then be oxidised easier, which after reaction with the alcohol leads to the ester (**Scheme 3.2.7.4**). With excess DBU more deprotonated Breslow intermediate **3.85** is present, leading to faster oxidation and higher yields of ester.

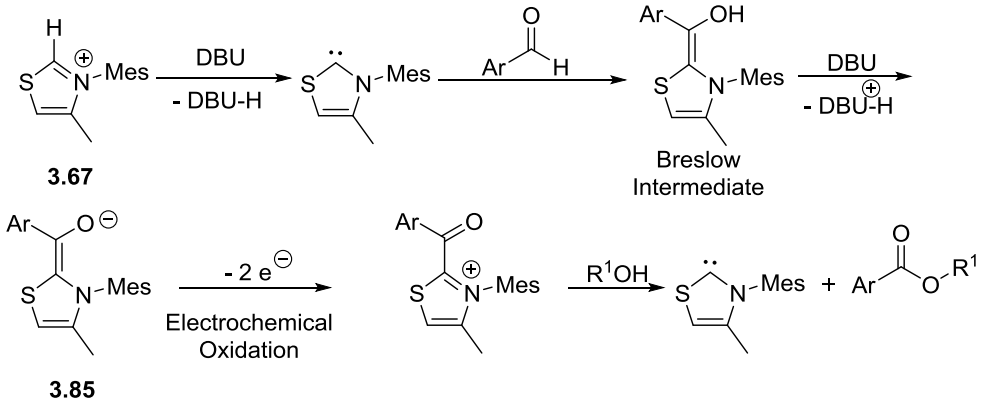

Scheme 3.2.7.4 - Effect of excess DBU on the electrochemical oxidation of the Breslow intermediate

The model predicted that an improved yield of 75-82% could be achieved with the following conditions:

- Voltage - 2.5 V
- Flow Rate - 0.1 mL min^{-1}
- Concentration of aldehyde **3.67** - 0.1 M
- DBU - 1.5 equiv.
- Methanol - 1.0 equiv.
- DMSO - 5.0 equiv.
- NHC Salt **3.67** - 1.0 equiv.
- Room temperature

When these conditions were tested a yield of 80% was achieved. Increasing the path length of the flow cell did not improve the yield under these conditions. Although it was shown 0.5 equiv. of NHC salt **3.77** could be used if the path length was doubled, with only a small decrease in yield (73%). With the optimised conditions in hand, the substrate scope was investigated (**Scheme 3.2.7.5**, **Table 3.2.7.5**). All yields for the substrate examples are of isolated purified material.

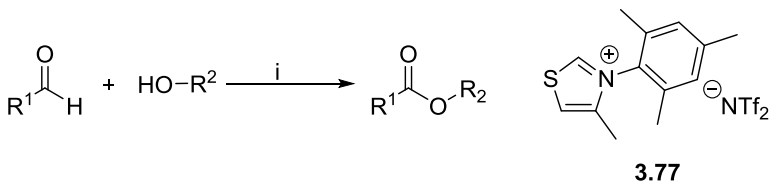

Scheme 3.2.7.5 - Electrochemical oxidative esterification. *Reagents & conditions* - i) Aldehyde (0.1 M), NHC salt **3.77** (1.0 equiv.), DBU (1.5 equiv.), alcohol (1.0 equiv.), DMSO (5.0 equiv.), THF, 0.1 mL min^{-1}, 2.5 V.

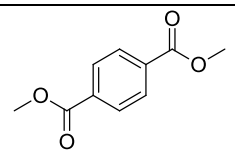

3.77 (80%)

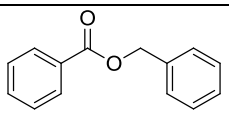

3.86 (68%)

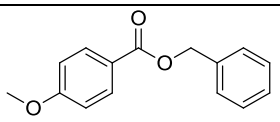

3.87 (74%)

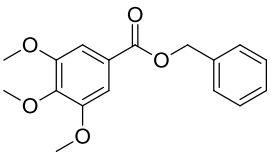

3.88 (73%)

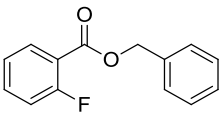

3.89 (50%)

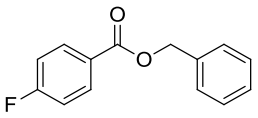

3.90 (81%)

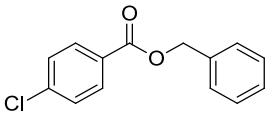

3.91 (83%)

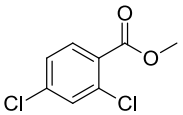

3.92 (52%)

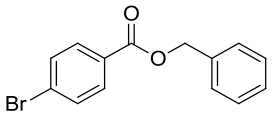

3.93 (93%)

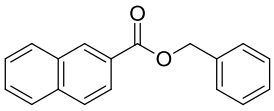

3.94 (88%)

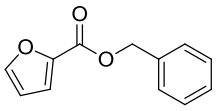

3.95 (71%)

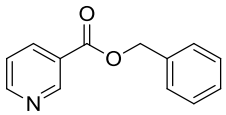

3.96 (70%)

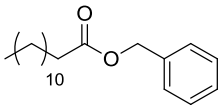

3.97 (56%)

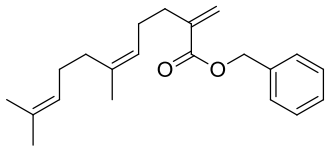

3.98 (45%)

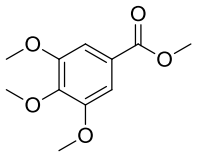

3.99 (75%)

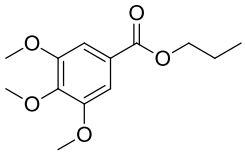

3.100 (75%)

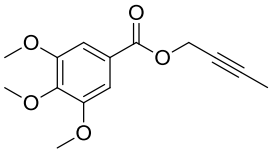

3.101 (76%)

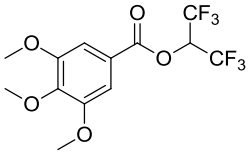

3.102 (39%)

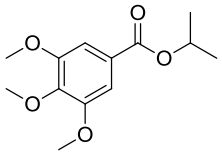

3.103 (57%)

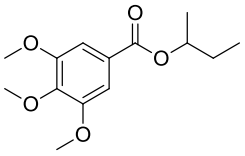

3.104 (45%)

Table 3.2.7.5 - Electrochemical oxidative esterification in microflow: Substrate scope.

Moderate to excellent isolated yields were achieved with a range of aldehydes and alcohols. Aromatic aldehydes gave good to excellent yields, possibly

because of the increased resonance stabilisation available for the intermediates, leading to longer lived Breslow intermediates. Good yields were achieved with heteroaromatic substrates such pyridine (**3.96**, 70%) and furan (**3.95**, 71%). Dodecanal gave ester **3.97** in an expected moderate yield (56%), due to the reduced ability to stabilise the intermediates by resonance, leading to a shorter lived Breslow intermediate. Oxidative esterification of cinnamaldehyde under these conditions led to a low yield and a mixture of saturated and unsaturated esters. The mixture of products can be accounted for by the internal redox pathway proceeding at a similar rate to the electrochemical oxidation. However, the α,β-unsaturated ester **3.98** was synthesised with no evidence of the saturated product, albeit in moderate yield (45%). The aldehyde **3.66**, used in the model reactions, gave mixtures of trans-esterified products if an alcohol other than methanol was used in the reaction. Trans-esterification is presumably promoted under the basic reaction conditions, or by reaction with the NHC which is then displaced by another alcohol. Primary alcohols gave higher yields than secondary alcohols possibly due to the increased steric bulk of the latter. A reduction in yield was also observed with *ortho*-substituted aromatic aldehydes, **3.89** and **3.92**, which could again be due to the increased steric bulk.

A combination of DoE and cyclic voltammetry has been utilised to successfully develop a new procedure for the electrochemical oxidative esterification in a microflow cell. A range of aldehydes and alcohols have been subjected to the reaction conditions, generating a range of esters in good to excellent yields at a rate of ~50-100 mg h^{-1}. After achieving these results our attention turned to developing a strategy for the more challenging oxidative amidation in the electrochemical flow cell.

3.2.8 Development of Direct Oxidative Amidation of Aldehydes

The conversion of aldehyde **3.105** to amide **3.106** was selected as the model reaction for initial study, on the basis of the aldehyde's good reactivity during the esterification reaction development (**Scheme 3.2.8.1**). All reported yields are of pure isolated material. Initial translation of the conditions used in the esterification reaction was unsuccessful in giving any amide (**Scheme 3.2.8.1**). This is most likely because of the competing imine formation reaction that has been reported previously by Struder.[126]

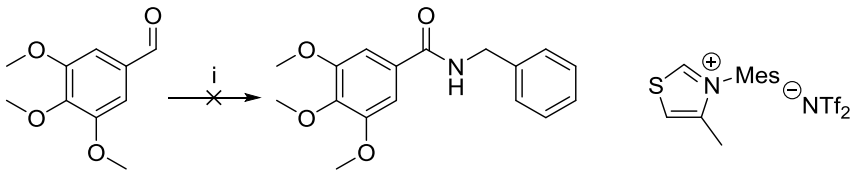

3.105 **3.106** **3.77**

Scheme 3.2.8.1 - Attempted formation of amide **3.106**. *Reagents & conditions* - i) Aldehyde **3.105** (0.1 M), NHC salt **3.77** (1.0 equiv.), DBU (1.5 equiv.), benzyl amine (1.0 equiv.), DMSO (5.0 equiv.), THF, 0.1 mL min^{-1}, 2.5 V, rt.

Performing the reaction in flow gives the opportunity to be able to flow in the amine solution after the formation of the Breslow intermediate. Therefore the flow arrangement was changed to accommodate this. A third pump was added to the set-up, which also added another level of complexity. Due to the three pump arrangement the total flow rate through the electrochemical cell was increased to 0.12 mL min^{-1}. The total flow rate through the electrochemical cell was created by flowing the aldehyde **3.105** and NHC salt **3.77** solution at 0.03 mL min^{-1} and mixing with the DBU solution flowing at the same rate. The combined reaction mixture flowing at a flow rate 0.06 mL min^{-1} was mixed with the benzyl amine solution flowing at the same rate to give a total flow rate of 0.12 mL min^{-1} entering the electrochemical cell (**Figure 3.2.8.1**). The concentrations of the solutions also needed to be considered. The 5.0 mL solution of aldehyde is 0.1 M, and when it is mixed with the DBU solution it is diluted to 0.05 M. Therefore to mix one equivalent of amine with the aldehyde a 10 mL solution of 0.05 M amine is required.

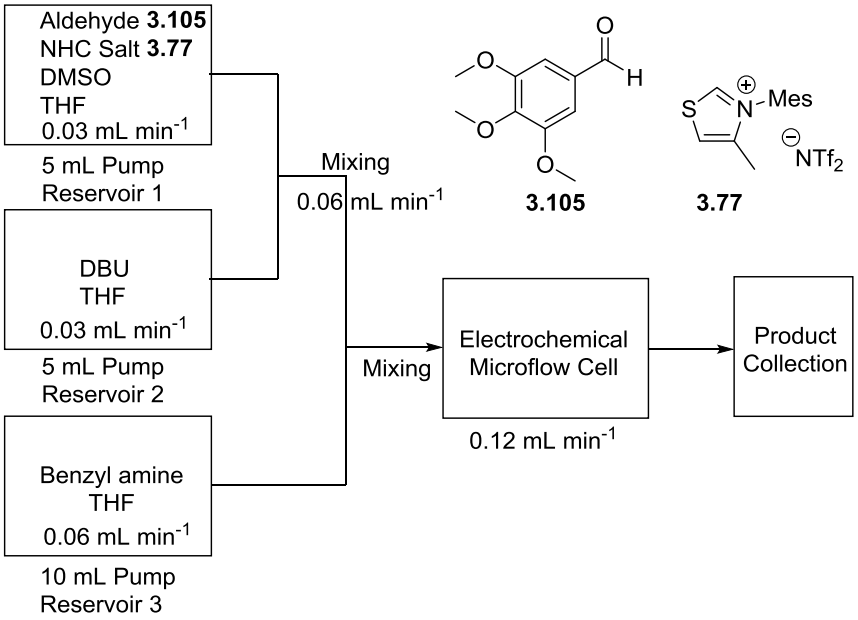

Figure 3.2.8.1 - Schematic of flow set-up for amidation reaction.

When the amidation reaction was tested using this arrangement the yields improved to around 40%. The ratios of NHC salt and amine to aldehyde were adjusted, but the yield did not improve. Orsisi has shown recently that oxidative amidations using an internal redox approach could be performed in $[BMIM]^+[BF_4]^-$ with electrogenerated NHCs.[142] They also reported how well the reaction worked in other solvents. Interestingly, THF only gave a yield of 18%, whereas DMF gave a yield of 78%.[142] Therefore, in our study, the solvent was changed from the mixed THF/DMSO system to DMF, and the model reaction was tested. DMF is considered to be a better electrochemical solvent because of its improved dielectric constant properties (37, compared to 7 for THF).[1] As DMF is a good electrochemical solvent there is no longer a need to add DMSO to the reaction mixture, removing a variable affecting the reaction. Furthermore the increased dielectric constant value of DMF allows for increased dissociation of ions, leading to lower resistivity across the cell. Therefore a lower voltage of 2.0 V can be applied to achieve the same current, reducing the possibility of side reactions. Pleasingly when the reaction was attempted an isolated yield of 80% of amide **3.106** was achieved (**Scheme 3.2.8.2**).

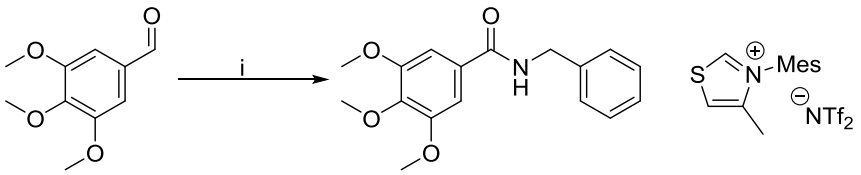

3.105 3.106 3.77

Scheme 3.2.8.2 - Electrochemical oxidative amidation in microflow. *Reagents & conditions* - i) Aldehyde **3.105** (0.1 M), NHC salt **3.77** (1.0 equiv.), DBU (1.0 equiv.), benzylamine (1.0 equiv.), DMF, 0.12 mL min^{-1}, 2.0 V, rt.

Voltammetry in the electrochemical flow cell was collected to confirm that the correct voltage was being applied to the reaction (**Figure 3.2.8.2**). Two peaks are observed, which correspond to each of the single electron transfers. The second peak occurs at approximately 1.8 V. At around 2.5 V there is a further increase in the current, which is related to over oxidation occurring or possibly a side reaction. Therefore an applied voltage of 2.0 V used during the optimised amidation reaction, is enough to drive the oxidation, but sufficiently low to reduce side reactions.

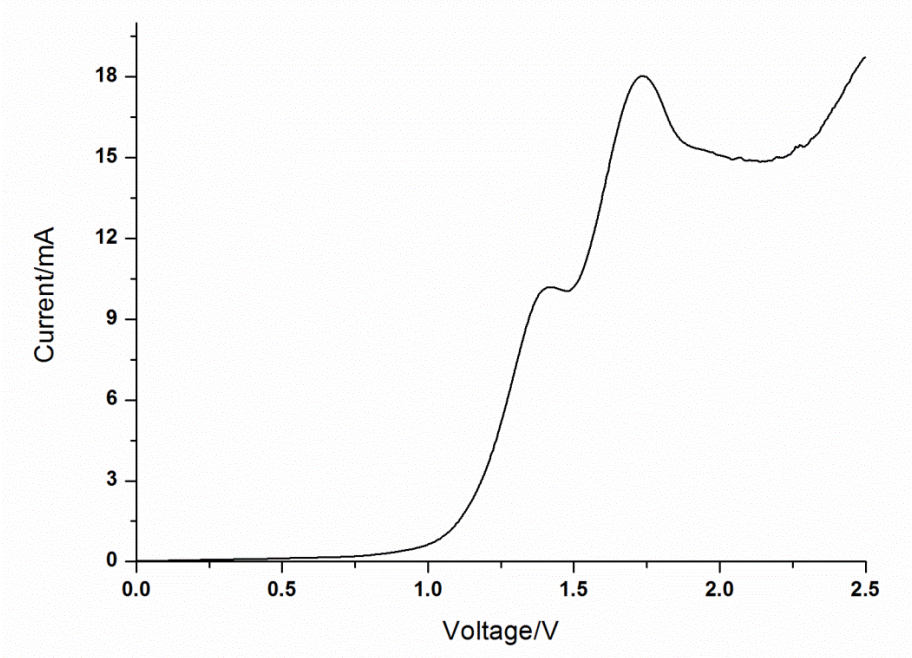

Figure 3.2.8.2 - Cyclic voltammetry of amidation reaction in the electrochemical miroflow cell.

The optimised conditions were then applied to a range of aldehydes and amines to investigate the scope of the reaction (**Scheme 3.2.8.3**). 22 examples were synthesised and the isolated yields are shown in **Table 3.2.8.1**.

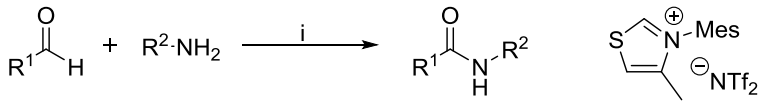

3.77

Scheme 3.2.8.3 - Electrochemical oxidative amidation reaction. *Reagents & conditions* - i) Aldehyde (0.1 M), NHC salt **3.77** (1.0 equiv.), DBU (1.5 equiv.), amine (1.0 equiv.), DMF, 0.12 mL min^{-1}, 2.0 V, rt.

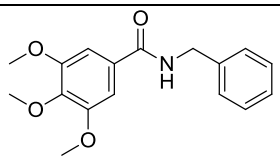

3.106 (80%)

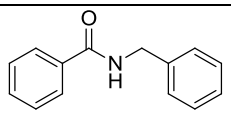

3.107 (66%)

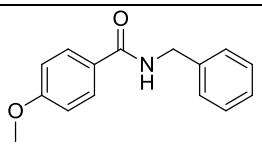

3.108 (71%)

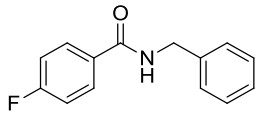

3.109 (83%)

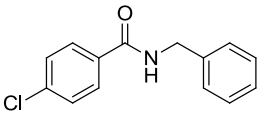

3.110 (82%)

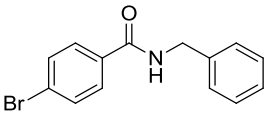

3.111 (91%)

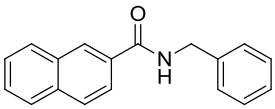

3.112 (84%)

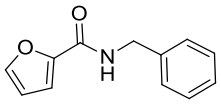

3.113 (75%)

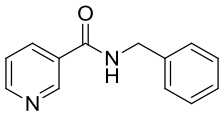

3.114 (74%)

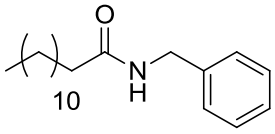

3.115 (59%)

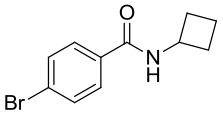

3.116 (67%)

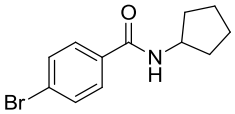

3.117 (65%)

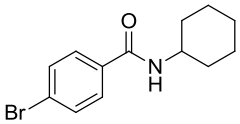

3.118 (67%)

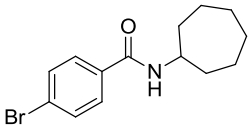

3.119 (72%)

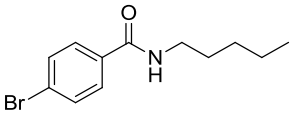

3.120 (89%)

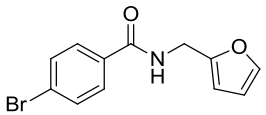

3.121 (75%)

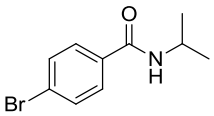

3.122 (70%)

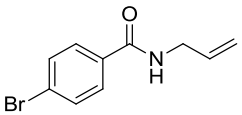

3.123 (92%)

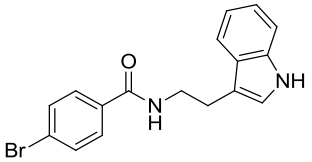

3.124 (73%)

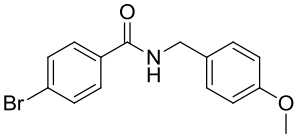

3.125 (84%)

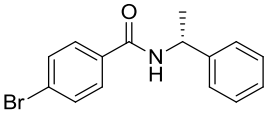

3.126 (66%)

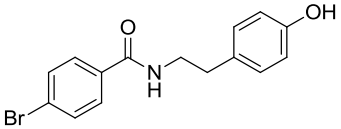

3.127 (66%)

Table 3.2.8.1 - Substrate examples for electrochemical oxidative amidation.

Good to excellent yields were achieved. Aromatic aldehydes again gave higher yields than aliphatic examples. Pyridyl amide **3.114** (74%) and furyl amide **3.113** (75%) also gave good yields. A range of amines with different functionality gave good yields. Interestingly when aldehyde **3.128** and amine **3.129** were subjected to the reaction conditions a mixture of amide **3.127** and amide **3.130** was formed in 66% and 32% yield respectively (**Scheme 3.2.8.4**).

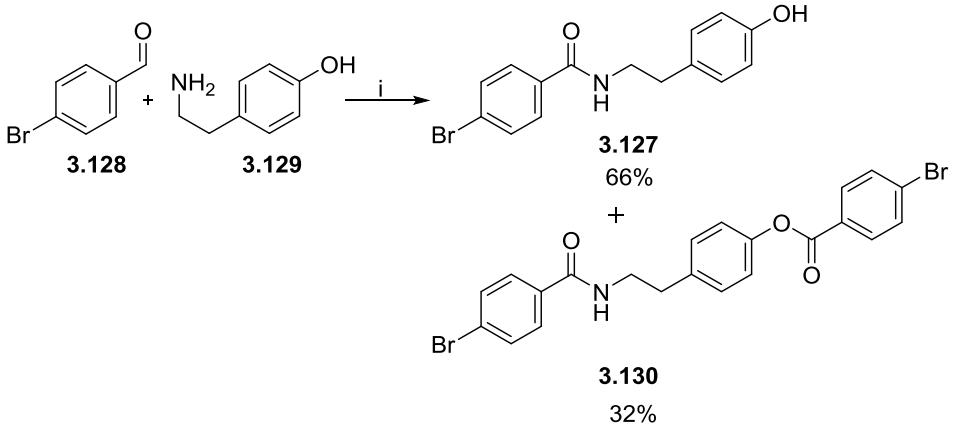

Scheme 3.2.8.4 - Formation of amides **3.127** and **3.130**. *Reagents & conditions* - i) Aldehyde **3.128** (0.1 M), NHC salt **3.77** (1.0 equiv.), DBU (1.5 equiv.), amine **3.129** (1.0 equiv.), DMF, 0.12 mL min^{-1}, 2.0 V, rt.

Secondary amines only gave traces of the amide product. Furthermore amines with bulkier groups attached gave slightly reduced yields. Similar observations were made with bulkier alcohols during the development of the esterification procedure as well. The reduced yield of amidation and esterification with bulkier amines and alcohols is postulated to be because of steric interactions. The approach of the larger amine or alcohol nucleophiles to the π* orbital *via* the Bürgi-Dunitz trajectory (105°) of the oxidised Breslow intermediate is partially blocked. The 3D model shows the oxidised Breslow intermediate **3.131** in a twisted conformation with the carbonyl centre surrounded with a lot of steric bulk (**Figure 3.2.8.3**). The methyl substituent of the mesityl group on the NHC is blocking the route of attack for the amine or alcohol in the activated acyl species **3.131**, from one side. For primary alcohols or amines with significantly lower steric bulk this does not appear to cause substantial reduction in yield. However, bulkier alcohol and amine substrates are more likely to clash with the large group surrounding the carbonyl centre, reducing the yield. To fully explore whether steric encumbrance is the source of the

reduced yield with larger alcohols and amines, computational studies of the transition state could be performed.

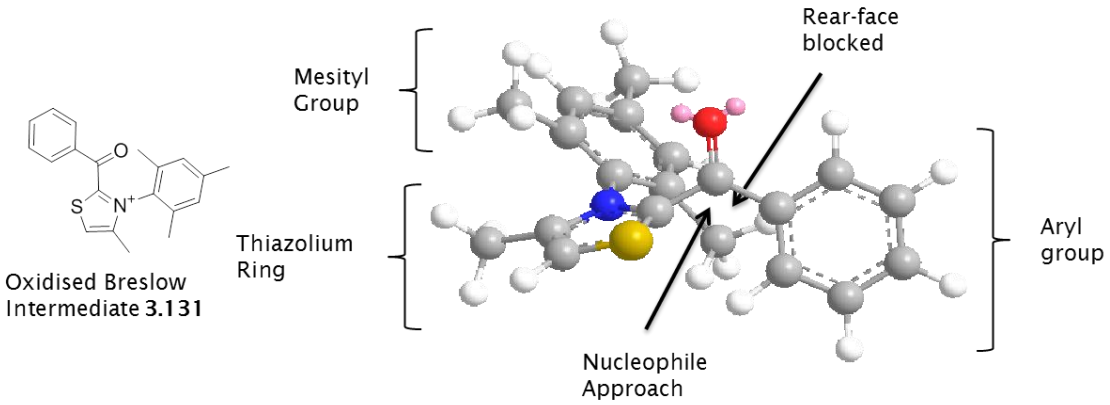

Figure 3.2.8.3 - Diagram depicting the steric interactions within the oxidised Breslow intermediate **3.131**.

The oxidative formation of amides with NHCs has previously been difficult to achieve with only a few examples discussed in the literature. Often this has been achieved by forming activated esters that are then displaced with amines. The research discussed in this section reports the first direct electrochemical oxidative amidation in good to excellent yields at a rate of ~50 mg h^{-1}, which is an advance compared to previous methods.

3.3 Conclusion and Future Work

The research discussed in this chapter has led to the successful development of electrochemical oxidative esterifications and amidations in flow, without the addition of electrolyte or excess alcohol or amine (**Scheme 3.3.1.1**). Research initially probing dual catalytic systems ultimately led to the effective implementation of a stoichiometric direct electrochemical oxidation. Both procedures have been applied to a range of substrates, showing a good tolerance of functional groups.

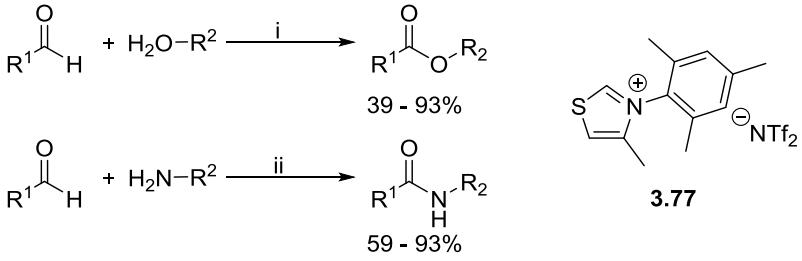

Scheme 3.3.1.1 - Oxidative esterification and amidation developed during this research. *Reagents & conditions* - i) Aldehyde (0.1 M), NHC salt **3.77** (1.0 equiv.), DBU (1.5 equiv.), alcohol (1.0 equiv.), DMSO (5.0 equiv.), THF, 0.1 mL min^{-1}, 2.5 V, rt. ii) Aldehyde (0.1 M), NHC salt **3.77** (1.0 equiv.), DBU (1.5 equiv.), amine (1.0 equiv.), DMF, 0.12 mL min^{-1}, 2.0 V, rt.

Design of Experiment software was applied to assist the optimisation of these reactions, and was helpful in the identification of the important factors, such as flow rate, voltage and DBU loading and how they affected the reaction. To generate the same information systematically, 60 to 100 experiments would have been required per design. The number of experiments performed was reduced to around twenty per model with the use of DoE software, highlighting the power of this approach when applied to reaction optimisation. Furthermore cyclic voltammetry experiments allowed quick investigation of the electrochemistry of oxidants and intermediates. This information was then directly used in the development and assisted in the understanding of the observations generated by the DoE models. For example the effect of increased DBU on the direct electrochemical oxidation of the Breslow intermediates, leading to improved esterification and amidation yields could be readily explained.

Future work will focus on developing an NHC catalyst/reagent which is more active for the oxidative esterification and amidation, with the intention of widening the scope of the reaction to involve bulkier alcohols and amines. Thiazole based NHC salts have been demonstrated to show the best reactivity towards the direct electrochemical oxidation of the Breslow intermediates. Replacing the aryl group for an alkyl chain would reduce the steric bulk around the oxidised Breslow intermediate, and also lead to more favourable ionic liquid properties.[152] The current NHC salt **3.77** is a very viscous ionic liquid and requires addition of co-solvent to facilitate its use in the flow cell. Thiazolium salt **3.132**, with the long alkyl chain would have reduced viscosity and increased hydrophobicity properties, which would be useful when considering alternative NHC sources (**Figure 3.3.1.1**).

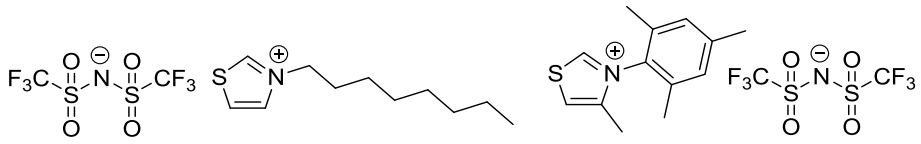

Figure 3.3.1.1 - Thiazolium NHC salt/ionic liquid for future development.

Three-dimensional models of the NHC salt **3.132** show that the oxidised Breslow intermediate would have less steric bulk surrounding where the approach of a nucleophile would occur *via* the Bürgi-Dunitz trajectory (**Figure 3.3.1.2**). This could potentially enable bulkier alcohols and amines to be utilised. To fully explore whether NHC salt **3.132** could improve yields, computational models of the transition state would provide a useful insight into the mechanism of the approach of the nucleophile.

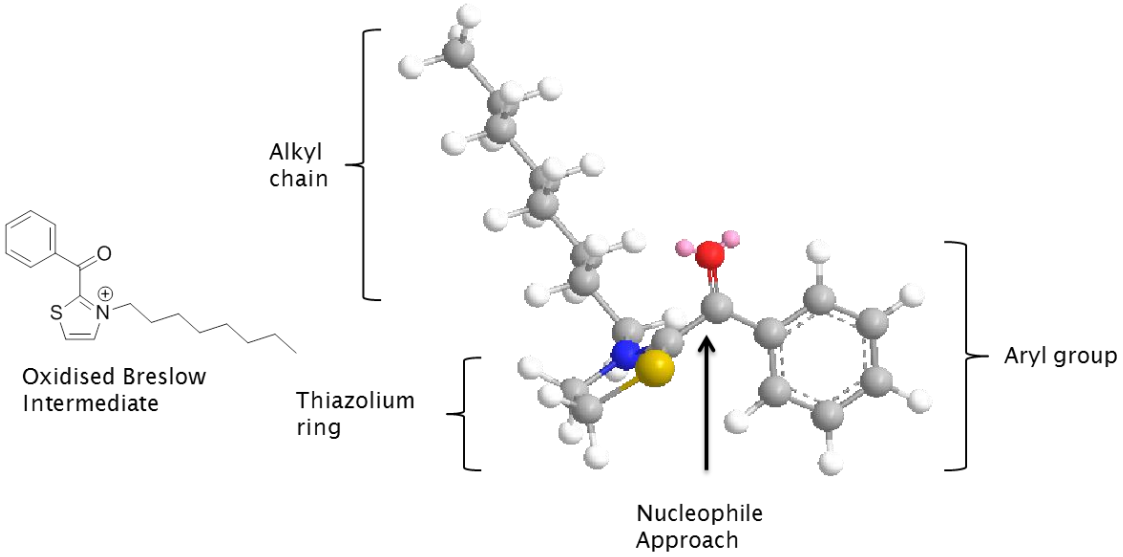

Figure 3.3.1.2 - Diagram depicting reduced steric crowding of oxidised Breslow intermediate.

Changing the groups present on the thiazole ring would also give information on what groups affect the oxidation, which could lead to milder oxidation protocols. Imidazolium salt $[BMIM]^+[BF_4]^-$ was shown to not be as effective at direct electrochemical oxidation. Furthermore attempts to perform cyclic voltammetry studies on the Breslow intermediate with imidazolium salts were unfruitful as no oxidation peaks were observed. This observation suggests the Breslow intermediate with imidazolium salts is less stable. The improved stability with thiazolium salts could be due to stability provided by the sulfur heteroatom. Alternatively, the mesityl group's ability to provide more resonance structures to be formed compared to the alkyl chain maybe more influential on the activity. Probing the effects on the substituents on the NHC using computational studies and electrochemical techniques could lead to a more active reagent.

Although this research has been highly successful in generating new oxidative procedures, the loading of NHC salt (1.0 equivalent) is likely to be prohibitive to its wider up-take. Research into developing a more active reagent/catalyst could lead to the reduction of the NHC loading, making these procedures more attractive. Our research has already shown that good yields can be achieved with the esterification using 0.5 equivalents of NHC salt with an extended path-length of the flow cell. Therefore a catalytic electrochemical oxidative esterification is feasible in the future with more development.

The development of a catalytic oxidative amidation may be more difficult to achieve, mostly because of the tendency of any free aldehyde to react with the amine generating an imine. Our research addressed this side reaction by engineering the flow path to avoid it. To develop a catalytic oxidative amidation is likely to require a more complex engineering solution, possibly requiring the development of a new electrochemical cell.

The research discussed in this chapter has laid the foundations for electrochemical oxidative esterifications and amidation with NHCs in flow. Further research into the factors affecting the activity of the NHC, using DoE experimentation, computational studies and electrochemical techniques, will eventually lead to more reactive reagents. This coupled with novel engineering solutions could lead to catalytic procedures, based on this work. This will lead to the wider up-take of this technology by synthetic chemists, achieving the ultimate goal of our research into flow electrosynthesis.

4 Experimental

4.1 General Methods

Chemicals were purchased from Sigma-Aldrich, Fisher Scientific, Alfa Aesar, Fluorochem or Apollo Scientific. All air/moisture sensitive reactions were carried out under an inert atmosphere, in oven-dried or flame-dried glassware. The solvents THF (over Na/benzophenone), CH_3CN, CH_2Cl_2 (over CaH_2) and MeOH (over $Mg(OMe)_2$) were distilled before use, and where appropriate, other reagents and solvents were purified by standard techniques.[168] TLC was performed on aluminium-precoated plates coated with silica gel 60 with an F_{254} indicator; visualised under UV light (254 nm) and/or by staining with anisaldehyde, ceric ammonium molybdate, iodine, phosphomolybdic acid, potassium permanganate or vanillin. Flash column chromatography was performed using; high purity silica gel, Geduran®, pore size 60 Å, 230-400 mesh particle size, purchased from Merck.

Fourier-transform infrared (FT-IR) spectra are reported in wavenumbers (cm^{-1}) and were collected as solids or neat liquids on a Nicolet 380 fitted with a Smart Orbit Goldengate attachment using OMNIC software package. The abbreviations s (strong), m (medium), w (weak) and br (broad) are used when reporting the spectra. Optical rotations were collected on an Optical Activity PolAAr 2001 machine. The solvents used for the measurement of the optical activity are detailed in the experimental.

^1H NMR and ^{13}C NMR spectra were recorded in $CDCl_3$, CD_3CN, CD_3SOCD_3 solutions (purchased from Cambridge Isotope Laboratories, Inc.) at 298 K using Bruker AC300, AV300 (300 and 75 MHz respectively) or Bruker DPX400 (400 and 100 MHz respectively) spectrometers. Chemical shifts are reported in δ units using $CHCl_3$ or DMSO as an internal standard (δ 7.27 ppm ^1H, δ 77.00 ppm ^{13}C, δ 2.05 ppm ^1H, δ 39.52 ppm ^{13}C respectively). All spectra were reprocessed using ACD/Labs software version: 12.1. Coupling constants (*J*) were recorded in Hz and are corrected. The following abbreviations for the multiplicity of the peaks are s (singlet), d (doublet), t (triplet), q (quartet), quin (quintet), sxt (sextet), spt (septet), oct (octet) br (broad), and m (multiplet).

Melting points were obtained using a Gallenkamp Electrothermal apparatus and are uncorrected. Electrospray resolution mass spectra were recorded on a Waters ZMD quadrupole spectrometer. High resolution mass spectra were recorded on a Bruker Daltonics MaXis mass spectrometer equipped with a time of flight analyser.

4.2 Electrochemistry

4.2.1 Cyclic Voltammetry

Cyclic voltammograms were recorded using a potentiostat/galvanostat (SP-150, BioLogic Science Instruments or Autolab PGStat101) and EC-Lab® software or Nova 1.9 software. The voltammetry was carried out using a three electrode, two compartment glass cell. The working electrode was a glassy carbon disc (area = 0.07 cm^2) sealed in a glass tube and it was separated from the SCE (saturated calomel electrode) reference electrode by a Luggin capillary whose tip was positioned close to the surface of the disc. The Pt counter electrode was in the same compartment as the working electrode. Between experiments, the glassy carbon disc was polished using fine alumina powder on a polishing cloth.

4.2.2 Solution Preparation

The pH was varied for the investigation into the electrochemical TEMPO mediated alcohol oxidation, by mixing different ratios of 0.1 M Na_2CO_3 and 0.1 M $NaHCO_3$, both in water as shown in **Table 4.2.2.1**. These aqueous solutions were then mixed 1:1 with ^{t}BuOH and the pH measured using a calibrated Hanna HI 8424 pH meter. All solutions were sonicated and degassed prior to use.

pH of Solution	Ratio of Na_2CO_3:$NaHCO_3$
9.3	1:99
9.4	1:50
9.5	1:25
9.8	1:10
10.7	1:1
11.3	10:1
11.5	25:1
11.6	50:1
11.7	99:1

Table 4.2.2.1 - Buffer solution preparation.

A higher pH buffer solution of 13.2 was achieved by mixing 0.2 M KCl with 0.2 M of NaOH in water in equal amounts. Alternatively a 0.25 M KOH solution in 1:1 ^{t}BuOH/water gave a pH of 13.4.

4.3 Gas Chromatography

4.3.1 General Procedure

Gas Chromatography was performed using a Shimdazu GC-2014 equipped with an autosampler and FID detector. The GC was fitted with an Agilent technologies HP5 column with the following dimensions; length - 30 m, internal diameter - 0.32 mm and film thickness - 0.25 μm. The results were processed using GC Solution Lite software. Separations were carried out using Helium as a carrier gas with a flow rate of 2.37 mL min^{-1} through the column. A split injection was conducted using a split ratio of 100:1. The injection and detector temperatures were maintained at 200 °C and 255 °C respectively. The oven temperature was initially held at 80 °C and then programmed to increase at 20 °C min^{-1} to 250 °C, where it was held constant for 3 minutes.

4.3.2 TEMPO Mediated Benzyl Alcohol Calibration

GC techniques were used to aid the investigation of the effect of pH on the TEMPO mediated benzyl alcohol oxidation (discussed in Chapter 2). This required the formation of calibration curves for benzaldehyde (**2.42**), benzyl alcohol (**2.42**) and TEMPO (**2.22**). Using the method described earlier effective separation of the compounds was achieved, with retention times of 2.41 min for benzaldehyde, 2.77 min for benzyl alcohol and 3.42 min for TEMPO (**Figure 4.3.2.1**)

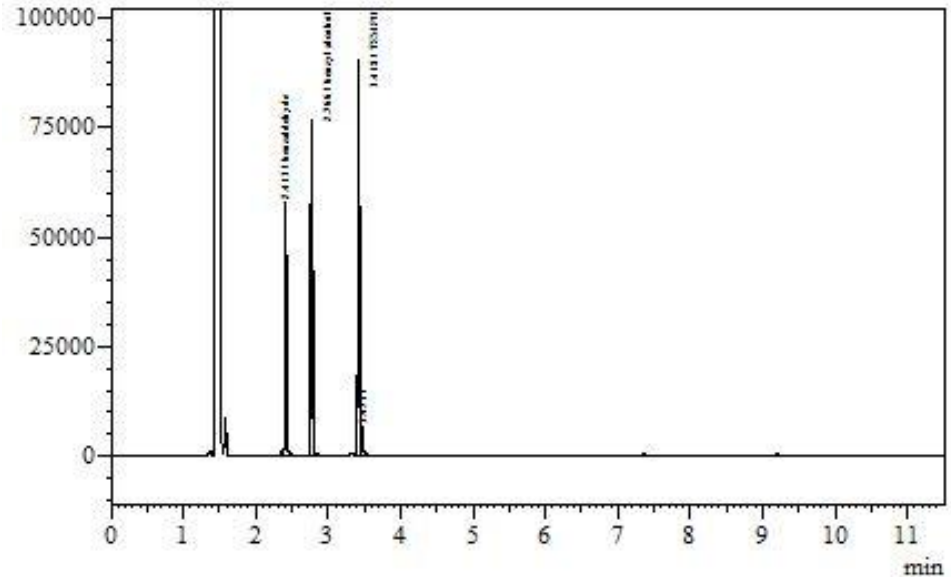

Figure 4.3.2.1- GC trace showing separation of benzaldehyde (**2.43**), benzyl alcohol (**2.42**) and TEMPO (**2.22**).

To create the calibration curves shown in **Figure 4.3.2.2**, the integration of the area of the peak was used, which was calculated by the software. This generated a straight line plot, from which the concentration of unknown solutions could be calculated.

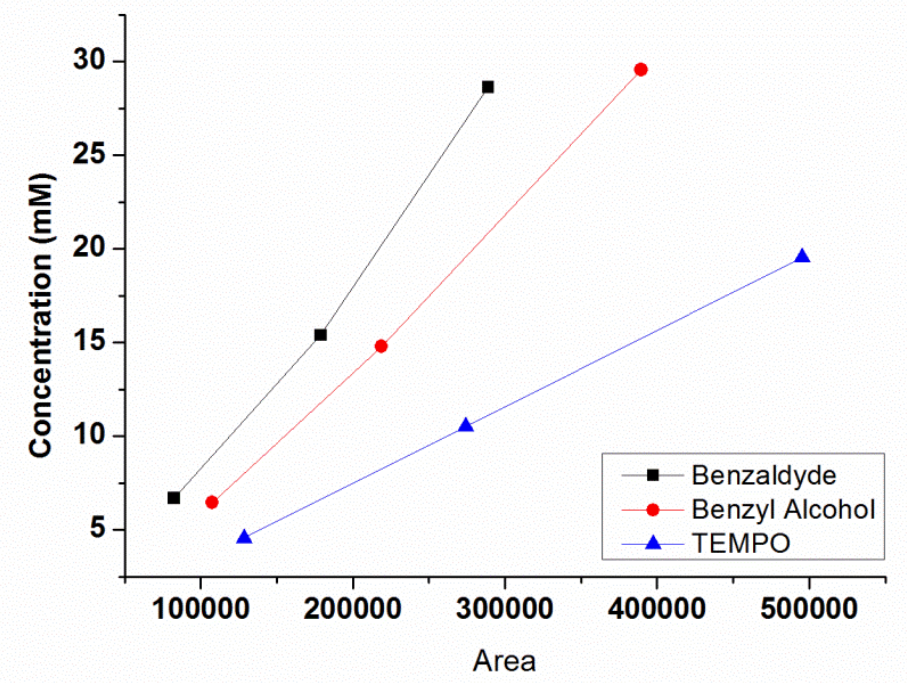

Figure 4.3.2.2 -Benzaldehyde, Benzyl alcohol and TEMPO calibration curves.

4.3.3 NHC Mediated Oxidative Esterifications Calibration

To increase the rate of optimisation the GC was employed to monitor the reaction. Aldehyde **3.66** and ester **3.67** (**Scheme 4.3.3.1**) were effectively separated using the method discussed earlier to give retention times of 4.67 min and 5.77 min respectively (**Figure 4.3.3.1**)

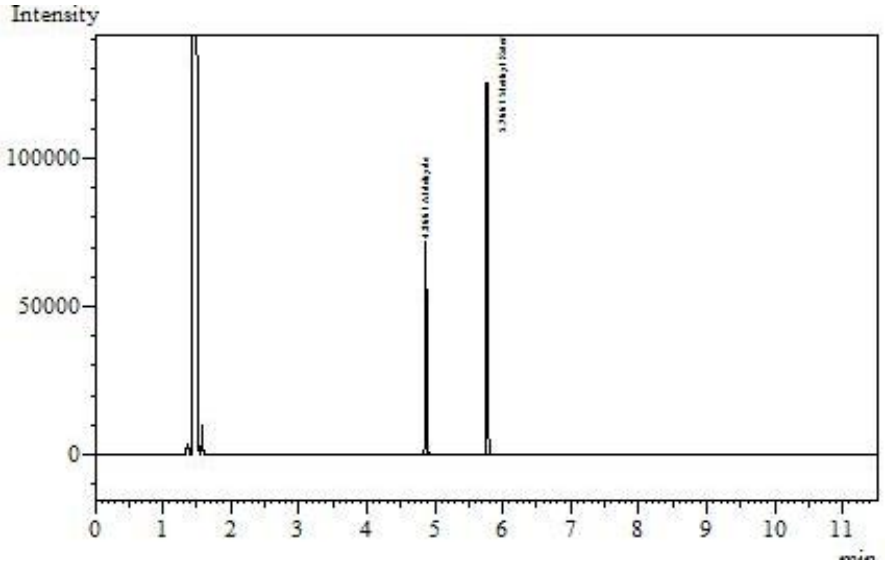

Figure 4.3.3.1 - GC trace showing separation of aldehyde **3.66** and ester **3.67**.

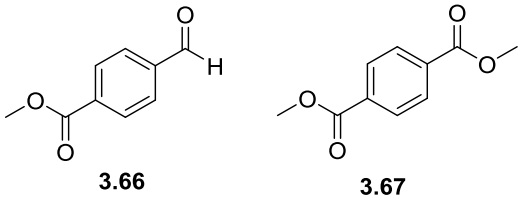

Scheme 4.3.3.1 - Structures of aldehyde **3.66** and ester **3.67**.

Calibration curves were created in order to use the GC to monitor the oxidative esterification optimisation. The calibration curves were obtained using three different concentrations of aldehyde **3.66** and ester **3.67**, plotting the integral of the response against concentration (**Figure 4.3.3.2**). The concentration of solutions of aldehyde **3.76** and **3.77** could be calculated, and therefore yields could be estimated.

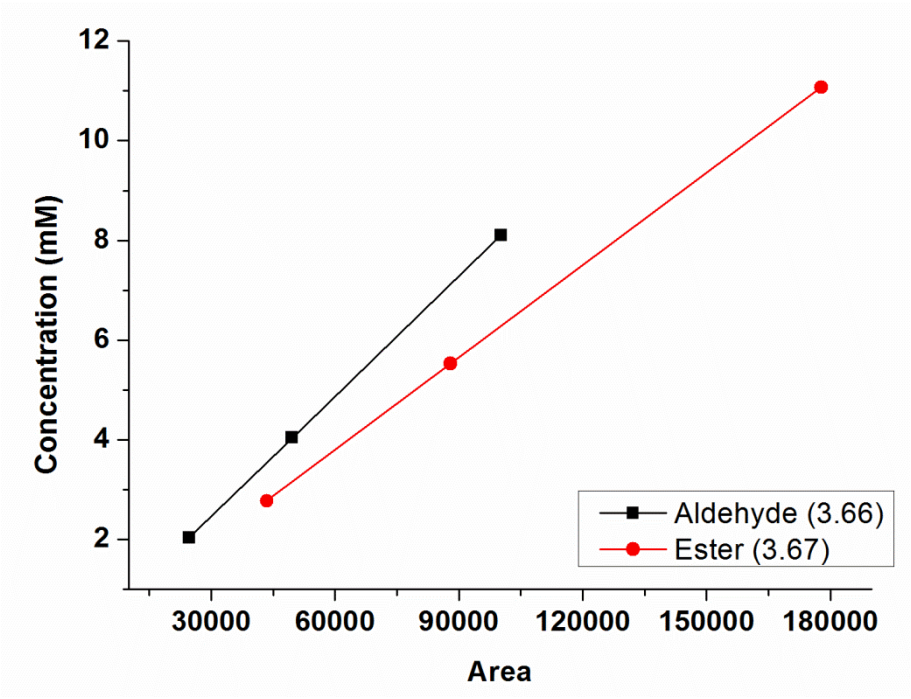

Figure 4.3.3.2 - Calibration curves for aldehyde **3.66** and ester **3.67**.

4.4 Procedures and Characterisation Data

4.4.1 2,2,6,6-Tetramethyl-1-oxopiperidin-1-ium tribromide (2.61)

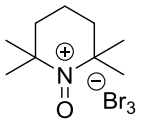

2.61
$C_9H_{18}Br_3NO$
393.95 g mol^{-1}

TEMPO (400 mg, 2.56 mmol 1.00 equiv.) was dissolved in hexane (10.0 mL). Bromine (412 mg 2.58 mmol, 1.01 equiv.) was added and the reaction mixture was stirred for 30 min. On completion a red precipitate had formed, which was collected by filtration, washed with hexane and dried under vacuum to give oxoammonium salt **2.61** (0.60 g, 1.52 mmol, 59%), as a red solid. Spectroscopic and physical data are consistent with the literature.[169]

MP: 84-86 °C [Literature: 78-80 °C (CCl_4)][169]

FT-IR (cm^{-1}) neat: 2985 (w), 2937 (w), 2864 (w), 1600 (m), 1462 (m).

LRMS: ESI^+ m/z 156.2 [M^+].

Elemental Analysis: Predicted: C (27.30), H (4.58), N (3.54)

Found : C (27.46), H (4.58), N (3.47).

4.4.2 2,2,6,6-Tetramethyl-1-oxopiperidin-1-ium tetrafluoroborate (2.62)

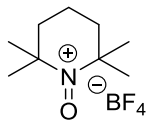

2.62

$C_9H_{18}BF_4NO$
243.05 g mol^{-1}

Procedure adapted from Studer *et al.*[89] TEMPO (1.00 g, 6.40 mmol, 1.00 equiv.) was taken up in water (5.00 mL) to give a red suspension. To this tetrafluoroboric acid (48% aq. solution, 1.30 mL, 6.40 mmol, 1.00 equiv.) was added dropwise. The reaction mixture was allowed to stir for 30 min, whereupon a yellow suspension formed. The reaction mixture was then cooled with an ice bath and NaOCl (2.30 mL, 3.20 mmol, 0.50 equiv.) was added dropwise. The reaction mixture was stirred with ice bath cooling for 1.5 h. The solids were filtered off and washed with 5% $NaHCO_3$ solution (5.00 mL), water (5.00 mL) and diethyl ether (40 mL), to give oxoammonium salt **2.62** (0.50 g, 2.06 mmol, 32%) as a yellow solid. Spectroscopic and physical data are consistent with the literature.[89,169,170]

MP: 155-157 ˚C [literature: 162-163 ˚C (H_2O)][169]

FT-IR (cm^{-1}) neat: 2999 (w), 2970 (w), 2943 (w), 1626 (m), 1462 (m), 1030 (s).

^{1}H NMR: 400 MHz, CD_3CN, δ ppm: 2.52-2.50 (4H, m, –C**H**$_2$–, x2), 2.43-2.39 (2H, m, –C**H**$_2$–), 1.67 (12H, s, –C**H**$_3$, x4).

^{13}C NMR: 100 MHz, CD_3CN, δ ppm: 118.4 (–**C**–N^+–**C**–), 41.5 (–**C**H_2–, x2), 29.7 (–**C**H_3, x4), 17.1 (–**C**H_2–).

^{19}F NMR: 282 MHz, CD_3CN, δ ppm: –151.8 (4F, B**F**$_4$).

LRMS: (ESI$^+$) m/z 156.2 [M^+].

(ESI$^-$) m/z 87.0 [M^-].

4.4.3 1-Methyl-1*H*-1,2,4-triazole (3.55)

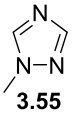

3.55

$C_3H_5N_3$

83.09 g mol^{-1}

The procedure was adapted from Belletire *et al.*[144] First a solution of NaOMe was prepared in flame-dried glassware, by adding sodium (1.66g, 72.0 g-atom, 1.00 equiv.) to ice cooled methanol (17 mL) slowly. 1,2,4-Triazole **3.54** (5.00 g, 72.0 mmol, 1.00 equiv.) was dissolved in methanol (40 mL). To this the NaOMe solution was added dropwise using a dropping funnel, whilst cooling the reaction mixture with an ice bath. On complete addition of the NaOMe solution the reaction mixture was warmed at 60 °C for 2 h. The reaction mixture was then cooled with an ice bath and methyl iodide (11.24 g, 79.0 mmol, 1.10 equiv.) was added dropwise. On complete addition the reaction mixture was warmed to reflux for 12 h after which the solvent was removed under reduced pressure. The crude was dissolved in water (20 mL), and the organic was extracted with hot chloroform (3 x 25 mL). The organic was dried with $MgSO_4$, filtered and the solvent removed to give a colourless oil. This was then purified by vacuum distillation (0.10 mbar, 60 °C) to give a colourless oil of methyl-triazole **3.55** (3.20 g, 38.5 mmol, 53%). Spectroscopic and physical data are consistent with the literature.[144]

FT-IR (cm^{-1}) neat: 3114 (w), 2948 (w), 1511 (s).

^{1}H NMR: 300 MHz, $CDCl_3$, δ ppm: 7.99 (1H, s, N=C**H**–N), 7.85 (1H, s, N=C**H**–N), 3.87 (3H, s, N–C**H**$_3$).

^{13}C NMR: (75 MHz, $CDCl_3$, δ ppm: 151.8 (N=**C**H–N), 143.3 (N=**C**H–N), 35.9 (**C**H$_3$).

LRMS: (ESI$^+$) m/z 84.1 [M + H$^+$].

4.4.4 1,4-Dimethyl-4*H*-1,2,4-triazol-1-ium iodide (3.49)

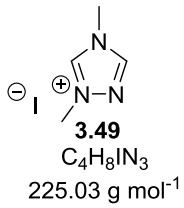

3.49

$C_4H_8IN_3$

225.03 g mol^{-1}

The procedure was adapted from Belletire *et al*.[144] To a dried RBF under N_2, methyl-triazole **3.55 (**2.00 g, 24.0 mmol, 1.00 equiv.) was added and dissolved in MeOH (5.00 mL). Then MeI (7.52 g, 52 mmol, 2.20 equiv.) was added. The reaction flask was covered with foil and left to stir for 4 days. Solvent was removed under reduced pressure to give a yellow solid. This was triturated with diethyl ether to give a pale yellow solid, which was collected by filtration and dried under high vacuum to give the triazolium salt **3.49** (3.87 g, 17.2 mmol, 72%) as a pale yellow solid. Spectroscopic and physical data are consistent with the literature.[144,171]

MP: 115-117 ˚C [Literature: 121-123 ˚C (EtOH)][171]

FT-IR (cm^{-1}) neat: 3025 (m), 2978 (m), 2929 (m), 1582 (m).

^{1}H NMR: 300 MHz, DMSO, δ ppm: 9.98 (1H, s, –N$^+$=C**H**–N), 9.11 (1H, s, N=C**H**–N), 4.06 (3H, s, –C**H**$_3$), 3.89 (3H, s, –C**H**$_3$).

^{13}C NMR: 75 MHz, DMSO, δ ppm: 145.3 (–N$^+$=**C**H–N–), 143.3 (–N=**C**H-N–), 38.6 (–**C**H$_3$), 34.0 (–**C**H$_3$).

LRMS: (ESI$^+$) m/z 98.1 [M$^+$].

(ESI$^-$) m/z 126.9 [M$^-$].

4.4.5 3,3',5,5'-Tetra-*tert*-butyl-4,4'-diphenoquinone (3.35)

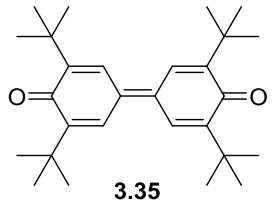

3.35
$C_{28}H_{40}O_2$
408.62 g mol^{-1}

The procedure was adapted from Omura *et al*.[172] A RBF was charged with 2,6-di-*tert*-butylphenol (**3.63**, 10.0 g, 48.0 mmol, 1.00 equiv.) and dissolved in MeOH (150 mL). Potassium hydroxide (20.9 g, 372 mmol, 7.75 equiv.) was added. Iodine flakes (12.4 g, 48.5 mmol, 1.01 equiv.) was dissolved in MeOH (100 mL) and added to the reaction mixture. The reaction mixture was stirred for 30 min, upon which a red/brown precipitate had formed. The precipitate was collected, washed with MeOH and dried to give the quinone (**3.35**, 9.80 g, 23.9 mmol, 100%) as a red solid. Spectroscopic and physical data are consistent with the literature.[173]

MP: 240-242 ˚C [literature: 240-242 ˚C (Benzene)][174]

FT-IR (cm^{-1}) neat: 2954 (m), 2908 (m), 2864 (m), 1600 (s), 1566 (m).

^{1}H NMR: 300 MHz, $CDCl_3$, δ ppm: 7.72 (4H,s, –C=C**H**–), 1.37 (36 H, s, 4 x ^{t}Bu).

^{13}C NMR: 75 MHz, $CDCl_3$ δ ppm: 186.5 (**C**=O, x2), 150.4 (–**C**-^{t}Bu, x4), 136.1 (–**C**=**C**–), 126.0 (–C=**C**–, x4), 36.0 (–**C**$(CH_3)_3$, x4), 29.6 (–C(**C**$H_3)_3$, x4).

LRMS: (EI) m/z 408.4 (4%) [M$^+$].

4.4.6 Tetra-acetylriboflavin (3.71)

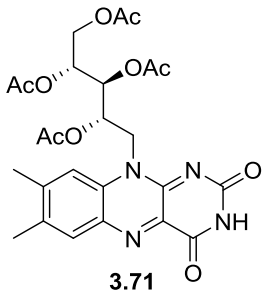

3.71

$C_{25}H_{28}N_4O_{10}$

544.51 g mol^{-1}

Procedure was adapted from Gust *et al.*[175] Riboflavin (**3.70**, 5.00 g, 13.3 mmol, 1.00 equiv.) was suspended in a mixture of acetic anhydride (60 mL) and pyridine (60 mL) and heated to reflux for 15 min. The reaction mixture was then allowed to cool and was diluted with DCM (90 mL), then poured onto ice-cooled HCl (2M, 60 mL). The product was extracted with DCM (3 x 100 mL) and then washed with HCl (2 M, 3 x 50 mL). The organic was dried over $MgSO_4$, filtered and the solvent removed to give an orange solid. The product was recrystallised from water to give tetra-acetylriboflavin **3.71** (4.75 g, 8.72 mmol, 66%) as orange crystals. Spectroscopic and physical data are consistent with the literature.[176]

MP: 237-239 ˚ C [literature: 238-242 ˚C (H_2O)][177]

FT-IR (cm^{-1}) neat: 3162 (w), 3101 (w), 3026 (m), 2809 (w), 1740 (s), 1712 (s), 1657 (s), 1575 (s), 1535 (s).

^{1}H NMR: 300 MHz, DMSO, δ ppm: 11.39 (1H, s, –N**H**), 7.87 (1H, s, Ar–**H**), 7.72 (1H, s, Ar–**H**), 5.59-5.43 (2H, m, –N-C**H**$_2$–), 5.31-5.29 (1H, m, –C**H**–), 5.04 (1H, br, –C**H**–), 4.83 (1H, d, *J*=13.5 Hz, –C**H**–), 4.37 (1H, dd, *J*=12.4, 2.6 Hz, –C**H**$_2$–), 4.20 (1H, dd, *J*=12.4, 6.2 Hz, –C**H**$_2$–) 2.50 (3H, s, –C**H**$_3$), 2.39 (3H, s, –C**H**$_3$), 2.19 (3H, s, –C**H**$_3$), 2.18 (3H, s, –C**H**$_3$), 1.99 (3H, s, –C**H**$_3$), 1.58 (3H, s, –C**H**$_3$).

^{13}C NMR: 75 MHz, $CDCl_3$ δ ppm: 170.1 (–**C**=O), 169.8 (–**C**=O), 169.6 (–**C**=O), 169.4 (–**C**=O), 159.7 (–**C**=O, Ar), 155.3 (–**C**=O, Ar), 150.6 (–**C**=N–, Ar), 146.3, (–**C**=N–, Ar), 136.9 (–**C**=C–, Ar), 135.9 (–**C**=C–, Ar), 133.6 (–**C**=C–, Ar), 131.1 (H_3C–**C**=C–,

x2, Ar), 116.3 (-**C**=C-) 84.9 (-**C**H-), 69.7 (-**C**H-), 68.7 (-**C**H-, x2), 61.5 (-**C**H_2-), 43.8 (-**C**H_2-N-), 20.8 (Ar-**C**H_3), 20.7 (OAc), 20.6 (OAc), 20.5 (OAc), 20.1 (OAc), 18.7 (Ar-**C**H_3).

LRMS: (ESI$^+$) m/z 1111.3 [2M + Na$^+$], 567.2 [M + Na$^+$].

4.4.7 3-Methylriboflavin Tetraacetate (3.36)

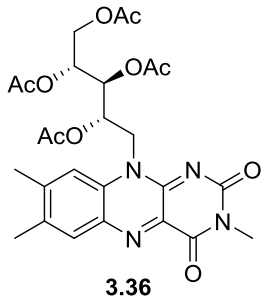

3.36
$C_{26}H_{30}N_4O_{10}$
558.54 g mol^{-1}

Procedure was adapted from Burkhard *et al.*[178] Tetra-acetylriboflavin **3.71** (4.00 g, 7.34 mmol, 1.00 equiv.) was dissolved in dry DMF (50 mL). Cs_2CO_3 (3.59 g, 11.0 mmol, 1.5 equiv.) and MeI (10.4 g, 73.4 mmol, 10.0 equiv.) was added to the reaction mixture and stirred for 16 h in the dark. Water (20 mL) was added to the reaction mixture, and the organic was extracted with chloroform (3 x 50 mL). The organic was washed with water (3 x 50 mL) and brine (3 x 50 mL), dried over $MgSO_4$ and the solvent removed. The product was purified by column chromatography (2% MeOH in chloroform), and finally recrystallised from MeOH, to give **3.36** (2.85g, 5.10 mmol, 70%) as orange crystals. Spectroscopic and physical data are consistent with the literature.[178]

MP: 175-177 ˚C [literature: 175 ˚C (MeOH)][177]

FT-IR (cm^{-1}) neat: 2981 (w), 2933 (w), 2357 (w), 2308 (w), 1741 (s), 1711 (s), 1666 (s), 1582 (s), 1540 (s).

^{1}H NMR: 300 MHz, $CDCl_3$, δ ppm: 8.05 (1H, s, Ar-**H**), 7.54 (1H, s, Ar-**H**), 5.68 (1H, m, -C**H**-), 5.49-5.39 (2H, m, -CH_2-), 4.91 (2H, br, -C**H**-), 4.44, (1H, dd, *J*=12.3, 2.4 Hz,

–C**H**–), 4.25 (1H, dd, *J*=12.4, 5.5 Hz, –C**H**–), 3.50 (3H, s, –C**H**$_3$), 2.56 (3H, s, –C**H**$_3$), 2.44 (3H, s, –C**H**$_3$), 2.31 (3H, s, –C**H**$_3$), 2.23 (3H, s, –C**H**$_3$), 2.08 (3H, s, C**H**$_3$), 1.74 (3H, s, –C**H**$_3$).

^{13}C NMR: 75 MHz, $CDCl_3$ δ ppm: 170.6 (**C**=O), 170.3 (**C**=O), 169.8 (**C**=O), 169.6 (**C**=O), 159.9 (**C**=O, Ar), 155.3 (**C**=O, Ar), 149.1 (–**C**=N–, Ar), 147.5 (–**C**=N–, Ar), 136.5 (–**C**=C–, Ar), 135.6 (–**C**=C–, Ar), 134.6 (–**C**=C–, Ar), 132.9 (–**C**=C–, Ar), 131.1 (–**C**=C–, Ar), 115.3 (–**C**=C–, Ar), 70.4 (–**C**H–), 69.4 (–**C**H–), 69.0 (–**C**H–), 61.9 (–**C**H$_2$–), 44.5 (–**C**H$_2$–), 28.7 (–N**C**H$_3$), 21.4 (Ar–**C**H$_3$), 21.0 (OAc), 20.9 (OAc), 20.7 (OAc), 20.3 (OAc), 19. 4 (Ar–**C**H$_3$).

LRMS: (ESI$^+$) m/z 1139.5 [2M + Na$^+$], 581.2 [M + Na$^+$].

4.4.8 3-Butyl-1-methyl-1*H*-imidazol-3-ium bromide [BMIM]$^+$[Br]$^-$ (3.75)

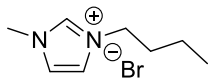

3.75
$C_8H_{15}BrN_2$
219.12 g mol^{-1}

The procedure was adapted from Kamal *et al.*[179] In flame-dried glassware 1-methylimidazole **3.73** (10.3 g, 125 mmol, 1.00 equiv.) was added followed by bromobutane **3.74** (18.4 g, 138 mmol, 1.1 equiv.). The reaction mixture was heated at 70 ˚C for 12 h, giving a yellow solution. The reaction mixture was cooled and the excess bromobutane was removed under reduced pressure to give [BMIM]$^+$[Br]$^-$ **3.65** (27.0g, 123 mmol, 99%), as a colourless oil, which gradually solidified. Spectroscopic and physical data are consistent with the literature.[179,180]

MP: 76-78 ˚C [literature: 77-78 ˚C ($CHCl_3$)][181]

FT-IR (cm^{-1}) neat: 3125 (w), 3081 (m), 2961 (m), 2867 (m), 2837 (w), 1566 (m).

^{1}H NMR: 300 MHz, DMSO, δ ppm: 9.26 (1H, s, –N–C**H**–N–), 7.82 (1H, s, –C**H**=CH–), 7.75 (1H, s, –CH=C**H**–), 4.18 (2H, t, *J*=7.1 Hz, N–C**H**$_2$–CH$_2$–), 3.86 (3H, s, N–C**H**$_3$), 1.76 (2H, quin, *J*=7.3 Hz, –N–CH$_2$–C**H**$_2$–), 1.25 (2H, sxt, *J*=7.3 Hz, –CH$_2$–C**H**$_2$–CH$_3$), 0.89 (3H, t, *J*=7.3 Hz, –CH$_2$–C**H**$_3$).

^{13}C NMR: 75 MHz, DMSO, δ ppm: 136.5 (–N–**C**=N–), 123.5, –**C**=C–), 122.2 (–C=**C**–), 48.4 (–N–**C**H$_2$–) 35.7 (–N–**C**H$_3$), 31.3 (–CH$_2$–**C**H$_2$), 18.7 (–**C**H$_2$–CH$_3$), 13.2 (–**C**H$_3$).

LRMS: ESI$^+$ m/z 139.2 [M$^+$].

ESI$^-$ m/z 80.9 [M(^{81}Br)$^-$], 78.9 [M(^{79}Br)$^-$].

4.4.9 3-Butyl-1-methyl-1*H*-imidazol-3-ium bis((trifluoromethyl)sulfonyl)amide [BMIM] [NTf_2] (3.72)

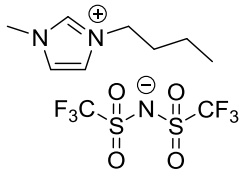

3.72

$C_{10}H_{15}F_6N_3O_4S_2$

419.36 g mol^{-1}

The procedure was adapted from Schmitzer *et al.*[182] $[BMIM]^+[Br]^-$ **3.75** (12.0 g, 54.8 mmol, 1.00 equiv.) was dissolved in water (25 mL). Lithium bis((trifluoromethyl)sulfonyl)amide was added, and the reaction mixture was stirred rapidly for 12 h. On completion two phases had formed. The product was separated from the aqueous and dried under high vacuum for 24 h, to give $[BMIM]^+[BF_4]^-$ **3.72** (22.9 g, 54.6 mmol, 98%) as a colourless liquid. Spectroscopic and physical data are consistent with the literature.[182]

FT-IR (cm^{-1}) neat: 3154 (w), 3113 (w), 2966 (w), 2945 (w), 2876 (w),1579 (w), 1346 (s), 1175 (s).

^{1}H NMR: 300 MHz, DMSO, δ ppm: 9.10 (1H, s, –N–C**H**–N–), 7.75 (1H, s, –C**H**=CH–), 7.69 (1H, s, –CH=C**H**–), 4.16 (2H, t, *J*=7.1 Hz, N–C**H**$_2$–CH_2–), 3.84 (3H, s, N–C**H**$_3$), 1.76 (2H, quin, *J*=7.3 Hz, –N–CH_2–C**H**$_2$–), 1.26 (2H, sxt, *J*=7.4 Hz, –CH_2–C**H**$_2$–CH_3), 0.90 (3H, t, *J*=7.4 Hz, –CH_2–C**H**$_3$).

^{13}C NMR: 75 MHz, DMSO, δ ppm: 136.5 (–N–**C**=N–), 123.6, –**C**=C–), 122.3 (–C=**C**–), 119.5 (q, J_{C-F}=320 Hz, F_3**C**–SO_2– x2) 48.5 (–N-**C**H_2–) 35.7 (–N-**C**H_3), 31.3 (–CH_2–**C**H_2), 18.7 (–**C**H_2–CH_3), 13.2 (–**C**H_3).

^{19}F NMR 282 MHz, DMSO, δ ppm: –78.8 (s, –C**F**$_3$ x2).

LRMS: (ESI$^+$) m/z 139.2 [M^+].

(ESI$^-$) m/z 280.0 [M^-].

4.4.10 3-Mesityl-4-methylthiazolie-2-(3*H*)-thione (3.81)

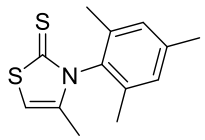

3.81
$C_{13}H_{15}NS_2$
249.39 g mol^{-1}

The procedure was adapted from Pesch *et al*.[183] In a RBF 2,4,6-trimethylaniline **3.78** (6.76 g, 50.0 mmol, 1.00 equiv.) was dissolved in DMSO (20 mL). To this a solution of NaOH (2.00 g, 50.0 mmol, 1.00 equiv.) in water (10 mL) was added dropwise. The reaction mixture was then cooled with an ice bath. Once cooled carbon disulfide **3.79** (3.80 g, 50.0 mmol, 1.00 equiv.) was added dropwise. The reaction mixture was allowed to warm to room temperature and stir for 1 h. Then the reaction mixture was cooled with an ice bath. Once cooled chloroacetone **3.80** (4.63 g, 50.0 mmol, 1.00 equiv.) was added dropwise. The reaction mixture was allowed to warm to room temperature and stirred for 1 h. Then ice cooled water (50.0 mL) was added, and the reaction mixture was rapidly stirred for 1 h, whilst cooled with an ice bath. This formed a viscous brown oil. Solvent and water was decanted away, and the oil was dissolved in ethanol (60 mL). Then conc. HCl (2.50 mL) was added dropwise. Gradually large crystals formed. The reaction mixture was then heated under reflux for 2 h. On cooling off-white crystals formed, which were collected by filtration, and washed with cold ethanol. The crystals were recrystallised from hot ethanol, collected, washed and dried under high vacuum to the give **3.81** (8.22 g, 34.6 mmol, 66%), as off-white crystals. Spectroscopic and physical data are consistent with the literature.[184]

MP: 137-139 ˚C

FT-IR (cm^{-1}) neat: 3132 (w), 2975 (w), 2943 (w), 2916 (w), 2857 (w), 1446 (m), 1591 (m).

^{1}H NMR: 400 MHz, $CDCl_3$, δ ppm: 7.03 (2H, s, Ar-**H**, x2), 6.38 (1H, q, *J*=1.0 Hz, -S-C**H**=C-), 2.35 (3H, s, Ar-C**H$_3$**), 2.04 (6H, s, Ar-C**H$_3$**, x2), 1.87 (3H, d, *J*=1.0 Hz, -C-C**H$_3$**).

^{13}C NMR: 100 MHz, $CDCl_3$, δ ppm: 188.3 (-**C**=S-), 139.6 (-N-**C**=C-),

139.2 (Ar), 135.1 (Ar, x2), 133.1 (Ar), 129.6 (Ar, x2), 106.4 (–S-**C**H=), 21.2 (Ar–**C**H_3), 17.4 (Ar–**C**H_3, x2), 15.3 (–**C**H_3).

LRMS: (ESI$^+$) m/z 250.2 [M + H^+].

4.4.11 3-Mesityl-4-methylthiazol-3-ium bis((trifluoromethyl)sulfonyl)amide (3.77)

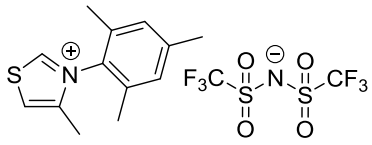

3.77

$C_{15}H_{16}F_6N_2O_4S_3$
498.48 g mol^{-1}

Method adapted from Pesch *et al.*[183] 3-Mesityl-4-methylthiazole-2(3*H*)-thione **3.81** (6.00 g, 24.0 mmol, 1.00 equiv.) was taken up in acetic acid (100 mL) and cooled with an ice bath. Once cooled H_2O_2 (30% Aqueous solution) (7.98 mL, 79.2 mmol, 3.30 equiv.) was added dropwise (caution, highly exothermic). The reaction mixture was allowed to stir for 1.5 hours. The acetic acid was removed under reduced pressure, with the last traces removed under high vacuum, to give a yellow oil. The oil was then dissolved in water (50.0 mL) and lithium bis((trifluoromethyl)sulfonylamide (6.89 g, 24.0 mmol, 1.00 equiv.) was added. The reaction mixture was stirred rapidly, giving two phases. The two phases were separated, and the organic was dissolved in chloroform (30 mL). This was then washed with water (3 x 50 mL). The solvent was removed under reduced pressure. This rapid stirring with water and water washes was repeated a further two times. Finally, the product was dried under high vacuum at 60 °C overnight to give thiazolium salt **3.77** (11.6 g, 23.2 mmol, 97%) as a viscous oil/ionic liquid.

FT-IR (cm^{-1}) neat: 3089 (w), 2359 (w), 2339 (w), 1740 (w), 1569 (w), 1481 (w), 1346 (s), 1178 (s).

^{1}H NMR: 400 MHz, $CDCl_3$, δ ppm: 9.76 (1H, d, *J*=2.5 Hz, –S–C**H**–N–), 8.11 (1H, d, *J*=1.5 Hz, –S–C**H**=C–), 7.09 (2H, s,

Ar–**H**, x2), 2.37 (3H, s, =C–C**H**$_3$), 2.24 (3H, s, Ar–C**H**$_3$), 1.92 (6H, s, Ar–C**H**$_3$, x2).

^{13}C NMR: 100 MHz, $CDCl_3$, δ ppm: 159.0 (–S–**C**=N–), 146.8 (–N–**C**=), 142.4 (Ar), 133.4 (Ar, x2), 131.8 (Ar), 130.3 (Ar, x2), 123.3 (–S–**C**H=), 119.7 (q, J_{C-F}=322 Hz, **C**F$_3$, x2), 21.0 (Ar–**C**H$_3$), 16.8 (Ar–**C**H$_3$, x2), 12.9 (=C–**C**H$_3$).

^{19}F NMR 282 MHz, $CDCl_3$, δ ppm: –79.00 (s, –C**F**$_3$, x2).

LRMS: (ESI^+) m/z 218.2 $[M^+]$.

(ESI^-) m/z 280.1$[M^-]$.

HRMS: (ESI^+) m/z calcd. for $C_{13}H_{16}NS$ [M] 218.0998, found 218.0994.

(ESI^-) m/z calcd for $C_2F_6NO_4S_2$ [M] 279.9178, found 279.9174.

4.4.12 General NHC mediated electrochemical oxidative esterification procedure

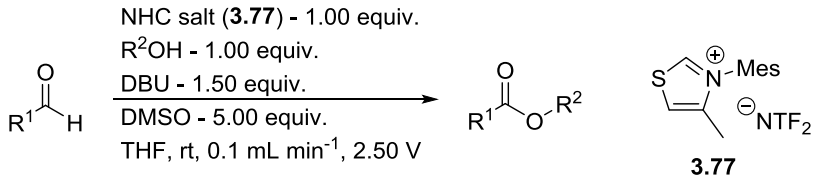

3.77

Glassware and electrodes were dried before use. A 0.10 M solution of aldehyde in THF (5.00 mL) was made, which also contained the NHC salt **3.77** (1.00 equiv.), alcohol (1.00 equiv.) and DMSO (5.00 equiv.). The solution was sonicated for 5 min. Another solution of 0.15 M DBU in THF (5.00 mL), was also made and sonicated for 5 min. The two 5.00 mL solutions were injected into separate sample loops and flowed at 0.05 mL min^{-1} into a T-piece, were they mixed (producing a red or yellow colour), to give a total flow rate of 0.10 mL min^{-1}. The reaction mixture was then flowed into the electrochemical cell at constant voltage of 2.50 V. On completion, solvents were removed under reduced pressure and the resultant product was extracted with EtOAc (30 mL), and purified by column chromatography, using mixtures of EtOAc and hexanes.

4.4.13 Dimethyl terephthalate (3.67)

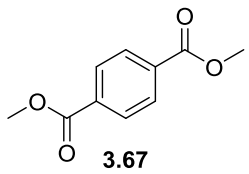

3.67

$C_{10}H_{10}O_4$
194.18 g mol^{-1}

Synthesised by the procedure described in **4.4.12** to give **3.67** (78 mg, 0.40 mmol, 80%) as white crystals. Spectroscopic and physical data are consistent with the literature.[185]

MP: 136-138 °C [Literature: 138-140 °C (Et_2O)][186]

FT-IR (cm^{-1}) neat: 3017 (w), 2960 (w), 2919 (w), 2848 (w), 2359 (w), 2339 (w), 1715 (s).

^{1}H NMR: 400 MHz, $CDCl_3$, δ ppm: 8.11 (4H, s, Ar–H, x4), 3.96 (6H, s, O–CH_3, x2).

^{13}C NMR: 100 MHz, CDCl3, δ ppm: 166.3 (C=O, x2), 133.9 (Ar, x2), 129.6 (Ar, x4), 52.4 (OCH_3, x2).

LRMS: (EI) m/z 194.1 (17%) [M^+], 163.1 (100%) [M^+ – OMe], 135.1 (18.5%) [M^+ – CO_2Me].

4.4.14 Benzyl benzoate (3.86)

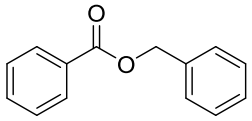

3.86
$C_{14}H_{12}O_2$
212.24 g mol^{-1}

Synthesised by the procedure described in **4.4.12** to give **3.86** (72 mg, 0.34 mmol, 68%) as an oil. Spectroscopic and physical data are consistent with the literature.[187]

FT-IR (cm^{-1}) neat: 3064 (w), 3032 (w), 2952 (w), 2361 (w), 2338 (w), 1714 (s), 1601 (w), 1584 (w).

^{1}H NMR: 400 MHz, $CDCl_3$, δ ppm: 8.10 (2H, dd, *J*=7.6, 1.0 Hz, Ar–**H**, x2), 7.58 (1H, tt, *J*=7.6, 1.0 Hz, Ar–**H**), 7.48-7.36 (7H, m, Ar–**H**, x7), 5.39 (2H, s, Ar–C**H**$_2$–O).

^{13}C NMR: 100 MHz, $CDCl_3$, δ ppm: 166.4 (**C**=O), 136.1 (Ar), 133.0 (Ar), 130.1 (Ar), 129.7 (Ar, x2), 128.6 (Ar, x2), 128.4 (Ar, x2), 128.2 (Ar), 128.1 (Ar, x2), 66.7 (O–**C**H$_2$–Ar).

LRMS: (EI) m/z 212.2 (34%) [M$^+$], 105.1 (100%) [M$^+$ – $OCH_2C_6H_5$].

4.4.15 Benzyl 4-methoxybenzoate (3.87)

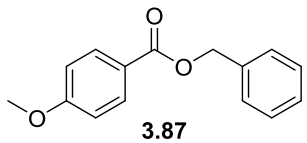

3.87

$C_{15}H_{14}O_3$

242.27 g mol^{-1}

Synthesised by the procedure described in **4.4.12** to give **3.87** (90 mg, 0.37 mmol, 74%) as an oil. Spectroscopic and physical data are consistent with the literature.[188]

FT-IR (cm^{-1}) neat: 3065 (w), 3032 (w), 3008 (w), 2956 (w), 2839 (w), 2360 (w), 2340 (w), 1708 (s), 1604 (s).

^{1}H NMR: 400 MHz, $CDCl_3$, δ ppm: 8.05 (2H, d, *J*=9.1 Hz, Ar–**H**, x2), 7.46 (2H, d, J=7.1 Hz, Ar–**H**, x2), 7.43-7.32 (3H, m, Ar–**H**, x3), 6.93 (2H, d, *J*=9.1 Hz, Ar–**H**, x2), 5.35 (2H, s, –O–C**H**$_2$–Ar), 3.87 (3H, s, O–C**H**$_3$).

^{13}C NMR: 100 MHz, $CDCl_3$, δ ppm: 166.2 (**C**=O), 163.4 (Ar), 136.3 (Ar), 131.7 (Ar, x2), 128.5 (Ar, x2), 128.1 (Ar), 128.1 (Ar x2), 122.6 (Ar), 113.6 (Ar, x2), 68.4 (-O-**C**H$_2$-Ar), 55.4 (–O–**C**H$_3$).

LRMS: (EI) m/z 242.2 (17%) [M^+], 135.2 (100%) [$M^+ - C_7H_7O$].

4.4.16 Benzyl 3,4,5-trimethoxybenzoate (3.88)

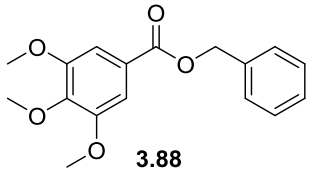

3.88

$C_{17}H_{18}O_5$
302.32 g mol^{-1}

Synthesised by the procedure described in **4.4.12** to give **3.88** (110 mg, 0.36 mmol, 73%) as an oil. Spectroscopic and physical data are consistent with the literature.[189]

FT-IR (cm^{-1}) neat: 2998 (w), 2940 (w), 2836 (w), 2359 (w), 2939 (w), 1710 (s), 1586 (s).

^{1}H NMR: 400 MHz, $CDCl_3$, δ ppm: 7.46-7.35 (7H, m, Ar–**H**, x7), 5.38 (2H, s, –OC**H**$_2$–Ar), 3.91 (3H, s, –OC**H**$_3$), 3.91 (6H, s, –OC**H**$_3$, x2).

^{13}C NMR: 100 MHz, $CDCl_3$, δ ppm: 166.1 (**C**=O), 153.0 (**Ar**–OCH_3, x2), 142.4 (**Ar**–OCH_3), 136.1 (Ar), 128.6 (Ar), 128.4 (Ar, x2), 128.2 (Ar, x2), 125.1 (Ar), 107.0 (Ar, x2), 66.8 (–O–**C**H_2–Ar), 60.9 (–O**C**H_3), 56.3 (–O**C**H_3, x2).

LRMS: (EI) m/z 302.2 (56 %) [M^+], 195.2 (50%) [M^+ – $OCH_2C_6H_5$].

4.4.17 Benzyl 2-fluorobenzoate (3.89)

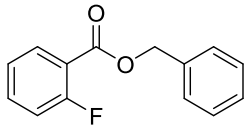

3.89
$C_{14}H_{11}FO_2$
230.23 g mol^{-1}

Synthesised by the procedure described in **4.4.12** to give **3.89** (58 mg, 0.25 mmol, 50%) as an oil. Spectroscopic and physical data are consistent with the literature.[190]

FT-IR (cm^{-1}) neat: 3066 (w), 3034 (w), 2952 (w), 1715 (s), 1612 (m).

^{1}H NMR: 400 MHz, $CDCl_3$, δ ppm: 7.98 (1H, ddd *J*=7.5, 7.5, 1.8 Hz, Ar–**H**), 7.55 (1H, m, Ar–**H**), 7.50-7.44 (2H, m, Ar–**H**, x2), 7.32-7.44 (3H, m, Ar–**H**, x2), 7.21 (1H, ddd, *J*=7.6, 7.6, 1.0 Hz, Ar–**H**), 7.15 (1H, ddd, *J*=10.6, 8.6, 1.0 Hz, Ar–**H**), 5.40 (2H, s, O–C**H**$_2$–Ar).

^{13}C NMR: 100 MHz, $CDCl_3$, δ ppm**:** 164.6 (d, J_{C-F}=119 Hz, **Ar**–F) 163.4 (**C**=O), 135.8 (Ar), 134.6 (d, J_{C-F}=8.8 Hz, Ar, x2), 132.2 (Ar), 128.4 (Ar, x2), 128.2 (Ar), 128.1 (Ar x2), 124.0 (d, J_{C-F}=4.4 Hz, Ar), 117.0 (d, J_{C-F}=22.0 Hz, Ar, x2) 66.9 (–O–**C**H$_2$–Ar).

^{19}F NMR: 282 MHz, $CDCl_3$, δ ppm: –109.1.

LRMS: (EI) m/z 230.3 (38%) [M^+], 123.2 (100%) [M^+ – $OCH_2C_6H_5$].

4.4.18 Benzyl 4-fluorobenzoate (3.90)

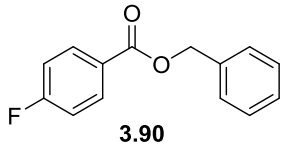

3.90

$C_{14}H_{11}FO_2$

230.23 g mol^{-1}

Synthesised by the procedure described in **4.4.12** to give **3.90** (93 mg, 0.40 mmol, 81%) as an oil. Spectroscopic and physical data are consistent with the literature.[188]

FT-IR (cm^{-1}) neat: 3067 (w), 3034 (w), 2953 (w), 2360 (w), 1715 (s), 1602 (m).

^{1}H NMR: 400 MHz, $CDCl_3$, δ ppm: 8.12-8.09 (2H, m, Ar–**H**, x2), 7.46-7.36 (5H, m, Ar–**H**, x5), 7.14-7.10 (2H, m, Ar–**H**, x2), 5.37 (2H, s, –OC**H**$_2$–Ar).

^{13}C NMR: 100 MHz, $CDCl_3$, δ ppm: 165.8 (d, J_{C-F}=255 Hz, **Ar**–F), 165.5 (**C**=O), 135.9 (Ar), 132.3 (d, J_{C-F}=8.80 Hz, Ar, x2), 128.6 (Ar, x2), 128.3 (Ar), 128.22 (Ar, x2), 126.4 (d, J_{C-F}=2.90 Hz, Ar), 115.6 (d, J_{C-F}=22.0 Hz, Ar, x2), 66.8 (–O–**C**H$_2$–Ar).

^{19}F NMR: 282 MHz, $CDCl_3$, δ ppm: –105.5.

LRMS: (EI) m/z 230.2 (31%) [M$^+$], 123.1 (100 %) [M$^+$ – $OCH_2C_6H_5$].

4.4.19 Benzyl 4-chlorobenzoate (3.91)

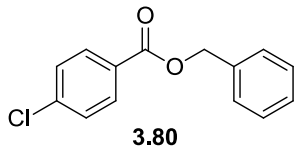

3.80
$C_{14}H_{11}ClO_2$
246.69 g mol^{-1}

Synthesised by the procedure described in **4.4.12** to give **3.91** (103 mg, 0.42 mmol, 84%) as an oil. Spectroscopic and physical data are consistent with the literature.[188]

FT-IR (cm^{-1}) neat: 3065 (w), 3033 (w), 2957 (w), 2360 (w), 2889 (w), 1716 (s), 1650 (m).

^{1}H NMR: 400 MHz, $CDCl_3$, δ ppm: 8.02 (2H, d, *J*=8.6, Ar–**H**, x2), 7.46-7.38 (7H, m, Ar–**H**, x7), 5.37 (2H, s, –O–C**H**$_2$–Ar).

^{13}C NMR: 100 MHz, $CDCl_3$, δ ppm: 165.5 (**C**=O), 139.5 (Ar–Cl), 135.8 (Ar), 131.1 (Ar, x2), 128.7 (Ar, x2), 128.6 (Ar, x2), 128.6 (Ar), 128.4 (Ar), 128.2 (Ar, x2), 66.9 (–O–**C**H$_2$–Ar).

LRMS: (EI) m/z 248.3 (6%), [M(^{37}Cl)$^+$], 246.3 (18%) [M(^{35}Cl)$^+$], 141.2 (25%) [M(^{37}Cl)$^+$ – $OCH_2C_6H_5$], 139.1 (81%) [M(^{35}Cl)$^+$ – $OCH_2C_6H_5$].

4.4.20 Methyl 2,4-dichlorobenzoate (3.92)

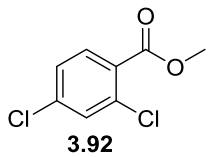

3.92

$C_8H_6Cl_2O_2$

205.04 g mol^{-1}

Synthesised by the procedure described in **4.4.12** to give **3.92** (53 mg, 0.26 mmol, 52%) as an oil. Spectroscopic and physical data are consistent with the literature.[191]

FT-IR (cm^{-1}) neat: 3092 (w), 3000 (w), 2952 (w), 2852 (w), 1731 (s), 1585 (s).

^{1}H NMR: 400 MHz, $CDCl_3$, δ ppm: 7.82 (1H, d, *J*=8.6 Hz, Ar–**H**), 7.49 (1H, d, *J*=2.0 Hz, Ar–**H**), 7.31 (1H, dd, *J*=8.3 , 1.8 Hz, Ar–**H**), 3.94, (3H, s, OC**H**$_3$).

^{13}C NMR: 100 MHz, $CDCl_3$, δ ppm: 165.2 (**C**=O), 138.3 (Ar–Cl), 135.0 (Ar–Cl), 132.5 (Ar), 131.0 (Ar), 128.3 (Ar), 127.0 (Ar), 52.5 (–O–**C**H$_3$).

LRMS: (EI) m/z 208.2 (2%) [M(^{37}Cl^{37}Cl)$^+$], 206.2 (11%) [M(^{35}Cl^{37}Cl)$^+$], 204.1 (21%) [M(^{35}Cl^{35}Cl)$^+$], 177.1 (9%) [M(^{37}Cl^{37}Cl)$^+$ – OCH_3], 175.1 (61%) [M(^{35}Cl^{37}Cl)$^+$ – OCH_3], 173.1 (100%) [M(^{35}Cl^{35}Cl)$^+$ – OCH_3].

4.4.21 Benzyl 4-bromobenzoate (3.93)

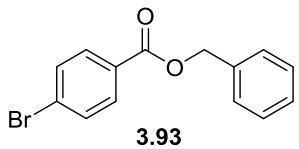

3.93

$C_{14}H_{11}BrO_2$

291.14 g mol^{-1}

Synthesised by the procedure described in **4.4.12** to give **3.93** (135 mg, 0.46 mmol, 93%) as a white solid. Spectroscopic and physical data are consistent with the literature.[188]

MP: 51-53 °C [literature 52-53 °C (EtOAc)][192]

FT-IR (cm^{-1}) neat: 3070 (w), 3035 (w), 2972 (w), 2894 (w), 2358 (w), 1710 (s), 1588 (m).

^{1}H NMR: 400 MHz, $CDCl_3$, δ ppm: 7.94 (2H, d, *J*=8.6, Ar–**H**, x2), 7.59 (2H, d, *J*=8.6, Ar–**H**, x2), 7.46-7.38 (5H, m, Ar–**H**, x5), 5.37 (2H, s, –O–C**H**$_2$–Ar).

^{13}C NMR: 100 MHz, $CDCl_3$, δ ppm: 165.7 (**C**=O), 135.8 (Ar), 131.7 (Ar, x2), 131.2 (Ar, x2), 129.0 (Ar), 128.6 (Ar, x2), 128.4 (Ar), 128.2 (Ar, x2), 128.2 (Ar–Br), 66.9 (–O–**C**H$_2$–Ar).

LRMS: (EI) m/z 292.2 (15%) [M(^{81}Br)$^+$], 290.2 (15%) [M(^{79}Br)$^+$], 185.1 (69%) [M(^{81}Br)$^+$ – OCH_2C_6H], 183.1 (77%) [M(^{79}Br)$^+$–$OCH_2C_6H_5$].

4.4.22 Benzyl 2-naphthoate (3.94)

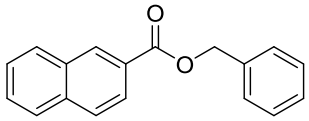

3.94
$C_{18}H_{14}O_2$
262.30 g mol^{-1}

Synthesised by the procedure described in **4.4.12** to give **3.83** (116 mg, 0.44 mmol, 89%) as a white solid. Spectroscopic and physical data are consistent with the literature.[188]

MP: 60-62 °C [literature 63-63.5 °C (MeCN)][193]

FT-IR (cm^{-1}) neat: 3392 (w), 3024 (w), 2967 (w), 2898 (w), 1701 (s).

^{1}H NMR: 400 MHz, $CDCl_3$, δ ppm: 8.66 (1H, s, Ar-**H**), 8.11 (1H, dd, *J*=8.6, 1.0 Hz, Ar-**H**), 7.96 (1H, d, *J*=8.1 Hz, Ar-**H**), 7.89 (2H, d, *J*=8.6 Hz, Ar-**H**, x2), 7.62-7.51 (4H, m, Ar-**H**, x4), 7.45-7.36 (3H, m, Ar-**H**), 5.45 (2H, s, -O-C**H**$_2$-Ar).

^{13}C NMR: 100 MHz, $CDCl_3$, δ ppm: 166.6 (**C**=O), 136.1 (Ar), 135.6 (Ar), 132.5 (Ar, x2), 131.2 (Ar), 129.4 (Ar x2), 128.6 (Ar, x2), 128.3 (Ar), 128.2 (Ar), 127.8 (Ar), 127.4 (Ar, x2), 126.7 (Ar), 125.3 (Ar), 66.9 (-O-**C**H$_2$-Ar).

LRMS: (EI) m/z 262.2 (37%) [M$^+$], 155.1 (100%) [M$^+$ - $OCH_2C_6H_5$].

4.4.23 Benzyl furan-2-carboxylate (3.95)

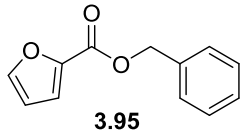

3.95

$C_{12}H_{10}O_3$
202.21 g mol^{-1}

Synthesised by the procedure described in **4.4.12** to give **3.95** (72 mg, 0.37 mmol, 71%) as an oil. Spectroscopic and physical data are consistent with the literature.[188]

FT-IR (cm^{-1}) neat: 3140 (w), 3033 (w), 2955 (w), 1714 (s), 1578 (m).

^{1}H NMR: 400 MHz, $CDCl_3$, δ ppm: 7.59 (1H, s, Ar–**H**), 7.46-7.33 (5H, m, Ar–**H**, x5), 7.22 (1H, dd, *J*=3.0, 0.8 Hz, Ar–**H**), 6.51 (1H, dd, *J*=3.5, 1.5 Hz, Ar–**H**), 5.36 (2H, s, O–C**H**$_2$–Ar).

^{13}C NMR: 100 MHz, $CDCl_3$, δ ppm: 158.5 (**C**=O), 146.4 (Ar), 144.6 (Ar), 135.6 (Ar), 128.6 (Ar, x2), 128.4 (Ar), 128.3 (Ar, x2), 118.2 (Ar), 111.8 (Ar), 66.5 (O–**C**H$_2$–Ar).

LRMS: (EI) m/z 202.2 (41%) [M$^+$], 95.1 (61%) [M$^+$ – $OCH_2C_6H_5$].

4.4.24 Benzyl nicotinate (3.96)

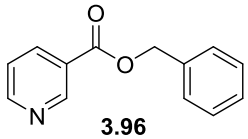

3.96

$C_{13}H_{11}NO_2$

213.23 g mol^{-1}

Synthesised by the procedure described in **4.4.12** to give **3.96** (75 mg, 0.35 mmol, 70%) as an oil. Spectroscopic and physical data are consistent with the literature.[194]

FT-IR (cm^{-1}) neat: 3034 (w), 2953 (w), 2359 (w), 2837 (w), 1718 (s), 1589 (m).

^{1}H NMR: 400 MHz, $CDCl_3$, δ ppm: 9.27 (1H, d, *J*=1.5 Hz, Ar–**H**), 8.78 (1H, dd, *J*=5.1, 1.5, Hz, Ar–**H**), 8.33 (1H, dt, *J*=8.0, 1.8 Hz, Ar–**H**), 7.47-7.37 (6H, m, Ar–**H**, x6), 5.41 (2H, s, –O–C**H**$_2$–Ar).

^{13}C NMR: 100 MHz, $CDCl_3$, δ ppm: 165.1 (**C**=O), 153.5 (Ar), 151.0 (Ar), 137.1 (Ar), 135.5 (Ar), 128.7 (Ar, x2), 128.5 (Ar), 128.3 (Ar, x2), 126.0 (Ar), 123.3 (Ar), 67.1 (O–**C**H$_2$–Ar).

LRMS: (EI) m/z 213.3 (55%) [M$^+$], 106.1 (81%) [M$^+$ – $OCH_2C_6H_5$].

4.4.25 Benzyl dodecanoate (3.97)

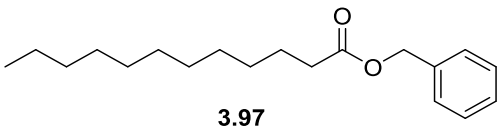

3.97

$C_{19}H_{30}O_2$

290.44 g mol^{-1}

Synthesised by the procedure described in **4.4.12** to give **3.97** (82 mg, 0.28 mmol, 57%) as an oil. Spectroscopic and physical data are consistent with the literature.[195]

FT-IR (cm^{-1}) neat: 2922 (s), 2853 (s), 2359 (w), 2338 (w), 1736 (s).

^{1}H NMR: 400 MHz, $CDCl_3$, δ ppm: 7.37-7.35 (5H, m, Ar–**H**, x5), 5.13 (2H, s, –O–C**H**$_2$– Ar), 2.36 (2H, t, *J*=7.6 Hz, –C**H**$_2$–), 1.67-1.62 (2H, m, –C**H**$_2$–), 1.35-1.25 (16 H, m, –C**H**$_2$–, x8), 0.89 (3H, t, *J*=6.8 Hz, –C**H**$_3$).

^{13}C NMR: 100 MHz, $CDCl_3$, δ ppm: 173.7 (**C**=O), 136.2 (Ar), 128.5 (Ar, x3), 128.1 (Ar, x2), 66.0 (–O–**C**H$_2$–Ar) 34.3 (–**C**H$_2$–), 31.9 (–**C**H$_2$–), 29.6 (–**C**H$_2$–, x2), 29.4 (–**C**H$_2$–), 29.3 (–**C**H$_2$–), 29.2 (–**C**H$_2$–), 28.1 (–**C**H$_2$–), 25.0 (–**C**H$_2$–), 22.7 (–**C**H$_2$–), 14.08 (–**C**H$_3$).

LRMS: (EI) m/z 290.4 (2%) [M^+], 205.4 (100%) [$M^+ - C_6H_{13}$].

4.4.26 (*Z*)-Benzyl 6,10-dimethyl-2-methyleneundeca-5,9-dienoate (3.98)

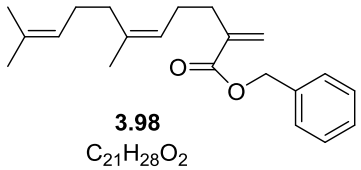

3.98
$C_{21}H_{28}O_2$
312.45 g mol^{-1}

Synthesised by the procedure described in **4.4.12** to give **3.98** (70 mg, 0.22 mmol, 48%) as an oil.

FT-IR (cm^{-1}) neat: 3033 (w), 2963 (m), 2918 (m), 2856 (m), 1717 (s), 1630 (m).

^{1}H NMR: 400 MHz, $CDCl_3$, δ ppm: 7.38-7.32 (5H, m, Ar–**H**, x5), 6.21 (1H, s, –C=C**H$_a$**H$_b$), 5.56 (1H, s, –C=CH$_a$**H$_b$**), 5.21 (2H, s, –O–C**H$_2$**–Ar), 5.14-5.11 (2H, m, –C=C**H**–), 2.36 (2H, t, *J*=8.1 Hz, –CH$_2$–C**H$_2$**–), 2.18 (2H, q, *J*=7.2 Hz, –C**H$_2$**–CH$_2$–), 2.02 (4H, br, –C**H$_2$**–C**H$_2$**–), 1.69 (6H, s, –C**H$_3$**, x2), 1.61 (3H, s, –C**H$_3$**).

^{13}C NMR: 100 MHz, $CDCl_3$, δ ppm: 167.1 (**C**=O), 140.3 (–**C**=CH$_2$), 136.2 (–**C**=CH–), 136.1 (Ar), 131.6 (–**C**=CH–), 128.5 (Ar, x2), 128.1 (Ar), 128.0 (Ar, x2), 125.2 (–C=**C**H$_2$), 124.3 (–C=**C**H–), 124.0 (–C=**C**H–), 66.3 (–O–**C**H$_2$–Ar), 32.2 (–CH$_2$–**C**H$_2$–), 31.9 (–CH$_2$–**C**H$_2$–), 26.7 (–**C**H$_2$–**C**H$_2$–), 26.6 (–**C**H$_2$–CH$_2$–), 25.7 (–**C**H$_3$), 23.3 (–**C**H$_3$), 17.6 (–**C**H$_3$).

LRMS: EI m/z 221.2 (20%) [M – $C_7H_7^+$], 91.1 (100%), [$C_7H_7^+$].

HRMS (ESI$^+$) m/z calcd. for $C_{21}H_{28}NaO_2$ [M + Na$^+$] 335.1982, found 335.1985.

4.4.27 Methyl 3,4,5-trimethoxybenzoate (3.99)

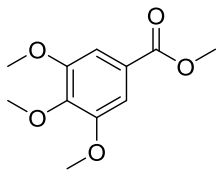

3.99
$C_{11}H_{14}O_5$
226.23 g mol^{-1}

Synthesised by the procedure described in **4.4.12** to give **3.99** (84 mg, 0.37 mmol, 74%) as a white solid. Spectroscopic and physical data are consistent with the literature.[196]

MP: 75-77 ˚C [literature: 75-76 ˚C (EtOH)][197]

FT-IR (cm^{-1}) neat: 3012 (w), 2951 (m), 2840 (w), 2358 (w), 2337 (w), 1712 (s), 1589 (s).

^{1}H NMR: 400 MHz, $CDCl_3$, δ ppm: 7.31 (2H, s, Ar–**H**, x2), 3.92 (12H, s, –OC**H**$_3$, x4).

^{13}C NMR: 100 MHz, $CDCl_3$, δ ppm: 166.7 (**C**=O), 152.9. (Ar, x2), 142.2 (Ar), 125.1 (Ar), 106.8, (Ar, x2), 60.9 (–O**C**H$_3$), 58.2 (–O**C**H$_3$, x2), 52.2 (–O**C**H$_3$).

LRMS: (EI) m/z 226.2 (100%) [M^+], 211.1 (49%) [M^+ – CH_3], 195.2 (24%) [M^+ – OCH_3].

4.4.28 Propyl 3,4,5-trimethoxybenzoate (3.100)

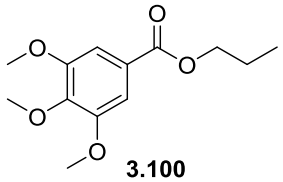

3.100

$C_{13}H_{18}O_5$
254.28 g mol^{-1}

Synthesised by the procedure described in **4.4.12** to give **3.100** (95 mg, 0.37 mmol, 75%) as an oil. Spectroscopic and physical data are consistent with the literature.[198]

FT-IR (cm^{-1}) neat: 2965 (m), 2837 (w), 1710 (s), 1587 (s).

^{1}H NMR: 400 MHz, $CDCl_3$, δ ppm: 7.31 (2H, s, Ar–**H**, x2), 4.28, (2H, t, *J*=6.8 Hz, –O–C**H**$_2$–), 3.92 (6H, s, –OC**H**$_3$, x2), 3.91 (3H, s, –OC**H**$_3$), 1.80 (2H, sxt, *J*=7.2 Hz, –CH_2–C**H**$_2$–CH_3), 1.03 (3H, t, *J*=7.6 Hz, –CH_2–C**H**$_3$).

^{13}C NMR: 100 MHz, $CDCl_3$, δ ppm: 166.3 (**C**=O), 152.9 (Ar, x2), 142.1 (Ar), 125.6 (Ar), 106.8 (Ar, x2), 66.7 (–O–**C**H_2–), 60.9 (–O**C**H_3), 56.2 (–O**C**H_3, x2), 22.1 (–**C**H_2–CH_3), 10.5 (–CH_2–**C**H_3).

LRMS: (EI) m/z 254.3 (100%) [M^+].

4.4.29 But-2-yn-1-yl 3,4,5-trimethoxybenzoate (3.101)

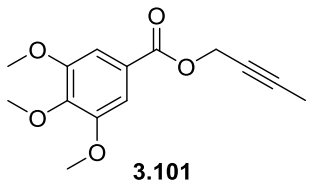

3.101

$C_{14}H_{16}O_5$

264.27 g mol^{-1}

Synthesised by the procedure described in **4.4.12** to give **3.101** (100 mg, 0.39 mmol, 76%) as a white solid.

MP: 97-99 °C

FT-IR (cm^{-1}) neat: 3015 (w), 2939 (w), 2842 (w), 2247 (w), 1706 (s), 1588 (s).

^{1}H NMR: 400 MHz, $CDCl_3$, δ ppm: 7.33 (2H, s, Ar–**H**, x2), 4.89 (2H, q, *J*=2.0 Hz, –O–C**H**$_2$–), 3.92 (6H, s,–OC**H**$_3$), 3.92 (3H, s, –OC**H**$_3$), 1.89 (3H, t, *J*=2.3 Hz,–C–C**H**$_3$).

^{13}C NMR: 100 MHz, $CDCl_3$, δ ppm: 165.7 (**C**=O), 152.9 (Ar, x2), 142.4 (Ar), 124.7 (Ar), 107.0 (Ar, x2), 83.4 (**C**–CH_3), 73.3 (CH_2–**C**–), 60.9 (–O**C**H_3), 56.3 (-O**C**H_3 x2), 53.4 (–O**C**H_2–), 3.7 (–**C**H_3).

LRMS: (EI) m/z 264.2 (79%) [M^+].

HRMS: (ESI^+) m/z calcd. for $C_{14}H_{16}NaO_5$ [M + Na^+] 287.0890, found 287.0886.

4.4.30 1,1,1,3,3,3-hexafluoropropan-2-yl 3,4,5-trimethoxybenzoate (3.102)

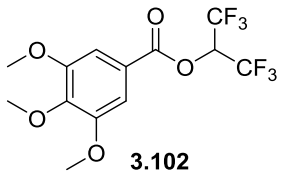

3.102

$C_{13}H_{12}F_6O_5$
362.22 g mol^{-1}

Synthesised by the procedure described in **4.4.12** to give **3.102** (70 mg, 0.19 mmol, 39%) as a white solid.

MP: 75-77 ˚C

FT-IR (cm^{-1}) neat: 3017 (w), 2978 (w), 2946 (w), 2847 (w), 2358 (w), 1734 (s), 1592 (m).

^{1}H NMR: 400 MHz, $CDCl_3$, δ ppm: 7.35 (2H, s, Ar–**H**, x2), 6.01 (1H, spt, J_{H-F}=6.1 Hz, –OC**H**–$(CF_3)_2$), 3.95, (3H, s, O–C**H**$_3$), 3.94 (6H, s, –OC**H**$_3$).

^{13}C NMR: 100 MHz, $CDCl_3$, δ ppm: 162.9 (**C**=O), 153.2 (Ar, x2), 144.0 (Ar), 121.4 (Ar), 120.9 (q, J_{C-F}=282 Hz, –**C**F_3), 120.9 (q, J_{C-F}=282 Hz, –**C**F_3) 107.8 (Ar, x2), 66.9 (spt, J_{C-F}=35.6 Hz, –O**C**H–$(CF_3)_2$), 61.0 (–O**C**H_3), 58.3 (–O**C**H_3, x2).

^{19}F NMR 282 MHz, $CDCl_3$, δ ppm: –73.15.

LRMS: (EI) m/z 362.1 (100%) [M$^+$].

HRMS: (ESI$^+$) m/z calcd. for $C_{13}H_{12}F_6NaO_5$ [M + Na$^+$] 385.0481, found 385.0489.

4.4.31 Isopropyl 3,4,5-trimethoxybenzoate (3.103)

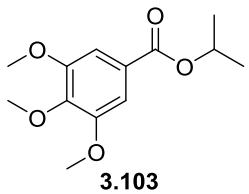

3.103
$C_{13}H_{18}O_5$
254.28 g mol^{-1}

Synthesised by the procedure described in **4.4.12** to give **3.103** (73 mg, 0.29 mmol, 57%) as an oil. Spectroscopic and physical data are consistent with the literature.[196]

FT-IR (cm^{-1}) neat: 2978 (w), 2939 (w), 2837 (w), 1707 (s), 1587 (s).

^{1}H NMR: 400 MHz, $CDCl_3$, δ ppm: 7.30 (2H, s, Ar–**H**), 5.24 (1H, spt, *J*=6.2 Hz, –O–C**H**–$(CH_3)_2$), 3.92 (6H, s,–OC**H**$_3$, x2), 3.90 (3H, s, –OC**H**$_3$), 1.38 (6H, d, *J*=6.6 Hz, CH–(C**H**$_3$)$_2$).

^{13}C NMR: 100 MHz, $CDCl_3$, δ ppm: 165.7 (**C**=O), 152.9 (Ar, x2), 142.0 (Ar), 125.9 (Ar), 106.7 (Ar, x2), 68.52 (-O**C**H-), 60.9 (–O**C**H$_3$), 59.2 (–O**C**H$_3$, x2), 21.9 (–CH–(**C**H$_3$)$_2$).

LRMS: (EI) m/z 254.2 (100%) [M$^+$].

4.4.32 Sec-butyl 3,4,5-trimethoxybenzoate (3.104)

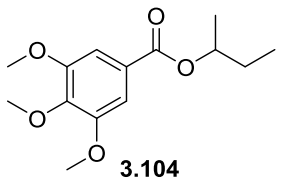

3.104
$C_{14}H_{20}O_5$
268.31 g mol^{-1}

Synthesised by the procedure described in **4.4.12** to give **3.104** (60 mg, 0.22 mmol, 45%) as an oil.

FT-IR (cm^{-1}) neat: 2970 (m), 2939 (m), 2837 (w), 1707 (s), 1587 (s).

^{1}H NMR: 400 MHz, $CDCl_3$, δ ppm: 7.31 (2H, s, Ar–**H**, x2), 5.09 (1H, sxt, *J*=6.3 Hz, –O–C**H**–), 3.92 (6H, s, –OC**H**$_3$), 3.91 (3H, s, –OC**H**$_3$), 1.72 (2H, m, –C**H**$_2$–CH$_3$), 1.35 (3H, d, *J*=6.1 Hz, –CH–C**H**$_3$), 0.98 (3H, t, *J*=7.3 Hz, –CH$_2$–C**H**$_3$).

^{13}C NMR: 100 MHz, $CDCl_3$, δ ppm: 165.8 (**C**=O), 152.9 (Ar, x2), 142.1 (Ar), 126.0 (Ar), 106.8 (Ar, x2), 73.1 (-O-**C**H-), 60.9 (–O**C**H$_3$), 56.2 (–O**C**H$_3$, x2), 28.9 (–**C**H$_2$–CH$_3$), 19.6 (CH–**C**H$_3$), 9.8 (–CH$_2$–**C**H$_3$).

LRMS: (EI) m/z 268.3 (60 %) [M$^+$].

HRMS: (ESI$^+$) m/z calcd. for $C_{14}H_{20}NaO_5$ [M + Na$^+$] 291.1203, found 291.1203.

4.4.33 General NHC mediated electrochemical oxidative amidation procedure

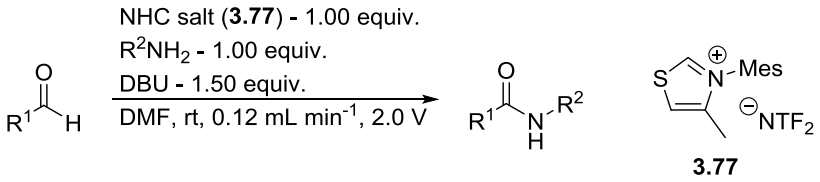

3.77

Glassware and electrodes were dried before use. A 0.10 M solution of aldehyde in DMF (5.00 mL) was made, which also contained the NHC salt (**3.77**) (1.00 equiv.). The solution was sonicated for 5 min. Separate solutions of 0.15 M DBU in DMF (5.00 mL) and amine (1.00 equiv.) in DMF (10.0 mL), were also prepared and sonicated for 5 min. The three solutions were injected into separate sample loops. The aldehyde and DBU solutions were flowed at 0.03 mL min^{-1} into a T-piece, were they mixed (producing a red or yellow colour), to give a total flow rate of 0.06 mL min^{-1}. The reaction mixture was then flowed into another T-piece, where it was mixed with the amine solution, flowing at 0.06 mL min^{-1}, to give a total flow rate of 0.12 mL min^{-1}. The reaction mixture was then flowed into the electrochemical cell at constant voltage of 2.00 V. On completion, solvents were removed under reduced pressure. The resulted crude was then diluted with EtOAc (20 mL), and washed with brine (3 x 20 mL). The organic was dried over $MgSO_4$, and the solvent was removed under reduced pressure. The product was then purified using mixtures of EtOAc and hexanes. The resulting products were then recrystallized from hot EtOAc/hexane mixtures.

4.4.34 *N*-benzyl-3,4,5-trimethoxybenzamide (3.106)

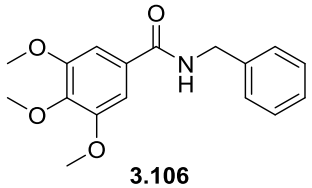

3.106
$C_{17}H_{19}NO_4$
301.34 g mol^{-1}

Synthesised by the procedure detailed in **4.4.33**, to give **3.106** (120 mg, 0.40 mmol, 80%) as white crystals.

MP: 132-134 ˚C [literature: 141˚C (Aq. EtOH)][199]

FT-IR (cm^{-1}) neat: 3301 (m), 3023 (w), 2942 (w), 2872 (w), 1624 (m), 1579 (m).

^{1}H NMR: 400 MHz, $CDCl_3$, δ ppm: 7.38-7.30 (5H, m, Ar–**H**, x5), 7.03 (2H, s, Ar–**H**, x2), 6.36 (1H, br, –N**H**–), 4.66 (2H, d, *J*=6.1 Hz, –NH–C**H**$_2$–Ar), 3.90 (6H, s, –OC**H**$_3$, x2), 3.89 (3H, s, –OC**H**$_3$).

^{13}C NMR: 100 MHz, $CDCl_3$, δ ppm: 167.0 (**C**=O), 153.2 (Ar, x2), 141.1 (Ar), 138.2 (Ar), 129.8 (Ar), 128.8 (Ar, x2), 128.0 (Ar, x2), 127.7 (Ar), 104.4 (Ar, x2), 60.9 (–O**C**H$_3$), 56.4 (–O**C**H$_3$, x2), 44.2 (–NH–**C**H$_2$–Ar).

LRMS: (ESI$^+$) m/z 625.2 [2M + Na$^+$].

HRMS: (ESI$^+$) m/z calcd. for $C_{17}H_{20}NO_4$ [M + H$^+$] 302.1387, found 302.1384.

4.4.35 *N*-Benzylbenzamide (3.107)

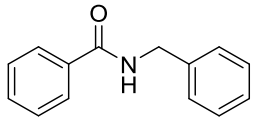

3.107
$C_{14}H_{13}NO$
211.26 g mol^{-1}

Synthesised by the procedure detailed in **4.4.33**, to give **3.107** (70 mg, 0.33 mmol, 66%) as white crystals. Spectroscopic and physical data are consistent with the literature.[200]

MP: 102-104 ˚C [literature 101-103 ˚C (Et_2O)][200]

FT-IR (cm^{-1}) neat: 3279 (m), 3089 (w), 3061 (w), 3030 (w), 2927 (w), 1636 (m), 1601 (m), 1545 (m).

^{1}H NMR: 400 MHz, $CDCl_3$, δ ppm: 7.80 (2H, d, *J*=7.6 Hz, Ar–**H**, x2), 7.53-7.30 (8H, m, Ar–**H**, x8), 6.41 (1H, br, –N**H**–), 4.67 (2H, d, *J*=6.1 Hz, –NH–C**H**$_2$–Ar).

^{13}C NMR: 100 MHz, $CDCl_3$, δ ppm: 167.3 (**C**=O), 138.2 (Ar), 134.4 (Ar), 131.5 (Ar, x2), 128.8 (Ar, x2), 128.6 (Ar, x2), 127.9 (Ar), 127.6 (Ar), 126.9 (Ar, x2), 44.1 (–NH–**C**H_2–Ar).

LRMS: (ESI^+) m/z 445.2 [2M + Na^+].

4.4.36 *N*-Benzyl-4-methoxybenzamide (3.108)

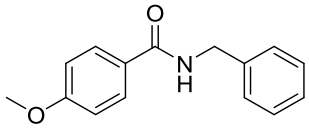

3.108
$C_{15}H_{15}NO_2$
241.29 g mol^{-1}

Synthesised by the procedure detailed in **4.4.33**, to give **3.108** (85 mg, 0.35 mmol, 71%) as white crystals. Spectroscopic and physical data are consistent with the literature.[200]

MP: 128-130 ˚C [literature: 128-129 ˚C (Et_2O)][200]

FT-IR (cm^{-1}) neat: 3248 (m), 3059 (w), 2957 (w), 2837 (w), 2556 (w), 1630 (m), 1604 (m), 1557 (m),

^{1}H NMR: 400 MHz, $CDCl_3$, δ ppm: 7.77 (2H, d, *J*=8.6 Hz Ar–**H**, x2), 7.37-7.27 (5H, m, Ar–**H**, x5), 6.92 (2H, d, *J*=9.1 Hz, Ar–**H**, x2), 6.37 (1H, br, –N**H**–), 4.64 (2H, d, *J*=5.6 Hz, –NH–C**H**$_2$–Ar), 3.85 (3H, s, –OC**H**$_3$).

^{13}C NMR: 100 MHz, $CDCl_3$, δ ppm: 166.9 (**C**=O), 162.2 (Ar), 138.4 (Ar), 128.7 (Ar, x4), 127.9 (Ar, x2), 127.6 (Ar), 126.7 (Ar), 113.8 (Ar, x,2), 55.4 (–O**C**H$_3$), 44.1 (–NH–**C**H$_2$–Ar).

LRMS: (ESI^+) m/z 505.2 [2M + Na^+].

4.4.37 *N*-Benzyl-4-fluorobenzamide (3.109)

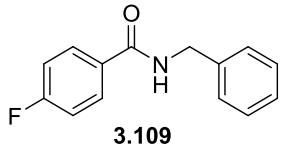

3.109
$C_{14}H_{12}FNO$
229.25 g mol^{-1}

Synthesised by the procedure detailed in **4.4.33**, to give **3.99** (95 mg, 0.41 mmol, 83%) as white crystals. Spectroscopic and physical data are consistent with the literature.[200]

MP: 135-137 ˚C [literature 142-144˚C (Et_2O)][200]

FT-IR (cm^{-1}) neat: 3815 (m), 3067 (w), 3032 (w), 2516 (w), 2357 (w), 1640 (m), 1595 (m), 1550 (m).

^{1}H NMR: 400 MHz, $CDCl_3$, δ ppm: 7.81 (2H, dd, *J*=8.6, 5.6 Hz, Ar–**H**), 7.38-7.30 (5H, m, Ar–**H**, x5), 7.10 (2H, t, *J*=8.6Hz, Ar–**H**), 6.46 (1H, br, –N**H**–), 4.63 (2H, d, *J*=5.6 Hz, –NH–C**H**$_2$–Ar).

^{13}C NMR: 100 MHz, $CDCl_3$, δ ppm: 166.3 (**C**=O), 164.7 (d, J_{C-F}=252 Hz, Ar–F), 138.0 (Ar), 130.5 (d, J_{C-F}=2.90 Hz, Ar), 129.3 (d, J_{C-F}=8.80 Hz, Ar, x2), 127.9 (Ar, x2), 127.9 (Ar, x2), 127.7 (Ar), 115.6 (d, J_{C-F}=22.0 Hz, Ar, x2), 44.2 (–NH–**C**H$_2$–Ar).

^{19}F NMR: 282 MHz, $CDCl_3$, δ ppm: –108.1.

LRMS: (ESI^+) m/z 481.2 [2M + Na^+].

4.4.38 *N*-Benzyl-4-chlorobenzamide (3.110)

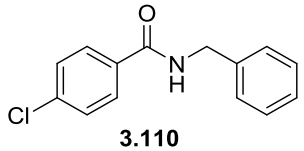

3.110

$C_{14}H_{12}ClNO$

245.70 g mol^{-1}

Synthesised by the procedure detailed in **4.4.33**, to give **3.110** (101 mg, 0.41 mmol, 82%) as white crystals. Spectroscopic and physical data are consistent with the literature.[200]

MP: 161-163 ˚C [literature 162-163 ˚C (Et_2O)][200]

FT-IR (cm^{-1}) neat: 3304 (m), 3085 (w), 3060 (w), 3027 (w), 2521 (w), 1638 (m), 1592 (w), 1550 (w).

^{1}H NMR: 400 MHz, $CDCl_3$, δ ppm: 7.73 (2H, d, *J*=8.6, Ar–**H**, x2), 7.40 (2H, d, *J*=8.1 Hz, Ar–**H**, x2), 7.37-7.29 (5H, m, Ar–**H**, x5), 6.46 (1H, Br, –N**H**–), 4.63 (2H, d, *J*=5.6 Hz, –NH–C**H**$_2$**N**–Ar).

^{13}C NMR: 100 MHz, $CDCl_3$, δ ppm: 166.3 (**C**=O), 137.9 (Ar), 137.8 (Ar), 132.7 (Ar), 128.8 (Ar, x3), 128.4 (Ar, x2), 127.8 (Ar, x2), 127.7 (Ar, x2), 44.2 (–NH–**C**H_2–Ar).

LRMS: (ESI$^+$) m/z 517.2 [2M(^{37}Cl^{37}Cl) + Na^+], 515.2 [2M(^{35}Cl^{37}Cl) + Na^+], 513.1 [2M(^{35}Cl^{35}Cl) + Na^+].

4.4.39 *N*-benzyl-4-bromobenzamide (3.111)

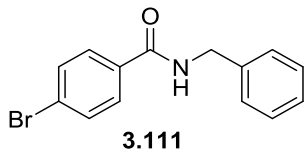

3.111
$C_{14}H_{12}BrNO$
290.16 g mol^{-1}

Synthesised by the procedure detailed in **4.4.33**, to give **3.111** (132 mg, 0.45 mmol, 91%) as white crystals. Spectroscopic and physical data are consistent with the literature.[200]

MP: 166-168 ˚C [literature 168 ˚C (Et_2O)][200]

FT-IR (cm^{-1}) neat: 3304 (m), 3084 (w), 3060 (w), 3028 (w), 2545 (w), 1637 (m), 1585 (m), 1545 (m).

^{1}H NMR: 400 MHz, $CDCl_3$, δ ppm: 7.66 (2H, d, *J*=8.6 Hz, Ar–**H**, x2), 7.56 (2H, d, *J*=8.1 Hz, Ar–**H**, x2), 7.39-7.30 (5H, m (Ar–**H**, x5), 6.44 (1H, br, –N**H**–), 4.63 (2H, d, *J*=5.6 Hz).

^{13}C NMR: 100 MHz, $CDCl_3$, δ ppm: 166.4 (**C**=O), 137.9 (Ar), 133.2 (Ar), 131.8 (Ar, x2), 128.8 (Ar, x2), 128.6 (Ar, x2), 127.9 (Ar, x2), 127.7 (Ar), 126.2 (Ar–Br), 44.2 (–NH–**C**H_2–Ar).

LRMS: (ESI$^+$) m/z 604.9 [2M(^{81}Br^{81}Br) + Na$^+$], 602.9 [2M(^{79}Br^{81}Br) + Na$^+$], 601.0 [2M(^{79}Br^{79}Br + Na$^+$].

4.4.40 *N*-Benzyl-2-naphthamide (3.112)

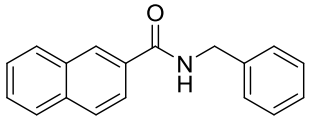

3.112
$C_{18}H_{15}NO$
261.32 g mol^{-1}

Synthesised by the procedure detailed in **4.4.33**, to give **3.112** (110 mg, 0.42 mmol, 84%) as white crystals. Spectroscopic and physical data are consistent with the literature.[200]

MP: 135-137 ˚C [literature 134-136 ˚C (Et_2O)][200]

FT-IR (cm^{-1}) neat: 3283 (m), 3081 (w), 3054 (w), 3027 (w), 2921 (w), 2353 (w), 2345 (w), 1635 (m), 1623 (m), 1601 (m), 1543 (m).

^{1}H NMR: 400 MHz, $CDCl_3$, δ ppm: 8.32 (1H, s, Ar–**H**), 7.92-7.85 (4H, m, Ar–**H**, x4), 7.59-7.52 (2H, m, Ar–**H**, x2), 7.42-7.32 (5H, m, Ar–**H**, x5), 6.61 (1H, br, –N**H**–), 4.72 (2H, d, *J*=5.6 Hz, –NH–C**H**$_2$–).

^{13}C NMR: 100 MHz, $CDCl_3$, δ ppm: 167.4 (**C**=O), 138.2 (Ar), 134.7 (Ar), 132.6 (Ar), 131.6 (Ar), 128.9 (Ar), 128.8 (Ar, x2), 128.5 (Ar), 128.0 (Ar, x2), 127.7 (Ar), 127.6 (Ar, x2), 127.4 (Ar), 126.7 (Ar), 123.6 (Ar), 44.3 (–NH–**C**H_2–Ar).

LRMS: (ESI$^+$) m/z 545.2 [2M + Na^+].

4.4.41 *N*-Benzylfuran-2-carboxamide (3.113)

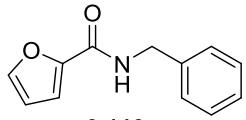

3.113
$C_{12}H_{11}NO_2$
201.22 g mol^{-1}

Synthesised by the procedure detailed in **4.4.33**, to give **3.113** (75 mg, 0.37 mmol, 75%) as white crystals. Spectroscopic and physical data are consistent with the literature.[201]

MP: 108-110 ˚C [Literature: 111-113 ˚C (EtOAc)][201]

FT-IR (cm^{-1}) neat: 3278 (m), 3123 (w), 3061 (w), 3030 (w), 1636 (m), 1572 (m), 1538 (m).

^{1}H NMR: 400 MHz, $CDCl_3$, δ ppm: 7.43 (1H, d, *J*=1.0 Hz, Ar–**H**), 7.37-7.29 (5H, m, Ar–**H**, x5), 7.16 (1H, d, *J*=3.5 Hz, Ar–**H**, 6.64 (1H, br, –N**H**–), 6.51 (1H, dd, *J*=3.3, 1.8 Hz, Ar–**H**), 4.63 (2H, d, *J*=6.1 Hz, –NH–C**H**$_2$–Ar).

^{13}C NMR: 100 MHz, $CDCl_3$, δ ppm: 147.9 (**C**=O), 143.8 (Ar), 138.0 (Ar), 128.8 (Ar, x2), 127.9 (Ar, x2), 127.6 (Ar, x2), 114.4 (Ar), 112.2 (Ar), 43.2 (–NH–**C**H$_2$–Ar).

LRMS: (ESI$^+$) m/z 265.2 [M + Na$^+$ + MeCN].

4.4.42 *N*-Benzylnicotinamide (3.114)

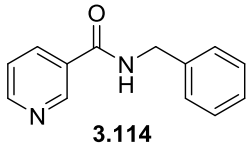

3.114

$C_{13}H_{12}N_2O$

212.25 g mol^{-1}

Synthesised by the procedure detailed in **4.4.33**, to give **3.114** (78 mg, 0.37 mmol, 74%) as white crystals. Spectroscopic and physical data are consistent with the literature.[202]

MP: 70-72 ˚C [Literature: 72-74 ˚C (EtOH)][203]

FT-IR (cm^{-1}) neat: 3281 (m), 3060 (w), 3030 (w), 2922 (w), 2831 (w), 2349 (w), 1632 (m), 1589 (m), 1538 (m).

^{1}H NMR: 400 MHz, $CDCl_3$, δ ppm: 8.99 (1H, d, *J*=1.2 Hz, Ar–**H**), 8.74 (1H, dt, *J*=4.0, 1.2 Hz, Ar–**H**), 8.15 (1H, dt, *J*=8.0, 1.9 Hz, Ar–**H**), 7.42-7.30 (6H, m, Ar–**H**, x6), 6.44 (1H, br, –N**H**–), 4.68 (2H, d, *J*=5.6 Hz, –NH–C**H**$_2$–).

^{13}C NMR: 100 MHz, $CDCl_3$, δ ppm: 165.4 (**C**=O), 152.4 (Ar), 147.8 (Ar), 137.7 (Ar), 135.1 (Ar), 130.0 (Ar), 128.1 (Ar, x2), 128.0 (Ar, x2), 127.9 (Ar), 123.5 (Ar), 44.3 (–NH–**C**H$_2$–).

LRMS: (ESI$^+$) m/z 659.3 [3M + Na$^+$], 447.2 [2M + Na$^+$].

4.4.43 *N*-Benzyldodecanamide (3.115)

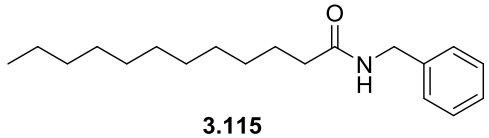

3.115

$C_{19}H_{31}NO$

289.46 g mol^{-1}

Synthesised by the procedure detailed in **4.4.33**, to give **3.115** (85 mg, 0.29 mmol, 59%) as white crystals. Spectroscopic and physical data are consistent with the literature.[204]

MP: 79-81 °C [literature: 77-79 °C (EtOAc)][204]

FT-IR (cm^{-1}) neat: 3289 (m), 3064 (w), 3034 (w), 2966 (w), 2915 (m), 2847 (m), 2357 (w), 1630 (m), 1551 (m),

^{1}H NMR: 400 MHz, $CDCl_3$, δ ppm: 7.36-7.27 (5H, m, Ar–**H**, x5), 5.73 (1H, br, –N**H**–), 4.45 (2H, d, *J*=5.6 Hz, –NH–C**H**$_2$–Ar), 2.22 (2H, t, *J*=7.8 Hz, –C**H**$_2$–), 1.72-1.63 (2H, m, –C**H**$_2$–), 1.30-1.26 (16H, m, –C**H**$_2$–, x8), 0.89 (3H, t, *J*=6.8 Hz, –C**H**$_3$).

^{13}C NMR: 100 MHz, $CDCl_3$, δ ppm: 173.0 (**C**=O), 138.4 (Ar), 128.7 (Ar, x2), 127.8 (Ar, x2), 127.5 (Ar), 43.6 (–NH–**C**H$_2$–Ar), 36.8 (–**C**H$_2$–), 31.9 (–**C**H$_2$–), 29.6 (–**C**H$_2$–, x2), 29.5 (–**C**H$_2$–), 29.3 (–**C**H$_2$–), 29.3 (–**C**H$_2$–, x2), 25.8 (–**C**H$_2$–), 22.7 (–**C**H$_2$–), 14.1 (–**C**H$_3$).

LRMS: (ESI$^+$) m/z 601.5 [2M + Na$^+$].

4.4.44 4-bromo-*N*-cyclobutylbenzamide (3.116)

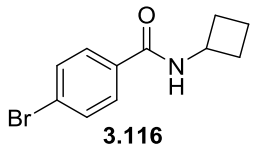

3.116
$C_{11}H_{12}BrNO$
254.12 g mol^{-1}

Synthesised by the procedure detailed in **4.4.33**, to give **3.116** (85 mg, 0.33 mmol, 67%) as white crystals.

MP: 160-162 ˚C

FT-IR (cm^{-1}) neat: 3296 (m), 2980 (w), 2942 (w), 2869 (w), 1634 (m), 1586 (m), 1567 (m).

^{1}H NMR: 400 MHz, $CDCl_3$, δ ppm: 7.63 (2H, d, *J*=8.6 Hz, Ar–**H**, x2), 7.56 (2H, d, *J*=8.6 Hz, Ar–**H**, x2), 6.25 (1H, br, –N**H**–), 4.58 (1H, sxt, *J*=8.1 Hz, –NH–C**H**–), 2.47-2.40 (2H, m, –C$\mathbf{H}_2$–), 2.00-1.92 (2H, m, –C$\mathbf{H}_2$–), 1.82-1.75 (2H, m, –C$\mathbf{H}_2$).

^{13}C NMR: 100 MHz, $CDCl_3$, δ ppm: 165.5 (**C**=O), 133.4 (Ar), 131.7 (Ar, x2), 128.5 (Ar, x2), 126.0 (Ar–Br), 45.3 (–NH–**C**H–), 31.3 (–**C**H_2–, x2), 15.2 (–**C**H_2–).

LRMS: (ESI$^+$) m/z 533.0 [2M(^{81}Br^{81}Br) + Na^+], 531.0 [2M(^{79}Br^{81}Br) + Na^+], 529.1 [2M(^{79}Br^{79}Br + Na^+].

HRMS: (ESI$^+$) m/z calcd. for $C_{11}H_{12}{}^{79}BrNNaO$ [M + Na^+] 275.9994, found 275.9995.

4.4.45 4-Bromo-*N*-cyclopentylbenzamide (3.117)

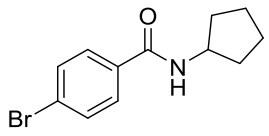

3.117
$C_{12}H_{14}BrNO$
268.15

Synthesised by the procedure detailed in **4.4.33**, to give **3.117** (87 mg, 0.32 mmol, 65%) as white crystals.

MP: 174-176 °C

FT-IR (cm^{-1}) neat: 3285 (m), 2947 (m), 2866 (m), 1631 (m), 1587 (m), 1536 (m).

^{1}H NMR: 400 MHz, $CDCl_3$, δ ppm: 7.62 (2H, d, *J*=8.1 Hz, Ar–**H**, x2), 7.56 (2H, d, *J*=8.1 Hz, Ar–**H**, x2), 6.02 (1H. br, –N**H**–), 4.39 (1H, sxt, *J*=7.0 Hz, –NHC**H**–), 2.14-2.08 (2H, m, –C**H**$_2$–), 1.76-1.61 (4H, m, –C**H**$_2$–, x2), 1.51-1.47 (2H, m, –C**H**$_2$–).

^{13}C NMR: 100 MHz, $CDCl_3$, δ ppm: 166.1 (**C**=O), 133.7 (Ar), 131.7 (Ar, x2), 128.4 (Ar, x2), 128.9 (Ar–Br), 51.8 (–NH–**C**H–), 33.2 (–**C**H$_2$–, x2), 23.8 (–**C**H$_2$–, x2).

LRMS: (ESI$^+$) m/z 557.1 [2M(^{81}Br^{81}Br) + Na$^+$], 559.1 [2M(^{79}Br^{81}Br) + Na$^+$], 561.1 [2M(^{79}Br^{79}Br + Na$^+$].

HRMS: (ESI$^+$) m/z calcd. for $C_{12}H_{14}{}^{79}BrNNaO$ [M + Na$^+$] 290.0151, found 290.0154.

4.4.46 4-Bromo-*N*-cyclohexylbenzamide (3.118)

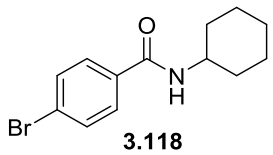

3.118

$C_{13}H_{16}BrNO$

282.18 g mol^{-1}

Synthesised by the procedure detailed in **4.4.33**, to give **3.118** (95 mg, 0.34 mmol, 67%) as white crystals. Spectroscopic and physical data are consistent with the literature.[205]

MP: 199-201 ˚C [literature: 201-205 ˚C (EtOAc)][205]

FT-IR (cm^{-1}) neat: 3284 (m), 3056 (m), 2853 (m), 2353 (w), 2321 (w), 1631 (m), 1589 (m), 1537 (m).

^{1}H NMR: 400 MHz, $CDCl_3$, δ ppm: 7.63 (2H, d, *J*=8.6 Hz, Ar–**H**, x2), 7.57 (2H, d, *J*=8.6 Hz, Ar–**H**, x2), 5.90 (1H, br, –N**H**–), 3.97 (1H, m, –NH–C**H**–), 2.05-2.02 (2H, m, –C**H**$_2$–), 1.79-1.74 (2H, m, –C**H**$_2$–), 1.66 (1H, m, –C**H**$_a$H$_b$–), 1.49-1.38 (2H, m, –C**H**$_2$–), 1.28-1.17 (3H, m, –C**H**$_2$–, –CH$_a$**H**$_b$–).

^{13}C NMR: 100 MHz, $CDCl_3$, δ ppm: 165.6 (**C**=O), 133.9 (Ar), 131.7 (Ar, x2), 128.4 (Ar, x2), 125.8 (Ar–Br), 48.8 (–NH–**C**H–), 33.2 (–**C**H$_2$– x2), 25.5 (–**C**H$_2$–), 24.9 (–**C**H$_2$– x2).

LRMS: (ESI$^+$) m/z 585.0 [2M(^{81}Br^{81}Br) + Na$^+$], 587.3 [2M(^{79}Br^{81}Br) + Na$^+$], 589.1 [2M(^{79}Br^{79}Br + Na$^+$].

4.4.47 4-Bromo-*N*-cycloheptylbenzamide (3.119)

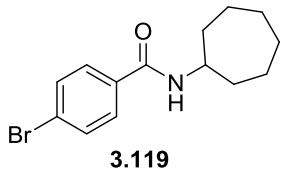

3.119
$C_{14}H_{18}BrNO$
296.20 g mol^{-1}

Synthesised by the procedure detailed in **4.4.33**, to give **3.119** (106 mg, 0.36 mmol, 72%) as white crystals.

MP: 185-187 ˚C

FT-IR (cm^{-1}) neat: 3234 (m), 3089 (w), 3056 (w), 2919 (m), 2854 (m), 2357 (w), 2312 (w), 1621 (m), 1587 (m), 1537 (m).

^{1}H NMR: 400 MHz, $CDCl_3$, δ ppm: 7.62 (2H, d, *J*=8.6 Hz, Ar–**H**, x2), 7.56 (2H, d, *J*=8.6 Hz, Ar–**H**, x2), 6.00 (1H, d, *J*=6.1 Hz, –N**H**–), 4.15 (1H, m, –NH–C**H**–), 2.05-2.01 (2H, m, –C**H**$_2$–), 1.67-1.49 (10H, m, –C**H**$_2$–, x5).

^{13}C NMR: 100 MHz, $CDCl_3$, δ ppm: 165.3 (**C**=O), 133.9 (Ar), 131.7 (Ar, x2), 128.4 (Ar, x2), 125.8 (Ar–Br), 51.0 (–NH–**C**H–), 35.1 (–**C**H$_2$– x2), 28.0 (–**C**H$_2$–, x2), 24.1 (–**C**H$_2$–, x2).

LRMS: (ESI$^+$) m/z 613.1 [2M(^{81}Br^{81}Br) + Na$^+$], 615.1 [2M(^{79}Br^{81}Br) + Na$^+$], 617.1 [2M(^{79}Br^{79}Br + Na$^+$].

HRMS: (ESI$^+$) m/z calcd. for $C_{14}H_{19}{}^{79}BrNO$ [M + H$^+$] 296.0645, found 296.0647.

4.4.48 4-Bromo-*N*-pentylbenzamide (3.120)

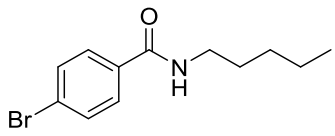

3.120
$C_{12}H_{16}BrNO$
270.17

Synthesised by the procedure detailed in **4.4.33**, to give **3.120** (120 mg, 0.44 mmol, 89%) as white crystals. Spectroscopic and physical data are consistent with the literature.[206]

MP: 97-99 ˚C [literature 94-96 ˚C (DCM)][206]

FT-IR (cm^{-1}) neat: 3230 (m), 3058 (w), 2950 (m), 2929 (m), 2864 (m), 2359 (w), 1629 (m), 1589 (m), 1536 (m).

^{1}H NMR: 400 MHz, $CDCl_3$, δ ppm: 7.63 (2H, d, *J*=8.6 Hz, Ar–**H**, x2), 7.56 (2H, d, 8.6 Hz, Ar–**H**, x2), 6.17 (1H, br, –N**H**–), 3.43 (2H, q, *J*=6.7 Hz, –NH–C**H**$_2$–), 1.67-1.58 (2H, m, –C**H**$_2$–), 1.37-1.34 (4H, m, –C**H**$_2$– x2), 0.92 (3H, t, *J*=6.8 Hz, –C**H**$_3$).

^{13}C NMR: 100 MHz, $CDCl_3$, δ ppm: 166.5 (**C**=O), 133.7 (Ar), 131.7 (Ar, x2), 128.4 (Ar, x2), 125.9 (Ar–Br), 40.2 (–NH–**C**H$_2$–), 29.3 (–**C**H$_2$–), 29.1 (–**C**H$_2$–), 22.3 (–**C**H$_2$–), 13.9 (–**C**H$_2$–).

LRMS: (ESI$^+$) m/z 561.0 [2M(^{81}Br^{81}Br) + Na$^+$], 563.1 [2M(^{79}Br^{81}Br) + Na$^+$], 565.2 [2M(^{79}Br^{79}Br + Na$^+$].

4.4.49 4-Bromo-*N*-(furan-2-ylmethyl)benzamide (3.121)

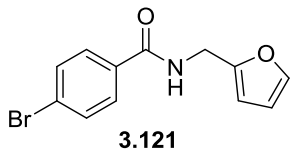

3.121

$C_{12}H_{10}BrNO_2$

280.12

Synthesised by the procedure detailed in **4.4.33**, to give **3.121** (105 mg, 0.37 mmol, 75%) as white crystals.

MP: 120-121 °C

FT-IR (cm^{-1}) neat: 3253 (m), 3074 (w), 2931 (w), 2851 (w), 2358 (w), 1634 (m), 1588 (m), 1544 (m).

^{1}H NMR: 400 MHz, $CDCl_3$, δ ppm: 7.65 (2H, d, *J*=8.6 Hz, Ar–**H**, x2), 7.57 (2H, d, *J*=8.6 Hz, Ar–**H**, x2), 7.39 (1H, d, *J*=1.0 Hz, Ar–**H**), 6.41 (1H, s, br –N**H**–), 6.35 (1H, m, Ar–**H**), 6.31 (1H, d, *J*=3.0 Hz, Ar–**H**), 4.64 (2H, d, *J*=5.6 Hz, –NH–C**H**$_2$–).

^{13}C NMR: 100 MHz, $CDCl_3$, δ ppm: 166.2 (**C**=O), 150.9 (Ar), 142.4 (Ar), 133.0 (Ar), 131.8 (Ar, x2) 128.6 (Ar, x2), 126.3 (Ar–Br), 110.6 (Ar), 107.9 (Ar), 37.1 (–NH–**C**H$_2$–).

LRMS: (ESI$^+$) m/z 581.0 [2M(^{81}Br^{81}Br) + Na$^+$], 583.0 [2M(^{79}Br^{81}Br) + Na$^+$], 584.9 [2M(^{79}Br^{79}Br + Na$^+$].

HRMS: (ESI$^+$) m/z calcd. for $C_{12}H_{10}{}^{79}BrNNaO_2$ [M + Na$^+$] 301.9787, found 301.9790.

4.4.50 4-Bromo-*N*-isopropylbenzamide (3.122)

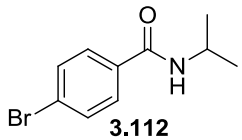

3.112

$C_{10}H_{12}BrNO$

242.11 g mol^{-1}

Synthesised by the procedure detailed in **4.4.33**, to give **3.122** (85 mg, 0.35 mmol, 70%) as white crystals. Spectroscopic and physical data are consistent with the literature.[207]

MP: 149-151 °C

FT-IR (cm^{-1}) neat: 3292 (m), 3064 (w), 2975 (w), 2932 (w), 2874 (w), 2359 (w), 1624 (m), 1585 (m), 1565 (m).

^{1}H NMR: 400 MHz, $CDCl_3$, δ ppm: 7.63 (2H, d, *J*=8.6 Hz, Ar–**H**, x2), 7.56 (2H, d, *J*=8.6 Hz Ar–**H**, x2), 5.87 (1H, br, –N**H**–), 4.28 (1H, oct, *J*=6.7 Hz, –NH–C**H**–), 1.27 (6H, d, *J*=6.6 Hz, –C**H**$_3$, x2).

^{13}C NMR: 100 MHz, $CDCl_3$, δ ppm: 165.7 (**C**=O), 133.8 (Ar), 131.7 (Ar, x2), 128.4 (Ar, x2), 125.9 (Ar–Br), 42.1 (–NH–**C**H–), 22.8 (–**C**H$_3$, x2).

LRMS: (ESI$^+$) m/z 505.1 [2M(^{81}Br^{81}Br) + Na$^+$], 507.0 [2M(^{79}Br^{81}Br) + Na$^+$], 509.0 [2M(^{79}Br^{79}Br + Na$^+$].

4.4.51 *N*-Allyl-4-bromobenzamide (3.123)

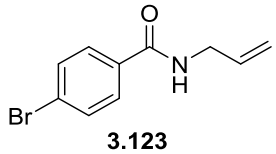

3.123
$C_{10}H_{10}BrNO$
240.10 g mol^{-1}

Synthesised by the procedure detailed in **4.4.33**, to give **3.123** (110 mg, 0.46 mmol, 92%) as white crystals. Spectroscopic and physical data are consistent with the literature.[208]

MP: 92-94 ˚C

FT-IR (cm^{-1}) neat: 3288 (m), 3074 (w), 3011 (w), 2979 (w), 2919 (w), 2868 (w), 2358 (w), 2312 (w), 1630 (m) 1588 (m), 1565 (m).

^{1}H NMR: 400 MHz, $CDCl_3$, δ ppm: 7.66 (2H, d, *J*=8.6 Hz, Ar-**H**, x2), 7.58 (2H, d, *J*=8.1 Hz, Ar-**H**, x2), 6.20 (1H, br, -N**H**-), 5.94 (1H, ddt, *J*=17.1, 10.3, 5.7 Hz, (-CH_2-C**H**=CH_2), 5.27 (1H, dtd, *J*=17.2, 1.5, 1.5 Hz, -CH=C**H**$_a$H$_b$), 5.20 (1H, dtd *J*=10.6, 1.0, 1.0 Hz, -CH=CH$_a$**H**$_b$), 4.08 (2H, m, -NH-C**H**$_2$-).

^{13}C NMR: 100 MHz, $CDCl_3$, δ ppm: 166.3 (**C**=O), 133.9 (Ar), 133.3 (-**C**=CH_2), 131.8 (Ar, x2), 128.5 (Ar, x2), 128.2 (Ar-Br), 116.9 (-CH=**C**H_2), 42.5 (-NH-**C**H_2-).

LRMS: (ESI^+) m/z 501.0 [2M(^{81}Br^{81}Br) + Na^+], 503.0 [2M(^{79}Br^{81}Br) + Na^+], 505.0 [2M(^{79}Br^{79}Br + Na^+].

4.4.52 *N*-(2-(1*H*-Indol-3-yl)ethyl)-4-bromobenzamide (3.124)

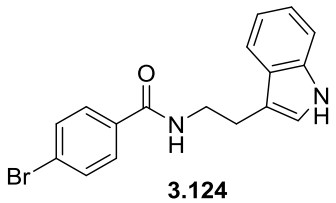

3.124
$C_{17}H_{15}BrN_2O$
343.22 g mol^{-1}

Synthesised by the procedure detailed in **4.4.33**, to give **3.124** (125 mg, 0.36 mmol, 73%) as white crystals.

MP: 146-148 ˚C

FT-IR (cm^{-1}) neat: 3390 (m), 3219 (w), 3056 (w), 2929 (w), 2864 (w), 1630 (m), 1589 (m), 1544 (m).

^{1}H NMR: 400 MHz, DMSO, δ ppm: 10.80 (1H, br s, –CH–N**H**–Ar), 8.68 (1H, t, *J*=5.6 Hz, –N**H**–CH_2–), 7.79 (2H, d, *J*=8.1 Hz, Ar–**H**, x2), 7.68 (2H, d, *J*=8.6 Hz, Ar–**H** x2), 7.57 (1H, d, *J*=8.1 Hz, Ar–**H**), 7.34 (1H, d, *J*=8.1 Hz, Ar–**H**), 7.17 (1H, d, *J*=1.5 Hz, –C=C**H**–NH–), 7.06 (1H, t, *J*=7.3 Hz, Ar–**H**). 6.98 (1H, t, *J*=7.3 Hz, Ar–**H**), 3.54 (2H, q, *J*=7.1 Hz, (NH–C**H**$_2$–), 2.95 (2H, t, *J*=7.3 Hz, –CH_2–C**H**$_2$–).

^{13}C NMR: 100 MHz, DMSO, δ ppm: 165.1 (**C**=O), 136.2 (Ar), 133.8 (Ar), 131.2 (Ar, x2), 129.4 (Ar, x2), 127.2 (Ar–Br), 124.7 (Ar), 122.6 (Ar), 120.9 (Ar), 118.2 (Ar), 118.2 (Ar), 111.8 (Ar), 111.3 (Ar), 40.25 (–**C**H_2–), 25.1 (–**C**H_2–).

LRMS: (ESI$^+$) m/z 707.0 [2M(^{81}Br^{81}Br) + Na$^+$], 708.8 [2M(^{79}Br^{81}Br) + Na$^+$], 710.9 [2M(^{79}Br^{79}Br + Na$^+$].

HRMS: (ESI$^+$) m/z calcd. for $C_{17}H_{15}{}^{79}BrN_2NaO$ [M + Na$^+$] 365.0260, found 365.0258.

4.4.53 4-Bromo-*N*-(4-methoxybenzyl)benzamide (3.125)

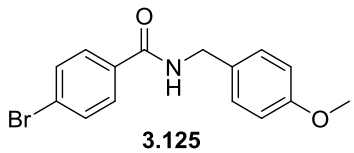

3.125
$C_{15}H_{14}BrNO_2$
320.18 g mol^{-1}

Synthesised by the procedure detailed in **4.4.33**, to give **3.125** (135 mg, 0.42 mmol, 84%) as white crystals.

MP: 142-144 °C

FT-IR (cm^{-1}) neat: 3319 (m), 3011 (w), 2930 (m), 2838 (m), 1637 (m), 1585 (m), 1509 (m).

^{1}H NMR: 400 MHz, $CDCl_3$, δ ppm: 7.65 (2H, d, *J*=8.6 Hz, Ar–**H**, x2), 7.56 (2H, d, *J*=8.6 Hz, Ar–**H**, x2), 7.28 (2H, d, *J*=8.6 Hz, Ar–**H**, x2), 6.89 (2H, d, *J*=8.6 Hz, Ar–**H**, x2), 6.37 (1H, br –N**H**–), 4.56 (2H, d, *J*=5.6 Hz, –NH–C**H**$_2$–), 3.81 (3H, s, –OC**H**$_3$).

^{13}C NMR: 100 MHz, $CDCl_3$, δ ppm: 166.2 (**C**=O), 159.2 (Ar–OCH_3), 133.2 (Ar), 131.7 (Ar, x2), 130.0 (Ar) 129.3 (Ar, x2), 128.6 (Ar, x2), 126.2 (Ar–Br), 114.2 (Ar, x2), 55.3 (–O**C**H$_3$), 43.7 (–NH–**C**H$_2$–).

LRMS: (ESI$^+$) m/z 661.1 [2M(^{81}Br^{81}Br) + Na$^+$], 663.1 [2M(^{79}Br^{81}Br) + Na$^+$], 665.1 [2M(^{79}Br^{79}Br + Na$^+$].

HRMS: (ESI$^+$) m/z calcd. for $C_{15}H_{14}{}^{79}BrNNaO_2$ [M + Na$^+$] 342.0100, found 342.0097.

4.4.54 (*R*)-4-Bromo-*N*-(1-phenylethyl)benzamide (3.126)

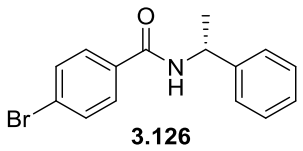

3.126

$C_{15}H_{14}BrNO$

304.18 g mol^{-1}

Synthesised by the procedure detailed in **4.4.33**, to give **3.126** (100 mg, 0.33 mmol, 66%) as white crystals.

$[\alpha]^{23}_{D}$ –14.7 (c 0.17, $CHCl_3$)

MP: 158-160 ˚C

FT-IR (cm^{-1}) neat: 3341 (m), 3031 (w), 2978 (m), 2925 (w), 2357 (w), 1639 (m), 1587 (m), 1527 (m).

^{1}H NMR: 400 MHz, $CDCl_3$, δ ppm: 7.65 (2H, d, *J*=8.6 Hz, Ar–**H**, x2), 7.57 (2H, d, *J*=8.6 Hz, Ar–**H**, x2), 7.41-7.28 (5H, m, Ar–**H**, x5), 6.25 (1H, d, *J*=6.8 Hz, –N**H**–), 5.33 (1H, quin, *J*=6.8 Hz, –NH–C**H**–), 1.62 (3H, d, *J*=6.8 Hz, –C**H**$_3$).

^{13}C NMR: 100 MHz, $CDCl_3$, δ ppm: 165.5 (**C**=O), 142.8 (Ar), 133.4 (Ar), 131.8 (Ar, x2), 128.8 (Ar, x2), 128.5 (Ar, x2), 127.6 (Ar), 126.2 (Ar, x2), 126.1 (Ar–Br), 49.4 (–NH–**C**H–), 21.6 (–**C**H$_3$).

LRMS: (ESI$^+$) m/z 629.0 [2M(^{81}Br^{81}Br) + Na$^+$], 631.0 [2M(^{79}Br^{81}Br) + Na$^+$], 633.0 [2M(^{79}Br^{79}Br + Na$^+$].

HRMS: (ESI$^+$) m/z calcd. for $C_{15}H_{14}{}^{79}BrNNaO$ [M + Na$^+$] 326.0151, found 326.0151.

4.4.55 4-Bromo-*N*-(4-hydroxylphenylethyl)benzamide (3.127) and 4-(2-(4-Bromobenzamido)ethyl)phenyl 4-bromobenzoate (3.130)

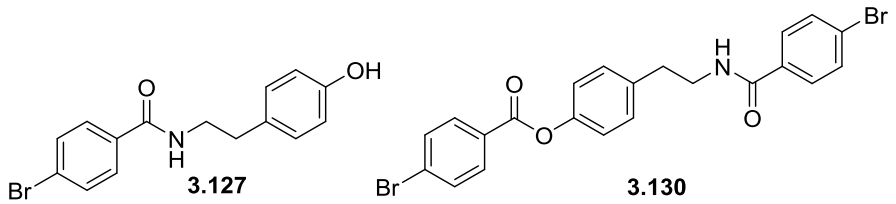

3.127
$C_{15}H_{14}BrNO_2$
320.18 g mol^{-1}

3.130
$C_{22}H_{17}Br_2NO_3$
503.18 g mol^{-1}

Synthesised by the procedure detailed in **4.4.33**, to give **3.127** (106 mg, 0.33 mmol, 66%) as white crystals and **3.130** (71 mg, 0.13 mmol, 32%) as a white crystalline by-product.

Spectroscopic and physical data for **3.127**.

MP: 170-172 ˚C

FT-IR (cm^{-1}) neat: 3315 (m), 2999 (w), 2917 (w), 2873 (w), 2801 (w), 2682 (w), 2594 (w), 1621 (m), 1590 (m), 1548 (m).

^{1}H NMR: 400 MHz, DMSO, δ ppm: 9.16 (1H, s, Ar–O**H**), 8.59 (1H, t, *J*=5.4 Hz, –N**H**–), 7.76 (2H, d, *J*=8.6 Hz, Ar–**H**, x2), 7.67 (2H, d, *J*=8.6 Hz, Ar–**H**, x2), 7.01 (2H, d, *J*=8.3 Hz, Ar–**H**, x2), 6.67 (2H, d, *J*=8.3 Hz, Ar–**H**, x2), 3.40 (2H, td, *J*=7.5, 5.4 Hz, –NH–C**H**$_2$–), 2.71 (2H, t, *J*=7.5 Hz, –CH$_2$–C**H**$_2$–).

^{13}C NMR: 100 MHz, DMSO, δ ppm: 165.1 (**C**=O), 155.6 (Ar–OH), 133.7 (Ar, x2), 131.2 (Ar, x2), 129.5 (Ar, x2), 129.2 (Ar, x2), 124.7 (Ar–Br), 115.1 (Ar, x2), 41.3 (–NH–**C**H$_2$–), 34.2 (–CH$_2$–**C**H$_2$–).

LRMS: (ESI$^+$) m/z 661.0 [2M(^{81}Br^{81}Br) + Na$^+$], 663.0 [2M(^{79}Br^{81}Br) + Na$^+$], 664.9 [2M(^{79}Br^{79}Br + Na$^+$].

HRMS: (ESI$^+$) m/z calcd. for $C_{15}H_{14}{}^{79}BrNNaO_2$ [M + Na$^+$] 342.0100, found 342.0094.

Spectroscopic and physical data for **3.130**.

MP: 216-218 ˚C

FT-IR (cm^{-1}) neat: 3338 (m), 3043 (w), 2931 (w), 2868 (w), 1721 (s), 1632 (m), 1587 (m), 1538 (m).

^{1}H NMR: 400 MHz, DMSO, δ ppm: 8.67 (1H, t, *J*=5.4 Hz, –N**H**–), 8.04 (2H, d, *J*=8.6 Hz, Ar–**H**, x2), 7.82 (2H, d, *J*=8.6 Hz, Ar–**H**, x2), 7.77 (2H, d, *J*=8.6 Hz, Ar–**H**, x2), 7.68 (2H, d, *J*=8.6 Hz, Ar–**H**, x2), 7.33 (2H, d, *J*=8.6 Hz, Ar–**H**, x2), 7.21 (2H, d, *J*=8.6 Hz, Ar–**H**, x2), 3.51 (2H, td, *J*=7.3, 5.4 Hz, –NH–C**H**$_2$–), 2.88 (2H, t, *J*=7.3 Hz, –CH_2–C**H**$_2$–Ar).

^{13}C NMR: 100 MHz, DMSO, δ ppm: 165.2 (**C**=O), 164.0 (**C**=O), 148.8 (Ar), 137.3 (Ar), 133.6 (Ar), 132.1 (Ar, x2), 131.7 (Ar, x2), 131.3 (Ar, x2), 129.7 (Ar, x2), 129.2 (Ar, x2), 128.2 (Ar–Br), 128.1 (Ar–Br), 124.8 (Ar), 121.6 (Ar, x2) 40.8 (–**C**H_2–NH–), 34.3 (–**C**H_2–CH_2–).

LRMS: (ESI$^+$) m/z 524.0 [M(^{81}Br^{81}Br) + Na$^+$], 526.0 [M(^{79}Br^{81}Br) + Na$^+$], 528.0 [M(^{79}Br^{79}Br + Na$^+$].

HRMS: (ESI$^+$) m/z calcd. for $C_{22}H_{17}{}^{79}Br^{81}BrNNaO_3$ [M + Na$^+$] 523.9465, found 523.9468.

5 References

(1) *Organic Electrochemistry*; 4th ed.; Marcel Dekker, **2001**.

(2) Pletcher, D. *A first course in electrode processes*; 2nd ed.; RSC Publising, **2009**.

(3) Nagib, D. A.; MacMillan, D. W. C. *Nature* **2011**, *480*, 224-228.

(4) Wang, J.; Sánchez-Roselló, M.; Aceña, J. L.; del Pozo, C.; Sorochinsky, A. E.; Fustero, S.; Soloshonok, V. A.; Liu, H. *Chem. Rev.* **2013**.

(5) Hagmann, W. K. *J. Med. Chem.* **2008**, *51*, 4359-4369.

(6) Purser, S.; Moore, P. R.; Swallow, S.; Gouverneur, V. *Chem. Soc. Rev.* **2008**, *37*, 320-330.

(7) Pagliaro, M.; Ciriminna, R. *J. Mater. Chem.* **2005**, *15*, 4981-4991.

(8) Fuchigami, T.; Inagi, S. *Chem. Commun.* **2011**, *47*, 10211-10223.

(9) Wiles, C.; Watts, P. *Eur. J. Org. Chem.* **2008**, *2008*, 1655-1671.

(10) Roberge, D. M.; Zimmermann, B.; Rainone, F.; Gottsponer, M.; Eyholzer, M.; Kockmann, N. *Org. Process Res. Dev.* **2008**, *12*, 905-910.

(11) Watts, P.; Wiles, C. *Chem. Commun.* **2007**, 443-467.

(12) Mason, B. P.; Price, K. E.; Steinbacher, J. L.; Bogdan, A. R.; McQuade, D. T. *Chem. Rev.* **2007**, *107*, 2300-2318.

(13) Ahmed-Omer, B.; Brandt, J. C.; Wirth, T. *Org. Biomol. Chem.* **2007**, *5*, 733-740.

(14) Watts, P.; Haswell, S. J. *Chem. Soc. Rev.* **2005**, *34*, 235-246.

(15) Pennemann, H.; Watts, P.; Haswell, S. J.; Hessel, V.; Löwe, H. *Org. Process Res. Dev.* **2004**, *8*, 422-439.

(16) Amemiya, F.; Horii, D.; Fuchigami, T.; Atobe, M. *J. Electrochem. Soc.* **2008**, *155*, E162-E165.

(17) He, P.; Watts, P.; Marken, F.; Haswell, S. J. *Green Chem.* **2007**, *9*, 20-22.

(18) Horii, D.; Atobe, M.; Fuchigami, T.; Marken, F. *J. Electrochem. Soc.* **2006**, *153*, D143-D147.

(19) He, P.; Watts, P.; Marken, F.; Haswell, S. J. *Angew. Chem. Int. Ed.* **2006**, *45*, 4146-4149.

(20) D. Horii; M. Atobe; T. Fuchigami; Marken, F. *Electrochem. Commun.* **2005**, *7*, 35-39.

(21) P. He; P. Watts; F. Marken; Haswell, S. J. *Electrochem. Commun.* **2005**, *7*, 918-924.

(22) Paddon, C.; Atobe, M.; Fuchigami, T.; He, P.; Watts, P.; Haswell, S.; Pritchard, G.; Bull, S.; Marken, F. *J. Appl. Electrochem.* **2006**, *36*, 617-634.

(23) C. A. Paddon; G. J. Pritchard; T. Thiemann; Marken, F. *Electrochem. Commun.* **2002**, *4*, 825-831.

(24) Ziogas, A.; Kolb, G.; O'Connell, M.; Attour, A.; Lapicque, F.; Matlosz, M.; Rode, S. *J. Appl. Electrochem.* **2009**, *39*, 2297-2313.

(25) Kashiwagi, T.; Amemiya, F.; Fuchigami, T.; Atobe, M. *J. Flow Chem.* **2013**, *3*, 17-22.

(26) Kashiwagi, T.; Amemiya, F.; Fuchigami, T.; Atobe, M. *Chem. Commun.* **2012**, *48*, 2806-2808.

(27) Watts, K.; Gattrell, W.; Wirth, T. *Beilstein J. Org. Chem.* **2011**, *7*, 1108-1114.

(28) Attour, A.; Rode, S.; Ziogas, A.; Matlosz, M.; Lapicque, F. *J. Appl. Electrochem.* **2008**, *38*, 339-347.

(29) Attour, A.; Rode, S.; Lapicque, F.; Ziogas, A.; Matlosz, M. *J. Electrochem. Soc.* **2008**, *155*, E201-E206.

(30) Renault, C.; Roche, J.; Ciumag, M. R.; Tzedakis, T.; Colin, S.; Serrano, K.; Reynes, O.; André-Barrès, C.; Winterton, P. *J. Appl. Electrochem.* **2012**, *42*, 667-677.

(31) Anis Attour; Patricia Dirrenberger; Sabine Rode; Athanassios Ziogas; Michael Matlosz; Lapicque, F. *Chem. Eng. Sci.* **2011**, *66*, 480-489.

(32) Simms, R.; Dubinsky, S.; Yudin, A.; Kumacheva, E. *Lab Chip* **2009**, *9*, 2395-2397.

(33) M. Küpper; V. Hessel; H. Löwe; W. Stark; J. Kinkel; M. Michel; Schmidt-Traub, H. *Electrochim. Acta* **2003**, *48*, 2889-2896.

(34) Horcajada, R.; Okajima, M.; Suga, S.; Yoshida, J.-i. *Chem. Commun.* **2005**, 1303-1305.

(35) Kristal, J.; Kodym, R.; Bouzek, K.; Jiricny, V.; Hanika, J. *Ind. Eng. Chem. Res.* **2011**, *51*, 1515-1524.

(36) E.R. Henquín; Bisang, J. M. *Electrochim. Acta* **2011**, *56*, 5296-5933.

(37) Karel Bouzek; Vladimír Jiřičný; Roman Kodým; Jiří Křišťál; Bystroň, T. *Electrochimica Acta* **2010**, *55*, 8172-8181.

(38) Suga, S.; Okajima, M.; Fujiwara, K.; Yoshida, J.-i. *J. Am. Chem. Soc.* **2001**, *123*, 7941-7942.

(39) J. Kuleshova; J. T. Hill-Cousins; P. R. Birkin; R. C. D. Brown; D. Pletcher; Underwood, T. J. *Electrochim. Acta* **2011**, *56*, 4322-4326.

(40) J. Kuleshova; J. T. Hill-Cousins; P. R. Birkin; R. C. D. Brown; D. Pletcher; Underwood, T. J. *Electrochim. Acta* **2012**, *69*, 197-202.
(41) Tojo, G.; Fernández, M. *Oxidation of Alcohols to Aldehydes and Ketones: A Guide to Current Common Practice*; Springer Science, **2006**.
(42) *Modern Oxidation Methods*; Wiley-VCH: Germany, **2004**.
(43) Poos, G. I.; Arth, G. E.; Beyler, R. E.; Sarett, L. H. *J. Am. Chem. Soc.* **1953**, *75*, 422-429.
(44) Bowden, K.; Heilbron, I. M.; Jones, E. R. H.; Weedon, B. C. L. *J. Chem. Soc.* **1946**, 39-45.
(45) J. C. Collins; W. W. Hess; F. J. Frank *Tetrahedron Lett.* **1968**, *9*, 3363-3366.
(46) E. J. Corey; Suggs, J. W. *Tetrahedron Lett.* **1975**, *16*, 2647-2650.
(47) Mancuso, A. J.; Huang, S.-L.; Swern, D. *J. Org. Chem.* **1978**, *43*, 2480-2482.
(48) Pfitzner, K. E.; Moffatt, J. G. *J. Am. Chem. Soc.* **1963**, *85*, 3027-3027.
(49) Albright, J. D.; Goldman, L. *J. Am. Chem. Soc.* **1965**, *87*, 4214-4216.
(50) Onodera, K.; Hirano, S.; Kashimura, N. *J. Am. Chem. Soc.* **1965**, *87*, 4651-4652.
(51) Omura, K.; Sharma, A. K.; Swern, D. *J. Org. Chem.* **1976**, *41*, 957-962.
(52) Parikh, J. R.; Doering, W. v. E. *J. Am. Chem. Soc.* **1967**, *89*, 5505-5507.
(53) Dess, D. B.; Martin, J. C. *J. Org. Chem.* **1983**, *48*, 4155-4156.
(54) M. Frigerio; Santagostino, M. *Tetrahedron Lett.* **1994**, *35*, 8019-8022.
(55) Griffith, W. P.; Ley, S. V.; Whitcombe, G. P.; White, A. D. *J. Chem. Soc. Chem. Commun.* **1987**, 1625-1627.
(56) Carey, J. S.; Laffan, D.; Thomson, C.; Williams, M. T. *Org. Biomol. Chem.* **2006**, *4*, 2337-2347.
(57) Sheldon, R. A.; Arends, I. W. C. E. *Adv. Synth. Catal.* **2004**, *346*, 1051-1071.
(58) Tebben, L.; Studer, A. *Angew. Chem. Int. Ed.* **2011**, *50*, 5034-5068.
(59) Nooy, A. E. J. d.; Besemer, A. C.; Bekkum, H. V. *Synthesis* **1996**.
(60) Adam, W.; Saha-Möller, C. R.; Ganeshpure, P. A. *Chem. Rev.* **2001**, *101*, 3499-3548.
(61) Alfonsi, K.; Colberg, J.; Dunn, P. J.; Fevig, T.; Jennings, S.; Johnson, T. A.; Kleine, H. P.; Knight, C.; Nagy, M. A.; Perry, D. A.; Stefaniak, M. *Green Chem.* **2008**, *10*, 31-36.
(62) Bobbitt, J. M.; Flores, M. C. L. *Heterocycles* **1988**, *27*, 509-533.

(63) Ciriminna, R.; Pagliaro, M. *Org. Process Res. Dev.* **2009**, *14*, 245-251.
(64) Calderon, F. *Synlett* **2006**, 657-658.
(65) Golubev, V. A.; Rozantsev, É. G.; Neiman, M. B. *Bull. Acad. Sci. USSR.* **1965**, *14*, 1898-1904.
(66) Lucio Anelli, P.; Biffi, C.; Montanari, F.; Quici, S. *J. Org. Chem.* **1987**, *52*, 2559-2562.
(67) Tromp, S. A.; Matijošytė, I.; Sheldon, R. A.; Arends, I. W. C. E.; Mul, G.; Kreutzer, M. T.; Moulijn, J. A.; de Vries, S. *ChemCatChem* **2010**, *2*, 827-833.
(68) Liu, R.; Liang, X.; Dong, C.; Hu, X. *J. Am. Chem. Soc.* **2004**, *126*, 4112-4113.
(69) Semmelhack, M. F.; Schmid, C. R. *J. Am. Chem. Soc.* **1983**, *105*, 6732-6734.
(70) Semmelhack, M. F.; Chou, C. S.; Cortes, D. A. *J. Am. Chem. Soc.* **1983**, *105*, 4492-4494.
(71) Inokuchi, T.; Matsumoto, S.; Torii, S. *J. Org. Chem.* **1991**, *56*, 2416-2421.
(72) K. Mitsudo; H. Kumagai; F. Takabatake; J. Kubota; Tanaka, H. *Tetrahedron Lett.* **2007**, *48*, 8994-8997.
(73) J. Kubota; Y. Shimizu; K. Mitsudo; Tanaka, H. *Tetrahedron Lett.* **2005**, *46*, 8975-8979.
(74) J. Kubota; T. Ido; M. Kuroboshi; H. Tanaka; T. Uchida; Shimamura, K. *Tetrahedron* **2006**, *62*, 4796-4773.
(75) M. Kuroboshi; T. Yoshida; J. Oshitani; K. Goto; Tanaka, H. *Tetrahedron* **2009**, *65*, 7177-7185.
(76) Y. Demizu; H. Shiigi; T. Oda; Y. Matsumura; Onomura, O. *Tetrahedron Lett.* **2008**, *49*, 48-52.
(77) H. Shiigi; H. Mori; T. Tanaka; Y. Demizu; Onomura, O. *Tetrahedron Lett.* **2008**, *49*, 5247-5251.
(78) Comminges, C.; Barhdadi, R.; Doherty, A. P.; O'Toole, S.; Troupel, M. *J. Phys. Chem. A* **2008**, *112*, 7848-7855.
(79) A. C. Herath; Becker, J. Y. *Electrochim. Acta.* **2008**, *53*, 4324-4330.
(80) Geneste, F.; Moinet, C.; Ababou-Girard, S.; Solal, F. *New J. Chem.* **2005**, *29*, 1520-1526.
(81) D. Liaigre; T. Breton; Belgsir, E. M. *Electrochem. Commun.* **2005**, *7*, 312-316.
(82) S. Kishioka; T. Ohsaka; Tokuda, K. *Electrochim. Acta* **2003**, *48*.

(83) E.M. Belgsir; Schäfer, H. J. *Electrochem. Commun.* **2001**, *3*, 32-35.

(84) S. Kishioka; S. Ohki; T. Ohsaka; Tokuda, K. *J. Electroanal. Chem.* **1998**, *452*, 179-186.

(85) Osa, T.; Kashiwagi, Y.; Mukai, K.; Ohsawa, A.; Bobbitt, J. M. *Chem. Lett.* **1990**, *19*, 75-78.

(86) M.F. Semmelhack; C. R. Schmid; Cortés, D. A. *Tetrahedron Lett.* **1986**, *27*, 1119-1122.

(87) A. Israeli; M. Patt; M. Oron; A. Samuni; R. Kohen; Goldstein, S. *Free Radic. Biol. Med.* **2005**, *38*, 317-324.

(88) Golubev, V. A.; Sen, V. D.; Rozantsev, É. G. *Bull. Acad. Sci. USSR. Chem. Sci.* **1979**, *28*, 1927-1931.

(89) Wertz, S.; Kodama, S.; Studer, A. *Angew. Chem. Int. Ed.* **2011**, *50*, 11511-11515.

(90) Manda, S.; Nakanishi, I.; Ohkubo, K.; Yakumaru, H.; Matsumoto, K.-i.; Ozawa, T.; Ikota, N.; Fukuzumi, S.; Anzai, K. *Org. Biomol. Chem.* **2007**, *5*, 3951-3955.

(91) Fish, J. R.; Swarts, S. G.; Sevilla, M. D.; Malinski, T. *J. Phys. Chem.* **1988**, *92*, 3745-3751.

(92) Hill-Cousins, J. T.; Kuleshova, J.; Green, R. A.; Birkin, P. R.; Pletcher, D.; Underwood, T. J.; Leach, S. G.; Brown, R. C. D. *ChemSusChem* **2012**, *5*, 326-331.

(93) Green, R. A.; Hill-Cousins, J. T.; Brown, R. C. D.; Pletcher, D.; Leach, S. G. *Electrochimica Acta* **2013**, *113*, 550-556.

(94) Golubev, V. A.; Sen', V. D. *Russ. J. Org. Chem.* **2011**, *47*, 869-876.

(95) G. Moad; E. Rizzardo; Solomon, D. H. *Tetrahedron Lett.* **1981**, *22*, 1165-1168.

(96) Arduengo, A. J.; Harlow, R. L.; Kline, M. *J. Am. Chem. Soc.* **1991**, *113*, 361-363.

(97) Arduengo, A. J.; Iconaru, L. I. *J. Chem. Soc. Dalton Trans.* **2009**, 6903-6914.

(98) Biju, A. T.; Kuhl, N.; Glorius, F. *Acc. Chem. Res.* **2011**, *44*, 1182-1195.

(99) Bourissou, D.; Guerret, O.; Gabbaï, F. P.; Bertrand, G. *Chem. Rev.* **1999**, *100*, 39-92.

(100) Dröge, T.; Glorius, F. *Angew. Chem. Int. Ed.* **2010**, *49*, 6940-6952.

(101)Enders, D.; Niemeier, O.; Henseler, A. *Chem. Rev.* **2007**, *107*, 5606-5655.

(102) Grossmann, A.; Enders, D. *Angew. Chem. Int. Ed.* **2012**, *51*, 314-325.

(103) Kirmse, W. *Angew. Chem. Int. Ed.* **2010**, *49*, 8798-8801.
(104) Knappke, C. E. I.; Imami, A.; Jacobi von Wangelin, A. *ChemCatChem* **2012**, *4*, 937-941.
(105) Kuhl, O. *Chem. Soc. Rev.* **2007**, *36*, 592-607.
(106) Marion, N.; Díez-González, S.; Nolan, S. P. *Angew. Chem. Int. Ed.* **2007**, *46*, 2988-3000.
(107) Melaimi, M.; Soleilhavoup, M.; Bertrand, G. *Angew. Chem. Int. Ed.* **2010**, *49*, 8810-8849.
(108) Nair, V.; Bindu, S.; Sreekumar, V. *Angew. Chem. Int. Ed.* **2004**, *43*, 5130-5135.
(109) Nair, V.; Vellalath, S.; Babu, B. P. *Chem. Soc. Rev.* **2008**, *37*, 2691-2698.
(110) Vora, H. U.; Wheeler, P.; Rovis, T. *Adv. Synth. Catal.* **2012**, *354*, 1617-1639.
(111) De Sarkar, S.; Biswas, A.; Samanta, R. C.; Studer, A. *Chem. Eur. J.* **2013**, *19*, 4664-4678.
(112) Wöhler; Liebig *Ann. Pharm.* **1832**, *3*, 249-282.
(113) Lapworth, A. *J. Chem. Soc. Trans.* **1903**, *83*, 995-1005.
(114) T. Ugai; S. Tanaka; Dokawa, S. *J. Pharm. Soc. Jpn.* **1943**, 269.
(115) Breslow, R. *J. Am. Chem. Soc.* **1958**, *80*, 3719-3726.
(116) Stetter, H. *Angew. Chem. Int. Ed.* **1976**, *15*, 639-647.
(117) Burstein, C.; Glorius, F. *Angew. Chem. Int. Ed.* **2004**, *43*, 6205-6208.
(118) Sohn, S. S.; Rosen, E. L.; Bode, J. W. *J. Am. Chem. Soc.* **2004**, *126*, 14370-14371.
(119) Reynolds, N. T.; Read de Alaniz, J.; Rovis, T. *J. Am. Chem. Soc.* **2004**, *126*, 9518-9519.
(120) Chow, K. Y.-K.; Bode, J. W. *J. Am. Chem. Soc.* **2004**, *126*, 8126-8127.
(121) Sohn, S. S.; Bode, J. W. *Org. Lett.* **2005**, *7*, 3873-3876.
(122) Corey, E. J.; Gilman, N. W.; Ganem, B. E. *J. Am. Chem. Soc.* **1968**, *90*, 5616-5617.
(123) Maki, B. E.; Chan, A.; Phillips, E. M.; Scheidt, K. A. *Org. Lett.* **2006**, *9*, 371-374.
(124) Zeitler, K.; Rose, C. A. *J. Org. Chem.* **2009**, *74*, 1759-1762.
(125) Maji, B.; Vedachalan, S.; Ge, X.; Cai, S.; Liu, X.-W. *J. Org. Chem.* **2011**, *76*, 3016-3023.
(126) De Sarkar, S.; Studer, A. *Org. Lett.* **2010**, *12*, 1992-1995.
(127) Vora, H. U.; Rovis, T. *J. Am. Chem. Soc.* **2007**, *129*, 13796-13797.

(128) Bode, J. W.; Sohn, S. S. *J. Am. Chem. Soc.* **2007**, *129*, 13798-13799.
(129) Sarkar, S. D.; Grimme, S.; Studer, A. *J. Am. Chem. Soc.* **2010**, *132*, 1190-1191.
(130) Wang, B.; Huang, P.-H.; Chen, C.-S.; Forsyth, C. J. *J. Org. Chem.* **2011**, *76*, 1140-1150.
(131) B. Wang; C. J. Forsyth *Synthesis* **2009**, 2873-2880.
(132) Orsini, M.; Chiarotto, I.; Sotgiu, G.; Inesi, A. *Electrochim. Acta* **2010**, *55*, 3511-3517.
(133) Orsini, M.; Chiarotto, I.; Feeney, M. M. M.; Feroci, M.; Sotgiu, G.; Inesi, A. *Electrochem. Commun.* **2011**, *13*, 738-741.
(134) Feroci, M.; Orsini, M.; Inesi, A. *Adv. Synth. Catal.* **2009**, *351*, 2067-2070.
(135) Feroci, M.; Elinson, M. N.; Rossi, L.; Inesi, A. *Electrochem. Commun.* **2009**, *11*, 1523-1526.
(136) Feroci, M.; Chiarotto, I.; Orsini, M.; Sotgiu, G.; Inesi, A. *Adv. Synth. Catal.* **2008**, *350*, 1355-1359.
(137) Feroci, M.; Chiarotto, I.; Orsini, M.; Pelagalli, R.; Inesi, A. *Chem. Commun.* **2012**, *48*, 5361-5363.
(138) Feroci, M.; Chiarotto, I.; Orsini, M.; Inesi, A. *Chem. Commun.* **2010**, *46*, 4121-4123.
(139) Chiarotto, I.; Feroci, M.; Orsini, M.; Sotgiu, G.; Inesi, A. *Tetrahedron Lett.* **2009**, *65*, 3704-3710.
(140) Chiarotto, I.; Feroci, M.; Orsini, M.; Feeney, M. M. M.; Inesi, A. *Adv. Synth. Catal.* **2010**, *352*, 3287-3292.
(141) Chiarotto, I.; Feeney, M. M. M.; Feroci, M.; Inesi, A. *Electrochim. Acta.* **2009**, *54*, 1638-1644.
(142) M. Feroci; I. Chiarotto; A. Inesi *Electrochim. Acta.* **2013**, *89*, 692-699.
(143) Tam, S. W.; Jimenez, L.; Diederich, F. *J. Am. Chem. Soc.* **1992**, *114*, 1503-1505.
(144) Belletire, J. L.; Bills, R. A.; Shackelford, S. A. *Synthetic Commun.* **2008**, *38*, 738-745.
(145) Guin, J.; De Sarkar, S.; Grimme, S.; Studer, A. *Angew. Chem. Int. Ed.* **2008**, *47*, 8727-8730.
(146) Zhou, J.; Rieker, A. *J. Chem. Soc., Perkin Tran. 2.* **1997**, 931-938.
(147) Tümer, M.; Aslantaş, M.; Sahin, E.; Deligönül, N. *Spectrochimica Acta Part A.* **2008**, *70*, 477-481.

(148) P. D. Astudillo; J. Tiburcio; González., F. J. *J. Electroanal. Chem.* **2007**, *604*, 57-64.

(149) Macías-Ruvalcaba, N. A.; Okumura, N.; Evans, D. H. *J. Phys. Chem. B.* **2006**, *110*, 22043-22047.

(150)Lehmann, M. W.; Evans, D. H. *J. Phys. Chem. B.* **2001**, *105*, 8877-8884.

(151) Gupta, N.; Linschitz, H. *J. Am. Chem. Soc.* **1997**, *119*, 6384-6391.

(152) Hallett, J. P.; Welton, T. *Chem. Rev.* **2011**, *111*, 3508-3576.

(153) Sowmiah, S.; Srinivasadesikan, V.; Tseng, M.-C.; Chu, Y.-H. *Molecules* **2009**, *14*, 3780-3813.

(154) S. Chowdhury; Mohan, R. S.; Scott, J. L. *Tetrahedron* **2007**, *63*, 2363-2389.

(155) Welton, T. *Coordination. Chem. Rev.* **2005**, *248*, 2459-2477.

(156) I, C.; M. Feroci; G. Sotgiu; Inesi, A. *Tetrahedron* **2013**, *69*, 8088-8095.

(157) Sawyer, D. T.; Komai, R. Y. *Anal. Chem.* **1972**, *44*, 715-721.

(158) G. Accorsi; F. Barigelletti; A. Farrán; F. Herranz; R. M. Claramunt; M. Marcaccio; G. Valenti; F. Paolucci; E. Pinilla; Torres., M. R. *J. Photochem. Photobio. A. Chem.* **2009**, *203*, 166-176.

(159) Iwahana, S.; Iida, H.; Yashima, E. *Chem. Euro. J.* **2011**, *17*, 8009-8013.

(160) C. Noonan; L. Baragwanath; Connon., S. J. *Tetrahedron Lett.* **2008**, *49* 4003-4006.

(161) Freire, M. G.; Neves, C. M. S. S.; Marrucho, I. M.; Coutinho, J. O. A. P.; Fernandes, A. M. *J. Phys. Chem. A.* **2009**, *114*, 3744-3749.

(162) Cho, C.-W.; Phuong Thuy Pham, T.; Jeon, Y.-C.; Yun, Y.-S. *Green Chem.* **2008**, *10*, 67-72.

(163) O'Mahony, A. M.; Silvester, D. S.; Aldous, L.; Hardacre, C.; Compton, R. G. *J. Chem. Eng. Data.* **2008**, *53*, 2884-2891.

(164) Huddleston, J. G.; Visser, A. E.; Reichert, W. M.; Willauer, H. D.; Broker, G. A.; Rogers, R. D. *Green Chem.* **2001**, *3*, 156-164.

(165) Finney, E. E.; Ogawa, K. A.; Boydston, A. J. *J. Am. Chem. Soc.* **2012**, *134*, 12374-12377.

(166) Barletta, G.; Chung, A. C.; Rios, C. B.; Jordan, F.; Schlegel, J. M. *J. Am. Chem. Soc.* **1990**, *112*, 8144-8149.

(167) Nakanishi, I.; Itoh, S.; Fukuzumi, S. *Chem. Euro. J.* **1999**, *5*, 2810-2818.

(168) Armarego, W. L. F.; Perrin, D. D.; Perrin, D. R. *Purification of Laboratory Chemicals*; 4th ed.; Butterworth-Heinemann Ltd.: Oxford, **1997**.

(169) Shibuya, M.; Tomizawa, M.; Iwabuchi, Y. *J. Org. Chem.* **2008**, *73*, 4750-4752.

(170) Vogler, T.; Studer, A. *Adv. Synth. Catal.* **2008**, *350*, 1963-1967.

(171) Myles, L.; Gathergood, N.; Connon, S. J. *Chem. Commun.* **2013**, *49*, 5316-5318.

(172) Omura, K. *J. Org. Chem.* **1984**, *49*, 3046-3050.

(173) Matsushita, M.; Kamata, K.; Yamaguchi, K.; Mizuno, N. *J. Am. Chem. Soc.* **2005**, *127*, 6632-6640.

(174) Kashparova, V. P.; Kagan, E. S.; Zhukova, I. Y.; Ivakhnenko, E. P. *Russ. J. Appl Chem.* **2004**, *77*, 964-967.

(175) Banekovich, C.; Ott, I.; Koch, T.; Matuszczak, B.; Gust, R. *Bioorg. Med. Chem. Lett.* **2007**, *17*, 683-687.

(176) Caelen, I.; Kalman, A.; Wahlström, L. *Anal. Chem.* **2003**, *76*, 137-143.

(177) Brown, P.; Hornbeck, C. L.; Cronin, J. R. *Organic Mass Spectrometry* **1972**, *6*, 1383-1399.

(178) Schmaderer, H.; Hilgers, P.; Lechner, R.; König, B. *Adv. Synth. Catal.* **2009**, *351*, 163-174.

(179) Kamal, A.; Chouhan, G. *Adv. Synth. Catal.* **2004**, *346*, 579-582.

(180) Brandt, A.; Hallett, J. P.; Leak, D. J.; Murphy, R. J.; Welton, T. *Green Chem.* **2010**, *12*, 672-679.

(181) Hu, A.; Cao, G. *Tetrahedron-Asymmetry* **2011**, *22*, 1332-1336.

(182) Gauchot, V.; Kroutil, W.; Schmitzer, A. R. *Chem. Eur J.* **2010**, *16*, 6748-6751.

(183) Pesch, J.; Harms, K.; Bach, T. *Eur. J. Org. Chem.* **2004**, *2004*, 2025-2035.

(184) Hirano, K.; Piel, I.; Glorius, F. *Adv. Synth. Catal.* **2008**, *350*, 984-988.

(185) Liu, C.; Wang, J.; Meng, L.; Deng, Y.; Li, Y.; Lei, A. *Angew. Chem. Int. Ed.* **2011**, *50*, 5144-5148.

(186) Joseph, T. C.; Dev, S. *Tetrahedron-Asymmetry* **1968**, *24*, 3809-3827.

(187) Gowrisankar, S.; Neumann, H.; Beller, M. *Angew. Chem. Int. Ed.* **2011**, *50*, 5139-5143.

(188) Zhao, J.; Mück-Lichtenfeld, C.; Studer, A. *Adv. Synth. Catal.* **2013**, *355*, 1098-1106.

(189) Rivero-Cruz, B.; Rivero-Cruz, I.; Rodríguez-Sotres, R.; Mata, R. *Phytochemistry* **2007**, *68*, 1147-1155.

(190) Rendina, V. L.; Kingsbury, J. S. *J. Org. Chem.* **2012**, *77*, 1181-1185.

(191) Sun, X.; Shan, G.; Sun, Y.; Rao, Y. *Angew. Chem. Int. Ed.* **2013**, *52*, 4440-4444.

(192) Y. Li; W. Du; Deng., W. P. *Tetrahedron* **2012**, *69*, 3611-3615.

(193) Vorbrüggen, H. *Angew. Chem.* **1963**, *75*, 296-297.

(194) Hatano, M.; Kamiya, S.; Ishihara, K. *Chem. Commun.* **2012**, *48*, 9465-9467.

(195) Manabe, K.; Iimura, S.; Sun, X.-M.; Kobayashi, S. *J. Am. Chem. Soc.* **2002**, *124*, 11971-11978.

(196) Tschaen, B. A.; Schmink, J. R.; Molander, G. A. *Org. Lett.* **2013**, *15*, 500-503.

(197) Liu, G.; Liu, C.; Sun, L.; Qu, R.; Chen, H.; Ji, C. *Chem. Heterocyc. Compd.* **2007**, *43*, 1290-1300.

(198) Baumert, M.; Albrecht, M.; Winkler, H. D. F.; Schalley, C. A. *Synthesis* **2010**, 953-958.

(199) Baker, W.; Glockling, F. *J. Chem. Soc.* **1950**, 2759-2764.

(200) Kawagoe, Y.; Moriyama, K.; Togo, H. *Tetrahedron-Asymmetry* **2013**, *69*, 3971-3977.

(201) Gernigon, N.; Al-Zoubi, R. M.; Hall, D. G. *J. Org. Chem.* **2012**, *77*, 8386-8400.

(202) Orliac, A.; Gomez Pardo, D.; Bombrun, A.; Cossy, J. *Org. Lett.* **2013**, *15*, 902-905.

(203) Williams, A.; Lucas, E. C.; Rimmer, A. R.; Hawkins, H. C. *J. Chem. Soc., Perkin Trans 2* **1972**, 627-633.

(204) Kunishima, M.; Kikuchi, K.; Kawai, Y.; Hioki, K. *Angew. Chem.* **2012**, *124*, 2122-2125.

(205) Ohshima, T.; Iwasaki, T.; Maegawa, Y.; Yoshiyama, A.; Mashima, K. *J. Am. Chem. Soc.* **2008**, *130*, 2944-2945.

(206) Petricci, E.; Mugnaini, C.; Radi, M.; Corelli, F.; Botta, M. *J. Org. Chem.* **2004**, *69*, 7880-7887.

(207) Sharma, S.; Park, E.; Park, J.; Kim, I. S. *Org. Lett.* **2012**, *14*, 906-909.

(208) Moon, N. G.; Harned, A. M. *Tetrahedron Lett.* **2013**, *54*, 2960-2963.